

ASSESSMENT OF EARTHQUAKE DAMAGES BY IMAGE-BASED TECHNIQUES

Mehdi Rezaeian

Zurich, 2010

DISS. ETH NO. 19178

Assessment of earthquake damages by image-based techniques

A dissertation submitted to
ETH Zurich

for the degree of
Doctor of Sciences

presented by

Mehdi Rezaeian
M.Sc. in the field of
Electrical Engineering - University of Tehran

Born September 22, 1970
Citizen of Iran

accepted on the recommendation of
Prof. em. Dr. Armin Grün, examiner
ETH Zurich, Switzerland
Prof. Dr. Marc Pollefeyts, co-examiner
ETH Zurich, Switzerland
Prof. Dr. Orhan Altan, co-examiner
Technical University of Istanbul, Turkey

2010

IGP Mitteilungen Nr. 107

Assessment of earthquake damages by image-based techniques
Mehdi Rezaeian

Copyright © 2010, Mehdi Rezaeian

Institut für Geodäsie und Photogrammetrie
Eidgenössische Technische Hochschule Zürich
Wolfgang Pauli-Strasse 15
8093 Zürich

All rights reserved

ISSN 0252-9335
ISBN 978-3-906467-90-0

ABSTRACT

Although natural disasters are inevitable and it is almost impossible to fully recoup the damage caused by the disaster, what the humans can change is the way they respond to disasters. The whole disaster management procedure requires urgent developments toward better, more elaborated and appropriate means for facing natural risks. This is already realized and accepted as a high priority task by many organizations, governments and companies in all over the world. Their prediction and preparedness along with an effective disaster management program can minimize the effect of damage. Thus, damage assessments have attracted significant attentions among researchers and practitioners of disaster management.

Remote sensing techniques both by space-borne and air-borne sensors could make a very effective contribution especially in response and recovery phases of disaster management. A fast ascertainment of the affected buildings and people is helpful for the disaster management in order to allocate the limited search and rescue resources (personnel and equipment) for each individual collapsed building. The possibility of a near real-time damage assessment could help the rescue operations. Furthermore, the spatial distribution of damages is very important for the emergency teams deployed immediately after the catastrophe. In this study, we mainly focus on rapid damage assessment methods using remotely sensed imagery data. Several kinds of remotely sensed data on damages may be available, such as aerial photography and digital imagery, satellite imagery, airborne laser scanning and synthetic aperture radar observations. Optical images can be interpreted visually as they depict the ground surface as it appears to the human eye. Within this realm, studies are based on either mono-temporal (only post-event images are available) or multi-temporal analysis (both pre- and post-event images are available). We present methods for local (buildings) damage classification using multi-temporal high-resolution optical images.

To evaluate methods and verifying numerical results, two datasets of Kobe and Bam were obtained from aerial images. The Kobe earthquake was a major earthquake in Japan. It was the first time in the world that a densely populated modern city area was directly hit by very strong ground shaking. The Bam earthquake in terms of human loss was the worst to occur in Iranian history.

We base our verification on visual inspection of the stereo images using number of objective assessment criteria. Damage identification via space/airborne images is restricted to some structural type of visible damages and visibility of details relies on view direction as well as image resolution. In the Bam area, a multilevel damage scale (totally collapsed, partially collapsed, uncollapsed) appears to be adequate in representing the distribution of individual house damages. In Kobe, due to large scale and high quality colored images, it is possible to extract more details of damaged buildings based on EMS98 and a damage catalogue.

The drawbacks of traditional photo interpretation techniques are pertained first to the time and cost needed for manual processing of the data and second to the difficulty in supporting coherent interpretation criteria in case there are large numbers of photo-interpreters working in parallel for interpretation of wide areas in a short time. The major contribution of this dissertation is to find solutions in order to automate interpretation tasks entirely or partially. Damage interpretation is divided into four main tasks: identifying objects, collecting relative attributes and evidences, detecting damaged objects and classification in meaningful categories. This research is divided into two main parts. In part one (Chapters 5 and 6); it is assumed that objects of interest (i.e. buildings) are already identified using auxiliary pre-event data such as building polygons or 3D models. In this

part, we will commence bi-level classification (i.e. collapsed and uncollapsed) and move toward multilevel classifications. We present and develop damage classification methods utilizing: only DSMs features, only imagery features and integration of both. In the second part (Chapter 7) we document the use of a novel methodology for assessing the damages of man-made objects and make efforts to extract the object and its damages at once. This method utilizes a methodology of applying Bayesian networks to a multi-view and multi-modal damaged object description.

Digital surface models extracted from airborne stereo image pairs before and after the earthquake can be used to identify collapsed buildings. However, simple pointwise comparison of DSMs generated automatically won't be reliable evidence to detect damaged points. The critical parameter is an optimum threshold value, which cannot be defined generally due to stochastic behavior of the model in different areas. Hypothesis testing suggested in Chapter 5 shows that the normalized value of "average height differences" (AHD) reveals the results with the best overall accuracies. In this method, some undamaged sample buildings are employed for evaluating the mean and variance values. These buildings must be distributed almost uniformly in a test area including a variety of buildings shape. The experiments are extended by replacing the pre-event DSM with 3D model of buildings extracted before the earthquake.

In the course of this research several methods for extracting imagery features for debris detection are examined. First and second order statistical descriptors including standard deviation, entropy and homogeneity are evaluated. The assessments show that this kind of descriptors, measuring image amplitude in terms of luminance or tristimulus values, are less sensitive to soft damage and suffer from miscellaneous textures in high-resolution images in urban area. We propose "Regularity indices" to describe the appearance of the building as regular or irregular. Three kinds of classification methods: k-NN, Bayesian and SVM are used and compared. The classification results are evaluated by a cross-validation method and by an independent visual interpretation test set. The Support Vector Machine (SVM) classifier is a relatively new method that proved to be quite effective for damage detection. The integration of object (DSMs) and image space features is applied through classifiers for labeling three attributes of buildings ("Uncollapsed", "Partially collapsed" and "Totally collapsed"). Regularity indices combined with normalized average height difference through an OVO-SVM classifier show that using multiple features can be useful to classify collapsed buildings automatically.

In Chapter 7, we develop a system that automatically interprets data produced by aerial sensors before and after an earthquake in order to arrive at a detailed damage map quickly after disaster. We assume no prior information about buildings position is available and the possibility of a near-real time damage assessment is examined and the results are compared. The proposed system applies image-understanding algorithms to recognize buildings prior to classifying the scene. Another aspect of proposed system is to handle "uncertainty" using Bayesian networks. The network provides pointwise analysis based on prior information of multi-image segments. For line detection and image segmentation, we design and develop a multi-stage line detection method, so called Hierarchical Permissive Hough Transform (HPHT) a modified version of HT. This algorithm iteratively detects obvious and obscure lines. To detect damaged points a symmetric form of Bayesian network includes two parts for detection before and after earthquake is suggested. The investigations with the Bam and Kobe dataset show that the proposed augmented Bayesian network improves the performance of the reasoning system. Within a building polygon, the presented method is able to detect and classify damaged points. We are able to extract detailed information about collapsed buildings. Empirical results show that the suggested approach is quite promising.

ZUSAMMENFASSUNG

Obwohl Naturkatastrophen nicht vermieden werden können und es fast unmöglich ist, die durch Naturkatastrophen entstandenen Schäden auszugleichen, können wir Menschen die Art, wie wir auf die Katastrophen reagieren, ändern. Das komplette Verfahren des Katastrophenmanagement muss verbessert, mehr ausgearbeitet und adäquate Mittel für die Bekämpfung der Naturgefahren zur Verfügung gestellt bekommen. Die Notwendigkeit dafür ist bereits von vielen Organisationen, Regierungen und Firmen auf der ganzen Welt realisiert und als Schwerpunktthema aufgenommen wurden. Die Vorhersage und die Bereitschaft für ein effizientes Katastrophenmanagementprogramm können daher die Auswirkungen des Schadens minimieren. Das ist auch ein Grund dafür, warum Schadensabschätzungen grosse Aufmerksamkeit von Forschern und Fachleuten für Katastrophenmanagement bekommen.

Fernerkundungstechniken (Satelliten- und Flugzeuggetragene Sensoren) haben die Möglichkeit, einen nachhaltigen Beitrag für die Reaktions- und Erholungsphase des Katastrophenmanagements zu leisten. Eine schnelle Erfassung der betroffenen Gebäude und Personen ist hilfreich, um die limitierten Such- und Rettungsressourcen (Personal und Equipment) auf die individuellen eingestürzten Gebäude aufzuteilen. Die Möglichkeit, die Schadensabschätzung in naher Echtzeit durchzuführen könnte die Rettungsaktionen unterstützen. Weiterhin ist die räumliche Erfassung des Schadens wichtig für den Einsatz der Notfallkräfte direkt nach der Katastrophe. Daher liegt der Schwerpunkt unserer Forschung auf einer schnellen Schadenserfassungsmethode unter Verwendung von aufgenommen Bilddaten. Verschiedene Arten von Fernerkundungsdaten, zum Beispiel analoge und digitale Luftbilder, Satellitenbilder, Luftgestütztes Laserscanning und Synthetic Aperture Radar (SAR), können verfügbar sein. Optische Bilder sind einfach zu interpretieren, da diese die Oberfläche so zeigen, wie wir sie mit dem Auge wahrnehmen. Auswertungen mit Bildern werden mit nur einer Aufnahme nach dem Event oder mit einer zeitlichen Bildabfolge vor und nach dem Event analysiert. In dieser Arbeit werden Methoden für lokale (Gebäude) Schadensklassifikation mittels Zeitreihen von hochauflösenden optischen Bildern gezeigt.

Um die Ergebnisse und Methoden zu evaluieren wurden zwei Luftbilddatensätze von Kobe und Bam verwendet. Das Erdbeben in Kobe war eines der stärksten Erdbeben in Japan, da zum ersten Mal auf der Erde eine stark besiedelte moderne Stadt direkt von den starken Erschütterungen betroffen war. Das Erdbeben in Bam war das schrecklichste in der iranischen Geschichte bezüglich der Anzahl der umgekommenen Menschen. Unsere Verifikation der Schadenskriterien ist basiert auf visuelle Inspektion mittels Stereobildern. Die Identifikation des Schadens mittels Satelliten- und Luftbildern ist limitiert durch die Aufnahmerichtung des Sensors und durch die Auflösung der Bilder. Im Bam-Gebiet wurde eine mehrstufige Schadensskalierung (Komplett, teilweise oder nicht eingestürzt) für die adäquate Darstellung der Schadensverteilung der Häuser verwendet. Auf Grund der höheren Auflösung und der guten Qualität der Farbbilder der Kobe-Daten konnte der Schaden der Gebäude mittels EMS98 und Schadenskatalog ausgewertet werden.

Die Nachteile der traditionellen Luftbildinterpretation sind zum Einem die Zeit und die Kosten für das manuelle Prozessieren der Daten und zum Zweiten die Schwierigkeit für verständliche Interpretationskriterien für die grosse Anzahl von Bilderauswertern, welche während der Interpretation des gesamten Gebietes in einer kurzen Zeit parallel arbeiten. Der wichtigste Beitrag dieser Promotionsarbeit liegt hierbei in der Lösungsfindung für die automatische oder teilweise automatische Interpretation. Die Schadensinterpretation ist dabei untergliedert in vier Schwerpunkte: Identifizierung von Objekten, Erfassung von relativen Attributen und Aussagen,

Erfassung der beschädigten Objekte und der Klassifikation in aussagekräftige Kategorien. Die Schwerpunkte der Arbeit sind in zwei Teile untergliedert. Im ersten Teil (Kapitel 5 und 6) besteht die Annahme das Objekte (Gebäude) durch Gebäudepolygone oder 3D-Modelle schon identifiziert wurden. Bei der Auswertung startet man mit einer „Bi-Level“ (Eingestürzt und nicht eingestürzt) Klassifikation, welche danach in eine Multi-Level Klassifikation übergeht. Hierbei unterscheiden wir DHM- und Bild-basierte Methoden oder eine Kombination von beiden. Im zweiten Teil der Arbeit (Kapitel 7) beschreiben wir eine neuartige Methode für die Schadenserfassung von künstlichen geschaffenen Objekten, wobei das Objekt und die Zerstörung zur gleichen Zeit erfasst werden. Diese Methode basiert auf „Bayesian Networks“ mit der Beschreibung von „multi-view“ und „multi-modal“ Beschreibung der zerstörten Objekte.

Digitale Oberflächenmodelle, welche aus Stereobildern vor und nach der Zerstörung generiert wurden, können für die Identifizierung der zerstörten Objekte verwendet werden. Hierbei führen einfache punktbasierte Vergleiche der Höhenmodelle nicht zu einer zuverlässigen Aussage über die beschädigten Punkte. Ein kritischer Parameter ist hierfür ein optimaler Grenzwert, welcher nicht aus dem stochastischen Verhalten des Modells der verschiedenen Gebiete abgeleitet werden kann. Der in Kapitel 5 vorgestellte Hypothesentest zeigt, dass der normalisierte Wert der durchschnittlichen Höhendifferenz (AHD) zu einem optimalen Grenzwert führt. Für die Varianz und Mittelwert im Hypothesentest werden Beispieldaten der nichtzerstörten Gebäude benötigt. Dabei müssen diese gleichmäßig über das Testgebiet verteilt und verschiedene Gebäudeformen beinhalten. Das Experiment wurde noch erweitert, in dem das Höhenmodell mit einem 3D-Modell der Gebäude ersetzt wurde.

Im Rahmen dieser Arbeit wurden verschiedene Methoden für die Extraktion von Bildmerkmalen für die Erfassung von Trümmern untersucht. Es wurden statistische Deskriptoren erster und zweiter Ordnung, wie zum Beispiel Standardabweichung, Entropie und Homogenität evaluiert. Die Bewertung zeigte, dass diese Art von Deskriptoren (Messung Bildamplitude bezüglich der Helligkeit und des Farbwertes) weniger sensitiv auf kleine Schäden sind und durch die verschiedenen Texturen der hochauflösten Bilder in Stadtgebieten beeinträchtigt werden. Für die Beschreibung des Äusseren der Gebäude (regulär oder irregulär) schlagen wir „Regularity indices“ vor. Zusätzlich werden drei Typen von Klassifikationsmethoden (k-NN, Bayesian und SVM) verwendet und verglichen. Durch unabhängige visuelle Interpretationstestsätze werden die verglichenen Klassifikationsergebnisse mittels entgegengesetzter (cross) Validierungsmethoden evaluiert. Der Klassifikation durch „Support Vector Machine (SVM)“ ist eine relativ neue Methode, welche recht erfolgreich Schäden detektiert. Die Integration von Objekten (Oberflächen) und bildbasierenden Merkmalen wird durch Klassifikatoren für Gebäude (nicht, teilweise oder komplett zerstört) realisiert. Die Kombination der „Regularity indices“ mit dem normalisierten Höhendifferenzdurchschnitt mittels OVO-SVM-Klassifikator zeigte, dass die Verwendung von mehrfachen Merkmalen hilfreich für die automatische Erkennung von zerstörten Gebäuden eingesetzt werden kann.

In Kapitel 7 wird das entwickelte System beschrieben, welches automatisch Daten vor und nach einem Erdbeben auswertet um eine Schadenskarte speditiv nach der Katastrophe zu erstellen. Es wird angenommen, dass keine Information über die Position der Gebäude verfügbar ist und das die Möglichkeit einer nahe Echtzeitschadenserfassung behandelt wurde und die Ergebnisse verglichen wurden. Um die Gebäude vor der Klassifikation identifizieren zu können wurde ein „image-understanding“ Algorithmus in das System integriert. Die Messunsicherheit wurde im System mittels „Bayesian Network“ integriert. Basierend auf Vorinformation der multiplen Bildsegmente liefert das Netzwerk punktbasierte Analysen. Für die Detektion und Bildsegmentation wurde eine mehrstufige Liniendetektion basierend auf der „Hierarchical Permissive Hough Transform

(HPHT)“ durchgeführt. Dieser Algorithmus detektiert eindeutige und nicht eindeutige Linien. Um beschädigte Punkte zu detektieren, wurde eine symmetrische Form des „Bayesian Network“ integriert, welches zwei Teile für die Detektion beinhaltet (vor und nach dem Erdbeben). Die Untersuchungen in Bam und Kobe zeigten, dass das erweiterte „Bayesian Network“ die Performance des Systems verbesserte und zu einem aussagekräftigen System etablierte. Die präsentierte Methode ermöglicht innerhalb der Gebäudepolygone zerstörte Punkte zu Detektieren und zu Klassifizieren. Dies ermöglicht uns detaillierte Informationen von zerstörten Gebäuden zu gewinnen. Die empirischen Ergebnisse zeigten, dass die vorgestellte Methode sehr viel versprechend ist.

CONTENTS

Abstract.....	iii
Zusammenfassung	v
1. INTRODUCTION	1
1.1. Motivation.....	1
1.2. Disaster Management.....	2
1.3. Remote Sensing Technology for Disaster Management.....	4
1.3.1. Before a Disaster	4
1.3.2. After a Disaster.....	5
1.4. Summary	5
2. METHODOLOGY OF DAMAGE ASSESSMENT USING REMOTE SENSING DATA.....	7
2.1. Sensors	7
2.2. Platforms and Resolution.....	9
2.3. Field of view and Monitoring	11
2.3. Summary	11
3. IMAGE-BASED LOCAL DAMAGE ASSESSMENT.....	13
3.1. System Framework	13
3.1.1. Input Data	14
3.1.2. Image Preparation.....	14
3.1.3. Interpretation	16
3.1.4. Assessment	16
3.2. Damage Scales.....	16
3.3. Visual Interpretation of Damage	19
3.4. Automatic Interpretation of Damage	22
3.4.1. Methodology.....	22
3.4.1.1 Review of Change Detection Methods	22
3.4.1.2 Review of Damage Detection Classification Methods	24
3.4.2. Automation and Uncertainty	25

3.5. Summary	27
4. EARTHQUAKE DATASETS	29
4.1. Kobe Earthquake.....	29
4.2. Bam Earthquake	30
4.3. Digital Surface Model (DSM) Generation	31
4.4. Visual Damage Interpretation	32
4.5. Criteria of Accuracy Assessment.....	32
4.6. Summary	33
5. HYPOTHESIS TEST FOR AUTOMATIC COLLAPSE DETECTION USING DSMS.....	37
5.1. DSM Error.....	37
5.2. Optimum Threshold Value.....	38
5.3. Hypothesis Test.....	39
5.4. Empirical Investigations	41
5.4.1. Automatic Collapse Detection using Pre- and Post-Event DSMs	41
5.4.2. Automatic Collapse Detection using Pre-Event 3D Models and Post-event DSM.....	42
5.5. Summary	44
6. DAMAGE CLASSIFICATION USING IMAGE FEATURES.....	47
6.1. Preprocessing	47
6.2. Features Generation	48
6.2.1. Statistical Descriptors	48
6.2.1.1. First-Order Statistics Features	48
6.2.1.2. Second-Order Statistics Features	49
6.2.2. Line Extraction and Analysis	50
6.2.2.1. Edge Detection - Canny Edge Detector	50
6.2.2.2. Line Detection - Standard Hough Transform (SHT)	51
6.2.2.3. Experimental Test	52
6.2.2.4. Line Detection - Hierarchical Permissive Hough Transform (HPHT)	53
6.2.3. Regularity Indices	56
6.3. Features Evaluation.....	57
6.3.1. Data Normalization.....	57
6.3.2. Class Separability Measure	57

6.4. Review of Classifiers	59
6.4.1. k-Nearest Neighborhood Classifier	60
6.4.2. Bayesian Classifier	61
6.4.3. Support Vector Machine (SVM) Classifier	63
6.5. Empirical Investigations	66
6.5.1. Automatic Collapse Detection using Post-event Imagery Data.....	66
6.5.2. Automatic Classification of Collapsed buildings using Pre- and Post-event Images and DSMs	69
6.6. Summary	73
7. AUTOMATIC RECOGNITION OF DAMAGED BUILDINGS USING MULTI-VIEW AERIAL IMAGES	77
7.1. Overview of Related Works for Automatic Buildings Extraction	77
7.2. Automatic Damage Classification.....	79
7.2.1. Overall View of Our Strategy.....	79
7.2.2. Problem Formulation and Approach	80
7.3. Image Segmentation.....	83
7.4. Features and Cues Extraction.....	85
7.4.1. Features Extracted from DSMs	86
7.4.2. Features Extracted from Images	88
7.4.2.1. Pixel Intensity and Color	88
7.4.2.2. Segment Shape.....	91
7.5. Reasoning System using Bayesian Network.....	92
7.5.1. Bayesian Network	92
7.5.2. Naïve Bayesian Network for Buildings Extraction	96
7.5.3. Augmented Bayesian Network for Buildings Extraction	99
7.5.4. Bayesian Network for Damage Assessment.....	103
7.6. Empirical Investigations	106
7.6.1. Experimental Results – Bam City (Gray-scaled Aerial Images)	106
7.6.2. Experimental Results – Kobe City (Colored Aerial Images)	106
7.7. Automatic Interpretation of Damaged Buildings	113

7.8. Summary	122
8. CONCLUSIONS AND OUTLOOK	125
8.1. Collapse Detection using DSMs Generated Automatically	125
8.2. Imagery Data and Related Features for Collapse Detection	126
8.3. Collapse Classification using Image and Object Space Features.....	126
8.4. Knowledge-Based Bayesian Framework for Damage Assessment	126
8.4.1. Pointwise Analysis Using Object-Based Features.....	127
8.4.2. Image Segmentation and Shape Index.....	127
8.4.3. Bayesian Reasoning For Multi-view Multi-modal System	127
8.4.4. EMS98 Damage and Collapse Classification by “if-then” Rules.....	128
8.5. Future Investigations and Improvements	128
Bibliography	131
Acknowledgments	145
Curriculum Vitae	147

INTRODUCTION

1.1. Motivation

Red Cross: 3M Haitians Affected by Quake GENEVA, Jan. 13, 2010

"I see a lot of people on the streets crying for help. I know there's a lot of people under the buildings collapsed. A lot of traffic, people crying, people bleeding. It's a disaster,"

Carel Pedrel, a radio show host in Haiti

(Source: CBS/AP 2010)

Natural hazards have always been associated with *disasters* and can be understood as unpredictable acts of nature, characterized by extremes in physical processes. Natural disasters are divided into geologic (earthquakes, tsunamis, volcanic eruptions...), atmospheric (tropical cyclones, tornadoes...) hydrologic (floods, droughts...) and biologic (epidemic diseases) categories (Smith 1996). Major disasters across the world are more and more reported because their impact in terms of human and economical losses is increasing. Geological disasters like earthquakes and tsunamis often leave a devastating impact on human life and cause a high degree of damage particularly in developing countries. In the first decade of the 21st century, a large number of devastating earthquakes attacked highly populated urban areas in the world, and a huge amount of human, structural, and socioeconomic losses were reported due to the earthquakes (Table 1-1). The 2003 Bam earthquake (death toll: 30'000), the 2004 Sumatra earthquake and the resulting tsunami (death toll: 230'000), the 2005 Kashmir earthquake (death toll: 80'000) and the 2008 Sichuan earthquake (death toll: 70'000) are recent devastating earthquakes. Although it may seem that we are having more earthquakes, earthquakes of magnitude 7.0 or greater have remained fairly constant. This increase is explained by the growing population and by its migration in areas that are prone to disasters like seacoasts. It is also pointed out that rapid expansion of urban areas in developing countries has made the areas more vulnerable to various natural disasters (Kreimer et al. 1992).

Table 1-1: Statistics of recent deadly earthquakes (Source: USGS)

	1980-1989	1990-1999	2000-2009
Earthquakes with 1000 or more death	11	14	9
Estimated death toll	58,880	114,646	465,357

Although natural disasters are inevitable and it is almost impossible to fully recoup the damage caused by the disaster, what the humans can change is the way they respond to disasters. The whole disaster management procedure requires urgent developments toward better, more elaborated and appropriate means for facing natural risks. This is already realized and accepted as a high priority

task by many organizations, governments and companies in all over the world. Their prediction and preparedness along with an effective disaster management program can minimize the effect of damage

Consistent and quantitative damage assessment tools for buildings and infrastructure in seismic active areas are urgently needed to ensure an efficient decision making process that facilitates the optimal allocation of available economical resources for the management of disasters. Thus, damage assessments before and after disasters have attracted significant attentions among researchers and practitioners of disaster management.

The work presented in this thesis was initiated as a part of the MERCI project (Management of Earthquake Risks using Condition Indicators). This interdisciplinary project (www.merci.ethz.ch) was intended for developing a generic decision theoretical framework for the consistent quantitative and rational management of earthquake risks in three situations, namely, before, during (shortly after) and after an earthquake. One of the critical activities during an earthquake is the “*search and rescue operation*” to provide specialized assistance after buildings or other structures collapse. In this thesis, we aim to develop the methods to generate a map of damaged buildings by using high-resolution air-borne images as automatically as possible.

1.2. Disaster Management

In general, “Disaster management” is the continuous process by which all individuals, groups, and communities manage hazards in an effort to avoid or reduce the impact of disasters resulting from the hazards. The nature of management depends on local economic and social conditions. However, effective disaster management relies on thorough integration of emergency plans at all levels of government and non-government involvement (Jiping et al. 2009, De Groot et al. 2010).

Disaster management is generally understood to consist of four phases: *mitigation*, *preparedness*, *response* and *recovery* (Figure 1-1). Mitigation takes place before or between events to reduce impacts. It includes zoning ordinance, building codes, structural improvements. It can involve actions such as developing, adopting, improving, and enforcing building codes and standards. Many researchers in the field of structural mechanics and earthquake engineering have dedicated extensive efforts to the reduction of earthquake induced human and property loss by improving design codes for buildings, bridges and other structures. The implementation of mitigation strategies can be considered a part of the recovery process if applied after a disaster occurs. Preparedness focuses on development of community training, preparation among rescue forces (e.g., police, ambulance, fire) and public awareness, logistical support and communications, basic supply needs, early warning, and monitoring. Activities should be designed to ensure that when a disaster strikes, appropriate personnel would be able to provide the best response possible. Another aspect of preparedness is casualty prediction, the study of how many deaths or injuries to expect for a given kind of event. This gives planners an idea of what resources need to be in place to respond to a particular kind of event. Response is the acute and time-critical phase occurring after the event. Response is defined as the actions taken to save lives and prevent further damage in a disaster or emergency situation. Response activities may include damage assessment, search and rescue, fire fighting, and sheltering victims. Recovery involves the actions taken to restore the affected area to its previous state and to return the community to normal following a disaster including: repairing, replacing, or rebuilding structures. The four disaster management phases illustrated here do not always, or even generally, occur in isolation or in this precise order. Often phases of the cycle overlap and the length of each phase greatly depends on the severity of the disaster.

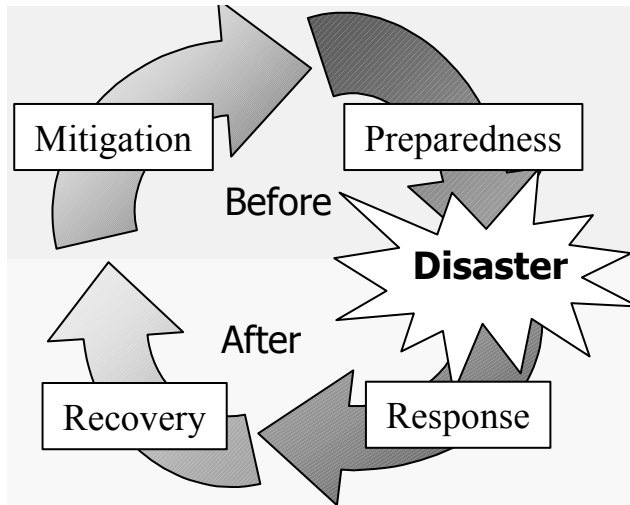


Figure 1-1: A graphic representation of the four phases in disaster management

Although all phases are interconnected and consequential, the response and recovery procedures are often viewed as the most critical in terms of saving lives. The quality of the relief efforts can be improved by an effective use of the available technical resources. Decisions in disaster management need to be based on a complete picture of a complex situation and have to be taken fast. Information systems for decision making need to combine uncertain information from multiple sources and present all relevant information in a clear and unambiguous way to decision makers in short time. For effective disaster management there is a need for a variety of geo-spatial information at different scales. Geo-information science, including geographic information systems (GIS), remote sensing (RS), and the Global Positioning System (GPS), can provide concrete support for disaster management activities in terms of efficiency, and speed up the data management, manipulation, analysis, output and lead to more informed decisions. The entire cycle of disaster management has greatly benefited from recent advancements in spatial information systems and related technology. The spatial data is very valuable for developing and implementing strategies for recovery and restoration of the affected areas (Murao et al. 2007). In this respect, obtaining real-time or near real-time information of seriously damaged areas immediately after a natural disaster is extremely useful for executing efficient search and rescue missions. The timely securing of spatial information can significantly assist the decision-making process, rescue lives and aid civilians. The spatial information may be obtained using either field survey or remote sensing technologies. Field inspection methods are very limited and basically too slow and static. Remote sensing and Geographic Information Systems (GIS) have had a significant impact, and are currently being used in a variety of ways during all phases of disaster management. Recent investigations give strong signals that disaster management users are interested to utilize three-dimensional dynamic analysis and visualization (Zlatanova 2008, Chengfeng et al. 2009, Purohit and Mantri 2009, Qiao and Zhang 2009, Tan and Fan 2009, Ajmar et al. 2010, Cygan and Patterson 2010).

In the following we give brief overview of remote sensing techniques related to disaster management procedures.

1.3. Remote Sensing Technology for Disaster Management

Earth remotely sensing has a long history but the modern connotation going back to the aircraft-mounted systems that were developed during the early part of the twentieth century. Remotely sensed data potentially provides valuable seismicity-related information in terms of both assessing the potential of risk and defining the state of vulnerability. The conclusions and recommendations of the different papers are generally consistent and strongly suggest that regional damage assessment using remotely sensed data is highly feasible (Altan and Kemper 2008, Kerle et al. 2008). The papers, however, acknowledge that more research is needed before these technologies can be used to make critical emergency response decisions. Remote sensing techniques either by air-borne or space-borne sensors were used in the last decades to detect, identify and monitor the impact and effects of natural disasters like earthquakes, landslides, tsunamis and floods. However, each disaster type in its spatio-temporal characteristics as well as its physical consequences requires an appropriate technical solution (Zhou 2009, Li et al. 2010, Nolte et al. 2010). Moreover, it has to be stressed that the basic knowledge of remote sensing is essential to decide on appropriate technology in an emergency situation. The suggestions on the use of appropriate satellite imagery were given by taking into account the spatial resolution, satellite's sensor type and action period, area to cover, and etc. (Kerle et al. 2008).

1.3.1. Before a Disaster

It is important to model the consequences of any large-scale disaster. An essential input into the model is a quantifiable representation of the built environment at risk. Three-dimensional data is produced by various sensors and some can be made available on-line or even in real-time. Standardization activities in developing models are essential for the entire life cycle of buildings (Kerle et al. 2008, Kolbe et al. 2008). In this regard, the overall aim of the research is to utilize advanced technologies to identify key physical characteristics of the built area for estimating potential earthquake damage. The model should convey information about the type, shape and other related information of the buildings. Exact inventories of the city are essential in order to realize economic, social and engineering consequences of the disaster. Therefore, the researchers are interested in the development of new techniques in quantifying inventory, relying on photogrammetry and remote sensing, Geographic Information Systems (GIS) and other advanced technologies (Altan et al. 2001, Sarabandi et al. 2005, Chung et al. 2006, Jiugang et al. 2009, Nolte et al. 2010). Buildings location, density and their configuration in footprint, height and size, age, structure type and occupancy deal with direct or indirect responses of structures to seismic stresses. These parameters serve as fundamental inputs in earthquake-related loss estimation models. They will be used to define inventory at risk, social and economic loss modeling, recovery and mitigation analysis (French & Muthukumar 2006). A pervasive problem for urban areas around the world is the lack of well-documented databases of their structures. Photogrammetric and remote sensing technology (aerial and satellite photography and airborne laser scans) can be used in order to define the building configuration footprint and the building height. The building height will then be turned (approximately) into the number of storeys of the structure. Building height information will also be used with other initial variables in knowledge-based systems in order to create and assign structure-type information for every building record in the database. High-resolution aerial images in combination with advanced image interpretation techniques have the potential to provide this data automatically.

1.3.2. After a Disaster

It is important to estimate and grasp damage situations during the early stage of response activity without depending on information sent from the interiors of the damaged area. Recent natural disasters have stressed the importance of a rapid and reliable damage assessment and loss estimate in order to support both short- and long-term emergency response. One important aspect, which helps determine the total number of fatalities after an earthquake, is the performance of search and rescue in the first few days. It has been demonstrated that the amount of earthquake damage is only partly due to the strength of the natural event; it also depends on the delay and inadequacy of the rescue and reconstruction intervention. Therefore, the development of early warning systems with an adequate array of monitoring instruments for the purpose of collecting necessary data and information for disaster evaluation is an essential aspect. An effective disaster response planning covers three activities which can be supported by remote sensing technology: 1) development of a practical model for damage simulation, 2) assessment of damaged structures rapidly after disaster, and 3) Deployment of limited rescue resources in an optimal way (Markus et al. 2000). Remote sensing techniques both by space-borne and air-borne sensors could make a very effective contribution especially to the first and second activities. In the next chapter, the methodology of damage assessment using remote sensing data is inspected.

1.4. Summary

Remote sensing techniques both by space-borne and air-borne sensors could make a very effective contribution especially in response and recovery phases of disaster management. A fast ascertainment of the affected buildings and people is helpful for the disaster management in order to allocate the limited search and rescue resources (personnel and equipment) for each individual collapsed building. The possibility of a near real-time damage assessment could help the rescue operations. Furthermore, the spatial distribution of damages being very important for the emergency teams deployed immediately after the catastrophe. Our research mainly focuses on rapid damage assessment methods using remotely sensed imagery data.

2

METHODOLOGY OF DAMAGE ASSESSMENT USING REMOTE SENSING DATA

Several kinds of remotely sensed data on damages may be available, such as aerial photography and digital imagery, satellite imagery, airborne laser scanning and synthetic aperture radar observations. In order to identify earthquake hazards it is necessary to have the expertise to recognize them and then obtaining the appropriate remote sensing data to respond them effectively. However, The analysis has shown that remotely sensed data without integration with reference data are not enough by themselves to fulfill the information requirements of the user. Auxiliary data showing the pre-disaster situation, such as population, road network, land use, ownership information, are crucial for an optimal use of the potential of remotely sensed data. Moreover, for an effective use and flow of information derived from remote sensing technology, there is a need for organizational improvements. Therefore the use of remote sensing as well as GIS has become essential in urban disaster management. For an effective cooperation, a personnel in the field asks for information that may be displayed by mobile devices and can add and communicate their observations and data (Brinkhoff 2008, Savorskiy & Tishchenkov 2008). Remote sensing provides an entire suite of “Platforms” and “Sensors” that allow relevant data in desired “Resolution” to be collected for “Monitoring” with different “Views” (Figure 2-1).

2.1. Sensors

Photogrammetric and remote sensing technologies include all forms of air- and space-borne platforms with sensors that *passively* or *actively* measure the earth’s surface. Passive systems include optical and infrared sensors that receive information from the earth’s surface. The variability of optical sensors is impressive. Optical sensors are widely used in damage observation and assessment. Optical images are easy to interpret as they depict the ground surface as it appears to the human eye. However, passive optical sensors especially are limited to daylight conditions and require cloud and smoke free situations. Traditional photographs used analogue camera, which are in a transition towards fully digital systems (Gua et al. 2009). Since digital cameras require less exposure light and can be processed and distributed directly, following a disaster are thus advantageous. Using video imagery we are able to capture dynamic events, but there are also some challenges to overcome. The cameras deployed are usually not calibrated and have much lower resolution, resulting either in very limited field of view or low detail (Kerle et. al. 2008). However, the images acquired by unmanned air vehicles (UAVs) equipped to GPS/INS systems can be captured with orientation data in high-resolution format and be transmitted in real-time to the ground control station (Eisenbeiss 2009).

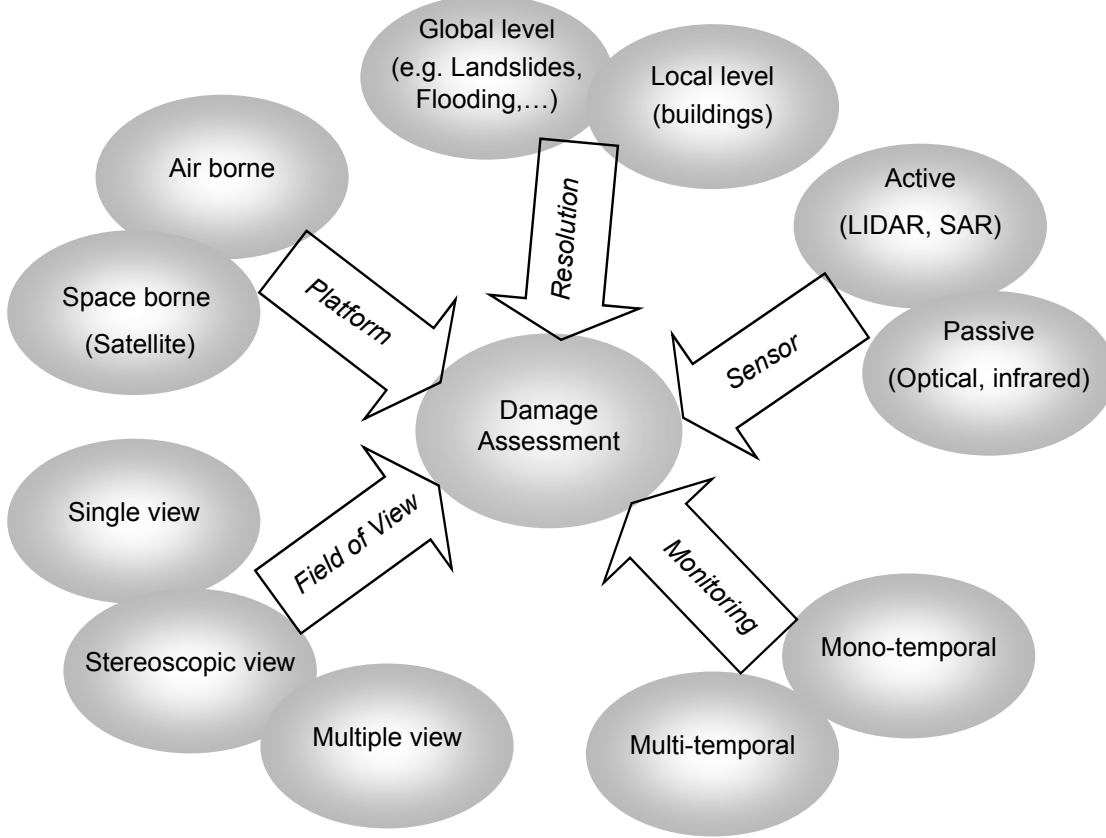


Figure 2-1: Remote sensing methodology for damage assessment

Active systems transmit signals to the earth from their respective platforms and receive the reflections from the object, like LIDAR and SAR. LIDAR, is an acronym for LIght Detection and Ranging, using a laser to measure distance from the sensor to points. It is also known as airborne laser scanning (ALS). ALS technology integrates several advanced technological units, including airborne laser, inertial measurement technology and global positioning systems (GPS). The range to an object is determined by measuring the time delay between transmission of a pulse and detection of the reflected signal. ALS usually does not yield photographic images, it delivers directly a so-called point clouds. ALS technology offers a great potential in extracting advanced urban building inventory information, such as building footprint, elevation and compactness. This technology bundled with advanced visualization software could be an essential ingredient for any major development project to generate high-precision digital topography for slope analysis in landslide risk mapping or for flood risk mapping. Laser scanning has proved to be a very effective tool for height determination and has very quickly become an operational tool in the context of emergency relief (Steinle & Bähr 1999, Vu et al. 2004a, Vögtle & Steinle, 2004, Li et al. 2008, Rehor et al. 2008). Generally, in LIDAR short wavelengths of the electromagnetic spectrum are used, typically in the ultraviolet, visible, or near infrared. Thus LIDAR is highly sensitive to aerosols and cloud particles and data acquisition during rain or fog through clouds is not possible.

Synthetic Aperture Radar (SAR) refers to the technique used to simulate a long antenna by combining signals (echoes) received by the sensor as it moves along a flight track. SAR systems have the capability of recording both the amplitude (intensity) and phase of backscattered echoes from objects on the earth's surface. The capability of SAR imagery has been demonstrated for

damage detection in large-scale natural disasters (Sharma et al. 2008, Singh et al. 2008). The great advantage of SAR is that it can be used irrespective of sunlight and weather conditions (Matsuoka & Yamazaki 2004). The analysis of the parameters of the models representing backscattered intensity or coherence values may be used to discriminate between damaged and undamaged areas and, to some extent, to evaluate the damage (Mansouri et al. 2005). The main problems are the unusual spectral signatures of microwave sensors, which are very different from the human visual system and as such not easy to interpret and the still very limited spatial resolution of SAR sensors. This is the reason why the use of SAR data is unlikely in a first step, although this may happen to be the only available data in case of poor weather conditions. A first damage mapping of limited accuracy in earthquake-stricken areas can be obtained using multi-temporal SAR data but it should be assisted by auxiliary information defining urban blocks (Trianni et al. 2008, Hosokawa et al. 2008).

2.2. Platforms and Resolution

The remotely sensed images can be acquired from various platforms with different temporal and spatial resolutions as illustrated in Figure 2-2.

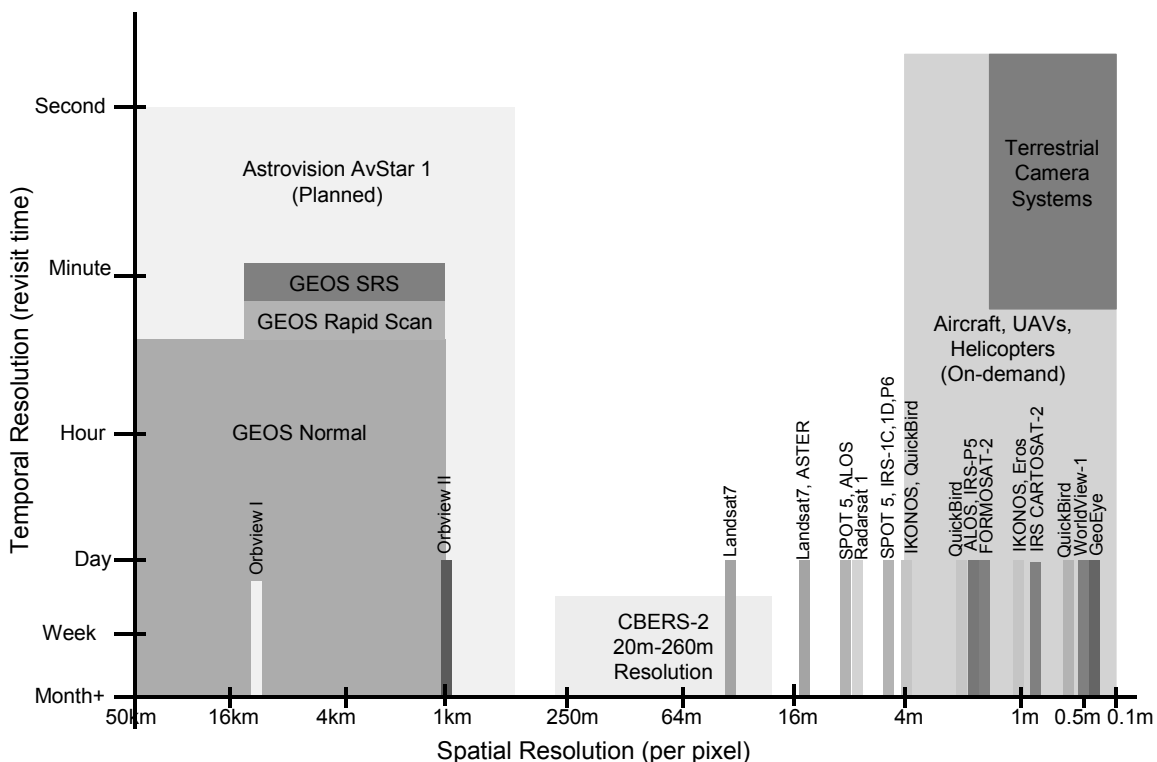


Figure 2-2: Various types of remotely sensed platforms and their spatial and temporal resolution, (adapted and redrawn from Rejaie and Shinozuka 2004)

Many types of information required for disaster management have a spatial component as well as temporal component. Spatial, temporal, spectral and radiometric resolution are properties of remote sensing instruments. Spatial resolution refers to sensor's ability to effectively image a

portion of the object surface in a single pixel and is typically expressed in terms of Ground Sample Distance, or GSD. GSD is a term containing the overall optical and systemic noise sources and is useful for comparing how well one sensor can "see" an object on the ground within a single pixel. Typically pixels may correspond to square areas ranging in side length from 0.1 to 1,000 meters. The temporal resolution specifies the revisiting frequency of a sensor for a specific location. For damage assessment, one important property of the remote sensing systems is the temporal resolution of the system that is the time elapse between successive dates of imagery acquisition for a given catastrophic area. The needed time is a function of the number of appropriate systems, the location of the disaster and financial considerations. A sensor's spectral resolution specifies the number of spectral bands in which the sensor can collect reflected radiance. This is related to the number of frequency bands recorded by the platform and the position of bands in the electromagnetic spectrum is important. Radiometric resolution or radiometric sensitivity refers to the number of digital levels used to express the data collected by the sensor. It is commonly represented by the number of required bits. Typically, this ranges from 8 to 14 bits, corresponding to 256 levels of the gray scale and up to 16,384 intensities of color, in each band. Practically, the level of accuracy in damage detection is limited by the resolution of the input images.

Image analysis studies, which were carried out using optical satellite images of lower spatial resolution, are limited to producing globally area-based damage assessment. Medium resolution imagery can be useful in strategic decision-making and can guide airborne data acquisition at the local level. At the national level, there is a need for global information about the damage and at the local level detailed information becomes most important for the user. To detect large-scale disasters such as landslides a resolution of about ten meters may be adequate (Richards, 1982). However, for more localized events, especially in urban areas, sub-meter detail may be necessary. The basis for these approaches is a multi-tiered procedure that allows broad regional damage assessments to be conducted using moderate-resolution data (SPOT, ALOS/PRISM, Cartosat-1, etc) (Adams et al. 2002, Turker and San 2003, Kohiyama and Yamazaki 2005, Jaya and Abe 2006, Danneels et al. 2007, Liu and Yamazaki 2008) and more detailed assessments using high-resolution information (QuickBird, IKONOS, aerial images) (Kouchi et al. 2004, Gusella et al. 2005, Sumer and Turker 2006, Chesnel et al. 2007, Suzuki and Yamazaki 2008).

Platforms for remote sensors may be situated on the ground, on an aircraft, helicopter, balloon (or some other platform within the Earth's atmosphere), or on a spacecraft or satellite outside of the Earth's atmosphere (Kerel et al. 2008). One of the key factors for the selection of a platform is the altitude that determines the ground resolution and which is also dependent on the instantaneous field of view of the sensor on board the platform. Airplanes have been the dominant platform in aerial remote sensing. Satellites are continuously in orbit, and their data collection either has to be simply activated or reprogrammed. If we want to get images over a large area, satellite imagery may be the most suitable tool, but the limitations of satellite images should be considered: 1- most satellite sensors have a limited resolution, 2- satellites cannot gather image data in several locations simultaneously, 3- satellites appear at a particular location on earth always at the same time of the day, and 4- optical satellite sensors have weather-related restrictions. On the contrary, aerial imagery can be obtained in a much more controlled fashion, both in terms of time and flight planning (data acquisition pattern) and with much higher geometric, spectral and radiometric resolution. In addition, with digital images we do have superior sharpness as well as real-time and on-line processing capabilities. However, manned vehicles are typically large and expensive. In addition, hazardous environments and operator fatigue can potentially threaten the life of the pilot. Therefore, there is a critical need for automating aerial monitoring using unmanned air vehicles (UAVs). UAV provides a platform for disaster area monitoring. It can be deployed to disaster areas quickly, or flown there from a distant location at a low altitude and at flight profiles close to the

objects where manned systems cannot be flown. UAVs have the advantage that they are more easily re-tasked, reconfigured, and upgraded to take advantage of different payloads or new sensor technology (Bendea et al. 2008, Eisenbeiss 2009).

2.3. Field of view and Monitoring

Without a depth perception, high spatial resolution images may not help to detect pancake collapse with intact roofs (please refer to section 3.2 and Figure 3.6). Some sensors, such as laser scanners, collect height information by design, while others, such as overlapping (i.e. stereo) aerial photographs or video frames allow extraction of 3D information using photogrammetric techniques. Stereoscopic images can be used to extract building height information. Stereoscopic aerial images are more suitable to obtain a very detailed inventory and to collect damage data of built environment. Damage in occluded faces of structures cannot be detected. In order to get around this difficulty, multiple images from different viewpoints are required. Within this realm, studies are based on either mono-temporal (only post-event images are available) or multi-temporal analysis (both pre- and post-event images are available). The mono temporal procedure mainly applies to the visual recognition of the damaged elements, and it is directly related to the image resolution. The image itself can give an immediate overview and may be the foundation for a qualitative survey or monitoring of consequential events. Although one may tag or pinpoint the image, an orthophoto, which is the orthographic view of an image, will be linked to digital maps or other geographic data. For a multi temporal analysis, the homogeneity (being comparable in terms of images resolution and angle of views) of the two images before and after the event is a basic condition for the treatments, independently of the approach. Moreover, the difficulties are amplified by a large temporal gap. A large temporal gap between images can lead to the impossibility of damage detection for the new buildings appeared in the after event scene. Pre- and post event 3D information allow valuable change detection, such as identification of collapsed buildings. This concept can be considerably assisted by an automated system, using digital photogrammetry and computer vision techniques. However, the image information is very complex and it is for instance difficult to extract the change of shapes of roads and buildings fully automatically.

2.4. Summary

In brief, data collected from the sensors - passively or actively - can be analyzed for change over time and provide dynamic descriptions of environmental characteristics. Since remote sensing data observed by various platforms have different parameters, it is necessary to consider the characteristics of each platform and sensor and the quality of the data. Basically, the platform and sensors should be selected considering the area to cover, urgency, resolution of images, and weather and time conditions. Some sensors are restricted in their operation by environmental factors and especially weather conditions (clouds, rain, etc.) may often obstruct the use of their information. In comparison with the active sensors, passive optical sensors and photogrammetric camera in particular, provide an easier, less complex and more reliable operation, and are cheaper. In this dissertation we have focused on multi-temporal high-resolution optical images for local (buildings) damage assessment. Next chapters commence with an outline of the system framework and goes on to present image-based systems for classifying damaged buildings due to earthquake, together with accuracy assessments.

3

IMAGE-BASED LOCAL DAMAGE ASSESSMENT

3.1. System Framework

Urban areas are most vulnerable with their concentration of buildings, infrastructure and population. Serious casualties and injuries are usually related to extreme damage experienced by a minority of buildings. Hence, after an earthquake, demolished structures have to be recorded in order to give a map of buildings damage and property losses. For quick mobilization of response and relief communities, data need to be captured and analysis result made available rapidly in the first 3 days after the earthquake, as people, injured or exposed by the disaster, usually normally survive between 4 and 7 days (Fiedrich et al. 2000) (One of the most curious events happened in Bam earthquake was that of a 97-year-old who was trapped in her home for eight days until she was rescued unhurt). Though less accurate, the image-based interpretation methods are very much less time-consuming than conventional field surveys. In this chapter, we present a framework of an image-based system for building damage assessment applying methods and tools to facilitate the estimation of damages using air/space borne images. The general architecture of the proposed image-based system is illustrated in Figure 3-1.

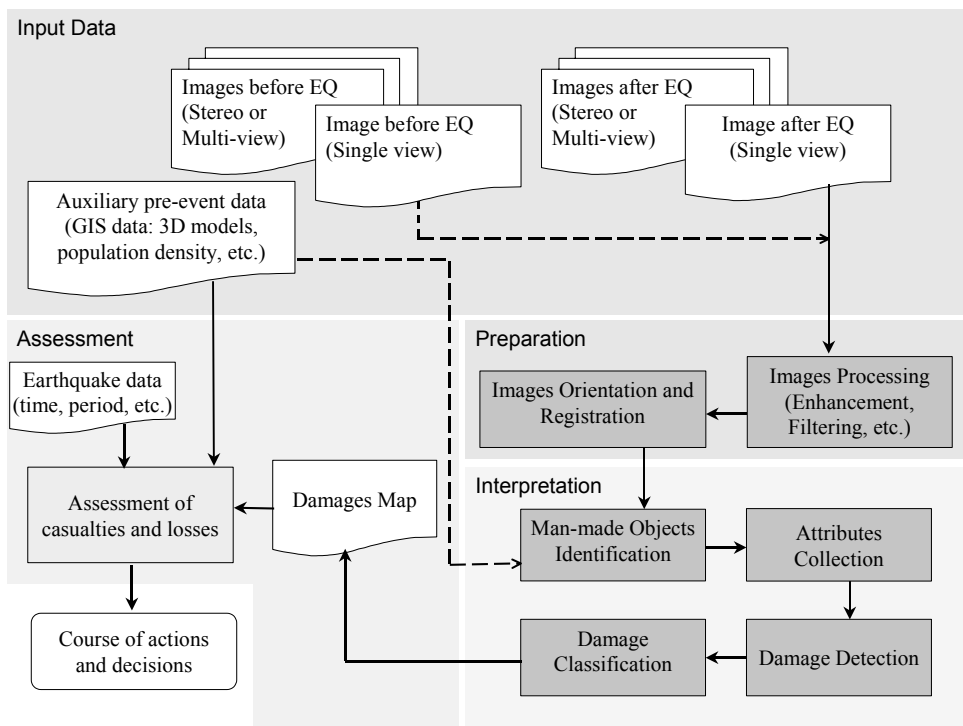


Figure 3-1: A flowchart for image-based damage assessment system

3.1.1. Input Data

Using imagery data, it is necessary that object of interest (i.e. building) be represented by groups of pixels as far as a human operator should be able to distinguish building textures. Roughly speaking, it can be satisfied by using images with pixel size less than one meter. The one-meter resolution enables the detection of damaged buildings one by one, the building size being considerably greater than the pixel size. With a medium resolution, (around 10 meters), only large zones completely destroyed can be observed. Although such a system has to work with a variety of input data, the performance of the image interpretation depends on the quality of the image and the quantity of information being carried out by them. After an earthquake, either due to constraints only monocular photos may be available or in a supplementary situation pre- and post-event imagery and GIS data may be obtained. A single view of high-resolution chromatic image can be utilized to identify heavy damages in the course of visual interpretation. However, using single view image not only confines depth perception but also limits the output data to the sketches and outlines without precise positions. One can also merge images taken from different viewpoints to create a true orthophoto to achieve a more accurate result taking into account occlusions. However, a prerequisite for the accurate extraction of orthophoto is the availability of a digital surface model. In this study, we have focused on multi-temporal approaches using pre- and post event imagery data. Furthermore, auxiliary pre-event information such as 3D buildings model accelerate damage assessment procedure. Obviously, integration different information layers can gain further knowledge particularly in assessment of casualties and losses.

3.1.2. Image Preparation

In the preparation phase, input data need to be processed before interpretation. Digital image processing modules have to be obtained to reduce radiometric problems caused by the variations in the sensor view angle, the sun angle and shadowing. Image noise is an unavoidable problem in digital images while both manually and automatically image interpretations are sensitive to image noise. Therefore, the images have to be pre-processed in order to reduce the image noise. Nowadays, many of the sensors have the ability to provide more than 8-bit/pixel high contrast digital images. Using of these images results in a major improvement for features detection especially for dark shadow area.

To compare images in multi-temporal approaches, it is necessary to form a pixel-by-pixel comparison of the same object field obtained from images at different times. Pointwise comparison between pre- and post-event scenes obtains more confidence in the result of image interpretation and damage detection (Figure 3-2).

To form this comparison, it is necessary to spatially register the images, and thereby to correct for relative translation shifts, rotational differences, scale differences and even perspective view differences. All remote sensing imageries are inherently subject to geometric distortions. These variations may be as a result of several reasons including: the perspective of the sensor optics, the motion of the scanning system, the platform altitude and velocity, the motion of the platform, the terrain relief and the curvature and rotation of the earth. Many of these distortions are systematic or predictable in nature and can be represented by accurate modeling of the sensor.

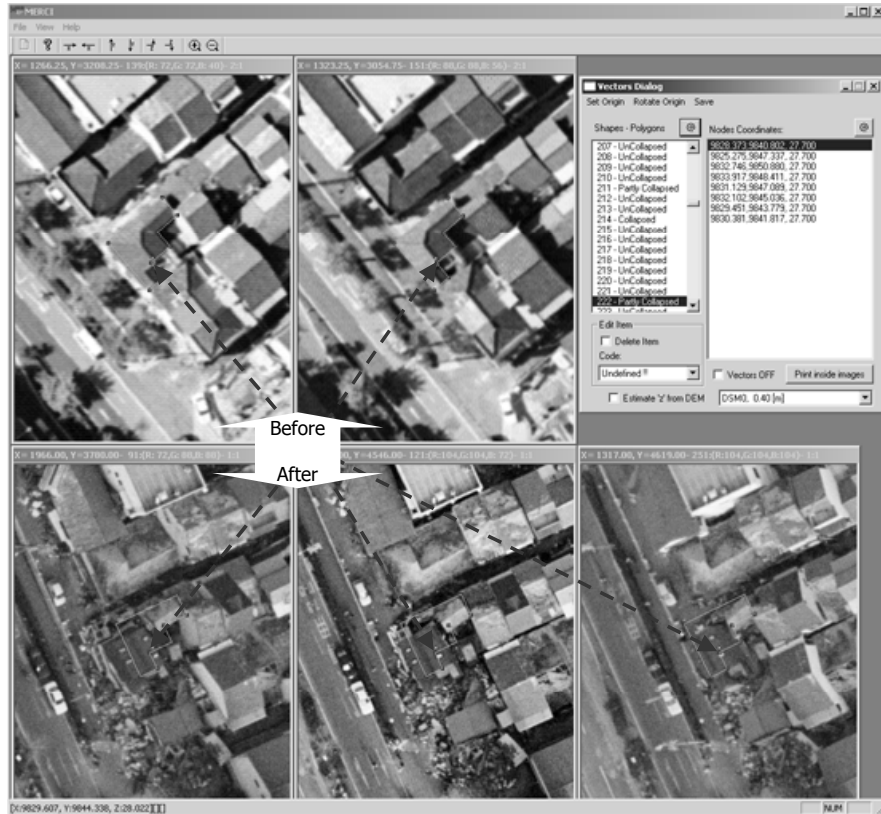


Figure 3-2: User interface of the developed image-based damage assessment system – Pointwise comparison of images (two images before and three images after earthquake) using geo-referenced aerial photos of Kobe city

The geometric registration process involves identifying 3D coordinates and the determination of three-dimensional coordinates from images requires the image orientation to be known. Therefore, geometric registration of the imagery to a known ground coordinate system must be performed. In recent years, a large amount of research has been devoted to sensor modeling and image orientation. The interior, relative and absolute (exterior) orientations are the fundamental orientation procedures in analog and digital photogrammetry. The interior orientation is required for the reconstruction of the bundle of rays. The location of the projection center has to be known in relation to the image points together with the geometric influence of the lens system. The exterior orientation describes the location and orientation of the bundle of rays in the object coordinate system generally with the parameters of projection center coordinates and the rotations around the axis. In aerial photogrammetry this task has been exclusively and very successfully solved using aerial triangulation for many decades. In conventional methods, corresponding image points have to be identified manually or automatically and to establish the relation between image and object space, one also needs to some ground control points. After a disaster, the access roads are restricted and it is important to estimate and grasp damage situations without depending on information sent from the interiors of the stricken area. We need to rapid data collection and short processing times to generate map products. Today the time consuming ground survey of control points can be reduced by block adjustment or even more by combined block adjustment with projection center coordinates from relative kinematic GPS-positioning. It is also possible to avoid control points like the measurement of image coordinates of tie points by direct sensor orientation with a combination of

GPS and an inertial measurement unit (IMU). Digital sensors and direct geo-referencing technologies have been proven to be an effective method in eliminating the need of aerial triangulation by directly measuring the exterior orientation parameters of each image. A direct geo-referencing system provides the ability to directly relate the data collected by a remote sensing device to the ground, by accurately measuring the geographic position and orientation of the device without the use of traditional ground based control points (Ip et al. 2008). However, even with available GPS/IMU data, it is advisable to perform an aerial triangulation and on-line triangulation techniques allow generating precise orientation data in a very fast mode. Today, autonomous software modules for interior and relative orientation are commercially available in digital photogrammetric workstations (DPWS), and so is automatic aerial triangulation. The absolute orientation has been successfully automated for a number of applications.

3.1.3. Interpretation

Interpretation and analysis of remote sensing imagery involves the identification and/or measurement of various targets in an image in order to extract damaged objects. This task can be performed full manual by a human interpreter or may be assisted by image processing techniques. In the optical imagery, damages are associated with major changes in the structure or in the contours of a given element. However, it is necessary to define specific criteria to define how a ‘change’ is translated to ‘damage’. In this study, our main goal is to find solutions in order to automate interpretation tasks entirely or partially.

3.1.4. Assessment

Estimation of human casualties is one of the most important issues in earthquake damage assessment. There are several methods to estimate casualties due to earthquake. The primary cause of deaths especially in developed country is still collapsed buildings (Yamazaki et al. 1996). In Kobe earthquake, over five thousand people were killed mostly due to the collapsed wooden houses. However, other parameters such as associated fire, time of the day, and period of the event, should be considered as modification factors. In estimation of directly earthquake-related casualties, the population density of an area to assess must be identified using GIS.

3.2. Damage Scales

A basic prerequisite for the interpretation is the development of the *damage scales*. One method for expressing the distribution of damage is a damage probability matrix. The spectrum of damage from none to total, is divided into damage states, each of which is described both by words and by a range of damage ratios. This may differ from country to country. Damages at buildings are generally described based on structural and non-structural damages. According to the performed studies, damage identification via space/airborne images is restricted to some structural type of visible damages, categories like: totally or partially collapsed (severely damaged), tilted and overturned building, displacement of building appendices, split in the middle of high-rise building and debris (Ogawa and Yamazaki 2000, Saito and Spence 2004, Yano et al. 2004). A standardized scale is needed in order to ensure consistent interpretation of remotely sensed images and data. Visual inspection of building damage could be conducted based on the classification of the European Macroseismic Scale 1998 (EMS98), shown in Table 3-1. Kouchi et al. (2004) and Yamazaki et al. (2005) utilized high-resolution satellite images (IKONOS, QuickBird) for damage interpretation based on EMS98. The performed studies show that this seems to give a reasonable accuracy for grade 4 and 5. Some amounts of omission and commission errors are observed

especially in grades 3 and 2. Principally, for actual classification based on EMS98, knowledge about buildings inventories as well as site inspection are required.

Table 3-1: Classification of damage (EMS98) and criteria for photo-interpretation

Damage Grade	Description	Summary	Criteria of photo interpretation
Grade 1	Uncollapsed	No significant damage	No structural damage, slight non-structural damage
Grade 2		Moderate damage	Slight structural damage, Moderate non-structural damage
Grade 3		Substantial damage	Moderate structural damage, Heavy non-structural damage
Grade 4	Collapsed	Partially collapsed	Heavy structural damage, very heavy non-structural damage
Grade 5		Totally collapsed	Very heavy structural damage

Different structural damage types require different search and rescue resources. At a minimum, the damage scale must distinguish between “collapsed” and “uncollapsed” structures. The principal cause of death in the most large-scale earthquake disasters is the collapse of buildings. Hence, one of the main deciding factors is the knowledge about the extent and the characteristic of a totally or partially collapsed building. People are often trapped in collapsed buildings and the survivors in collapsed buildings could often be rescued by fast and efficient measures. For trapped persons the probability of surviving decreases in time and depends on different factors. This probability has been recorded for several earthquakes with different types of collapsed buildings by Coburn et al. 1991 (Figure 3-3). For debris heap, the probability of surviving decreases in time rapidly in compare to pancake collapsed building. Therefore in urban areas, the number and type of collapsed buildings should be known quickly. In addition, the required rescue team and equipment for each collapsed building depends mainly on the construction and the damage type of the building, the building size, the degree of the collapse and the number of casualties.

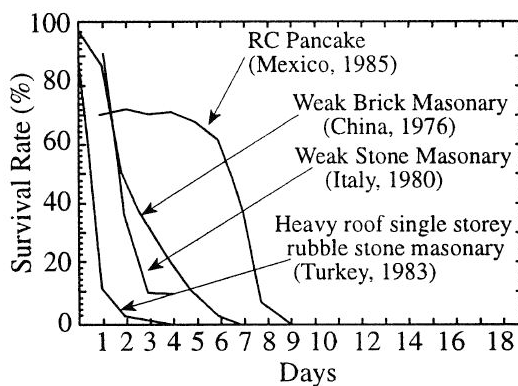


Figure 3-3: Empirical survival rate for collapsed buildings presented by Coburn et al. 1991

Thus a classification system of collapsed buildings is necessary to coordinate the operations and to allocate the limited search and rescue resources of the disaster area in an optimal way. Schweier and Markus (2004) developed the concept of the “damage catalogue”, which contains the characterization of real damaged buildings by defined geometrical features. The damage catalogue was set up using various after-action and damage reports as well as photographs of damaged buildings, which were collected and analyzed for this purpose. The result is a catalogue with different damage types and the geometrical features that characterize them (Figure 3-4). They presented five groups of damage types: “Inclined layers”(I) including (1) inclined planes (2) multi layer collapse (3) outspread multi layer collapse, “Pancake collapse”(P) including (4) pancake collapse – one storey (5) pancake collapse – all/several storeys, “Heap of debris”(H) including (6) heap of debris on uncollapsed storeys (7) heap of debris / with plates / with vertical elements, “Overturned”(O) including (8) overturn collapse-separated (9) overturn collapse –inclination, and (10) “Overhanging elements”. Due to many years of experience with these damage patterns, the position of trapped victims, their survival chances and the related rescue works can be inferred. The damage type “overhanging elements” is rarely observed after earthquakes and cannot be easily detected from vertical images. It is included in the damage catalogue for the sake of completeness. These damage types can be classified as partially or totally collapsed based on number of the collapsed storeys as well as rate of volume reduction (Schweier and Markus 2004). Overturned-inclined buildings can be used as indicators for soil liquefaction (Buchheister and Rezaeian 2008).

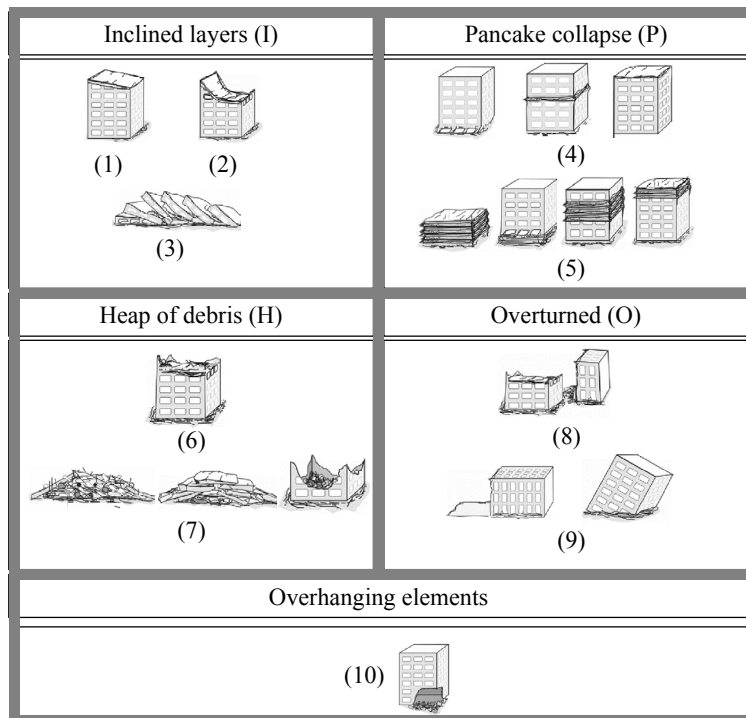


Figure 3-4: Types of collapsed buildings proposed by Schweier and Markus (2004). (1) Inclined planes (2) multi layer collapse (3) outspread multi layer collapse (4) pancake collapse – one storey (5) pancake collapse – all/several storeys (6) heap of debris on uncollapsed storeys (7) heap of debris / with plates / with vertical elements (8) overturn collapse-separated (9) overturn collapse –inclination (10) Overhanging elements

3.3. Visual Interpretation of Damage

Visual (manual) interpretation and analysis dates back to early beginning of aerial and remote sensing imaging. Photo-interpretation analysis can be a reliable technique for earthquake damage assessment, depending on the objectives and the image resolution. When a human operator performs images interpretation, the proficiency and expertise of working with air/space-borne photos raise the reliability and veracity of generated damage map. Manual interpretation is a subjective process, meaning that the results will vary with different interpreters (Ogawa and Yamazaki 2000). Using only visual information can serve as a first approximation of damaged buildings footprint area. Because of the differences between undamaged buildings and damaged ones in texture, figuration, grayscale and shadow, etc. one can find damaged buildings by manual interpretation relying on the differences and own experiences. However, the extraction of all desired information by visual interpretation is limited and depends on the specifications of the images as well as on the objects of interest. Furthermore, there may be non-visible parts due to shadows or occlusions, fire, smoke or bad weather. Also, visibility of details relies on image resolution as well as view direction. Stereoscopic viewing is an efficient tool in monitoring of spatial objects with respect to location, form and shape. Its main advantage lies in fact that the interpretation and measurement are done in three-dimensional virtual space so that many of detailed acquisition of deformation can be done afterwards. In addition, using both pre and post-event stereo images expedite the process of change detection and damage classifications (Figure 3-5).



**Figure 3-5: Stereoscopic view of Kobe city (a) before and (b) after earthquake (anaglyph images)
(c) 3D model of buildings of same area before earthquake**

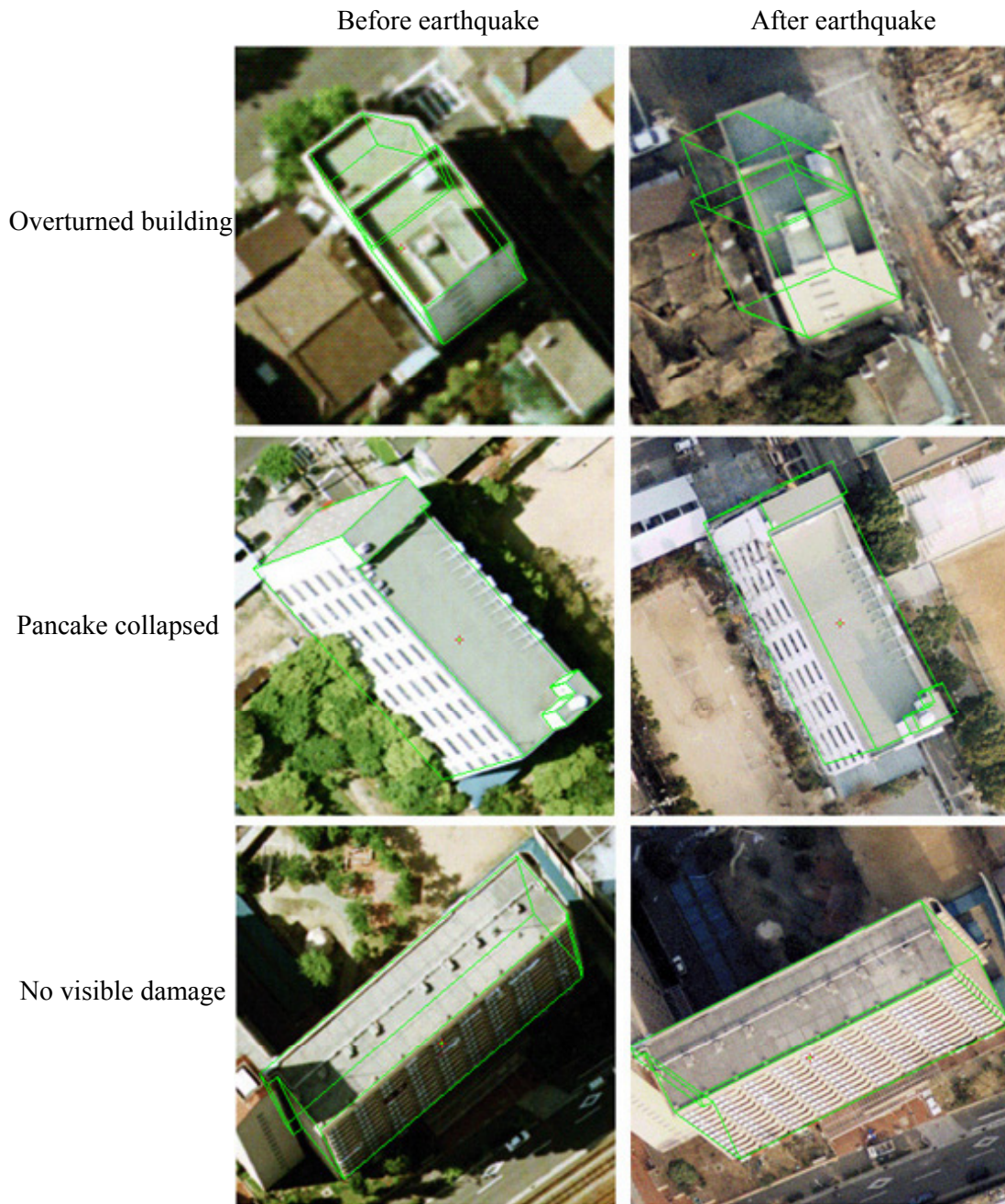


Figure 3-6: Visual interpretation with the aid of superimposed wire-frame models

Superimposed 3D model of buildings on post-event images can help to rapidly discover building displacements. An important difference in the texture or in the contour of a building before and after the earthquake is interpreted like a direct consequence of the structural damage (Figure 3-6).

To discover the damage types (damage classification) in the course of the damage interpretation, geometrical attributes that are detectable when comparing the pre- and post-event data, have to be defined. For this purpose, three-dimensional measurements must be done and

related geometrical features can be determined by means of stereoscopic photographs as well as airborne laser scanning. The following geometrical attributes can be employed to evaluate damage extent and damage classification:

- Initial height and area of buildings
- Average height/volume reduction
- Volume of debris heap
- Dimension of broken plates
- Size of the rubbles and broken parts that surround the building
- Tilt and plane inclination
- The region outside the building footprint covered by debris

In aerial photogrammetry, the accuracy of planimetry measurement is directly proportional to the image scale. The accuracy of photogrammetric measurement will also depend on points up on which measurements are being made. For targeted and very well defined points, an approximate estimation of the planimetry accuracy would be about one-third of the terrain pixel size and the altimetry accuracy would be 2 to 3 times worse than that. We can measure up to 5-10 cm point accuracy but this has to be considered as a limit value. Nevertheless, we are able to measure the building frame and its significant displacements (Figure 3-7).

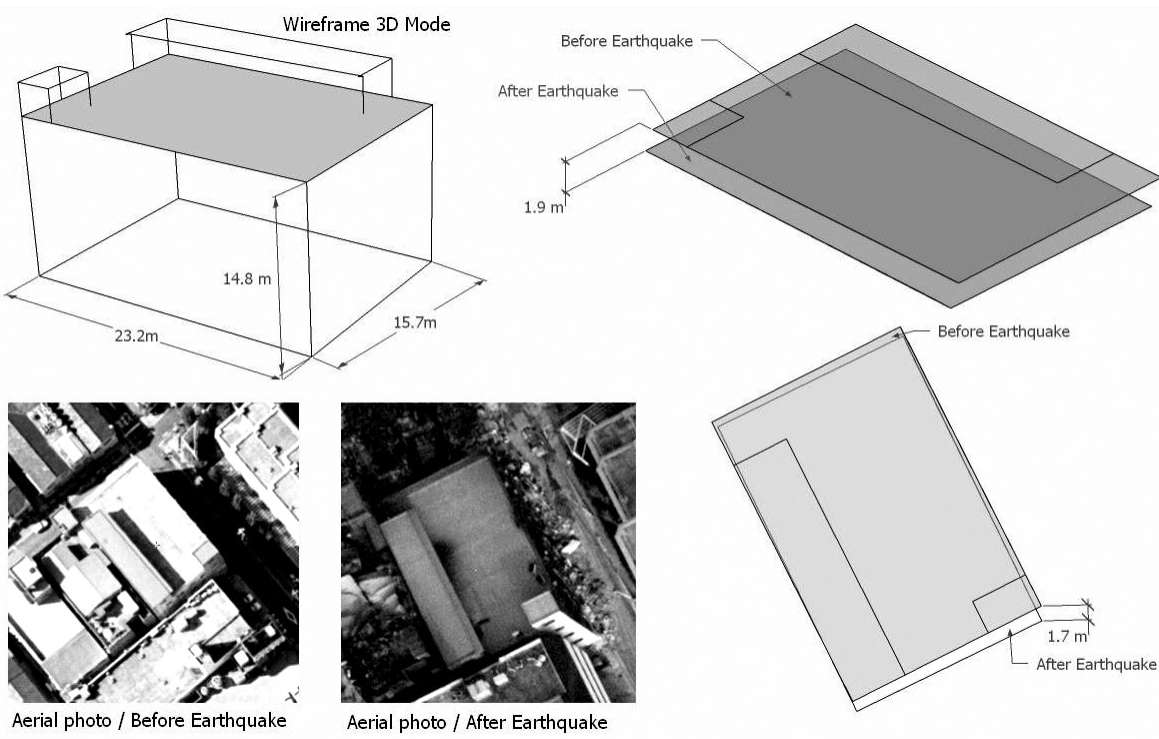


Figure 3-7: Displacement measurements using photogrammetric measurements (Building 'A' in Figure 3-5)

3.4. Automatic Interpretation of Damage

3.4.1. Methodology

For the human eye is very simple to recognize similar objects in two images (or even one image) and to detect change, and also to define what a building is and what not. Although visual interpretation is a powerful tool and has a high degree of reliability but it is a subjective and time-consuming process, which is of critical importance in the time of emergency. Automation could be a way for eliminating the time-consuming procedures, which are usually carried out by human operators. A possible definition for the amount of automation is the type of knowledge that is required for the software to run. Here the “knowledge” is the encoded information injected into the software, which lowers the amount of user interaction. Heuel (2004) distinguishes between four degrees of automation: “1) fully automatic: no interaction needs to be done; 2) automatic: simple yes/no decision have to be made or a selection of two or more alternatives; 3) semi-automatic: some quantitative parameters have to be set by mouse or keyboard; 4) interactive: the user continuously steers the acquisition”. It is doubted that (full-) automatic systems can achieve success rates comparable to human operators within the next few decades. The basic problem in fully automated object extraction stems from the fact that automated image understanding is still operating at a very rudimentary level. The challenge is to replace visual interpretation of optical remote sensing images, accomplished by expert photo-interpreters, with automatic or semi-automatic classification techniques. In general, the change detection-based method, which compares pre- and post-earthquake images, may lead to more accurate and reliable results.

3.4.1.1 Review of Change Detection Methods

The detection of changes is a crucial issue for a variety of tasks in image analysis. Change detection techniques can be employed in many fields like remote sensing, video surveillance, medical imaging and etc. Over the past years, researchers have proposed vast numbers of change detection methods of remote sensing images and classified them from different viewpoints. This interest stems from the wide range of applications of change detection in remote sensing topics such as environmental monitoring, agricultural surveys and damage assessment. Many change detection techniques have been developed and in Lu et al. (2004), Radke et al. (2005) and Pacifici (2007) very extensive reviews are given. In the following some of the change detection techniques are summarized.

The goal of a change detection algorithm is to detect “significant” changes while rejecting “insignificant” ones. To make this distinction, one needs to model all the expected types of changes (significant and insignificant) for a given application and integration of these models into an effective algorithm. Therefore, we need to consider and resolve any image-based differences before detecting real changes on the surface of the Earth. The requirements on image pre-processing ways vary among different change detection methods. However, radiometric corrections and image registration are important and indispensable steps.

One of the most widely used approaches of change detection is “image differencing” (Singh 1989). The registered images, which are acquired at two different times, are subtracted to generate a new image, namely “difference image”. It can be expected that the pixels associated with the changes be presented by significantly different values from those of the pixels associated with the unchanged areas. Other techniques, like Normalized Difference Vegetation Index (NDVI), make the same kind of comparison by using, instead of a spectral band, vegetation indices or other linear or nonlinear combinations of the original bands. The changed and unchanged regions are determined

by selecting the appropriate threshold value. The selection of a threshold value can be performed empirically that gives the best visual representation of changes (Sohl 1999). However, simple differencing with a global threshold is sensitive to noise and variations in illumination, which significantly affect the reliability and accuracy of the final change detection map. Some researchers propose the statistical frameworks to select optimum threshold value (Nelson 1983, Fung and Ledrew 1988, Bruzzone and Prieto 2000, Rogerson 2002, Rosin 2002).

There are several methods that are closely related to image differencing. For example, image ratioing produce the difference image by computing the ratio, instead of the difference, between images (Singh 1989, Shaoqing and Lu 2008). Also the widely used Change Vector Analysis (CVA) technique exploits a similar concept based on a multi-spectral dataset (Malial 1980). Change vector analysis involves a spectral change vector for each pair of corresponding pixels, which is computed as the difference between the feature vectors at the two times. Then, computing and analyzing the components of this vector identify the changes. The statistical analysis of the magnitudes of the spectral change vectors allows one to detect the presence of changes, while their directions make it possible to distinguish among different kinds of transitions (Malial 1980, Bruzzone and Prieto 2002, Rogan and Chen 2004, Bovolo and Bruzzone 2007).

Principal component analysis (PCA) is a commonly used statistical method for many aspects of remote sensing image analysis. The techniques based on the PCA can be used to perform change detection by applying the principal component transformation separately to the feature space at single time or to the merged feature space at two times. Many studies have used principal component analysis to detect change successfully (Byrne 1980, Li and Yeh 1998, Diermayer and Hostert 2007, Deng et al. 2008).

The decision for separation between changed and unchanged classes can be defined in terms of Bayes decision theory. For this purpose, a given mathematical model (e.g. Gaussian model) for the statistics of the changed and unchanged classes is assumed. Under the assumption that the gray-level values of the pixels in the difference image are independent of one another, the estimation of the model parameters could be performed using the Expectation Maximization (EM) algorithm. However, the difference image might be analyzed using a Markov Random Field (MRF) approach that considers the spatial contextual information in order to increase the accuracy of the final change-detection map (Aach and Kaup 1995, Bruzzone and Prieto 2000, Kasetkasem and Varshney 2002, Van Oort 2005).

Post classification comparison (PCC) is a well-known method based on a logical comparison of two independent classification maps. In the post-classification approach, any change detection problem can be defined as a classification problem where a change class and a no-change class have to be distinguished. The methods of change detection can be divided into the “unsupervised” and the “supervised” approaches (Pacifici 2007). The former is defined by no need for prior knowledge about the characteristics of the changed and unchanged areas. By contrast, the latter is based on supervised classification methods, which require the availability of a suitable training set for the learning process of the classifiers. All types of supervised and unsupervised classifications can be used according to the image characteristics for change detection. In this way, it is possible to detect changes and to understand the kinds of transitions that have taken place. However, the performance of the PCC technique crucially depends on the accuracies of the initial classifications. A variety of studies have produced good results with post classification techniques (Mas 1999, Sohl 1999, Ahlqvist 2008, Volpi et al. 2009, Zhang et al. 2009).

Contrary to PCC, in direct multidata classification (DMC) a single multi-temporal classification is performed and the dependency between the two images is considered directly. The pixels are

characterized by a vector obtained by stacking the feature vectors related to the images acquired at two times. Then, change detection is performed by considering each transition as a class and by training a classifier to recognize the transitions. In medium and high-resolution images, this approach has resulted into a better description of the changed and unchanged regions. In such a case, supervised classification is performed over the complete set to predict ground transition (Schiavon et al. 2003, Pacifici 2007, Volpi et al. 2009).

The Mutual Information (MI) between two variables is based on information theory concept and measures the amount of information that one variable contains about another. MI was introduced as a similarity measure between images (both 2D and 3D) simultaneously by Viola et al. 1997 and Maes et al. 1997. The degree of similarity between two images could be a natural candidate to estimate dissimilarities. In recent years, mutual information has appeared as an impressive similarity measure for comparing images mainly in the field of medical imagery. It assumes a statistical relationship that can be captured by analyzing the images' joint entropy. Entropy can be interpreted as a measure of the mean uncertainty reduction that is obtained when one of the particular values is found during sampling. One of their principal properties is their capability to operate in the multi-sensor case and the presented results are promising and indicate similarity measures as possible tools to detect changes of the Earth surface (Pluim et al. 2004, Alberga et al. 2007, Alberga 2009). However, one important drawback to mutual information as a way of comparing images is that it fails to take geometry into account since it considers only pixel values and not pixel positions (Russakoff et al. 2004). In the next section, we describe more details about the methods of damage detection and classification in an urban area after the earthquake.

3.4.1.2 Review of Damage Detection and Classification Methods

There are different approaches for automatic damage detection and classification, principally pixel-based and object-based (Bitelli et al. 2004, Gusella et al. 2005). In pixel-based approaches, images are processed as they are based on the analysis of the individual pixels each pixel is assigned a separate damage state based on the characteristics of the pixel. Often, adjacent pixels are then aggregated to assign an average damage level to an area. This approach could be conducted based on the obtained frequency distribution of the differences in the optical sensor values, which show significant changes in the reflectance due to the effects of the earthquake. The threshold values for the reflectance in the image are defined based on the values of the selected training data. The change areas are detected by subtracting the image brightness values of the merged pre- and post- image. Some contextual information from adjacent pixels (e.g., texture, edges) may also be used in assigning the damage state (Estrada et al. 2001, Yusuf et al. 2001, Turker and San 2003). Although some of the existing methods provide a very useful basis for change detection studies, they have limited capabilities for structural damage assessment. These methods do not focus on structural damage assessment of the scene. In other words, they do not distinguish any change caused by structural damage from other kinds of change. Correlation analysis usually fails to detect structural change, especially if images are acquired under different lighting conditions (Shinozuka and Rejaie 2001). It is crucial to recognize that any major structural damage induces change in the captured images but not all changes are due to structural damage. In this regard, it is necessary to identify 'object' and define how a 'demolished object' is perceived in images and how it is reflected as a 'change' in image data. In object-based algorithms, images are firstly divided into meaningful regions, to simulate the abstraction done by a human interpreter. In object-based analysis, all subsequent analyses are performed on objects and damage levels are assigned to each object as a whole. The object-oriented approach can speed up and increase the accuracy of the extraction process. Here it is assumed that related pixels are actually part of an object with special properties in object space and these properties are represented as features in image space. An automated

procedure of object-based damage assessment needs multi-tiered procedures, which follow a string of operations.

In Figure 3-1 we proposed four main tasks of image interpretation: man-made objects identification, attributes (cues) collection, damage detection and classification. Automatic extraction of man-made structures from images is difficult for many reasons. Space- and air-borne images, especially in urban areas, have a wide variety of structured and unstructured content. They have different properties that make it hard to develop generic algorithms and methods for the extraction. Buildings may have complicated structures and can be occluded by other buildings or vegetation. Together this gives a challenging research problem. However, target buildings might be already identified using pre-event auxiliary data in desired format (e.g. building polygons). To determine the damaged buildings in the course of the damage detection from imagery data, evidence features must be collected which are detectable when comparing the pre- and post-event data. For this purpose, pictorial attributes like edges, texture or shadows can be extracted. For instance, the presence/absence of shadows in a pre/post event pair is a signal of a collapsed building (Turker and San 2004, Vu *et al.* 2004b, Turker and Sumer 2008) and texture analysis can be conducted for debris detection (Sumer and Turker 2005, Rehor and Vögtle 2008, Samadzadegan and Rastiveisi 2008). In these papers, after extracting the building position from vector maps, by measuring and comparing different textural features for extracted buildings in both pre- and post-event images, building conditions are evaluated. 3D information from intensity level matching or range data is also an important cue. Geometrical properties of buildings can be recorded from a digital surface model, which is extracted either from stereo images or laser scan data. Stereo or multiple images give reliable cues to infer 3D structures. In fact, it requires only a small extra cost to obtain stereo or multiple images in case of aerial images. Height differences to initial height, volume reduction rate, debris size, change of roof structure and inclination can be employed in order to assess building damages (Rehor and Bähr 2007). It is suggested that both image and object space cues should be exploited to perform more accurate change detection and classification (Rezaeian and Gruen 2007).

All evidences extracted from object and image spaces have to be integrated through a ‘decision making system’ in order to detect and classify damages. One important aspect that has to be considered is the concept of ‘uncertainty’. Making a rational decision on uncertain evidence is a major topic for artificial intelligence (AI). Researchers handle uncertainty using probability theory (Bayesian networks), Dempster-Shafer theory, and fuzzy logic (Rehor and Bähr 2007, Samadzadegan and Rastiveisi 2008, Rezaeian and Grün 2010).

3.4.2. Automation and Uncertainty

The most important assumption is that automation is intended to assist the human operator and the automation and the human must work together to accomplish the tasks. The programs, which solved such problems, are called “Expert Systems” and such reasoning requires prior knowledge. It is necessary to have the knowledge that the damages exhibited a particular group of evidences. One method of knowledge representation is through if, then... rules. This means if a targeted building has a group of cues, then it may reflect a particular damage. But information is sometimes factual and at other times, uncertain. Factual knowledge has clear cause to effect relationships, where clear conclusions could be drawn from concrete rules. Uncertainty is often treated as a single uniform concept that simply represents the absence of precise information. The uncertainty sometimes results from a random process; it sometimes results only from the lack of information that induces some ‘belief’ (instead of some ‘knowledge’). Data error is considered to be well-defined and measurable part of uncertainty (e.g. DSM error). However, in reasoning systems, important distinctions have been made between different varieties of uncertainty and the different conditions

that produce them. One of these distinctions is between instances of uncertainty that are ‘vague’ and those that are ‘ambiguous’. Vague uncertainty exists when there is a general lack of information regarding a judgment or a particular target. In terms of classification, a vague target would be one where there is only weak evidence for membership to any specific class. For example, altering texture intensity in pre- and post event images is only weakly related to the categories ‘collapse’, ‘partial collapse’ or ‘no damage’ (especially in high-resolution image which reflects miscellany of textures). In contrast, ambiguous uncertainty exists when there is an abundance of conflicting information regarding a possible judgment or a particular target. In terms of classification, an ambiguous target would be one where there is strong evidence for membership in two or more mutually exclusive categories. For example, inconformity of pre-event 3D building model superimposed on post-event images is strongly related to both the negative category ‘damaged building’ and positive category ‘renovated building’ (Figure 3-8).

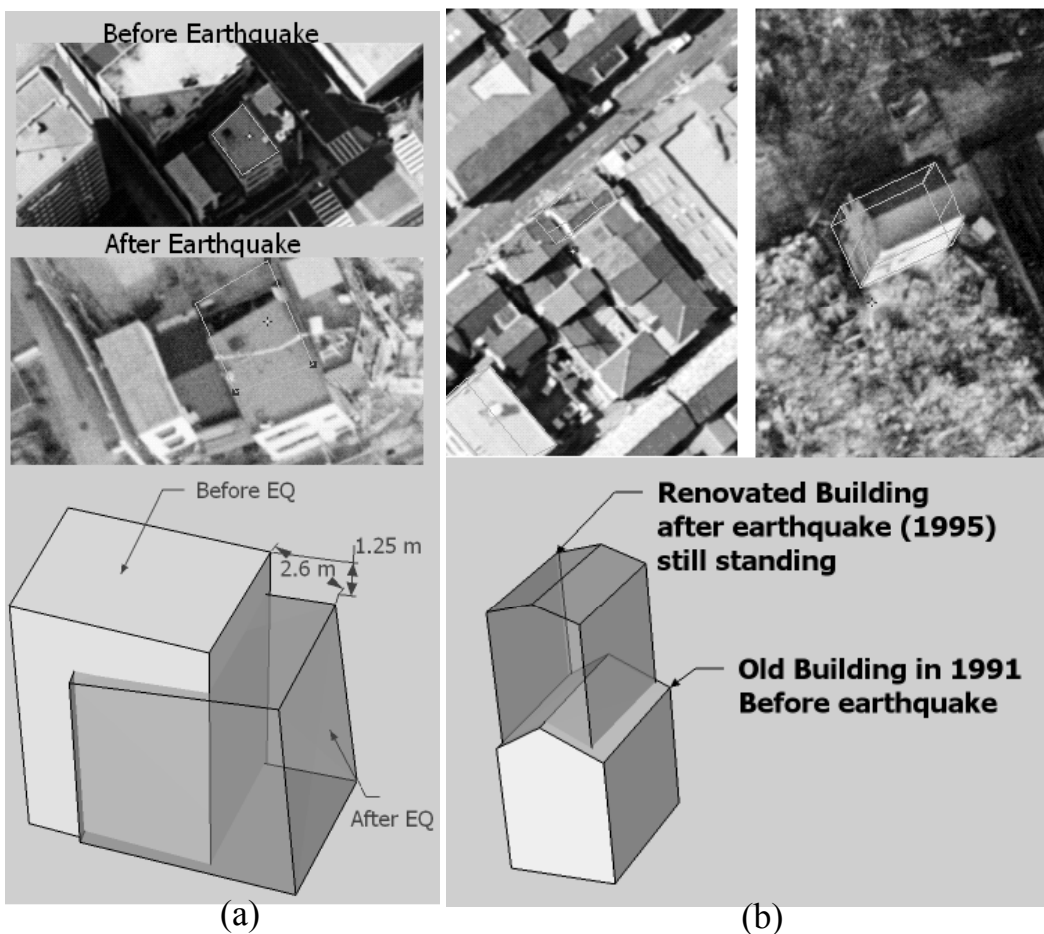


Figure 3-8: Inconformity of a superimposed model can be related to: (a) negative category ‘damaged building’ (Building ‘B’ in Fig. 3-5) and (b) positive category ‘renovated building’ (Building ‘C’ in Fig 3-5)

3.5. Summary

We need to collect appropriate features and attributes of objects before and after the earthquake. These attributes should be extracted from 2D (image) space as well as 3D (object) space. In

particular, the availability of DTMs (Digital Terrain Models) and DSMs (Digital Surface Models) is a major concern for damage detection. With the recent evolution of new sensors (digital camera, high resolution satellites, LIDAR data) and the development of efficient algorithms, the automatic production of urban DSMs is now possible. Furthermore, to mathematically model imprecise information, we need an appropriate language and effective arrangement to represent and manipulate uncertain evidences. Bayesian Networks (BN) are developed as principle formalisms for representing and reasoning under uncertainty in the presented system. In a BN, entities of interest (e.g., decision criteria and sub-criteria, factors that influence them) are treated as random variables and represented as nodes in the network, connected by directed arcs indicating probabilistic dependencies between them. The network structure, together with conditional probability tables associated with each node; provide a compact representation of the joint probability distribution of all variables.

For establishing a semi-automatic damage assessment system, we assume that images (at least a pair of stereo images) before and after the earthquake are available. Moreover, digital surface models should be already generated either manually (using stereoscopic images) or automatically (using matching software or by LIDAR systems). In this study, the field of interest is urban area and the detection and evaluation of damaged buildings is the main target.

4

EARTHQUAKE DATASETS

To evaluate methods and verifying numerical results, two datasets were obtained from aerial images. In our research, parts of the Kobe and Bam cities are selected as study regions (Figure 4-1).

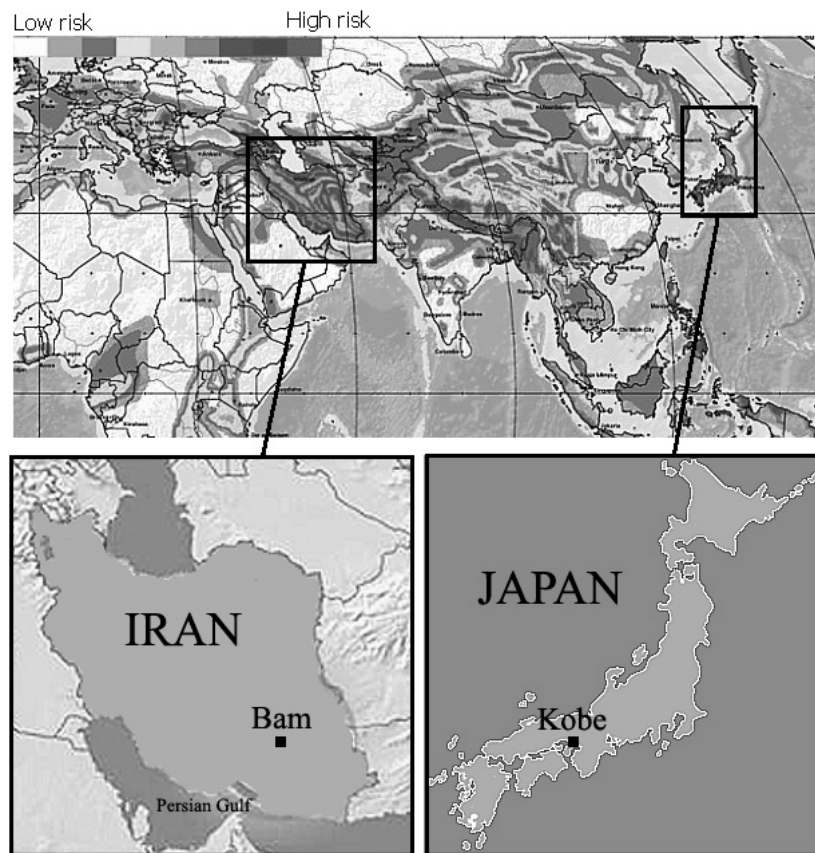


Figure 4-1: Global seismic hazard map produced by Global Seismic Hazard Assessment Program (GSHAP)

4.1. Kobe Earthquake

The Great Hanshin earthquake or Kobe earthquake was a major earthquake in Japan. The earthquake happened in the early morning at 5:46 JST (Japan Standard Time) on January 17, 1995. The epicenter was at Akachi and it was measured 7.2 on Richter scale. Among all major cities, Kobe with its population of 1.5 million was the closest to the epicenter and hit by the strongest tremors. Approximately 5,000 people lost their lives. About 4,600 of them were from Kobe and 350,000 were made homeless and about 200'000 buildings collapsed (Kobe City FIRE Bureau

2006). This was one of the worst earthquakes in Japan. Inner city problems such as densely populated urban areas with old wooden houses and very narrow streets intensified the severity of damage. The earthquake was particularly devastating because a densely populated modern city area was directly hit by very strong ground shaking (Yamazaki et al. 1996). A set of aerial photographs, which were taken before (1991) and after (1995) the earthquake was prepared. It includes RGB colored stereo pairs of images before and stereo triplet of images after the earthquake. The pre-event images were acquired by the aerial camera system Wild 15/4 with focal length 153.05mm. They were taken at a flight altitude 986m with an image scale of 1:6000. The post-event images were acquired by the aerial camera system RC-30 Leica with focal length 152.95mm and were taken at flight altitude 750m and 1:5000 image scale. The pre- and post-event photographs were scanned at 30 and 20 micron, respectively (ca. 18 and 10cm of pixel size on object space).

4.2. Bam Earthquake

A powerful earthquake struck the ancient city of Bam in Iran at 5:26 IST (Iran Standard Time) on December 26, 2003. The epicenter has been reported by the United States Geological Survey (USGS) to be located about 185km south east of Kerman city (roughly 10 km southwest of Bam city). The earthquake had a local magnitude of 6.6 on Richter scale. The earthquake was particularly destructive, most of the mud brick buildings in the historical city, including its ancient citadel collapsed and the death toll amounted to 27,000 people and injured 30,000 residents. In terms of human loss the quake was the worst to occur in Iranian history. One stereo pair of before earthquake and a triplet set of after earthquake (gray-scale photographs) with 1:10,000 scales were used for the analysis. The National Cartographic Center (NCC) of Iran acquired pre- and post-earthquake aerial images of Bam in 1994 and 2003 (3 days after the earthquake). The pre-event images were acquired by the aerial camera system RC-20 with focal length 153.17mm at flight altitude 1500m. The post-event images were acquired by the aerial camera system RMKTOP15 with focal length 152.84mm and were taken at flight altitude 1600m of 1:10000 scale. The pre- and post-event photographs were scanned at 21-micron pixel size, giving a footprint of 21 cm on the object. The calibration reports of the cameras and ground control points were available and used as input information for the interior and exterior orientation procedures.

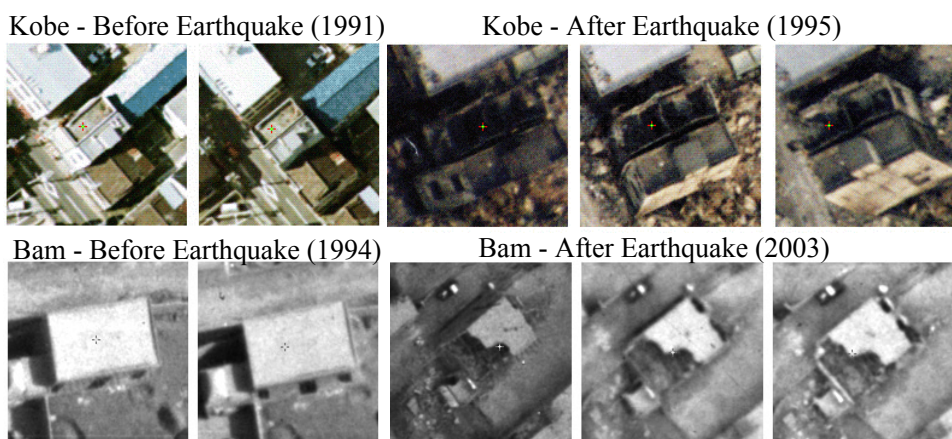


Figure 4-2: Sample windows of aerial photos – Kobe & Bam - before and after earthquake

4.3. Digital Surface Model (DSM) Generation

Digital surface models (DSM) were created automatically from both pre- and post-earthquake aerial images using the SAT-PP software, which is an efficient in-house developed software of IGP-ETHZ. The DSMs generated were then assessed. To evaluate the DSMs, many buildings corners, street lines, and some single points on the roofs are manually measured which considered as three dimensional check points. The heights of these points were measured on DSMs to be assessed and compared with their corresponding heights measured manually on stereo models. The mean, max and root mean square error (RMSE) values for checkpoints in pre- and post-earthquake DSM difference are given in Table 4-1.

Table 4-1: Statistics of DSM difference in checkpoints

DSM accuracy		Grid size (m)	Number of check points	Maximum Absolute (m)	Mean (m)	RMSE (m)
Kobe	Before	0.5	518	20.18	-0.59	2.37
	After	0.4	535	24.46	0.02	2.13
Bam	Before	1.0	4944	8.1	0.34	1.6
	After	1.0	4530	7.5	0.14	1.5

In order to provide a normalized DSM ($n\text{DSM} = \text{DSM} - \text{DTM}$), digital terrain model (DTM) is extracted. The $n\text{DSM}$ refers to the surface that suppresses the terrain height to an equal level. It gives the real heights of the objects above the ground and can be segmented according to a certain height threshold. Morphological operators are used to remove aboveground features, like buildings, trees, cars, and other objects since they are proved to be suitable for such shape processing of the objects. A morphological filter performs first a close operation to fill the pits in the DSM. A close operator dilates the DSM first and erodes it then. After that, the morphological filter performs an open operation to remove surface obtrusions such as buildings, trees and cars. The size of morphological element is decided by the size of the maximum object to be removed. Since removing aboveground features with a large-scale element will cause step effects in the DTM, a low pass filter is used to smooth the DTM. Then, subtracting DTM from DSM can generate the $n\text{DSM}$.

Using pre-event stereo images, 3D prismatic models (which describe a building by its polygonal ground plane and a height) are extracted for both dataset of Kobe and Bam. For this purpose, we developed our software for extracting building polygons and their heights. Table 4-2 reports the number and height statistics of buildings for those buildings within study area (Figure 5-3).

Table 4-2: Statistics of buildings height within study regions

Building Height	Study area of	Study area of
	Kobe city (ca. 0.2 Km ²)	Bam city (ca. 1 Km ²)
Less than 3m	90	87
$3 < H \leq 5$	191	665
$5 < H \leq 10$	276	138
$10 < H \leq 20$	71	0
$20 < H$	9	0
Total number of buildings	637	890

4.4. Visual Damage Interpretation

A visual inspection of building damages is conducted, based on stereo pairs of aerial photos before and after the earthquake to generate reference data for evaluating proposed methods. In the Bam dataset, the problem is the nine years elapsed time between the date of pre-earthquake photo acquisition and the date of post-earthquake aerial photo acquisition. For this reason, the stereo-photos of both dates were visually crosschecked and those buildings that existed in both pre- and post-earthquake images were used in the assessments. A multilevel damage scale (totally collapsed, partially collapsed, uncollapsed) appears to be adequate in representing the distribution of individual house damages (Figure 4-3). In Kobe, due to large scale and high quality colored images, it is possible to extract more details of damaged buildings. Based on EMS98 the buildings are labeled as Grade 1 to 5 by means of criteria described in Table 3-1. In addition, partially and totally collapsed buildings (i.e. G4 and G5) were carefully scrutinized for classifying in four levels of collapsed buildings: Inclined layers (I), Pancake (P), Heap of debris (H) and Overturned (O) (Figure 4-4). The convention of the selected grades and their qualitative descriptions may be roughly correlated to human fatalities due to demolition. Table 4-3 shows the statistics of buildings attribute for Kobe and Bam dataset.

Table 4-3: The number of buildings and their attributes

Bam												
Uncollapsed	Collapsed											
	Partially collapsed				Totally collapsed							
408	184				298							
Kobe												
Uncollapsed G1&G2	G3	Collapsed										
		Partially collapsed (G4)				Totally collapsed (G5)						
246	31	I	P	H	O	I	P	H				
		9	13	13	20	4	3	295				
								3				

4.5. Criteria of Accuracy Assessment

Accuracy assessment is an important step in the classification process. The goal is to quantitatively determine how effectively buildings were grouped into the correct damage classes in the area under investigation. The assessment is done based on data obtained by visual interpretation. Once a classification method is performed an error matrix (also referred to as confusion matrix) is developed (Table 4-4).

Table 4-4: Error matrix for accuracy assessment

		Reference data (Visually Classified)		
		Class 1	Class 2	Class 3
Classified data	Class 1	N ₁₁	N ₁₂	N ₁₃
	Class 2	N ₂₁	N ₂₂	N ₂₃
	Class 3	N ₃₁	N ₃₂	N ₃₃

This table is used to properly analyze the validity of each class as well as the classification. The following accuracy indices are generated:

The *overall accuracy*: it is the total number of correctly classified samples divided by total number of samples. It measures the accuracy of the whole data without any indication of the accuracy of individual categories.

$$\text{Overall accuracy} = \frac{\sum_i N_{ii}}{N} \quad (4-1)$$

The *producer's accuracy*: it is the number of correctly classified samples of a specific category divided by the total number of reference sample for that class. It is an estimate of how many of buildings in each category are classified correctly. It is a measure of the omission error.

$$\text{Producer's accuracy (for class k)} = \frac{N_{kk}}{\sum_i N_{ik}} \quad (4-2)$$

The *user's accuracy*: it is the number of correctly classified samples of a specific category divided by the total number of samples being classified as that category. It means, a user might wish to know what proportion of buildings assigned to specific class were correctly assigned. It measures the commission error.

$$\text{User's accuracy (for class k)} = \frac{N_{kk}}{\sum_i N_{ki}} \quad (4-3)$$

The *Kappa* (coefficient of agreement) developed by Cohen (1960): it is a measure of the difference between the actual agreement between reference data and an automated classifier and the chance agreement between the reference data and a random classifier (Lillesand and Kiefer 1994). It uses all cells in the error matrix and takes into account both commission and emission errors. Briefly, Kappa statistic considers a measure of overall accuracy of classification and individual category accuracy as a means of actual agreement between classification and observation. The value of Kappa lies between -1.0 and +1.0, where 0 represents agreement due to chance only and +1.0 represents complete agreement between the two data sets (i.e. a perfectly classified map with 100% accuracy). Negative values can occur but they are spurious.

$$Kappa = \frac{N \sum_i N_{ii} - \sum_i \left(\sum_j N_{ij} \times \sum_j N_{ji} \right)}{N^2 - \sum_i \left(\sum_j N_{ij} \times \sum_j N_{ji} \right)} \quad (4-4)$$

4.6 Summary

To evaluate methods and verifying numerical results, two datasets of Kobe and Bam were obtained from aerial images. In the Kobe earthquake a densely populated modern city area was

directly hit by very strong ground shaking. The Kobe photos exhibit varieties of damages including low-rise and high-rise collapsed buildings. Bam is an ancient city with masonry buildings represented by low-texture images. Pre and post-event DSMs were extracted automatically using the SAT-PP software. In addition 3D prismatic models of buildings were extracted using stereoscopic aerial images. We base our verification on the visual inspection of the stereo images using a number of objective assessment criteria. In the Bam area, a multilevel damage scale (totally collapsed, partially collapsed, uncollapsed) appears to be adequate in representing the distribution of individual house damages. In Kobe, due to the larger scale and high quality colored images, it is possible to extract more details of damaged buildings based on EMS98 and damage catalogue.



Figure 4-3: Study Area in Bam city, results of visual damage interpretation

■: Uncollapsed, ■: Partially collapsed, ■: Totally collapsed

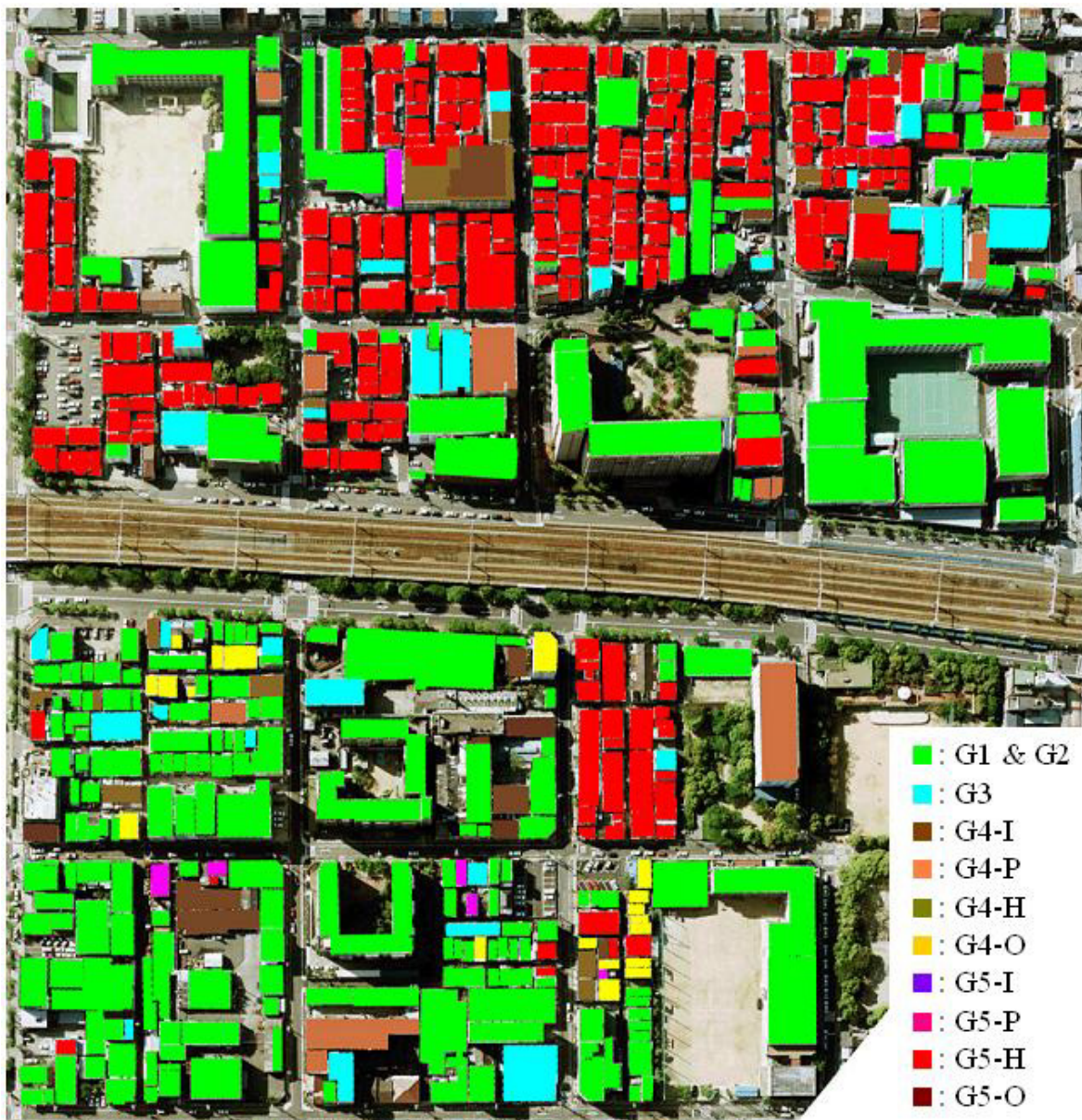


Figure 4-4: Study Area in Kobe, results of visual damage interpretation

(For classification please refer to Table 3-1 and Figure 3-4)

5

HYPOTHESIS TEST FOR AUTOMATIC COLLAPSE DETECTION USING DSMS

5.1. DSM Error

After disaster, comparing geometrical data in the form of digital surface model (DSM) can be major approach to detecting and understanding the extent of demolished area. Reduction of point's elevation would be significant cue to detect the damaged objects. DSMs can be derived from variety of sources requiring different processing methods, including digitization of contour map, interpolation from spot height measurements collected in the field, matching techniques applied to aerial images and processing of radar or laser measurements. In urban area, using stereoscopic (multiple) aerial photographs together with LIDAR technology are more prevalent. These remotely sensed DSM production methods provide users with high resolution DSM data that have stated vertical and horizontal accuracies in centimeters. As such, any resultant DSM is subject to both the precision and accuracy of the measurement sensor as well as the quality of digitizing or interpolation methods, and thus is subject to errors from these multiple sources. Therefore, the DSM elevation of given point P_n can be represented as a random process \tilde{Z}_n :

$$\forall P_n : (X_n, Y_n) \quad \tilde{Z}_n = Z_n + e_n \quad (5-1)$$

Where, Z_n denotes actual elevation (deterministic value) and e_n denotes DSM error (stochastic process). Here, the term error implies the deviation of a measurement from its true value and is therefore implicitly associated with any DSM. Usually, both the magnitude and spatial distribution of the error at any particular location are unknown. Different types of error are often listed: blunders, systematic and random errors as being typical in DSMs. Blunders are gross errors, which occur less frequently in DSM products. The avoidance and detection of blunders in the automatically generated DSM by image matching are critical issues for current researches. Systematic errors show a common trend or dependency, and can be the results of processing or recording procedures. Random errors originate from a variety of sources, and no trend can be observed. Fisher and Tate (2006) summarize the three main sources of such DSM errors:

- Measurement and generation of source data
- Data processing and DSM generation from source data
- The properties of the terrain surface being modeled with respect to its representation in a DSM

The third of these sources of error is particularly important since it emphasizes a fundamental and often neglected consideration when working with DSMs. The resolution and representation of a terrain surface and the derivation of products from that terrain surface introduce ambiguities and can thus best be categorized as uncertainty. Where no spatial dependency of error can be identified, assumptions about the spatial correlation of errors must be made, or all of the errors must be

modeled as random noise. Root mean square errors (RMSE) and standard deviations can be generated for DSMs by using data, which being assumed to have higher accuracy. When modeling errors using the RMSE, it is often assumed to be normally distributed. However, it has been suggested that this assumption is not generally valid and more complex distributions of random errors should be modeled (Wechsler 2006).

5.2. Optimum Threshold Value

The building changes can be automatically detected by simply subtracting one of the DSM data sets from another. The critical value for damage detection is a threshold to which the difference of point's elevation - before and after earthquake - is compared to determine whether or not the building is damaged. For all building polygons the difference of its pre- and post-event average elevation could be analyzed and classified as follow:

Average Height Difference (AHD):

$$\begin{aligned} \text{if } \bar{h}_{\text{diff}} = \bar{h}_{\text{before}} - \bar{h}_{\text{after}} > \text{Threshold} \\ \text{then } & \text{"Collapsed building"} \quad \text{else } \quad \text{"Uncollapsed building"} \end{aligned} \quad (5-2)$$

It closely resembles the method proposed by Turker and Cetinkaya (2005). Similarly, we (Rezaeian and Gruen 2008) proposed the method by using ratio of building volumes (V_a/V_b) to detect collapsed buildings:

Volumes Ratio (VR):

$$\begin{aligned} \text{if } \frac{V_a}{V_b} < \text{Threshold} \\ \text{then } & \text{"Collapsed building"} \quad \text{else } \quad \text{"Uncollapsed building"} \end{aligned} \quad (5-3)$$

V_b, V_a denote building volumes before and after earthquake, respectively. The optimum threshold value can be determined by a method proposed by Fung and LeDrew (1988). This threshold is identified as a value that provides the maximum overall accuracy.

Table 5-1 shows the overall accuracies using different thresholds. The thresholds of 0 for AHD and 0.1 for VR were chosen in the first iteration, and in each stage it is increased. Error matrices are produced and analyzed for each threshold calculating overall accuracies (c.f. section 4.5).

Using volume ratio (VR), the maximum overall accuracies for Kobe and Bam dataset are appeared 92.3% and 83.7%, respectively. Although, there is not significant difference between AHD and VR methods, the optimum threshold values differ considerably between Kobe and Bam dataset. It may be as a result of shape and height of buildings together with arrangement of collapsed buildings. Therefore, optimum threshold value must be used in an adaptive manner. Setting up and testing hypotheses is an essential part of statistical inference, which can be a general solution. Considering conventional stochastic theories, we introduce following hypothesis test to improve collapse detection without knowing optimal thresholds.

Table 5-1: Optimum threshold values computed from error matrices

Volumes Ratio (VR)	Overall accuracy % (Correct decision)		Average Height Difference (AHD)	Overall accuracy % (Correct decision)	
Threshold	Kobe	Bam	Threshold [m]	Kobe	Bam
0.10	69.4	59.2	0	78.8	55.5
0.15	74.7	64.6	0.5	90.3	57.0
0.20	78.3	70.4	1.0 ← Optimum for Kobe	91.8	61.0
0.25	80.1	75.2	1.5	90.1	66.0
0.30	81.5	79.7	2.0	88.2	70.7
0.35	82.9	83.3	2.5	86.3	76.7
0.40←Optimum for Bam	83.7	83.7	3.0	81.0	81.7
0.45	84.3	82.8	3.5	73.3	82.7
0.50	85.1	80.9	4.0 ← Optimum for Bam	70.5	83.0
0.55	85.7	78.0	4.5	67.5	78.8
0.60	86.7	75.8	5.0	59.5	69.9
0.65	87.4	71.1	5.5	50.4	62.6
0.70	88.9	68.2	6.0	45.8	56.7
0.75	90.1	64.5	6.5	44.3	52.8
0.80	91.8	61.5	7.0	44.0	50.0
0.85←Optimum for Kobe	92.3	59.3	7.5	44.0	48.3
0.90	91.2	57.4	8.0	43.8	46.7
0.95	87.6	56.5	8.5	43.8	46.3

5.3. Hypothesis Test

The question of interest is simplified into two competing claims/hypotheses between which we have a choice; the null hypothesis denoted H_0 : “Building is not changed”, against the alternative hypothesis, denoted H_1 : “Building is changed”. The outcome of a hypothesis test is ‘reject H_0 ’ or ‘do not reject H_0 ’. Despite the fact that rejecting the null hypothesis does not imply accepting the alternative, the buildings are classified according to Table 5-2. The operations are carried out in an attempt to disprove or reject the null hypothesis and it cannot be rejected unless the evidence against it is sufficiently strong.

Table 5-2: Decision using hypothesis test

Decision	Actual condition	
	H_0 True (Changed)	H_0 False (Unchanged)
Do not reject H_0	Correct decision	False negative error
	False positive error	Correct decision

In a hypothesis test, there are two kinds of error, classified as "Type I error" and "Type II error": Type I error, also known as an “error of the first kind”, an α error, or a "false positive": the error of rejecting a null hypothesis when it is actually true. Type II error, also known as an "error of the second kind", a β error, or a "false negative": the error of not rejecting a null hypothesis when the

alternative hypothesis is the true state of nature. The *power* of a study is defined as $1 - \beta$ and is the probability of rejecting the null hypothesis when it is false.

As long as we are committed to making decisions in the face of incomplete knowledge, as every scientist is, we cannot avoid making Type I and Type II errors. Simply speaking, “false positive” occurs when we are observing a difference when in truth there is none (or more specifically - no statistically significant difference) and “false negative” occurs when we are failing to observe a difference when in truth there is one. Statistical tests always involve a trade-off between the acceptable level of false positives (in which an uncollapsed is declared to be collapsed) and the acceptable level of false negatives (in which an actual damaged is not detected). It should also be noted that in damage detection false elimination of damaged buildings is typically much more costly than a false addition of uncollapsed buildings as collapsed ones.

We define a new variable of difference between before and after heights:

$$\forall P_n : (X_n, Y_n) \quad d_n = \tilde{Z}_n^b - \tilde{Z}_n^a = (Z_n^b + e_n^b) - (Z_n^a + e_n^a) \quad (5-4)$$

if $(P_n \in \text{Unchanged Object})$ then: $Z_n^b = Z_n^a \rightarrow d_n = e_n^b - e_n^a$

Where, \tilde{Z}_n^b & \tilde{Z}_n^a denote random variables of DSMs elevations, Z_n^b & Z_n^a denote true elevations of P_n and e_n^b & e_n^a represent DSM errors, before and after earthquake respectively. The central limit theorem is critical to applying inferential statistics and hypothesis testing. Let $d_1, d_2, d_3, \dots, d_N$ be a sequence of N independent and identically distributed (i.i.d) random variables each with finite mean and variance. The central limit theorem states that as the sample size N increases, the distribution of the sample average of these random variables approaches the normal distribution irrespective of the shape of the original distribution. There are many versions of the central limit theorem. Several of these place additional restrictions but do not require being identically distributed. Generally the additional restrictions are designed to prevent one or a handful of random variables from dominating the average, which might happen if one random variable has a standard deviation far greater than the rest (Lyapunov or Lindeberg conditions) (Durrett 1996). Roughly speaking, a sum of many small independent random variables will be nearly normally distributed. Although, this assumption might be invalidated locally due to systematic errors, we assume that the differences between systematic errors for DSMs (before and after) are negligible if both DSMs are generated by one system through similar procedures. We define following one-sided hypothesis test:

$$\forall P_n \text{ within building polygon: } \bar{d} = \frac{1}{N} \sum_n d_n \quad (5-5)$$

$$\begin{cases} H_0: \text{building is unchanged} & \bar{d} = \mu_0 + \delta \\ H_1: \text{building is changed} & \bar{d} > \mu_0 + \delta \end{cases}$$

The p-value provides an objective measure of the strength of evidence, which the data supplies in favor of the null hypothesis. For all building polygons, the following p-value is calculated and the value of δ which cause to reject null hypothesis is computed:

$$p\text{-value} = \frac{\bar{d} - \mu_0 - \delta}{\sigma_0 / \sqrt{N}} \quad (5-6)$$

$\alpha = 0.05 \quad \text{if } p\text{-value} > 1.645 \Rightarrow \text{Reject } H_0$

Here, μ_0 and σ_0 represent the sample mean and standard deviation of $\{d_n\}$ for undamaged buildings, respectively, and δ denotes an estimation of height reduction for collapsed buildings. N denotes total number of points surrounded by building polygon, which has to be sufficiently large. Therefore, the hypothesis test could not be reliable for buildings with small area.

5.4. Empirical Investigations

5.4.1. Automatic Collapse Detection using Pre- and Post-Event DSMs

After automatically generating the DSMs from both pre- and post-earthquake aerial photographs, in order to obtain μ_0 and σ_0 , some uncollapsed buildings are selected. Each building polygon encompasses several points of DSMs (before and after) and so $\{d_n\}$ can be calculated for uncollapsed sample buildings. μ_0 and σ_0 are estimated using following estimators:

$$\mu_0 = \frac{1}{M} \sum_{n=1}^M d_n \quad , \quad \sigma_0 = \sqrt{\frac{\sum_{n=1}^M (d_n - \mu_0)^2}{M-1}} \quad (5-7)$$

Where, M denotes total number of points belong to fifteen samples of uncollapsed buildings. We applied the above-mentioned hypothesis test for any building of both datasets. In a conventional test, it is assumed that δ equals zero and H_0 is rejected if p-value would be greater than 1.645 (for $\alpha = 5\%$). We determine the boundary value of δ for rejecting H_0 and make a decision based on the δ value. Obviously, it is anticipated that the greater the demolition, the larger the value of δ . For bi-level classification assuming that if $\delta < 1m$ then the building is classified as “Uncollapsed” and $\delta \geq 1m$ the building is classified as “Collapsed”. This value is selected according to our criteria to interpret collapsed buildings. Table 5-3 shows the numerical results. The overall accuracies are computed to be 91.8% and 82.7% for Kobe and Bam, respectively. Producers’ accuracy (i.e. 1 - false negative error) for collapsed buildings are computed 90.3% and 72.0% for Kobe and Bam, respectively. In Kobe, a concentration of heavily collapsed structures plus a few numbers of partly collapsed buildings may be the cause of the better producer’s accuracy in comparison with the Bam dataset.

One important result is that using the proposed hypothesis test, the computed overall accuracy will be very close to overall accuracy of using optimum threshold values of both Kobe and Bam data set (Table 5-1 and Table 5-3). In addition, false positive errors that are calculated for Kobe: $(17 \div 277) \times 100 = 6.1\%$ and for Bam $(19 \div 408) \times 100 = 4.7\%$, appear to be remarkably close to $\alpha=5\%$. These numerical results indicate to us that performed hypothesis test is supported by an appropriate statistical model. This approach is promising for detection of collapsed buildings using pre- and post-event DSMs of any dataset.

Table 5-3: Results of hypothesis tests for damage detection using pre- and post-event DSMs

		Visual interpretation			
		Kobe		Bam	
Hypothesis test		Uncollapsed	Collapsed	Uncollapsed	Collapsed
Decision	δ [m]	Uncollapsed	Collapsed	Uncollapsed	Collapsed
Uncollapsed	$\delta < 1$	260	35	389	135
Collapsed	$1 \leq \delta$	17	325	19	347
Accuracy Assessment					
Overall accuracy		91.8%		82.7%	
Producer's accuracy		93.9%	90.3%	95.3%	72.0%
User's accuracy		88.1%	95.0%	74.2%	94.8%
Kappa		83.5%		65.9%	

5.4.2. Automatic Collapse Detection using Pre–Event 3D Models and Post–event DSM

In the advent of mega-cities the availability of reliable and up-to-date 3D city models for technical and environmental planning tasks becomes increasingly urgent. There is an increasing need for 3D descriptions of urban areas for various applications such as town planning, telecommunication and disaster management. Hence, before an earthquake, it is an important task to collect spatial data like building models and to update them in short cycles.

Building models define the representation used for describing the form and size of buildings. We only refer to the exterior boundary of buildings, not their interior structure. Simple building models only cover a limited percentage of buildings or provide quite generalized building descriptions. The work on building reconstruction reveals essentially two different basic modeling schemes for the description of the building object, parametric and generic models. Parametric models describe a building by a small set of parameters. In the case of the parametric object model, the type and relations between model primitives are fixed, but their geometry is unknown. This type of model is usually realized in a database of predefined building types, or simple volumetric building primitives. Parametric models are matched with the respective features in images or cues such as a DSM to reconstruct the building instance. In the case of the generic object model, the numbers of model primitives as well as their geometry and topological relations are unknown. We may distinguish three important subclasses of generic building models: prismatic, polyhedral and CSG (constructive solid geometry) models. In the prismatic model the building is specified by a polygonal ground plan, vertical walls and a roof composed of prismatic elements. In polyhedral models, one assumes the building to be bounded by planar surfaces. CSG models allow the composition of complex models from simple parts, which usually are parametric models. Geometric similarity between 3D building model and digital surface model depends on level of details, model accuracy and density of measured points (Figure 5-1). It is possible to evaluate the fitness of pre-event building models on post-event DSM data in terms of parameters like volumetric features.

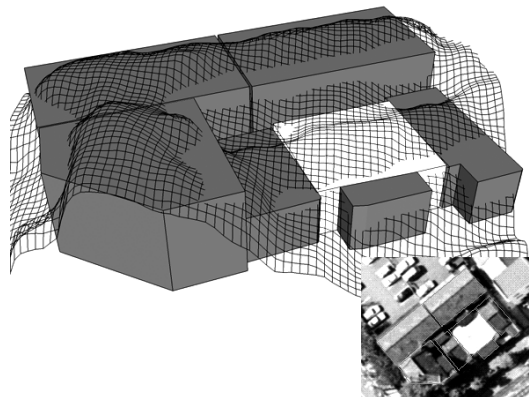


Figure 5-1: The comparison between DSM and prismatic models of buildings

The average height difference (AHD) between post-event DSM and pre-event model of buildings can be used for detecting damaged buildings as well. It is assumed that the pre-event building models have already been generated and are available after the earthquake. In this research, the prismatic models (building polygons with their heights) are generated manually using a digital photogrammetry workstation. Figure 5-2 depicts the distribution of uncollapsed buildings with respect to AHD between pre- and post-event DSMs in comparison with the AHD between prismatic models and post-event DSM. It shows that for both datasets the histograms (probability density functions) are similar in appearance to Gaussian distributions, however, the mean and variance are changed. Therefore, the proposed hypothesis test can be performed using the new values of mean and variance of AHD for DSM and prismatic model of uncollapsed buildings.

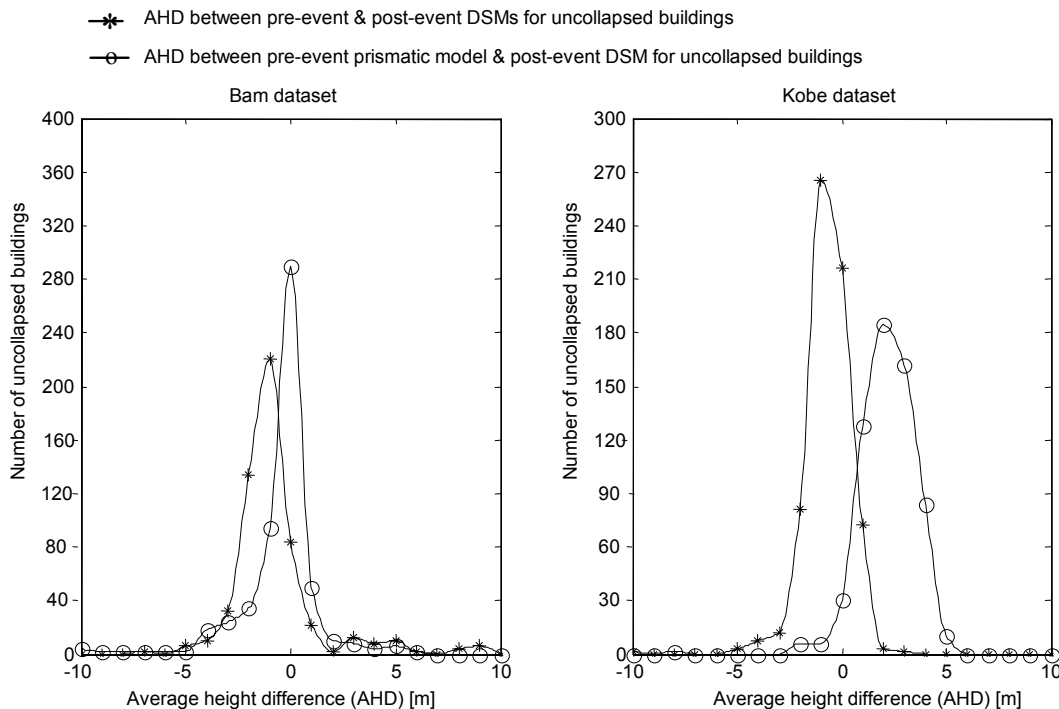


Figure 5-2: Histogram of uncollapsed buildings vs. average height difference

Once again, the mean (μ_0) and standard deviation (σ_0) of AHD between building models and DSM points for fifteen uncollapsed buildings are estimated. The hypothesis test is performed for all buildings in the Bam and Kobe datasets. Table 5-3 presents numerical results. The overall accuracy is computed to be 80.3% for the Bam dataset, which is close to the result of comparing pre- and post-event DSMs (82.7% in Table 5-3). However, the accuracy of the classifier significantly has decreased for Kobe dataset (79.6% in Table 5-4 vs. 91.8% in Table 5-3). In Bam city, the majority of buildings are simple with onefold rooftop, therefore, the prismatic model perfectly represents most of the buildings. On the other hand prismatic models are unable to exhibit detailed surfaces of modern buildings and complex rooftops in Kobe city (Figure 5-3). Nevertheless, it indicates to us that 3D city modeling is an essential pre-event task for disaster management and generates extremely valuable data for damage assessment.

Table 5-4: Results of hypothesis tests for collapse detection using pre-event building prismatic models and post-event DSM

Input data: post-event DSM + Buildings prismatic model		Visual interpretation			
		Kobe		Bam	
Hypothesis test		Uncollapsed	Collapsed	Uncollapsed	Collapsed
Decision	δ [m]				
Uncollapsed	$\delta < 1$	250	103	396	163
Collapsed	$1 \leq \delta$	27	257	12	319
Accuracy Assessment					
Overall accuracy		79.6%		80.3%	
Producer's accuracy		90.3%	71.4%	97.1%	66.2%
User's accuracy		70.8%	90.5%	70.8%	96.4%
Kappa		59.8%		61.5%	

5.5. Summary

In this chapter, approaches for detecting “Collapsed” and “Uncollapsed” buildings using surface models were presented. We focused on three-dimensional information extracted before and after the earthquake. Although we are utilizing DSMs generated automatically by SAT-PP, which is one of the best image matcher software, the systematic errors and blunders especially in densely constructed regions will be unavoidable. A simple pointwise comparison between pre- and post-event DSMs won’t be a reliable source for damaged points. To model the statistical behavior of DSM points we applied hypothesis tests for the mean value of height difference between clustered points, which are enclosed by the building polygon. The Kobe and Bam datasets contain vast varieties of real collapsed buildings and the results achieved for our dataset are very promising. Moreover, airborne LIDAR data can be used allowing a rapid and extensive acquisition of height data and the advantages of such DSMs is that the height component is usually better than the height component of DSMs acquired by matcher software. Considering rooftops details, we may replace pre-event DSM with 3D models of buildings.

There are some aspects that have to be improved in the next chapters. Actually, our definition for “Partially collapsed” is not always related to average height reduction and using image data can improve results of classification. We should utilize imagery features and bi-level classification (i.e. collapsed or uncollapsed) has to be extended to multi-level classification (i.e. Totally, Partially and Un-collapsed).

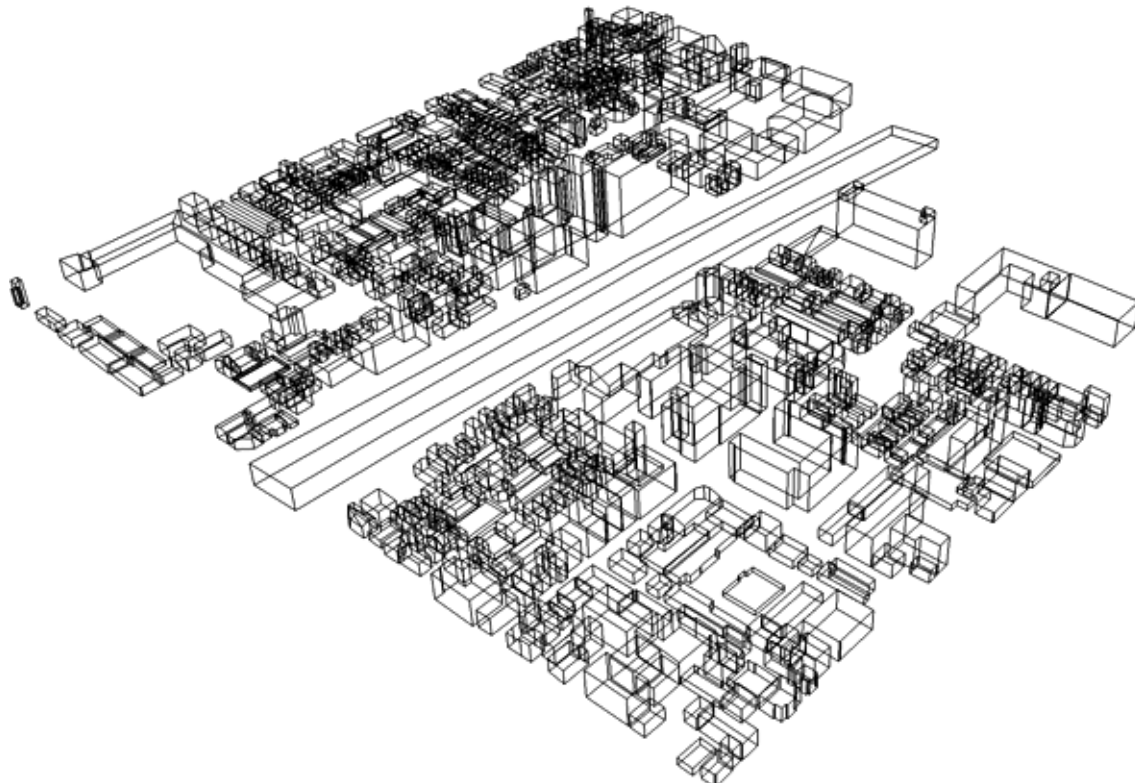


Figure 5-3: Wire-frame 3D model of Kobe dataset generated by a digital photogrammetry workstation

6

DAMAGE CLASSIFICATION USING IMAGE FEATURES

An essential step in finding building damages is the search for changes in its image data. The main topic of this section concerns the possibility of using optical imagery data for earthquake damage assessment in urban areas. Here, the main focus of interest is those imagery features, which are extracted within buildings boundary. Automatic damage detection can be conducted using data fusion integrating imagery information content with the geometrical attributes obtained from DSMs. The purpose behind this idea is to develop a framework for extracting as much as possible basic robust features from different type of data or different cues. Thereafter, the basic features could be integrated into the classification system for damage assessments.

Obviously, not all types of damage occurring at buildings reflect similar imagery features and not any image change indicate building damages. The difficulty of detecting building damages from aerial or other optical images arises from the fact that the damages to be detected are not those of optical surface characteristics of buildings, but those of 3D surface geometry, which cannot be directly observed through optical sensors. However, large-scale images show certainly the high level of details related to single buildings and small structures. Using high-resolution images, the human interpreter looks for the remaining ruins and debris from damaged buildings. The first goal of the semi-automated image classification is to be able to distinguish recent debris from other objects on the ground. The presence and amount of debris can be translated to damaged structures and rate of its demolition. The type of debris in terms of its material, shape and formation is generally complex and its reflectance characteristics can be very different in images. Nevertheless, the image descriptors, which provide measures of properties such as smoothness, coarseness and regularity, can intuitively be utilized for debris detection. Moreover, a building collapse leads to disappearance of the building shadow and also to weaker or even lack of roof edges.

6.1. Preprocessing

The aim of pre-processing is to improve the image appearance to a human viewer or better suited to machine processing. In order to get better results, the image should be enhanced at first. Examination of the histogram of the images reveals that the luminance histogram is skewed toward darker levels and the majority of the pixels possess a luminance less than the average, therefore we followed the histogram modification methods. We have applied an adaptive histogram equalization technique in which histograms are generated only at a rectangular grid of points and the mappings at each pixel are generated by interpolating mappings of the four nearest grid points (Gonzalez and Woods 2002). In addition, optical images which are taken just after an earthquake are subject to noise and haze of dust and smoke. Debris pattern generally contains high-frequency components and it is so difficult to distinguish from noise added to image, which similarly has a high spatial frequency spectrum. Since linear low-pass filtering may degrade feature generation results, the images are smoothed only with a 3by3 non-linear median filter in order to limit impulse noise effects.

6.2. Features Generation

The texture of an image region is determined by the way the gray levels are distributed over the pixels in this region. We are in a position to describe an image by the look of it as fine or coarse, smooth or irregular, homogeneous or inhomogeneous and so forth. There is no clear definition of “debris texture”. It is often qualitatively characterized by its coarseness in the sense that a patch of rubbles is coarser than a patch of intact building roof under the same viewing condition. Our goal in this subsection is to generate appropriate features that somehow quantify this property of an image within the building footprint. Various approaches have been used to investigate the textural and spatial structural characteristics of image data for damage detection, including first and second order statistical features, wavelet transform, morphological descriptors, variograms and density or dissimilarity of edge pixels (Mitomi et al. 2001, Huyck et al. 2005, Rathje et al. 2005, Shirzaei et al. 2006, Sertel et al. 2007, Rehor and Vögtle 2008, Gueguen et al. 2009). It should be noted that texture is a neighborhood property of an image points and therefore, texture measures are inherently dependent on the image scale.

6.2.1. Statistical Descriptors

6.2.1.1. First-Order Statistics Features

One approach to region description is to quantify its texture content using statistical moments of the gray-level histogram of an image globally or regionally. Measurements should be restricted to windows of relative uniformity. This can be computed in terms of the first-order histogram of image pixels within a neighborhood. The first order histogram estimate ($P(b)$, b represents quantized amplitude gray-level $0 \leq b \leq L-1$) is simply computed in a neighborhood window centered about (i,j) :

$$P(b) = \frac{\text{number of pixels with gray level } b}{\text{total number of pixels in the region}} \quad (6-1)$$

We select the following descriptors as quantitative measures:

Standard Deviation: $SD = \left[\sum_{b=0}^{L-1} (b - \bar{b})^2 P(b) \right]^{\frac{1}{2}}, \bar{b} : \text{the mean value of } b \quad (6-2)$

Entropy: $E = - \sum_{b=0}^{L-1} P(b) \log_2 P(b) \quad (6-3)$

The second moment (variance) is of particular importance in texture description. In the literature, the standard deviation image feature is sometimes called the *image dispersion* (Pratt 1991). This is a measure of gray-level contrast that can be used to represent relative smoothness. Entropy is a measure of histogram uniformity. The closer to the uniform distribution ($P(b)=\text{constant}$) the higher the E . In this study, for every point within the building area, small windows are selected and standard deviation and entropy are computed. In order to analysis the

texture of building image, average standard deviation (ASD) and average entropy (AE) are computed and assigned to each building polygon.

6.2.1.2. Second-Order Statistics Features

Measures of texture computed using only histograms suffer from the limitation that they carry no information regarding the relative position of pixels with respect to each other. This type of information can be extracted from second-order histograms where the pixels are considered in pairs. Second-order statistics also account for the spatial inter-dependency or co-occurrence of two pixels at specific relative positions. Two more parameters enter into the scene: relative distance among pixels and their relative orientation. The relative distance (d) is measured in pixel numbers and the orientation (ϕ) can be quantized in four directions: horizontal, diagonal, vertical and anti-diagonal ($0^\circ, 45^\circ, 90^\circ, 135^\circ$). Each element of (i,j) in the normalized P is the joint probability occurrence of pixel pairs with a defined spatial relationship having gray level values b_i and b_j in the image:

$$P(b_i, b_j) = \frac{\text{number of pairs of pixels at position } (d, \phi) \text{ with values } (b_i, b_j)}{\text{The total number of pixels in the measurement window}} \quad (6-4)$$

The joint amplitude histogram may be regarded as a $L \times L$ normalized gray-level co-occurrence matrix (GLCM) so that the sum of its elements is equal to one. The basic idea is to characterize the content of GLCM via descriptors. Haralick et al. (1973) have proposed a number of texture features based on the two-dimensional histogram of pixel pairs. For our purpose, the following useful descriptor is selected to be computed for every building area:

$$\text{Homogeneity:} \quad H = \sum_{i,j}^{L-1} \frac{P(b_i, b_j)}{1 + |i - j|} \quad (6-5)$$

‘H’ returns a value that measures the closeness of elements in the GLCM to the diagonal matrix (‘H’ is 1 for a diagonal matrix).

Figure 6-1 contains several examples of first and second order texture field discrimination tests. In these tests, the variance is computed for 3-by-3 and the entropy is computed for 9-by-9 neighborhoods around the corresponding pixel. The average values of standard deviation and entropy for building polygon are represented by ASD and AE, respectively. The GLCM is computed for a pair ($d = 1, \phi = 45^\circ$) and the homogeneity factor is computed for corresponding pixels within the building area. A preliminary investigation shows that these features can be helpful to discriminate between undamaged planar roofs and heap of debris (Figures 6-1(a),(b) and (e),(f)). However, complex intact roofs as well as broken structures could reflect similar attributes in terms of imagery statistics features. For instance, the uncollapsed buildings in Figures 6-1(c) and (d) are equivalent to the collapsed buildings in Figures 6-1(g) and (h) in terms of ASD, AE and H.

Direction, interconnection and clarity of lines may be key signal for human perception to discern devastated structures. The main characteristic feature for uncollapsed building can be the well-ordered distinct lines and their “regularity”. The degree of geometric regularity, not only at the building level itself but also at higher levels of spatial hierarchy can also be exploited. To measure “lines regularity” one has to define criteria that give a numerical index. We commence with a proposal of an algorithm for line detection and afterwards introduce two indices for representing line regularity (RI_1 and RI_2).

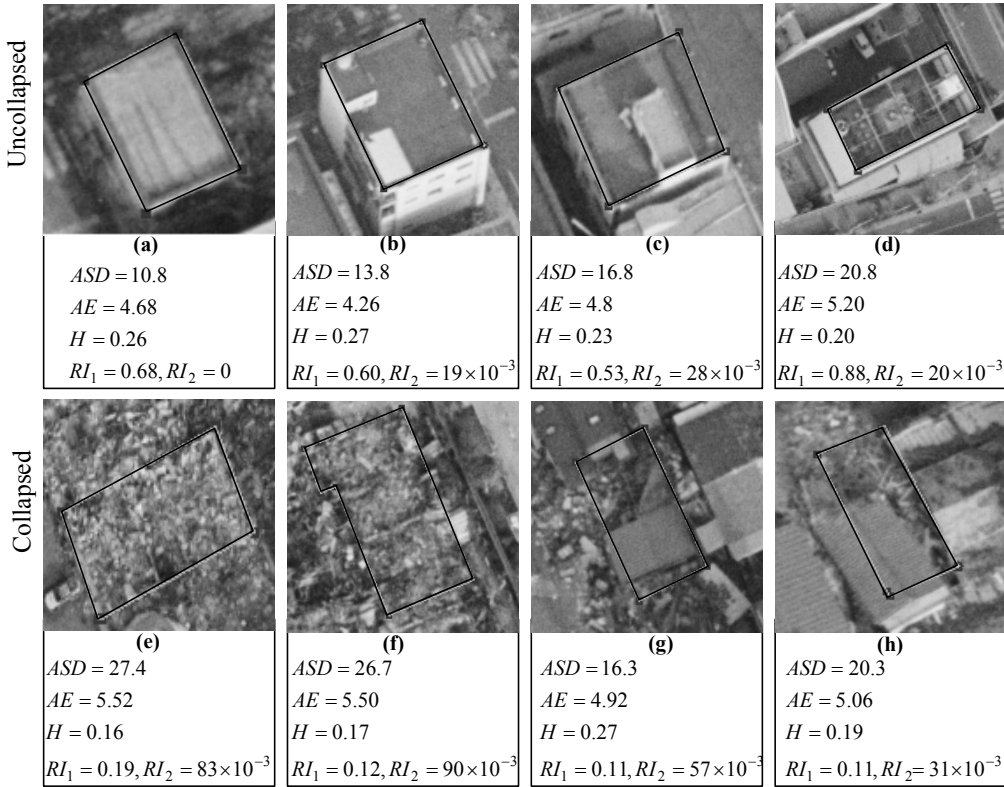


Figure 6-1: Numerical examples of statistical features (ASD: Average Standard Deviation, AE: Average Entropy, H: Homogeneity) and Regularity Indices (RI_1 and RI_2) for collapse detection

6.2.2. Line Extraction and Analysis

Straight-lines occur in various natures and man-made objects and many complex objects can often be identified by their distinct combination of linear features. In urban areas, straight-line segments of various relative orientations provide important information about buildings and polyhedral man-made objects. The degree of lines regularity in such man-made structures helps to tackle the problem of damage detection. In this section, we will first give a review on the basic Canny edge detector, and then briefly describe Standard Hough Transform and the involved problems. Finally we will present our method, a stratified model of Hough Transform as a means to resolve the problem.

6.2.2.1. Edge Detection - Canny Edge Detector

Canny edge detector (Canny 1986) is considered to be the ideal edge detection algorithm for images that are corrupted with white noise. The Canny operator works in a multi-stage process. It firstly smoothes the image to eliminate the image noise and then a derivative operator is applied to the smoothed image to highlight regions. The algorithm then tracks along these regions and suppresses all pixels that are not at the maximum, a process known as non-maximal suppression. The tracking process exhibits hysteresis controlled by two thresholds. If the magnitude is below the first threshold, it is set to zero, and if the magnitude is between the two thresholds, it is set to zero unless there is a path from this pixel to a pixel with gradient above the second threshold. This hysteresis helps to ensure that noisy edges are not broken up into multiple edge fragments. The result of the

Canny operator is determined by three parameters: the width of the Gauss kernel used in the smoothing phase, and the upper and lower thresholds used by the tracker. Increasing the width of the Gauss kernel reduces the detector's sensitivity to noise, at the expense of losing some of the finer detail in the image. The localization error in the detected edges also increases slightly as the Gauss width is increased. Usually, edge thresholding is normally done in an ad-hoc manner, often requiring user tuning of parameters. Setting the lower threshold too high will cause noisy edges to break up. Setting the upper threshold too low increases the number of spurious and undesirable edge fragments appearing in the output. A threshold can be determined automatically using an algorithm developed by Voorhees and Poggio (1987). They showed that if the image noise consists of additional Gaussian noise then the magnitude of the gradient of the image has a Rayleigh distribution. For an acceptable proportion of false edges, a threshold is calculated with risk probability factor of 0.1-0.2% and estimated peak of Rayleigh distribution (Zhang 2005). However, in practice the edge distribution in a real image is a combination of different sources of noise and significant features, complicating the identification of the non-noise components in the edge magnitude histogram. Another problem with the basic Canny operator is occurred where three ridges meet in the gradient magnitude image (Y-junction). Such junctions can occur where an edge is partially occluded by another object. The tracker will treat two of the ridges as a single line segment, and the third one as a line that approaches, but doesn't quite connect to that line segment.

6.2.2.2. Line Detection - Standard Hough Transform (SHT)

The Hough transform is a global, robust technique for the detection of predefined shapes in images, especially straight lines. The Hough Transform is well known as a method of determining the parameters of one or more straight lines which pass through a set of edge points. The main advantage of the Hough Transform technique is that it is tolerant to gaps in feature boundary descriptions and is relatively unaffected by image noise, unlike edge detectors. It is based on transformation of the candidate edge points to parameter space (Figure 6-2). Lines can be represented uniquely by two parameters either in Cartesian coordinates (slope-intercept parameters) or in corresponding polar coordinate as follows:

$$r = x \cos \theta + y \sin \theta \quad (6-6)$$

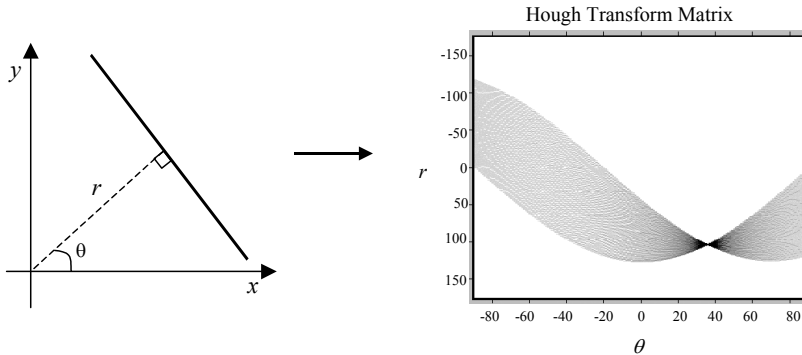


Figure 6-2: The principal of Hough Transform

Any line passing through (x,y) must have parameters which lie on the sinusoid in parameter space determined by the equation above. This parameterization (r,θ) yields a bounded parameter space and maps an edge point onto a sinusoidal curve. This equation can also be interpreted as a constraint on the parameters (r,θ) to ensure the line passes through the point (x,y) . The Hough approach involves creating an accumulator matrix in the (r,θ) space. Each edge point votes for the line parameters that could pass through that point. Infinite lines are detected by interpretation of accumulator when all edge points have been transformed. The line parameters are estimated by determining points with the greatest number of votes, which appear as peaks. The most basic way to detect lines is to set some threshold for the accumulator and interpret all values above threshold as a line. Furthermore, a post processing is still needed to extract segment lines. Figure 6-3 depicts a flow diagram of line detection process and input parameters.

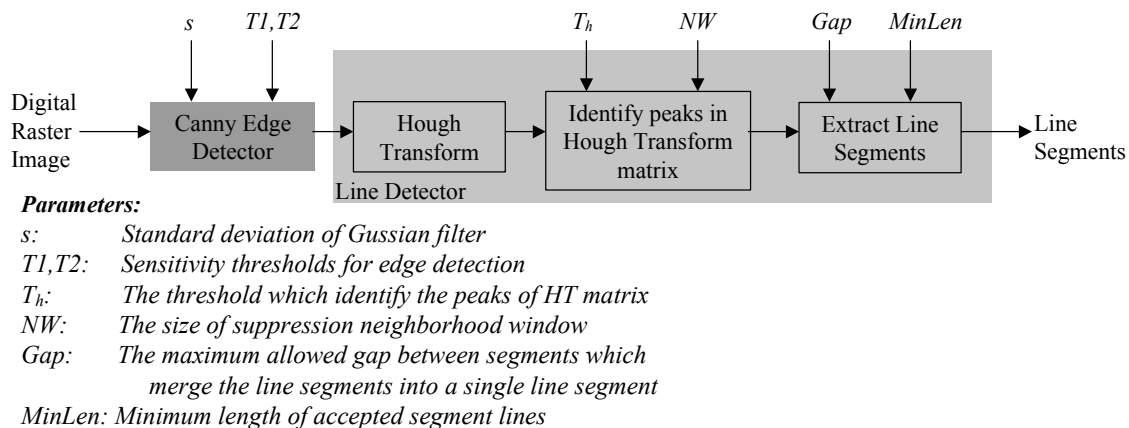


Figure 6-3: Flow diagram of Standard Hough Transform algorithm for segment line detection

6.2.2.3. Experimental Test

As a preliminary numerical experiment, first we used an artificially generated image, which was degraded by added Gaussian noise after blurring. The image contains four rectangle shapes; three of them are aligned so that the middle one slightly rotated and the fourth one is appeared with low contrast. Initially, we utilized a set of ready functions implemented in Matlab (R2007a) software package. For Canny Edge detector, the first threshold ($T1$) was set as a value higher than the gradient values of 70% pixels and the second threshold $T2=0.4T1$. The standard deviation 1.0 was used for Gaussian kernel. The Hough Transform generates a parameter space with one pixel and one degree spacing for r, θ , respectively. To locate peaks in the HT matrix, the threshold was set to 20% of the maximum value in the accumulator. Figure 6-4 shows the results of the line detection procedure using Matlab functions with different parameters. The Standard Hough Transform (SHT) is a well-established strategy but a detailed inspection reveals several problems which some of them are listed below:

- A naïve way of quantization the parameter space leads to generate the multi-short-line segments that seldom characterize the whole line segment completely. This effect could be augmented by the noise and large gaps between points.
- There is not unproblematic way to determine the optimum value of parameters. For instance, the size of suppression neighborhood window (NW) should be small enough to detect all line components, but small value has a tendency to detect several (almost identical) lines for each true

line. This makes confusion for the distant segment lines that are closely aligned (aligned boxes in Figure 6-4(c)).

- It is basically difficult to distinguish two equal-sized group points such that the one is short and densely distributed while the other is long but sparse.

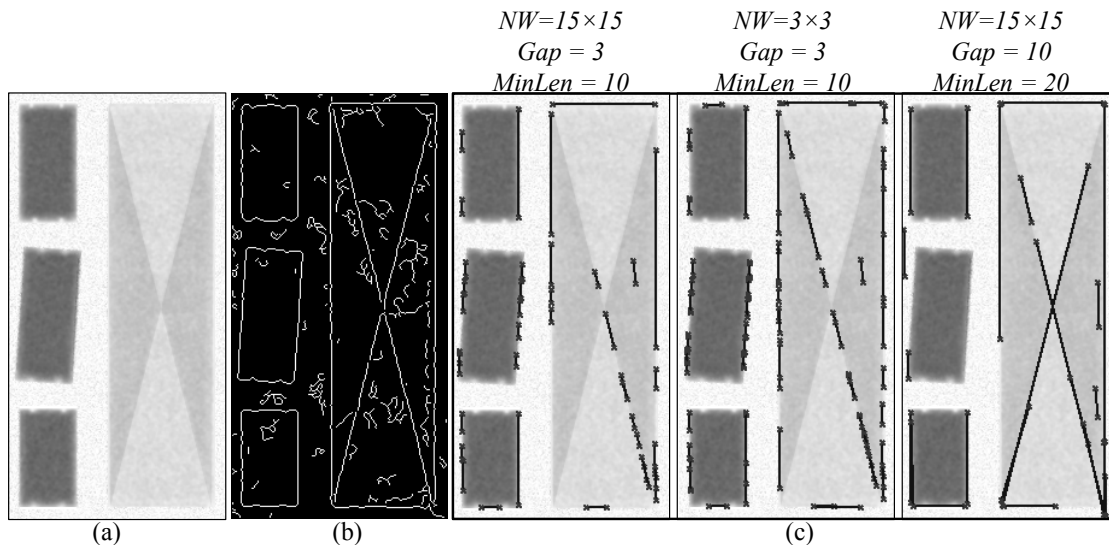


Figure 6-4: (a) Original image (b) Canny edge detection (c) Standard Hough Transform line detection with different input parameters

6.2.2.4. Line Detection - Hierarchical Permissive Hough Transform (HPHT)

Hierarchical detection has been traditionally used in edge detection approaches and was applied by Tuytelaars et al. (1997) to develop an effective procedure for line detection. Inspired by the success of their work, in this section, we present our method for line detection that satisfactorily solves the problems found in the aforementioned algorithm. We start with definition of our goals:

- The algorithm should be robust against discretization effect as well as noise. In fact, a digital line that can be accepted in a binary image is a sequence of discrete points that lie on grids almost close to a geometrical line.
- The algorithm should collect all obvious lines and also trying to detect obscure ones.
- The algorithm should report the longest line segment without considering the shorter overlapped line segments.

The proposed method for detecting straight lines from edge images can be divided into the following steps (Figure 6-5):

- 1- Mapping of edge points to the Hough space and storage in an accumulator. In this step, each point puts one vote in the corresponding bins.
- 2- Thresholding of the accumulator to yield lines with minimum vote. The threshold value should be selected base on minimum permitted length. The algorithm returns the line segments, which being longer than minimum length.

3- Corresponding to any infinite line, every bin of the accumulator reserves a certain number of votes. The edge image is searched along a corridor around that line to find the longest segment of connected pixels. Each edge pixel inside this corridor, which belongs to the longest line segment, is permitted to re-vote. The weight of re-voting is selected proportional to the distance from the target line (Figure 6-6(a)). Since the longer line segments have the upper priority, the candidate lines will be arranged descendingly according to the new scores.

4- Searching in edge image along specified lines to find the longest segments of pixels either continuous or exhibiting gaps not exceeding a given threshold. We used an inverse mapping from accumulator space to the edge data in order to re-analysis of the image. The lines to be detected remove the common pixels and a band around it. Bresenham's line drawing algorithm (Bresenham, 1965) has been used to brush up the edge points those parts of the selected line. This ensures that lines of connected votes are drawn as opposed to use of line equation that can lead to gaps in the drawn line.

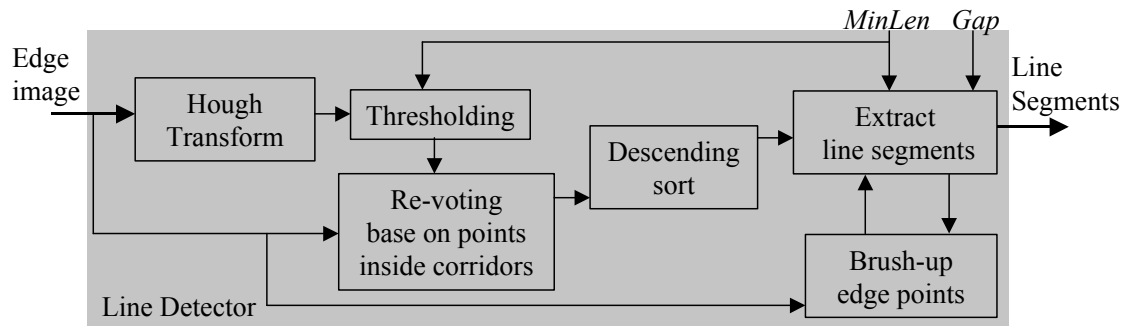


Figure 6-5: Block diagram of Hierarchical Permissive Hough Transform (HPHT)

The methods are implemented and developed in our system. Figure 6-6(b) shows the result of detected lines on artificial image.

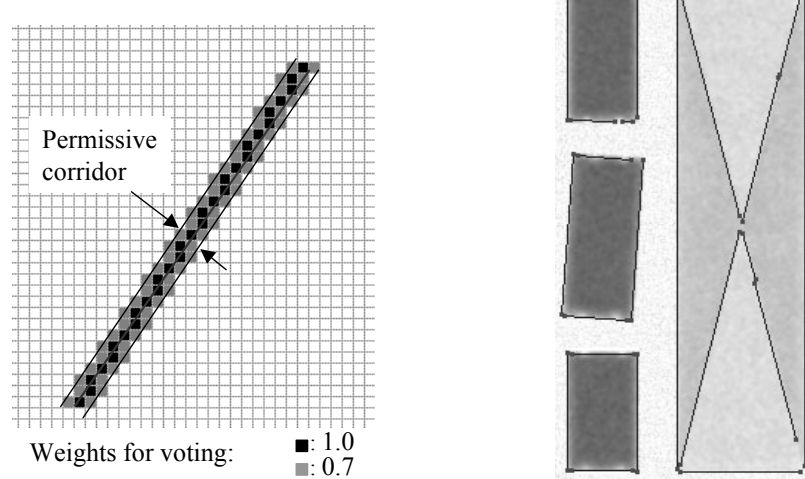


Figure 6-6: (Left): The weight of re-voting is selected proportional to the distance from the target line, (Right): Line detection using HPHT algorithm

In order to detect obvious line segments as well as obscure ones, we have proposed and implemented the stratified form of line detection procedure (Figure 6-7). This can be performed iteratively. The algorithm detects edges using the well-known Canny edge operator. In the first iteration, thresholds are set to high values resulting in the detection of strong edges. In the second iteration, the threshold values are set to lower values in order to detect weaker edges and it proceeds after deleting edge points, which previously detected as lines. Besides, in the first iteration, line detector should be permissive but in the second iteration should be restricted to ensure that the actual lines are detected.

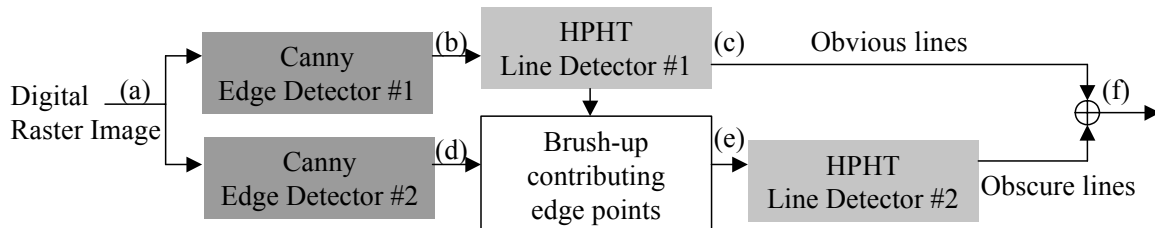


Figure 6-7: Flow diagram of multistage line detection method using HPHT; e.g. (a)-(f) from Figure 6-8

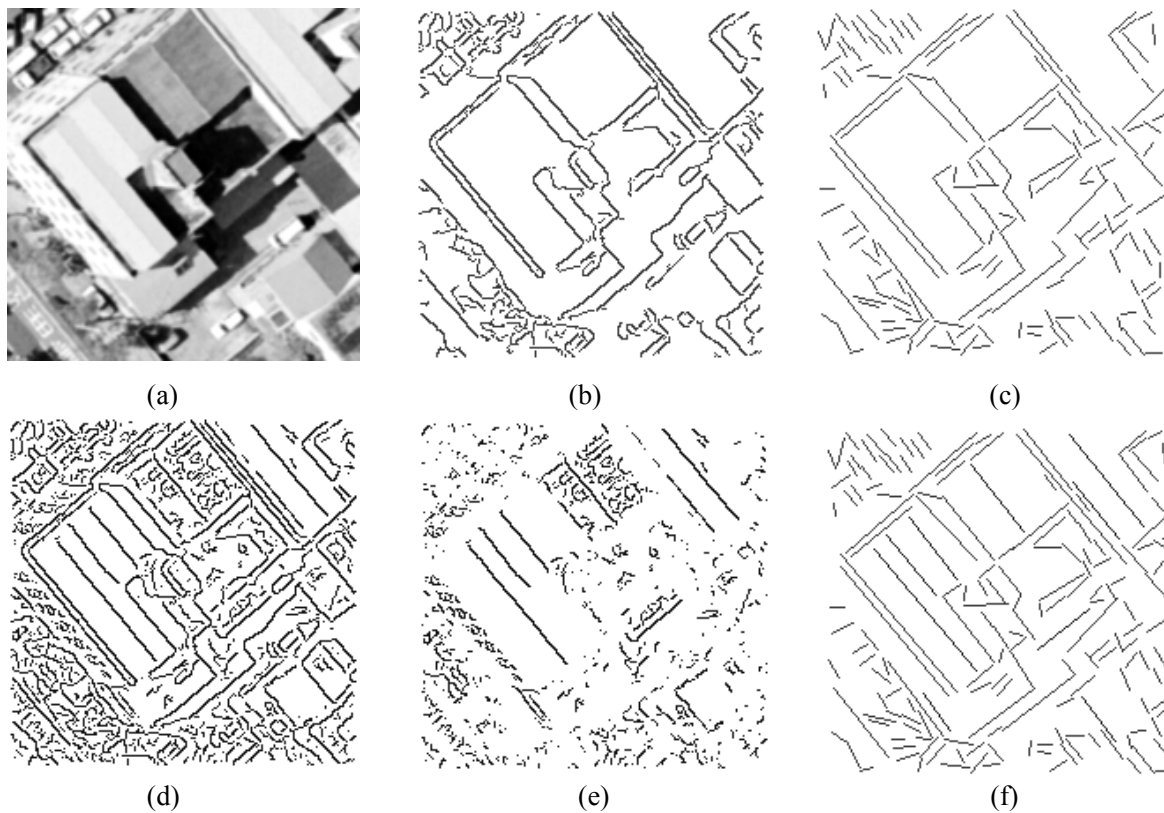


Figure 6-8: (a) A window of the Kobe aerial image (b), (c) The detection of strong edges and corresponding lines (the obvious lines) (d) The process is repeated and threshold values are set in order to detect weaker edges (e), (f) The detection of the obscure lines after deleting edge points which previously detected as the obvious lines

6.2.3. Regularity Indices

For the purpose of improving the classification of building damage types, especially to detect debris and rubbles, we present two kinds of features using linear features. Line detection of standing buildings exhibits a sketchy outlines draft. The composition of lines could be a remarkable cue of scene regularity. Here, regularity might be defined based on line directions with respect to the predefined building model. Regularity indices are defined for exterior and interior zones: the narrow strip around the border of building and the region surrounded by building polygon (Figure 6-9). Because of using Hough Transform, detected lines are accompanied by their direction angle and so that is simply possible to separate lines with similar directions from others. At the border of the building polygon, the output lines are compared with vector lines, which being already extracted from pre-event images. In order to evaluate the degree of fit of line segments to the pre-defined polygons two parameters were used: 1) the angle between segmented lines and actual polygon lines (α) 2) the length of segmented lines (l). To measure the degree of the match between the detected segment lines and delineated vectors of building polygons, the following formula is established for the first regularity index:

$$RI_1 = f \left(\frac{\sum l_i \cos \alpha_i}{\sum l_i} \right) \quad (6-7)$$

The function f describes the rate of fit between detected line segments and actual polygon lines. The second regularity index (RI_2) is defined based on density of line segments. For this index, those lines within building polygon which their direction are not close to the direction of polygon lines would be selected and density of pixels is calculated (Figure 6-9). Figure 6-1 shows regularity indices for several sample buildings. In comparison with the conventional statistical features, regularity indices show better results. In the next section, a numerical evaluation of the proposed features for damage classification will be presented.

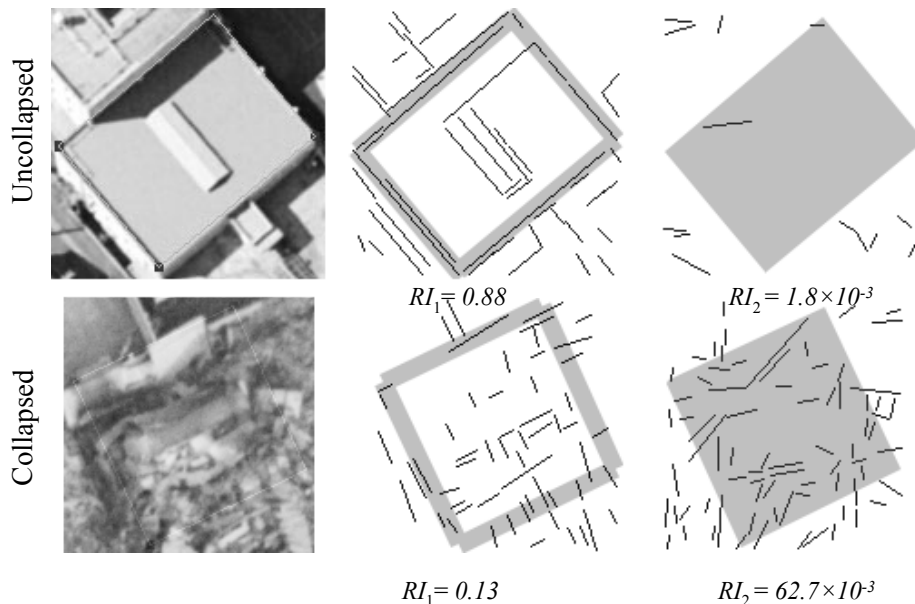


Figure 6-9: Regularity indices (RI_1 , RI_2) are computed for exterior and interior regions

6.3. Features Evaluation

In the previous section, we endeavored to study and propose methods to generate efficient imagery features for damage detection. The goal of this section is to evaluate features and estimate the classification error probabilities. Using our dataset Kobe and Bam, we evaluate the following features extracted from imagery data: average standard deviation (ASD), average entropy (AE), homogeneity (H), and regularity indices (RI_1 , RI_2). Inasmuch as there are triplet-views of the study area after the earthquake, the average values extracted from the post-event images corresponding to each building polygon was employed to obtain final results. We should aim to find features that take distant values in the different classes and closely located values in the same class. A first step is to look at each of the generated features independently and test their discriminatory capability for the problem at hand. However, looking at the features independently is far from optimal and may not be effective for features with high mutual correlation. We focus on techniques measuring the classification capabilities of feature vectors.

6.3.1. Data Normalization

Ideally a classification system wants the same range of values for each input feature in order to minimize bias within different types of features (φ_i). The problem is overcome by normalizing the features so that their values lie within similar ranges. The rescaling is accomplished by using a linear interpolation formula such as that given in the following:

$$\varphi'_i = \frac{\varphi_i - \min(\varphi_i)}{\max(\varphi_i) - \min(\varphi_i)} \quad (6-8)$$

It puts the normalized data in a range of 0 to 1. When the min-max normalization is applied the underlying distributions of the corresponding features will remain the same while preserving all relationship in the data and it does not introduce any bias.

6.3.2. Class Separability Measure

One important step in the design of a classification system is to evaluate image features. There are two quantitative methods for the evaluation of imagery features: prototype performance and figure of merit (Pratt 1991). In the prototype performance method, an example image is classified by a classification procedure. The classification error is then measured for each features set. The figure-of-merit approach to feature evaluation involves the establishment of some functional distance measurements between sets of image features such that a large distance implies a low classification error, and vice versa. In this section, the performance of proposed features are evaluated using a figure-of-merit method by “Fisher discriminant ratio” and “B-distance” criteria.

Fisher's discriminant ratio is suggested in a more primitive fashion, independent of the underlying statistical distributions. It is built upon information related to the way feature vector samples are scattered in the feature space. The following formula is defined (Theodoridis and Koutroumbas 2003):

$$FDR = \frac{(\mu_1 - \mu_2)^2}{\sigma_1^2 + \sigma_2^2} \quad (6-9)$$

μ_i and σ_i^2 denote mean and variance of the features. However, such methods neglect to take into account the correlation that unavoidably exists among various features and influences the classification capabilities of the feature vectors that are formed. The *Bhattacharyya distance (B-distance)* can be another scalar function of the probability densities of features of a pair of classes: “Collapsed”, “Uncollapsed” (ω_1, ω_2). The B-distance is applicable only for Gaussian distributed feature data and defined as (Pratt 1991):

$$B(\omega_1, \omega_2) = \frac{1}{8} (\boldsymbol{\mu}_1 - \boldsymbol{\mu}_2)^T \left(\frac{\boldsymbol{\Sigma}_1 + \boldsymbol{\Sigma}_2}{2} \right)^{-1} (\boldsymbol{\mu}_1 - \boldsymbol{\mu}_2) + \frac{1}{2} \ln \left[\frac{\frac{1}{2} |\boldsymbol{\Sigma}_1 + \boldsymbol{\Sigma}_2|}{|\boldsymbol{\Sigma}_1|^{\frac{1}{2}} |\boldsymbol{\Sigma}_2|^{\frac{1}{2}}} \right] \quad (6-10)$$

where $|\cdot|$ denotes the determinant of the respective matrix and $\boldsymbol{\mu}_i$ and $\boldsymbol{\Sigma}_i$ represent the feature mean vector and the feature covariance matrix of the classes, respectively. It can be shown (Theodoridis and Koutroumbas 2003) that the B-distance is related monotonically to minimum attainable classification error or *Chernoff bound* for the probability of classification error using a Bayes classifier and it is used as a class separability measure.

The values of the criteria are computed for each of the features and then are ranked in order of descending values. The best values can describe the classification effectiveness of individual features or feature vectors. Features of potential interest include the average standard deviation (ASD), average entropy (AE), homogeneity (H) and the proposed regularity indices (RI_1, RI_2). These features are computed for each one of the building polygons from the reference data (“Collapsed” and “Uncollapsed” visually classified buildings, please refer to Table 4-3). Fisher discriminant ratio and one-dimensional B-distance measurements of these imagery features are calculated and presented in Table 6-1.

Table 6-1: FDR and B-distance of one-dimensional features (texture features) for bi-level classification (“Collapsed” and “Uncollapsed”)

Kobe data set					
	RI_2	RI_1	H	AE	ASD
FDR	2.43	1.96	1.06	0.75	0.73
B-distance (One-dimensional)	0.68	0.50	0.30	0.24	0.18
Bam data set					
	RI_1	RI_2	ASD	AE	H
FDR	1.10	0.89	0.68	0.15	0.05
B-distance (One-dimensional)	0.35	0.23	0.17	0.10	0.04

In this table the discrimination properties of individual features are presented. Both B-distance and FDR measurements indicate that the regularity indices are marginally more effectual separators for “Collapsed” and “Uncollapsed” buildings categories. In Bam city most buildings were made of clay bricks, and resulting textural features are not robust separators, although using boundary feature (RI_1) yields the best result with the largest B-distance.

Table 6-2: The performance of n-dimensional features evaluated by B-distance criterion for bi-level classification (“Collapsed” and “Uncollapsed”)

B-distance for Kobe data set					
2-dimesional feature vector		3-dimensional feature vector		4-dimensional feature vector	
RI ₁ , RI ₂	1.26	H, RI ₁ , RI ₂	1.71	AE, H, RI ₁ , RI ₂	2.22
H, RI ₁	1.24	AE, RI ₁ , RI ₂	1.71	ASD, AE, RI ₁ , RI ₂	2.21
AE, RI ₁	1.18	ASD, H, RI ₁	1.70	ASD, H, RI ₁ , RI ₂	2.17
ASD, RI ₁	1.16	ASD, AE, RI ₁	1.68	ASD, AE, H, RI ₁	2.16
AE, RI ₂	0.93	AE, H, RI ₁	1.67	ASD, AE, H, RI ₂	1.90
H, RI ₂	0.93	ASD, RI ₁ , RI ₂	1.66	5-dimensional feature vector	
ASD, RI ₂	0.87	AE, H, RI ₂	1.43	ASD, AE, H, RI ₁ , RI ₂	2.71
ASD, H	0.74	ASD, AE, RI ₂	1.41		
ASD, AE	0.70	ASD, H, RI ₂	1.37		
AE, H	0.69	ASD, AE, H	1.14		
B-distance for Bam data set					
2-dimesional feature vector		3-dimensional feature vector		4-dimensional feature vector	
RI ₁ , RI ₂	0.80	AE, RI ₁ , RI ₂	1.28	ASD, AE, RI ₁ , RI ₂	1.77
ASD, RI ₁	0.80	ASD, RI ₁ , RI ₂	1.28	ASD, H, RI ₁ , RI ₂	1.72
ASD, RI ₂	0.78	ASD, AE, RI ₁	1.28	AE, H, RI ₁ , RI ₂	1.70
AE, RI ₂	0.78	H, RI ₁ , RI ₂	1.22	ASD, AE, H, RI ₁	1.69
H, RI ₂	0.73	AE, H, RI ₂	1.22	ASD, AE, H, RI ₂	1.66
AE, RI ₁	0.72	ASD, AE, RI ₂	1.22	5-dimensional feature vector	
H, RI ₁	0.66	ASD, H, RI ₁	1.21	ASD, AE, H, RI ₁ , RI ₂	2.19
ASD, AE	0.61	ASD, H, RI ₂	1.19		
ASD, H	0.58	AE, H, RI ₁	1.13		
AE, H	0.53	ASD, AE, H	1.04		

A better alternative is to examine feature vectors. B-distance measurements for all possible combinations of features are presented in Table 6-2. These tests indicate that those combinations which including regularity indices, are superior to the other combinations. However for collapse detection, combination of all five features yields maximum B-distance value (5-dimentional feature vector).

6.4. Review of Classifiers

In this study, a major effort will be devoted to the design of supervised classifiers in a pattern recognition system. Supervised classification methods require prior knowledge of the classes present in the data and identification of training data. It means that a human expert has to determine a set sample of buildings, which are categorized into most likely of damage class. This set of known buildings is called the training set because it is used by classification procedure to learn how to classify buildings. In a general form, feature vectors consist of L feature measurements:

$$\Phi = [\varphi_1, \varphi_2, \dots, \varphi_L]^T \quad (6-11)$$

and the known class labels:

$$\Omega = \{\omega_1, \omega_2, \dots, \omega_C\} \quad (6-12)$$

Assuming the training set of size R as pairs of the form:

$$\{(\Phi_i, \omega) | \omega \in \Omega, i = 1, 2, \dots, R\} \quad (6-13)$$

The objective is to predict the class label of a building, which is attributed by a new observation Φ using the knowledge from the training set.

The main objective of this section is to compare three classification methods for damage classification: k-Nearest Neighbors (k-NN), Bayesian classification and Support Vector Machines (SVM). We will initially focus on the two-class ($C = 2$) case “Collapsed” and “Uncollapsed”, later on we will extend our experimental results to recognize “Collapsed”, “Partially collapsed” and “Uncollapsed” categories. An evaluation of the cross validation method to estimate the error matrix is carried out, comparing the results obtained by these methods with the independent visual interpretation test.

6.4.1. k-Nearest Neighborhood Classifier

The k-Nearest Neighbor (k-NN) technique is a simple and appealing method to address supervised classification. k-NN is one of the most straightforward instance-based learning algorithms (Aha 1997). In instance-based methods, the learning algorithms are lazy-learning algorithms, as they delay the induction process until classification is performed. It bypasses the density function estimation and goes directly to decision rule. k-NN is based on the principle that the instances within a dataset will generally exist in close proximity to other instances that have similar properties. It assumes that points close to each other in feature space are likely to belong to the same class. If the instances are tagged with a classification label, then the value of the label of an unclassified building can be determined by observing the class of its nearest neighbors. The k-NN locates the k nearest instances to the query instance and determines its class by identifying the most frequent class label. In Figure 6-10 visualization of this method, it is assumed there are only two features (φ_1, φ_2) and two different classes. Query ‘?’ is here being classified by its 5 nearest neighbors.

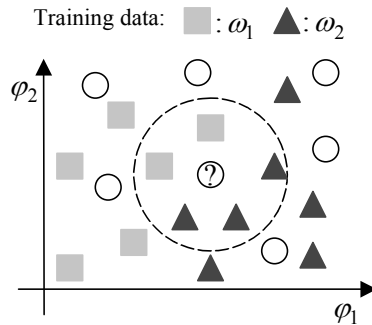


Figure 6-10: k-nearest neighborhood rule, classification into the most abundant class amongst its k neighbors

In general, instances can be considered as points within L -dimensional space. The distance metric must minimize the distance between two similar instances while maximizing the distance between different ones. Various distance measures can be used, including Euclidean and Mahalanobis distance. The choice of distance measure becomes crucial in determining the outcome of nearest neighbor classification. The Euclidean distance measure implies that the input space is isotropic, however, this assumption is generally invalid in practical application. It is clear that the choice of k is critical, since it represents a trade-off between local and global approximation of the probability measures. A serious drawback with k -NN techniques is the complexity and large computation time in search of the nearest neighbors among R available training samples. The problem becomes particularly severe in high dimensional feature spaces. As such, the expected accuracy of k -NN can be a function of parameters including the number of training instances, the number of relevant and irrelevant features, the probability of each attribute, the signal to noise ratio for each type of features and of course k (Guo et al. 2003).

6.4.2. Bayesian Classifier

The Bayesian classifier builds upon probabilistic arguments stemming from statistical nature of the generated features. This is a probabilistic classifier based on applying Bayes' theorem. Bayesian theory gives a mathematical calculus of degrees of belief, describing what it means for beliefs to be consistent and how they should change with evidences (extracted features). Given a classification task of C classes (Ω) and unknown pattern, which is represented by a feature vector Φ , Bayes classifier forms conditional probabilities: $P(\omega_i/\Phi), i=1,2,\dots,C$ which are referred to as "*a posterior probabilities*". Each of this conditional probability represents the probability that unknown pattern belongs to the respective class ω_i given that the corresponding feature vector takes the value Φ . It is assumed that the "*a prior probabilities*" $P(\omega_i)$ are known, if they are not known, they can easily be estimated from available training feature vectors. Indeed, if R is the total number of available training patterns, and R_i of them belong to ω_i then $P(\omega_i) \approx R_i/R$.

The distribution of the feature vectors in each of the classes is conditional probability density functions: $f(\Phi/\omega_i)$. It is referred to as *likelihood function* of ω_i with respect to Φ and assuming that to be known. Recall from probability course basics the Bayes rule:

$$P(\omega_i/\Phi) = \frac{f(\Phi/\omega_i)P(\omega_i)}{f(\Phi)} \quad (6-14)$$

where $f(\Phi)$ is the probability density function of Φ and for which we have:

$$f(\Phi) = \sum_{i=1}^C f(\Phi/\omega_i)P(\omega_i) \quad (6-15)$$

The Bayes classification rule can now be stated as:

$$\forall j, j \neq i \quad \text{if} \quad P(\omega_i/\Phi) > P(\omega_j/\Phi) \quad \text{then} \quad "\Phi \text{ is classified to } \omega_i" \quad (6-16)$$

It is equivalent to partitioning the feature space into C regions by a decision surface in the multidimensional feature space. In practice, one of the most commonly density functions, which models adequately a large number of data, is the Gaussian density function. The likelihood

functions of ω_i with respect to Φ in the L -dimensional feature space follow the general multivariate normal density:

$$f(\Phi/\omega_i) = \frac{1}{(2\pi)^{L/2} |\Sigma_i|^{L/2}} \exp\left(-\frac{1}{2} (\Phi - \mu_i)^T \Sigma_i^{-1} (\Phi - \mu_i)\right), i = 1, 2, \dots, C \quad (6-17)$$

where $\mu_i = E[\Phi]$ is the mean value of the ω_i class and Σ_i the $L \times L$ covariance matrix:

$$\Sigma_i = E[(\Phi - \mu_i)(\Phi - \mu_i)^T] \quad (6-18)$$

From a mathematical point of view, instead of working with probabilities it may be more convenient to work with a discriminant function $h_i(\Phi)$, which is a monotonically increasing function. The decision test is now stated as:

$$\text{if } h_i(\Phi) > h_j(\Phi), \forall i \neq j \quad \text{then} \quad " \Phi \text{ is classified to } \omega_i " \quad (6-19)$$

We can define the decision surfaces for separating class regions:

$$h_{ij}(\Phi) \equiv h_i(\Phi) - h_j(\Phi) = 0, \quad i, j = 1, 2, \dots, C, i \neq j \quad (6-20)$$

To design discriminant function for Bayesian classifier the exponential form is preferable:

$$h_i(\Phi) = \ln(f(\Phi/\omega_i)P(\omega_i)) = -\frac{1}{2}(\Phi - \mu_i)^T \Sigma_i^{-1} (\Phi - \mu_i) + \ln P(\omega_i) - \frac{L}{2}(\ln 2\pi + \ln |\Sigma_i|) \quad (6-21)$$

In general this is a nonlinear quadratic form and the Bayesian classifier is a quadratic classifier and the decision surfaces are hyperquadrics. If we assume that the covariance matrix is the same in all classes, that is, $\Sigma_i = \Sigma$, thus we may redefine $h_i(\Phi)$ as:

$$h_i(\Phi) = \mathbf{a}_i^T \Phi + b \quad (6-22)$$

where:

$$\mathbf{a}_i = \Sigma^{-1} \mu_i, \quad b = \ln P(\omega_i) - \frac{1}{2} \mu_i^T \Sigma^{-1} \mu_i \quad (6-23)$$

Hence $h_i(\Phi)$ is a linear function of Φ and respective decision surfaces are hyperplanes. We can fit a multivariate normal density to each class with a pooled estimate of covariance. This method cannot be applied if a determinant of the covariance matrix derived from some training data becomes zero and an inverse of its matrix does not exist. For these reasons, the principal component analysis is applied before the maximum likelihood classification (Theodoridis and Koutroumbas 2003).

6.4.3. Support Vector Machine (SVM) Classifier

The Support Vector Machines (SVM) classifier is based on statistical learning theory proposed by Vapnik and Chervonenkis (Vapnik 1995). In the case of SVM, we suppose some given data points (extracted features) each belong to one of two classes (ω_1, ω_2) and the goal is to know whether it can separate L -dimensional feature points with $(L-1)$ -dimensional hyperplane. SVM revolve around the notion of a margin in either sides of a hyperplane that separates two data classes. This classification procedure is an extension of the optimum margin algorithm. Maximizing the margin and thereby creating the largest possible distance between the separating hyperplane and the instances on either side of it has been proven to reduce an upper bound on the expected generalization error. The model complexity of an SVM is unaffected by the number of features encountered in the training data. For this reason, SVMs are well suited to deal with learning tasks where the number of features is large with respect to the number of training instances (Kotsiantis 2007).

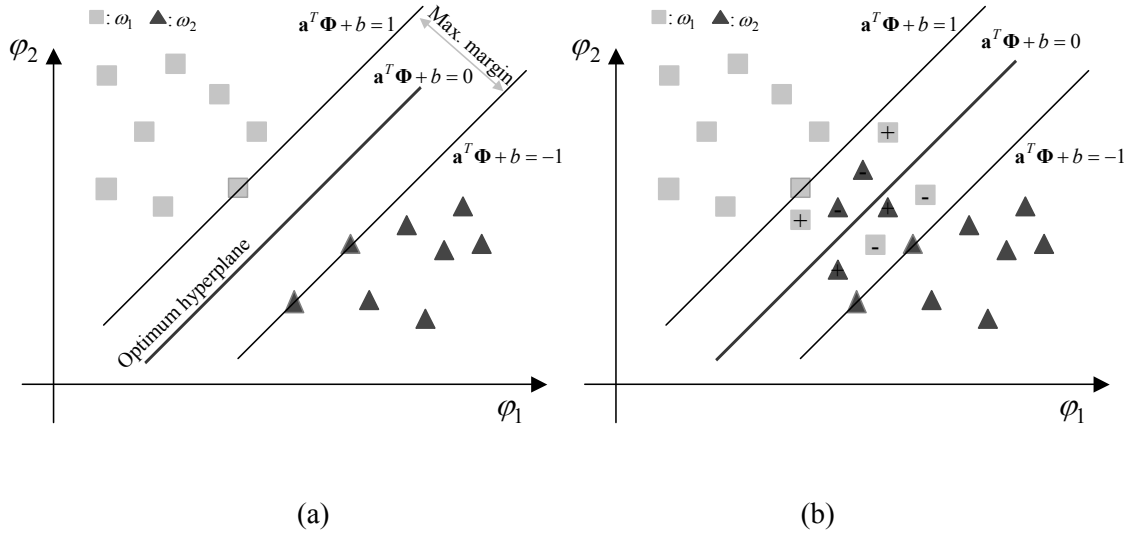


Figure 6-11: Maximum-margin hyperplane and margins for a SVM trained with samples from two classes. Samples on the margin are called the support vectors. a) Separable b) Not separable

If the training data is linearly separable, then the respective decision hypersurface in the L -dimensional feature space is a hyperplane, that is:

$$h(\Phi) = \mathbf{a}^T \Phi + b = 0 \quad (6-24)$$

where $\mathbf{a} = [a_1, a_2, \dots, a_L]^T$ is normal vector perpendicular to the hyperplane. Once the optimum separating hyperplane is found, data points that lie on its margin are known as support vector points and the solution is represented as linear combination of only these points. We want to choose the ' \mathbf{a} ' and ' b ' to maximize the margin, or distance between parallel hyperplanes that are as far apart as possible while still separating the data. It is reasonable to select that hyperplane which has the same distance from respective support vector points in ω_1 and ω_2 (Figure 6-11). Our goal is to search the direction that gives the maximum possible margin. The distance d of a point Φ from a hyperplane $h(\cdot)$ is given by:

$$d = \frac{|h(\Phi)|}{\|\mathbf{a}\|} \quad (6-25)$$

where $| \cdot |$ and $\| \cdot \|$ denote the absolute value and Euclidean norm, respectively. We can now scale \mathbf{a} , b so that the value of $h(\Phi)$, at the nearest points in ω_1 and ω_2 is equal to 1 and -1. These hyperplanes can be described by the equations:

$$\begin{aligned} \forall \Phi \text{ is classified to } \omega_1 : & \quad \mathbf{a}^T \Phi + b \geq 1 \\ \forall \Phi \text{ is classified to } \omega_2 : & \quad \mathbf{a}^T \Phi + b \leq -1 \end{aligned} \quad (6-26)$$

The distance between these two hyperplanes is $\frac{2}{\|\mathbf{a}\|}$, so we want to minimize $\|\mathbf{a}\|$. The minimization can be set up as a convex quadratic programming (QP) problem:

$$\underset{\mathbf{a}, b}{\text{Minimize}} \quad \frac{1}{2} \|\mathbf{a}\|^2 \quad (6-27)$$

$$\text{subject to} \quad c_i (\mathbf{a}^T \Phi_i + b) \geq 1 \quad i = 1, 2, \dots, R \quad (6-28)$$

For each Φ_i the corresponding class indicator is denoted by c_i where: $c_i = +1$ for ω_1 and $c_i = -1$ for ω_2 . This is a nonlinear optimization task subject to a set of linear inequality constraints, which can be solved by standard quadratic programming techniques and programs (Kotsiantis 2007).

In the case where the classes are not separable, the above setup is not valid any more. The problem can be addressed by using a *soft margin* that accepts some misclassifications of the training instances. The method introduces positive slack variable $\xi_i, i = 1, 2, \dots, R$, which measure the degree of misclassification of the datum:

$$c_i [\mathbf{a}^T \Phi_i + b] \geq 1 - \xi_i \quad i = 1, 2, \dots, R \quad (6-29)$$

There are three categories of training feature vectors corresponding to this slack variable:

$\xi_i = 0$: Vectors that fall outside the band and are correctly classified.

$0 < \xi_i \leq 1$: Vectors falling inside the band but still are correctly classified (Figure 6-11(b) '+' sign).

$\xi_i > 1$: Vectors that are misclassified (Figure 6-11(b) '-' sign).

The goal now is to make the margin as large as possible but at the same time to keep the number of points with $\xi_i > 0$ as small as possible. This is equivalent to minimize following cost function:

$$\begin{aligned} \underset{\mathbf{a}, b, \xi}{\text{Minimize}} \quad & \frac{1}{2} \|\mathbf{a}\|^2 + K \sum_{i=1}^R \xi_i \\ \text{subject to} \quad & c_i [\mathbf{a}^T \Phi_i + b] \geq 1 - \xi_i, \xi_i \geq 0, i = 1, 2, \dots, R \end{aligned} \quad (6-30)$$

The parameter K controls the trade-off between the slack variable penalty and the size of margin. The problem is again a convex programming and can be solved using Lagrange multipliers (Theodoridis and Koutroumbas 2003). However, there is an elegant property in the SVM methodology that can be exploited for non-linear classifiers by applying the kernels functions. The resulting algorithm is formally similar, except that every inner product is replaced by a nonlinear kernel function (Genton 2001).

The SVM is only directly applicable for two-class tasks. Therefore, algorithms that reduce the multi-class task to several binary problems have to be applied. Due to various complexities, a direct solution of multi-class problems using a single SVM formulation is usually avoided. The better approach is to use a combination of several SVM classifiers to solve a given multi-class problem. In particular, one technique in practice has been one-versus-all classifiers (OVA), and to choose the class which classifies the test datum with greatest margin. OVA constructs C binary classifiers, a feature point would be classified under a certain class if and only if that class's SVM accepted it and all others rejected it. Another strategy is to build a set of one-versus-one (OVO) classifiers, and to choose the class that is selected by the most classifiers. This method constructs one binary classifier for every pair of distinct classes and so, all together $C(C-1)/2$ binary classifiers are constructed. The binary classifier c_{ij} is trained taking the examples from ω_i as positive and examples from ω_j as negative. For a new example Φ , if classifier c_{ij} says Φ is in class ω_i the vote for class ω_i is added by one, otherwise, the vote for class ω_j is increased by one. After each of the $C(C-1)/2$ binary classifiers makes its vote, OVO strategy assigns Φ to the class with the largest number of votes. This method leaves regions of the feature space undecided where more than one class accepts or all classes reject (Figure 6-12). As suggested by Platt (2000) the OVO approach is an efficient multi-class SVM and was therefore used in our study.

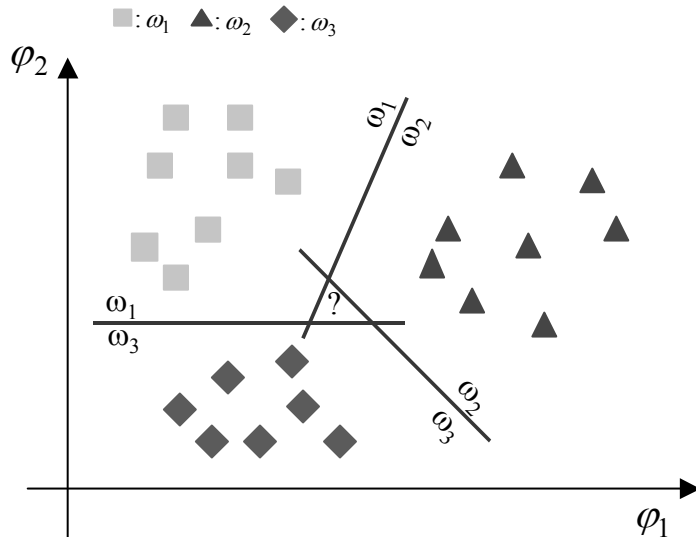


Figure 6-12: Diagram of One-Versus-One (OVO) SVM decision boundaries on a basic problem, “?” represents unclassified region

6.5. Empirical Investigations

6.5.1. Automatic Collapse Detection using Post-event Imagery Data

Figure 6-13 depicts a flowchart of operations for collapse detection using imagery features. Here, we use only the post-earthquake images and the pre-earthquake images are not needed. The regions of interest are delineated with the aid of prismatic model of buildings. Since our data set includes aerial images, the object to image transformation will be established using traditional aerial photogrammetry knowledge. The implemented program extracts all attributes including statistical features (average standard deviation, average entropy and homogeneity) and regularity indices for any building polygon.

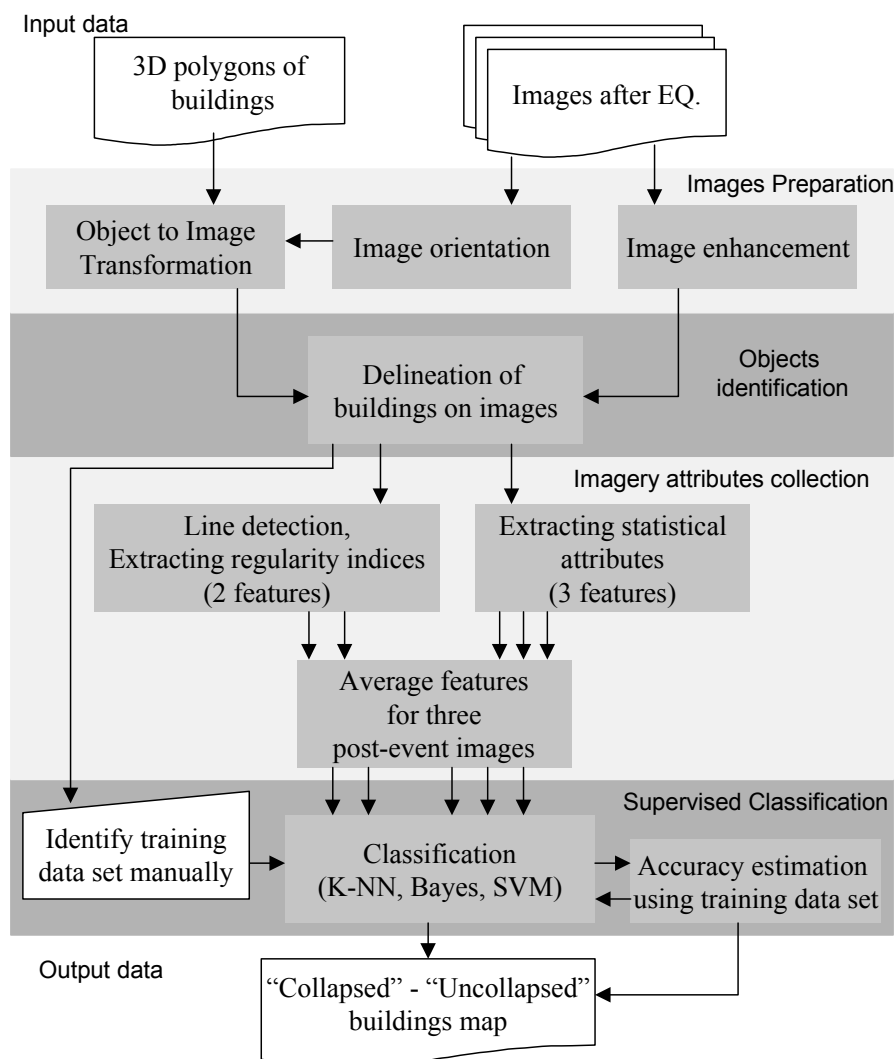


Figure 6-13: The processing flowchart collapse detection using post-event imagery features

The variables resulting from this procedure are calculated for a triplet set of post-event aerial images and final normalized features are generated from average values. The variance of the features can provide us with a quantitative basis to screen out non-discriminative features before feature subset selection. Our study compares three classification methods (k-Nearest Neighbors, Bayesian and Support Vector Machines) for the production of collapse maps from aerial images.

After performing the classification, it is important to evaluate the quality of the results. The ideal process is to have an independent set of test data. Unfortunately this kind of information is rarely available. An alternative form is to split the training data into two sets: one to be used for training and the other for validation. The classification results were evaluated by a cross-validation method and by an independent visual interpretation test set. We used cross-validation techniques for assessing how the results of classification will generalize to an independent data set. We used *random sub-sampling validation* technique. This method randomly splits the dataset into training and validation data. For each such split, the classifier is retained with training data and validated on the remaining data. The process is repeated for each of the subsets as validation. The error matrix from each split can then be averaged. In this method all observations are used for both training and validation. The goal of cross-validation is to estimate the expected level of accuracy to a data set that is independent of the data that were used to train the model. Primarily, a bi-level classification is tested in order to generate a map of “Collapsed” and “Uncollapsed” buildings and draw a comparison with the hypothesis test results in Chapter 5.

The procedures of image enhancement and orientation are performed by commercial software but features extraction - especially line detection algorithm (Hierarchical Permissive Hough Transform) - are implemented with customized codes. We used combination codes of C++ and Matlab (ver. 7.4.0 R2007a) to implement the described procedures in Figure 6-13. Statistical features as well as the second regularity index (RI_2) are calculated only for pixels within building polygons so that only roof textures are employed for classification. However, the first regularity index (RI_1) looks for intact lines around the building footprint. Therefore, the collapsed buildings such as “pancake” and “overturned” that shifted from initial position can be detected using this attribute (RI_1).

The k-nearest neighbor classifier was conducted with Euclidian distance metric. A direct majority vote from the nearest three neighbors ($k = 3$) was employed. The naive version of the algorithm is easy to implement by computing the distances from the test sample to all stored vectors, but it is computationally intensive, especially when the size of the training set grows. The experiments showed that the performance of k-NN was not sensitive to the exact choice of k when k was large. Although for small values of k , the k-NN algorithm was more robust than the 1-NN algorithm. We used a linear form of Bayesian classifier using a pooled estimate of covariance matrix. The experiments showed that for our data set there is no significant preference between quadratic or linear form of this classifier. The major advantage of the naïve Bayes classifier is its short computational time for training. We used Matlab ready functions for SVM classification using a linear kernel. For training, a Sequential Minimal Optimization (SMO) method is conducted. SMO is a simple algorithm, which is conceptually incomplex, easy to implement without any extra matrix storage and without using numerical quadratic programming optimization at all (Platt 2000). To control the tradeoff between margin width and misclassification we specified a scalar value 0.5 (Equation 6-30) for the box constraint parameter of soft margin.

Table 6-3 present average error matrix and accuracy assessments for the three classifiers: 3-NN, Bayesian and SVM. Sample buildings (fifteen buildings for each class) were acquired as a training set. Validations are performed 100 times each time with new training data set for obtaining average values of error matrix components.

Table 6-3: Average error matrix of 100 times cross validation for collapse detection – image features

Input data: post-event aerial images + building polygons	Visual interpretation			
	Kobe		Bam	
	Uncollapsed	Collapsed	Uncollapsed	Collapsed
3-NN classifier				
Uncollapsed	247	51	333	119
Collapsed	30	309	75	363
Accuracy Assessment - 3-NN classifier				
Overall accuracy	87.3%		78.2%	
Producer's accuracy	89.2%	85.8%	81.6%	75.3%
User's accuracy	82.9%	91.2%	73.7%	82.9%
Kappa	74.4%		56.5%	
Bayesian classifier	Uncollapsed	Collapsed	Uncollapsed	Collapsed
Uncollapsed	241	35	340	123
Collapsed	36	325	68	359
Accuracy Assessment - Bayesian classifier				
Overall accuracy	88.9%		78.5%	
Producer's accuracy	87.0%	90.3%	83.3%	74.5%
User's accuracy	87.3%	90.0%	73.4%	84.1%
Kappa	77.3%		57.2%	
SVM classifier	Uncollapsed	Collapsed	Uncollapsed	Collapsed
Uncollapsed	244	36	342	116
Collapsed	33	324	66	366
Accuracy Assessment - SVM classifier				
Overall accuracy	89.2%		79.6%	
Producer's accuracy	88.1%	90.1%	83.8%	75.9%
User's accuracy	87.1%	90.8%	74.7%	84.7%
Kappa	78.0%		59.2%	

The results achieved with Bayesian and SVM classifier are better than with the 3-NN classifier. The advantages of each classifier can be evaluated by comparing their performance in two different stages: the learning process and the classification process. While the Bayesian classifier performed faster on the learning process, the SVM classifier is faster in the classification process. The advantage of Bayesian classifier is the facility to build the classifier. The basic k-NN has usually

only a single parameter (k), which is relatively easy to tune. Although the SVM shows better overall accuracy, it has more parameters than other techniques and the process of training in SVM classifier is more complicate. However, k -NN is generally considered intolerant of noise and its similarity measures can be easily distorted by errors in attribute values, thus leading it to misclassify a new instance on the basis of the wrong nearest neighbors. The size of the training set has to be sufficiently large. Table 6-4 shows results of using different sizes of training data sets for the Bayesian classifier. In fact, employing large number of buildings as training data increase the accuracy as well as reliability of classifier. Also, using more training data causes difference between the actual accuracy and estimated accuracy - calculated based on the training data set - to be decreased. Our experiments revealed that for both the Kobe and Bam datasets minimum fifteen buildings per each class could be suitable for training procedure. Numerical results show that damage detection using only imagery attributes and hypothesis test method using height difference are in competition with each other (Tables 5-3,4). However, in our study, hypothesis test is made based on DSMs being generated automatically from imagery data. Next section, we will propose an integrated system of both types of features extracted from object and image space in order to perform multi-level damage classification.

Table 6-4: Average overall accuracies (\pm std.) and difference between actual and estimated values of 100 times cross-validation for various sizes of training sets

Bayesian classifier	Number of buildings selected as training set for each class – Kobe dataset					
	5	10	15	30	60	100
Overall accuracy	%81±7	%87±3	%89±2	%90±1	%90±1	%91±1
Average difference between estimated accuracy and actual accuracy	%16.5	%8.3	%4.9	%2.1	%1.2	%0.3
Bayesian classifier	Number of buildings selected as training set for each class- Bam data set					
	5	10	15	30	60	100
Overall accuracy	%70±9	%78±4	%79±2	%81±1	%82±1	%82±0.5
Average difference between estimated accuracy and actual accuracy	%24.4	%10.8	%5.0	%3.2	%1.0	%0.5

6.5.2. Automatic Classification of Collapsed buildings using Pre- and Post-event Images and DSMs

What are presented so far only describe methods to detect damaged buildings through bi-level classification. In this section we will present an integration system for multi-level damage classification. Figure 6-14 describes a flow diagram of the implemented system which endeavor to detect uncollapsed, partially collapsed (G4) and totally collapsed (G5) buildings using image and object space features together. As before, we assume building polygons have been already identified and objects of interest are already determined in both image and object spaces.

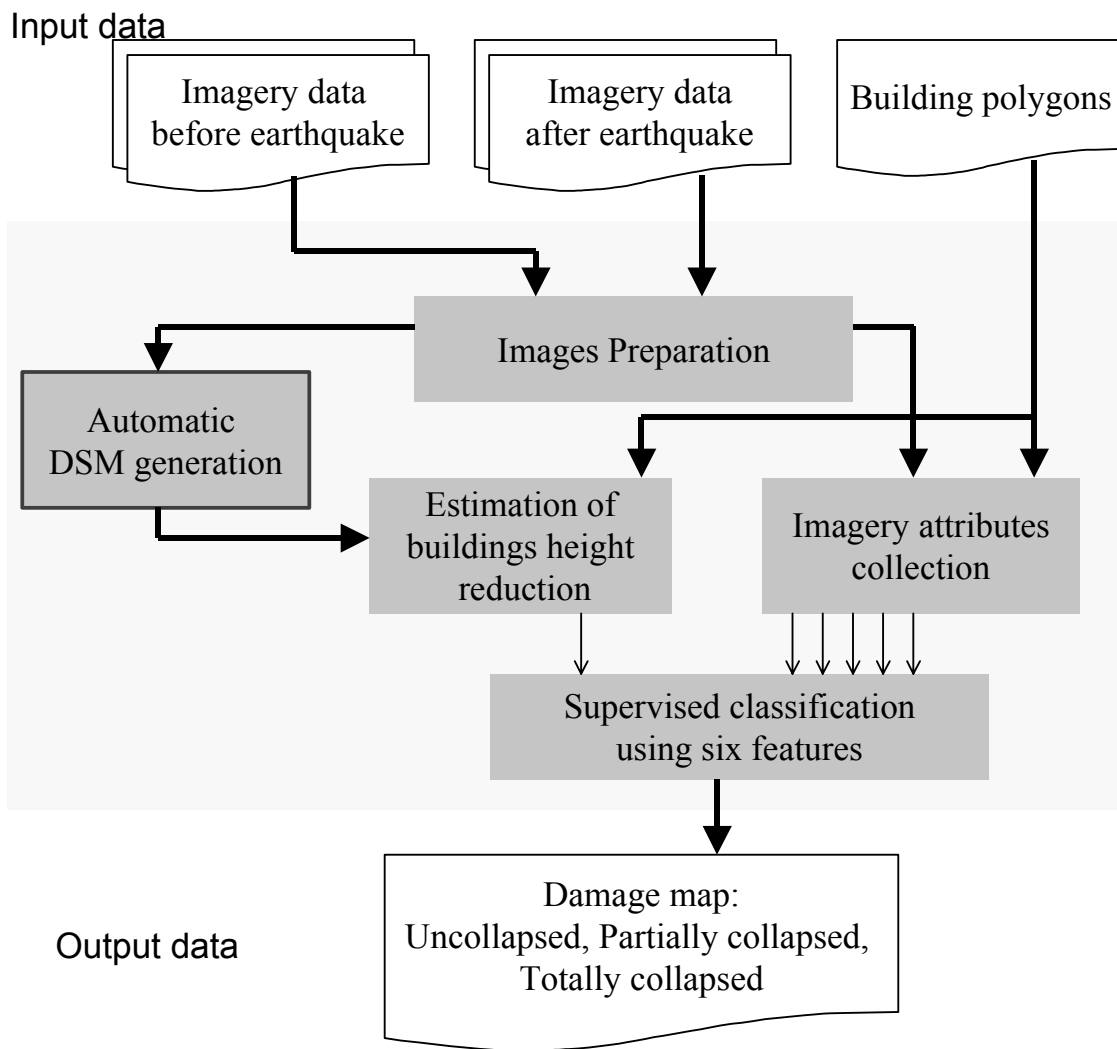


Figure 6-14: The processing flow diagram for automatic classification of collapsed buildings using object and image space features

In Chapter 5, it became clear that comparing even imprecise digital surface models could help to detect collapsed buildings. We used a p-value of average height difference (AHD) between before and after earthquake for the hypothesis test. Here, we append this p-value as a new feature to the imagery features input into the multi-level supervised classification procedure. Among other features, the average height difference as well as regularity indices have the most potential for separating damage categories. It is expected that fully collapsed buildings (G5-H) reflect large values of AHD accompanied by lack of borderlines (low RI₁) and rough texture (high RI₂). The inclined, pancake and overturned buildings can be discriminated by shifted footprints (low RI₁) but regular textures (low RI₂). The buildings with slight height reduction and irregular texture should be classified as partially collapsed. Figure 6-15 shows a three dimensional feature space and their classes for Kobe data set. We perform tri-level classification into “Uncollapsed”, “Partially collapsed” and “Totally collapsed” categories. Table 6-5 presents numerical results of cross-validation for applying three classifier: 3-NN, Bayesian and one-versus-one SVM method. To

implement OVO-SVM, we used three bi-level SVMs voting for possible combinations. Buildings without majority vote have to be identified as “Unclassified” which needs to be inspected visually. Some sample buildings (fifteen buildings for each damage class) were acquired as a training set. A high degree of agreement is evident between the assessment results and the reference data in the “Totally collapsed” state. Using a Bayesian classifier, of these buildings 258 were correctly labeled obtaining producer’s and user’s accuracy of 84.6% and 92.5% respectively in Kobe, and in Bam 249 out of 298 severely damaged buildings were correctly labeled as “Totally collapsed” resulting producer’s and user’s accuracy of 83.6% and 88.3%, respectively.

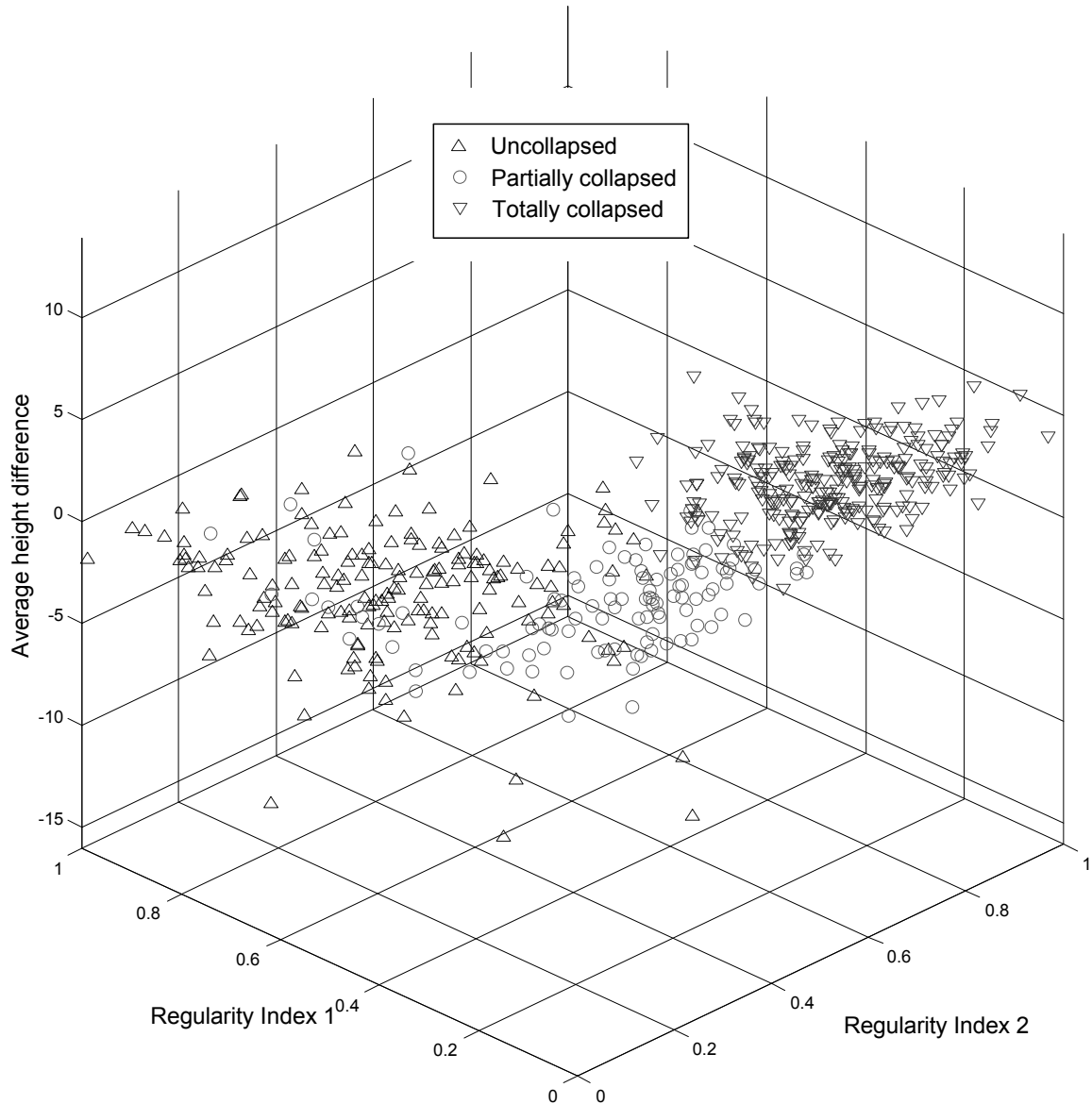


Figure 6-15: Feature space and actual distribution of labeled buildings (determined by visual interpretation for Kobe dataset)

Table 6-5: Average error matrix of 100 times cross validation for collapse classification

Input data: post-event aerial images, DSMs + building polygons		Visual interpretation				
		Kobe			Bam	
3-NN classifier	Uncollapsed	Partially collapsed	Totally collapsed	Uncollapsed	Partially collapsed	Totally collapsed
	Uncollapsed	200	27	9	273	41
	Partially collapsed	69	19	44	121	112
	Totally collapsed	8	9	252	14	31
Accuracy Assessment - 3-NN classifier						
Overall accuracy	73.9%			71.2%		
Producer's accuracy	72.2%	34.6%	82.6%	66.9%	60.9%	83.6%
User's accuracy	84.8%	14.4%	93.7%	85.6%	40.4%	84.7%
Kappa	57.9%			56.5%		
Bayesian classifier	Uncollapsed	Partially collapsed	Totally collapsed	Uncollapsed	Partially collapsed	Totally collapsed
	Uncollapsed	208	24	7	296	42
	Partially collapsed	59	20	40	103	118
	Totally collapsed	10	11	258	9	24
Accuracy Assessment - Bayesian classifier						
Overall accuracy	76.3%			74.5%		
Producer's accuracy	75.1%	36.4%	84.6%	72.5%	64.1%	83.6%
User's accuracy	87.0%	16.8%	92.5%	86.6%	44.4%	88.3%
Kappa	61.2%			61.1%		
SVM classifier OVO method	Uncollapsed	Partially collapsed	Totally collapsed	Uncollapsed	Partially collapsed	Totally collapsed
	Uncollapsed	213	24	7	315	39
	Partially collapsed	57	22	34	83	121
	Totally collapsed	5	8	263	5	19
Unclassified	2	1	1	5	5	4
Accuracy Assessment - SVM classifier, one versus one method						
Overall accuracy	78.6%			78.7%		
Producer's accuracy	77.5%	40.7%	86.5%	78.2%	67.6%	86.0%
User's accuracy	87.3%	19.5%	95.3%	88.2%	50.0%	91.3%
Kappa	64.9%			67.2%		

The user's accuracies of "Partially collapsed" buildings were computed as 16.8% and 44.4% using a Bayesian classifier and 19.5% and 50.0% using an OVO-SVM classifier for Kobe and Bam, respectively. Since, the average value of height reduction is the dominant feature to detect "Partially collapsed" buildings, using imprecise DSMs increases the commission errors. In other words, some uncollapsed buildings with error in their height values may be categorized as partially collapsed, which decrease the user's accuracy.

The erroneous categorized buildings were investigated to find out what might have caused them to deviate from the reference data. There seem to be two reasons that cause false classifications. The first and main reason is the problems in the DSM generation due to occlusions, shadows and trees. Therefore the height estimation is not of sufficient accuracy in this area and leads to an overlap between "Partially collapsed" and "Uncollapsed" in feature space (Figure 6-15). The second reason is the absence of the imagery features in the area where the buildings are hidden in the shadows or occluded by other objects. It should be noted that for complex shapes building borderlines couldn't be matched exactly with building polygon. It is therefore impossible to find line segments corresponding to the line of the building polygon. Moreover, the interpretation of damages in the Bam usually is a straight choice, mainly either fully collapsed or partly collapsed both converted to debris heap. But in the Kobe earthquake, partly damaged buildings mainly are classified as inclined, overturned and pancake buildings. To detect these categories one needs to the more detailed and precise geometrical data. This is the reason why user's accuracy of "Partially collapsed" in Bam is better than Kobe (because most of the damaged buildings exhibit simple shape). However, it revealed that for both dataset less than ten buildings (about 2%) of totally collapsed category were classified as "Uncollapsed" which is quite encouraging. The results of the analysis show that using multiple features can be useful to classify damages automatically and with high success rate. This can give first very valuable hints to rescue teams.

6.6. Summary

Imagery features are valuable data for detecting damaged structures, although buildings may reflect different and diverse forms of imagery features. In this chapter, three statistical features (ASD, AE, H) of collapsed and uncollapsed buildings were evaluated. Moreover, we presented two features based on composition of lines, so called "Regularity Indices" (RI_1 and RI_2). For this purpose, a modified version of the Hough Transform was implemented for the line detection procedure. Functional distance measurements of class separability as well as numerical results showed that using regularity indices significantly improve bi-level classification of damaged buildings (i.e. "Collapsed" and "Uncollapsed"). Three kinds of classification methods: k-NN, Bayesian and SVM were used and compared. The classification results were evaluated by a cross-validation method and by the independent visual interpretation test set. The Support Vector Machine (SVM) classifier is a relatively new method that proved to be quite effective for damage detection. Also, an integration of object and image space features was applied through classifiers for detecting three attributes of building ("Uncollapsed", "Partially collapsed" and "Totally collapsed"). The results of the analysis showed that using multiple features can be useful to classify collapsed buildings automatically and with high success rate.

In next chapter and according to previous studies, we are going to open new aspects of the research for damage classification. We aim to reach the following objectives:

- Until now, building position has been assumed to be known by a supporting data, we intend to extract buildings as automatically as possible

-For multi-level damage classification, an evidence base expert system using Bayesian networks will be presented. This system utilize following possibilities:

- Use of multi-image data that helps against occlusions and gives more reliability in feature extraction.
- Use of color images – this improves the image information (better radiometric depth allows to look into the shadows as well as using color information).



Figure 6-16: Study Area in Bam city, results of automatic collapse classification using OVO-SVM classifier, ■: Uncollapsed, □: Partially collapsed, ▢: Totally collapsed, □: Unclassified



Figure 6-17: Study Area in Kobe city, results of automatic collapse classification using OVO-SVM classifier, ■: Uncollapsed, □: Partially collapsed, ▢: Totally collapsed, □: Unclassified

AUTOMATIC RECOGNITION OF DAMAGED BUILDINGS USING MULTI-VIEW AERIAL IMAGES

Automated image understanding is an entire branch of the computer vision and photogrammetry fields, which is devoted to understand and duplicate the functions that the human visual system performs on a regular basis. In this chapter, we seek to develop a system that automatically interprets data produced by aerial sensors before and after an earthquake in order to arrive at a detailed damage map quickly after disaster. The research focuses on the interpretation of aerial images of urban areas so that prior information about building positions is not available. Given the set of aerial images of a city, the proposed system selectively applies image-understanding algorithms to recognize buildings prior to classifying the scene. Information gathered by the recognition algorithms should guide the damage classification of the scene as completely and as accurately as is possible given the available data. We aim to apply recent techniques of uncertain reasoning and decision making to damage detection and classification. We introduce a pointwise analysis technique for the recognition and subsequent classification of a different level of damage types. By using this technique in concert with other algorithms, we show that the decision procedure for each point of object space can be performed based on extracted evidences from image segments as well as surface models.

7.1. Overview of Related Works for Automatic Buildings Extraction

Over the past several years, considerable research was directed toward extracting buildings from remote sensing data. Comprehensive overviews are given in Baltsavias 2004 and Brenner 2005 and many studies are presented in the books of the Ascona Workshops (Gruen *et al.* 1995, Gruen *et al.* 1997, Baltsavias *et al.* 2001) and the SMATI2 book (Förstner and Plümer 1997). Principally, automatic object extraction consists of three steps: detection, reconstruction and attribution (Gruen 2000). Detection does not necessarily require the knowledge of the object outline, but, as a minimum requirement, should be able to produce image windows containing the outline. Reconstruction creates the 3-D geometric model of the object with the level of required detail. The model should convey information about type, shape and other related information of the building. With attribution, we mean semantic/functional properties or topological information. It would be helpful in assessing the damage. There is a wide range of data, which is used for the detection and reconstruction of building objects: aerial and satellite imagery with single, stereo, or multiple image frames, LIDAR, SAR, existing maps, GIS, etc. The images are may be in grayscale, color or multi-spectral. Moreover, there are supporting data such as scanned maps or existing 2D GIS data, plus additional information and knowledge such as position of the sun, time of primary data acquisition, texture, shadows, and reflection properties (Durupt and Taillandier 2006).

Detection of buildings can rely on simple characteristics, which distinguish buildings from non-buildings. In fact, depending on the type of basic data, the utilized methods vary. In digital surface

models (DSMs) this might be the relative height and size of regions with heights larger than the surroundings. DTMs/DSMs could be derived directly from laser scanning data or photogrammetric techniques. By subtracting the DTM from the DSM (i.e. nDSM) and by applying a threshold to the height differences, an initial building mask is created (Weidner, 1997; Ameri, 2000). An alternative method to DSM normalization was proposed in (Baltsavias et al. 1995). It is based on the use of multiple height bins. In this method the DSM heights are grouped into consecutive bins (height ranges) of a certain size that are always closed and are easy to extract. But besides buildings also trees are objects that represent local peaks (blobs) in the DSM. Using DSMs, the various approaches have been presented to separate man-made objects from vegetation. Obviously, a determinative parameter to adopt the approaches is DSM accuracy. The local variations of the DSM normal vectors can be used to eliminate these areas. The vegetation regions can be eliminated by evaluating a “terrain roughness” criterion derived by an analysis of the second derivatives of the DSM (Maas 1999, Oude Elberink and Maas 2000, Niederöst 2003). Brunn and Weinder (1997) discriminated buildings and vegetation by utilization of differential geometry via Bayesian networks. Using exact DSM generated by LIDAR system gives possibilities for discriminating between buildings and vegetation area. Attributes derived from the height information such as variance of surface normals as indicator for crease edges, height texture such as the co-occurrence matrix and contrast texture measures and distribution of gradient directions were used to extract vegetation areas and building roof structures. In the pulsed laser system, a part of the laser beam penetrates to foliage and is reflected by the ground, which is called “last echo”. The comparison between first and last echo of the laser pulse allows the detection of vegetation regions (Steinle and Vögtle 2000). Additional to multiple pulse measurements the intensity of the returned pulses is also measured. Different surfaces in the landscape will absorb/reflect pulses differently and therefore it may be possible to use this information in classifying points. Moffiet et al. (2005) investigated the capabilities of the different returns (ground and vegetation, first, last, and single pulse) as well as the related intensity to classify diverse tree types. Tovari and Vögtle (2004) used laser pulse intensities among other features. They used a fuzzy logic classifier in order to discriminate buildings, vegetation, and terrain. It should be reminded that after an earthquake, blobs on DSM might be reflections of remainders of damaged objects and therefore individually cannot be conclusive evidences for building detection. Thus a method has to be devised to separate man made objects from vegetation objects based on various input data sets such as, infrared imagery or color imagery. However, image features cannot be extracted reliably, due to image noise, low contrast, disturbing objects etc.

For building reconstruction from images the situation is more complicated and the quality of results is closely related to the complexity of the scenes been processed. When analyzing images and in order to prevent simple solutions there are some characteristics of image data, which have to be taking into account (Förstner 1999): 1) 2D data in image causes indeterminism about the form of 3D objects, 2) The objects are occluded by themselves or by other objects, causing lack of information, while other object parts lead to additional irrelevant data. Taking the projection into account, rectangles formed by image edges are an efficient way to set up hypotheses. The selected hypotheses undergo a validation process based on the shadow and/or wall verification process (Irvin and McKeown 1989, Wang and Schenk 1992). In (Lin et al. 1995) a system is described for detection and description of buildings from the monocular views of arbitrary aerial scenes. Such system generally uses a perceptual grouping approach (Huertas and Nevatia 1988, Mohan and Nevatia 1989, Huertas et al. 1993, Collins et al. 1995) to generate the roof hypotheses based upon very specific geometric properties of the building structures, which restrict the shapes of buildings to be a single or composition of rectangular parallelepipeds. For high-resolution images of densely built-up urban areas (such as Kobe dataset), automatic building extraction is very difficult because

of some intrinsic challenges. Firstly, there are hundreds of buildings with diverse appearances in the same scenes. They may appear very differently in intensity levels, shapes and structures. Moreover, accompanied with the increase of the image resolution, most buildings' sub-structures are visible which make discrimination between buildings and their sub-structures difficult and intrinsically ambiguous (Song et al. 2008).

Recently, there is a strong trend towards information fusion and introducing approaches using combinations of DSM data and high-resolution images (Sohn and Dowman 2007, Yong and Huayi 2008). Cues such as color and DSM data have proved to be particularly valuable to be combined. A conceptual framework for automated building detection analyzing multiple cue data is described in (Zimmermann 2005). The proposed framework integrates several low-level image-processing algorithms to derive from different cues as color, texture, edges and elevation data features to detect and recognize buildings. Results of combining points from laserscanners and image data prove that very high quality models can be generated (Dorninger and Nothegger 2007). Cues derived from different sources should support and supplement each other. However, numerous conflicting cues appear in case of complex scenes. Kulszewski and Koch (1999) reported a method for building recognition based on a dynamic Bayesian network in a single aerial image. The image features, faces of walls and roofs are detected in a face adjacency graph and aggregated to buildings. The Bayesian network is used in order to deal with decisions under uncertainties (Brunn and Weidner 1997, Nevatia et al. 1999). Bayesian networks appear a promising tool for qualitative recognition of buildings in aerial images.

7.2. Automatic Damage Classification

7.2.1. Overall View of Our Strategy

In this research, we aim to detect the points belong to buildings rooftop and comparing these points before and after earthquake in order to detect damaged points. In the proposed method, we deal with decision making for each single point of object space employing features extracted from segments in image space (Figure 7-1). Therefore, the goal is to detect and discern damaged points rather than extracting geometrical model of buildings. Within a particular area, the number and severity of the damaged points are translated to damage scale while this area can either a building rooftop or a district zone or even the whole of a city. Another aspect of the proposed system is to handle “uncertainty” based on available information. The system emphasizes a knowledge-based framework that directs basic geometric pattern of damages and combines evidences from different sources to reach most likely description of related category of damage. The framework is constructed so that the underlying specialized algorithms for evidence acquisition are nearly independent of the engineered domain knowledge and reasoning system (Figure 7-1). Thus, changes to the knowledge base often will not require significant changes to the underlying image understanding algorithms. This generality allows the system to categorize damage types from imagery data with only minimal changes to the knowledge base and no changes to the specific image understanding algorithms. Knowledge is represented in our system as a set of obvious assumptions about damaged or undamaged man-made objects. This is accomplished through the selective application of algorithms to segmented fields in data and combining their result in a Bayesian network. The network provides pointwise classification based on prior information of image segments. The use of Bayesian networks to represent prior knowledge about the scene proves to be a straightforward technique for designing knowledge-based vision systems.

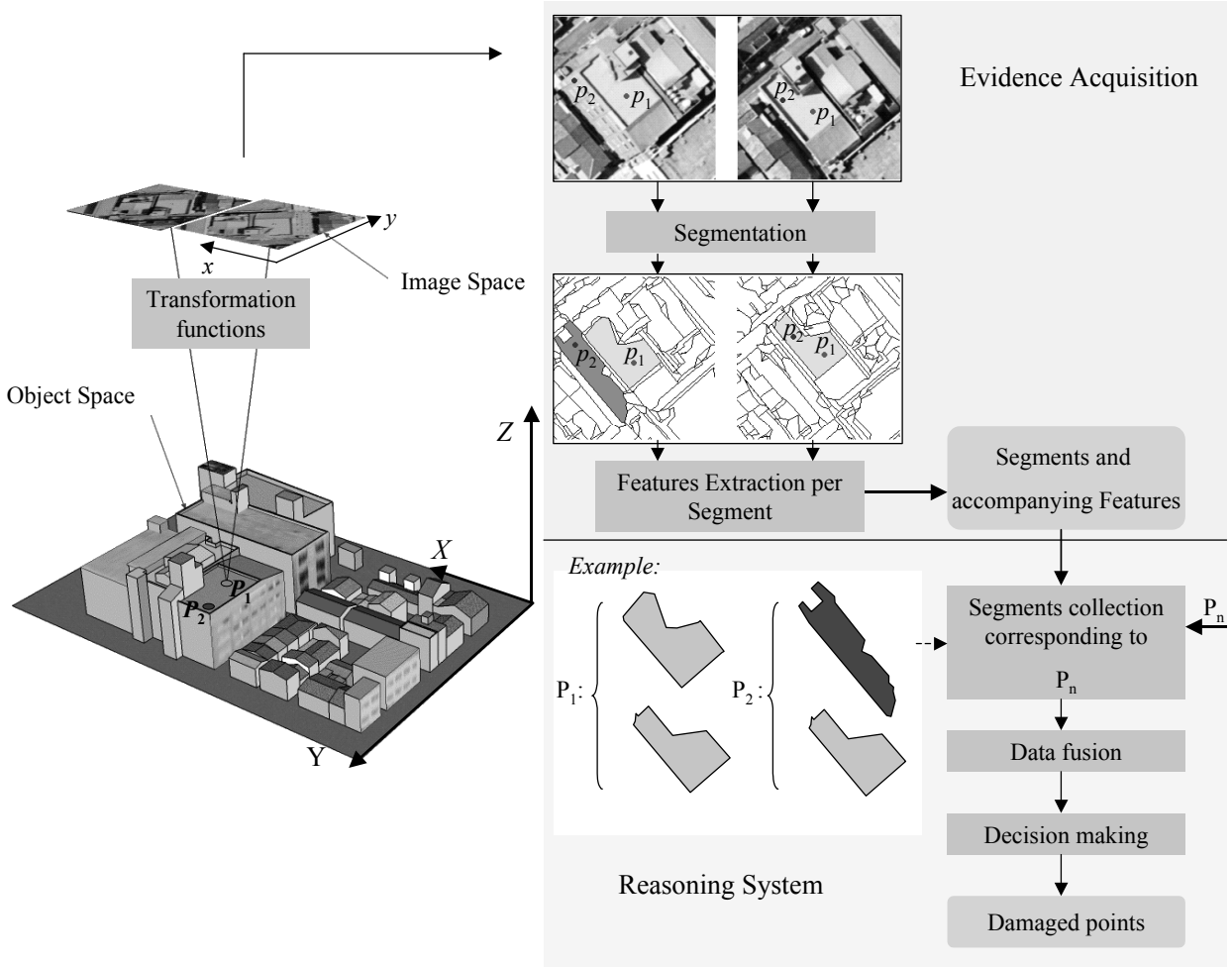


Figure 7-1: The reasoning system will make a decision for given points (P_n) based on the collected evidences from corresponding image segments – (P_2 is projected on different segments due to DSM error)

7.2.2. Problem Formulation and Approach

In general, we assume the object space to be a set of infinite discrete three-dimensional points at a given time t :

$$O^t = \{P_n : (X_n, Y_n, Z_n)\} \quad n = 1, 2, \dots ; t = (\text{before, after}) \text{ disaster} \quad (7-1)$$

The image space is a collection of image data accompanied by their orientation parameters (transformation functions). These parameters establish a geometrical relationship between image and object space (Figure 7-1):

$$IMG_i^t = \left\{ \{pixel_m : (\mathbf{p}_m; \lambda_m)\}_i^t, T_i^t \right\}, \quad \mathbf{p}_m = \begin{bmatrix} x_m \\ y_m \end{bmatrix}; i = 1, \dots, I^t; m = 1, \dots, M_i^t \quad (7-2)$$

where IMG_i^t and T_i^t denote the i th image and corresponding transformation function at a given time t . \mathbf{p}_m represents the coordinates of the m th pixel in an image, and λ_m stand for the spectral characteristics of this specific pixel. λ_m may represent B/W, colored or multi-spectral images. I^t represents the total number of available images and M_i^t denotes the number of pixels for the i th image at a given time t .

A digital surface model, generated by either stereo (multiple) images or laser scanner, can be referred to as an estimation of actual Z_n values (\tilde{Z}_n):

$$DSM^t \equiv \tilde{O}^t = \{\tilde{P}_n : (X_n, Y_n, \tilde{Z}_n)\} \quad (7-3)$$

The corresponding image points plus the estimated scene height represent points of the DSM, which are visible in the images:

$$IMG_i^t : \forall pixel_m, \exists \tilde{P}_n : \mathbf{p}_m = T_i^t(\tilde{P}_n) \quad (7-4)$$

If there is more than one \tilde{P}_n that satisfies the aforementioned formula, one with higher Z value is selected.

Here, the main goal is to answer the following questions: does the specific point (P_n) belong to a man-made object? If so, is this a demolished point or not? We endeavor to respond to these questions without any other extra information. For this purpose, we discriminate man-made objects as polyhedral objects, which reflect straight lines in images. Accordingly, we partition each image into polygonal segments. Such segments of image space may represent polyhedral planes in object space. Thus

$$\begin{aligned} S_{i,j}^t &= \{pixel_m : (\mathbf{p}_m; \lambda_m; \tilde{P}_n)\}_{i,j}^t \\ m &= 1, \dots, M_{i,j}^t \quad \text{where: } M_i^t = \sum_j M_{i,j}^t \end{aligned} \quad (7-5)$$

Further, a set of meaningful features is extracted per segment:

$$S_{i,j}^t \xrightarrow{\Gamma^L} \Phi_{i,j}^t = \{\varphi_1, \varphi_2, \dots, \varphi_L\}_{i,j}^t \quad (7-6)$$

Γ^L is the collection of L functions to expose particular aspects of a man-made surface. Hence, for every specific point P_n , one can define a set of features as:

$$\forall P_n : \Omega_n^t = subset\left(\{\Phi_1, \Phi_2, \dots, \Phi_{I'}\}_n^t\right) = \left\{ \Phi_{i,j}^t \mid \text{for } i = 1, 2, \dots, I' \text{ find } j : \mathbf{p}_m = T_i^t(\tilde{P}_n) \& pixel_m \in S_{i,j}^t \right\} \quad (7-7)$$

The next task is to investigate how to best combine various pieces of evidence available for the presence of a damaged point. Since the information sources are not fully reliable, it is also desirable to assign a confidence value to the decision. It is the one that makes a decision of whether a point of

an object is actually damaged with high enough confidence. It may be used in further selections depending on the utility of the decision for a particular task.

One challenge we face, reasoning on multi-view and multi-modal information, is that the numbers of evidence features that are used for the reasoning may vary at runtime because the numbers of segments used are not fixed and some image data may not always be available (i.e. the number of elements of Ω'_n is not fixed, it may be an empty set). Therefore, a reasoning tool for varying numbers of evidence and missing data is needed.

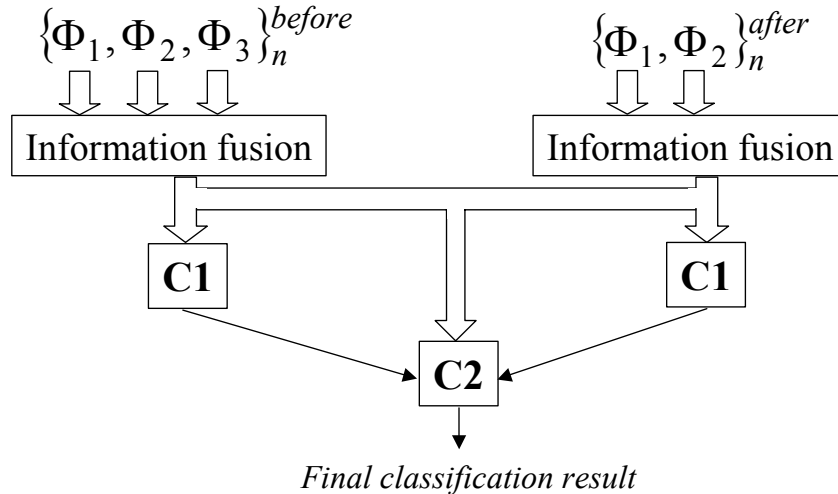


Figure 7-2: The classification flowchart for the proposed method, (e.g. 3 images before and 2 images after earthquake are available)

Figure 7-2 shows an example where three images before and two images after the event are available. For the first step, information fusion techniques such as majority voting, linear combinations (weighted sum) and certainty factor analysis may be considered. The first classifier (C1) is designed to take the fused data and produce a preliminary outcome at a given time t . The second classifier (C2) is designed to utilize both fused data plus primary results to produce the final classification (Kim and Müller 1995). Note that many classifiers, such as Bayesian classifiers, give likelihood values, not just binary decisions. Bayesian networks have several advantages for this problem domain. Bayesian networks are transparent, as all the parameters are represented as probabilities, making it easier for the system developer to understand their meaning in helping design improvements. Also any causal relationship can easily be represented in a Bayesian network. It gives a formal representation of the problem and we get the probabilistic optimum given the available evidence. Thus, it is desirable that C1 and C2 can take advantage of these values.

This data structure enables us to combine 2D and 3D information and to integrate a knowledge base or models by combining features derived from different views or cues that we get from additional attributes. An argument can be made that the success of such system relies on the existence of robust computer vision algorithms relevant to the contexts that will be encountered by the system. In fact, it is restricted by the underlying effectiveness of each of its algorithmic components. The overall system is comprised of smaller components that control the execution of a set of algorithms for specific algorithms designed for detecting the presence of a specific feature or computing a particular image property under predefined conditions. Straightforward algorithms can

lead to a complex and successful system if they are combined in a robust manner. The proposed method is done in three steps:

Image segmentation: The image is subdivided into independent regions using line detection and line grouping using geometric criteria.

Features and cues extraction: A characterization of objects derived from segmentation, based on their intrinsic properties (geometric, spectral and structural).

Reasoning system: A major challenge for processing multi-cue data is the handling of uncertainties during object extraction. The objects of similar specific characteristics are grouped into thematic classes using Bayesian Networks.

7.3. Image Segmentation

Successful image segmentation can be a central procedure to productivity in almost any object-oriented image processing. Several general-purpose algorithms and techniques have been developed for image segmentation. Since there is no general solution to the image segmentation problem, these techniques often have to be combined with domain knowledge in order to effectively solve an image segmentation problem for a problem domain. Image segmentation methods are divided into two main domains: data driven (bottom up) methods and model driven (top down) methods. Data driven methods group pixels to spatial clusters that meet certain criteria of homogeneity and heterogeneity and the generated segments are only image object primitives. In model driven approach the user already know what he wants to extract from the image, by formulating a model of the desired objects, the system tries to find the best methods of image processing to extract them. However, the generation of correct model hypotheses depends on the completeness of the extracted imagery data. The central assumption of such an approach is that structures of interest have a repetitive form of geometry. It is up to the user to determine what kind of real world objects the generated image objects represent. A primary focus of our system for damage detection is the man-made objects or buildings. Man-made objects such as buildings represent structures that are not random but have specific geometric properties. Those properties can be used to organize the extracted features or image primitives into roof and building hypotheses. Our goal of a segmentation algorithm is to partition the image of a city into a number of regions that correspond to surfaces in object space. Straight-line segments in urban areas can provide important information about the type (and number) of objects present in a local area of the image. High-order properties of the underlying image features such as colinearity and parallelism are assumed to be associated with human-made structure in the image. The power of perceptual organization for the extraction of structure in aerial scenes is well known and several researchers have made use of line grouping techniques in conjunction with geometric constraints to extract building rooftop boundaries (Lin et al. 1994, Jaynes 2000, Guler and Turker 2003, Jaw and Cheng 2008). Neighborhood relations between two lines can be tested for collinearity, parallelity and orthogonality. We used the concepts based on studies presented by Fuchs and Förstner (1995). We assume ideally each segment separated by a line and lines separated by a point. In order to form segments, neighborhood relations between two lines are tested and grouped into higher-level aggregate features based on geometric constraints such as colinearity, proximity, perpendicularity and parallelism (Figure 7-3). A specific grouping technique that leads to closed polygons has been developed. This approach uses Hierarchical Permissive Hough Transform (HPHT) algorithm (c.f. section 6.2.2.4) for the detection of straight lines and projects each line to a nominal plane in the world, based on the known camera parameters. This allows constraints to be expressed in terms that are independent of the perspective projection for a particular image. For example, the angle of intersection of two lines is dependent

upon the perspective transform, so the search for right angles is conducted on a nominal horizontal plane in the world where line angles are invariant, and right angles from horizontal facets in the world appear as right angles in the plane.

For neighboring lines the six semantically different relations collected in Figure 7-3(a) can be accepted. The feasible region of the end points position along line actually is not symmetric. We choose club's shape regions to fill short gaps between lines (Figure 7-3(b)). Line detection algorithm generates a table of lines and their related information (i.e. endpoint coordinates, direction angle, length). The generation of the hypotheses about the geometric properties of the lines is based on the endpoints adjacency derived from the information of segment lines. All neighboring lines are tested iteratively for three regions with different sizes (7-3(b)). To determine a set of relevant corner hypotheses, pairs of line segments with spatially proximate endpoints are grouped together into candidate image corner features.

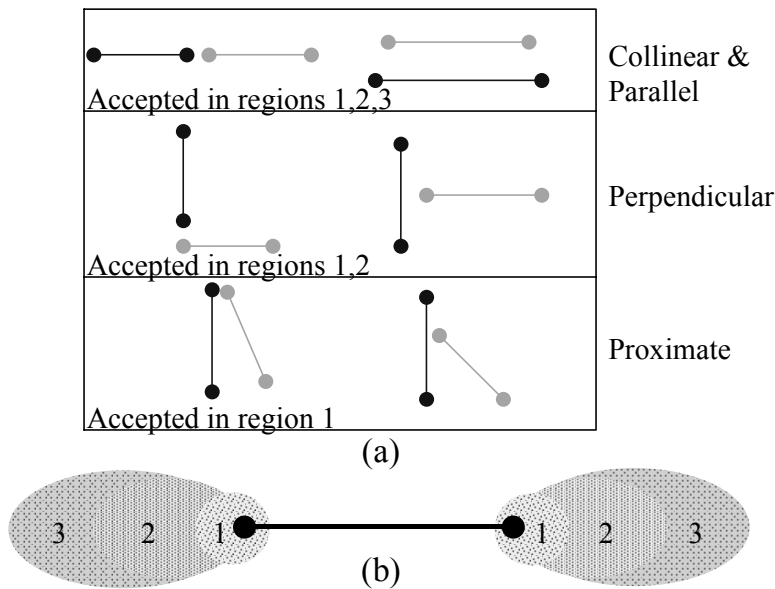


Figure 7-3: (a) Relations between straight-line segments (b) club shape neighborhood regions

There are two problems common in all image segmentation algorithms: over-grown and under-grown regions. For example, when an edge between two surfaces in object space does not appear in the image due to low contrast, lighting condition or shadow the corresponding regions will overgrow in the segmented image. The general approach to the correction has been based on an ability of the human brain that is often referred to as perceptual completion. There is, however, an ambiguity problem associated with perceptual completion. In our implemented approach, the incomplete features are intentionally completed so that the under-grown effect is more likely to occur. The segmented images for sample windows are shown in Figure 7-4.

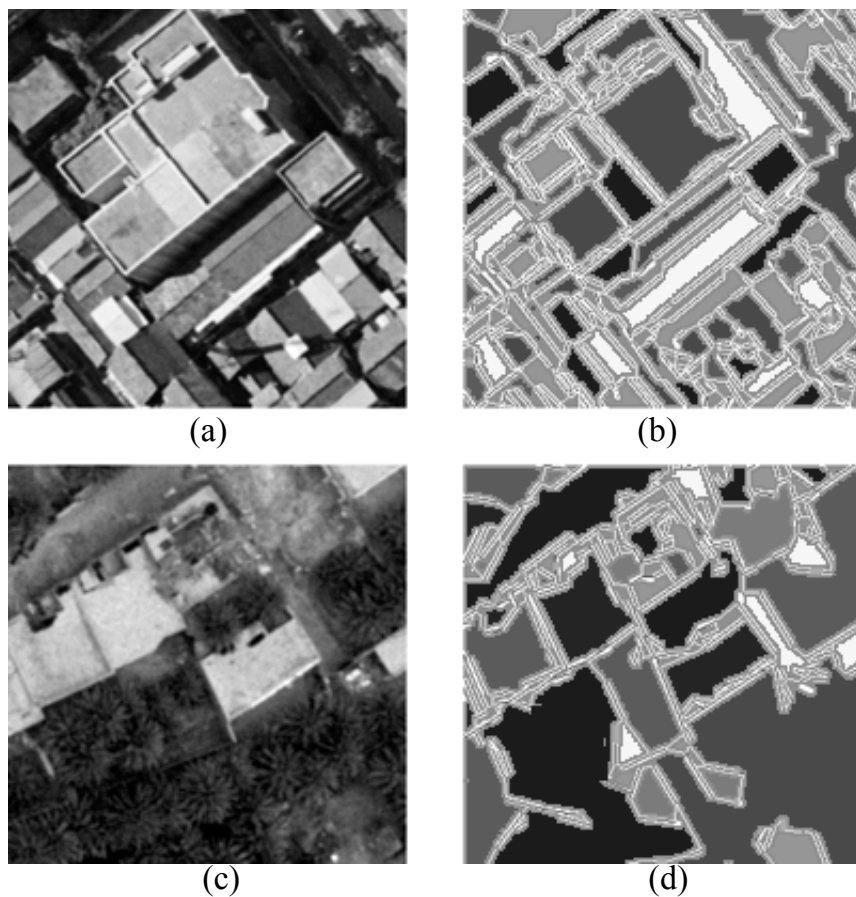


Figure 7-4: Two samples of (a) Kobe and (c) Bam aerial photos and (b)&(d) results of segmentation

7.4. Features and Cues Extraction

The idea behind the system is to develop a framework for extracting as much as possible basic robust features from different type of data or different cues. These basic features should be extracted and stored for all further processes, that means for building detection, recognition and damage classification processes. The system tries to derive necessary useful low-level information for each image segment in order to fuse related information. The introduced features are directly related to object and image spaces so that geometrical attributes derived from DSMs as well as imagery properties extracted from camera sensor (i.e. optical sensor). It is obvious that the result of a system for digital surface modeling can be corrupted by both the imperfection of measuring devices and matching algorithms. Additionally, the image segmentation may be imperfect and somewhere cannot reflect the polyhedral faces appropriately. All these influences add a certain amount of noise or uncertainty to the true and ideal values and we have to take uncertainty into account for practical applications. Using multi-images data together with statistical characteristics of grouped points, which clustered within image segments, can lessen the impact of these effects. The following features are proposed based on this idea.

7.4.1. Features Extracted from DSMs

We use DTM and DSM data to derive general features as height and slope of the segmental surfaces. Comparing these data before and after earthquake could be conducted for detecting damaged points (Chapter 5). For this purpose, each segment of image(s) should be projected down in object space using transformation functions and then those points of DSM within the projected segment will be processed to estimate planar surface (Figure 7-5).

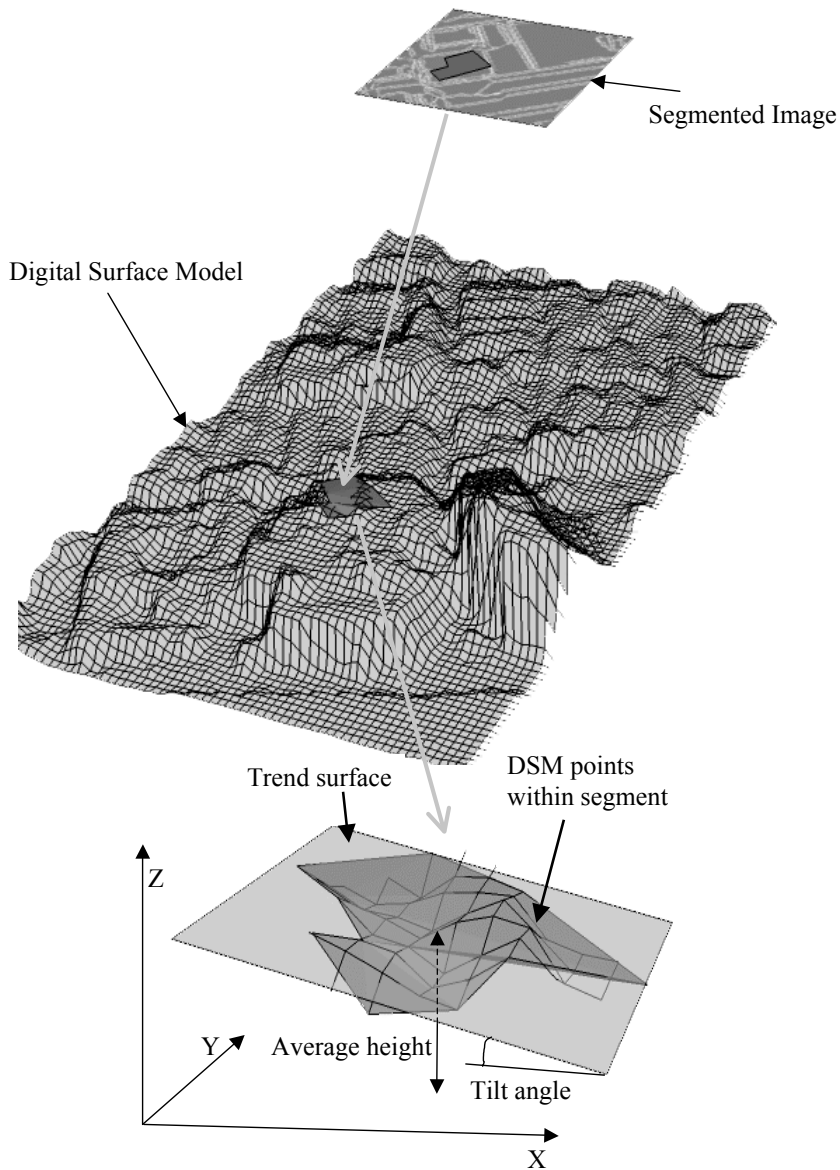


Figure 7-5: Trend surface of points belonging to an image segment

Simple regression techniques have been widely applied in spatial analysis for a very long time. The general form of model employed can be represented by the expression: $Z = f(X, Y, \mathbf{A})$ and the first order linear trend surface equation has the form:

$$Z(X, Y) = A_0 + A_1 \cdot X + A_2 \cdot Y \quad (7-8)$$

In the above equation there exist three unknown parameters (A_0, A_1, A_2). For a solution to be found, a minimum of three points must be known. Therefore the trend of those segments that contain minimum three points of DSM ($K > 3$ in equation 7-9) can be processed, in that a minimum of three points also fix a plane in space. When more than three points exist a least squares solution can be found by minimizing the deviations (e_n) from the trend to the observed points:

$$\begin{bmatrix} \tilde{Z}_1 \\ \tilde{Z}_2 \\ \vdots \\ \tilde{Z}_K \end{bmatrix} = \begin{bmatrix} 1 & X_1 & Y_1 \\ 1 & X_2 & Y_2 \\ \vdots & \vdots & \vdots \\ 1 & X_K & Y_K \end{bmatrix} \begin{bmatrix} A_0 \\ A_1 \\ A_2 \end{bmatrix} + \begin{bmatrix} e_1 \\ e_2 \\ \vdots \\ e_K \end{bmatrix} \quad (7-9)$$

Mathematically, using linear least squares the best approximation is defined as which minimizes the sum of squared differences between the data values and their corresponding trend values. Normal equations could be found as follow:

$$\mathbf{H} = \begin{bmatrix} K & \sum X_n & \sum Y_n \\ \sum X_n & \sum X_n^2 & \sum X_n Y_n \\ \sum Y_n & \sum Y_n X_n & \sum Y_n^2 \end{bmatrix}, \quad \mathbf{A} = \begin{bmatrix} A_0 \\ A_1 \\ A_2 \end{bmatrix}, \quad \mathbf{L} = \begin{bmatrix} \sum \tilde{Z}_n \\ \sum X_n \tilde{Z}_n \\ \sum Y_n \tilde{Z}_n \end{bmatrix} \quad (7-10)$$

$$\mathbf{H} \cdot \mathbf{A} = \mathbf{L}$$

By breaking the equation down further we can conclude that A_0 elevates the trend above a datum and A_1 and A_2 represent the slope in each direction. Using nDSM, the features such as average height and tilting angle with respect to horizon plane can be registered for each image segment. A trend-surface of a given order can be fit to any set of data, but does not guarantee that it is a meaningful or worthwhile model. It is necessary to compute measure of the *goodness of fit* of the function to the data and to determine if the function components are statistically significant. One measure of *goodness of fit* can be obtained by the residual mean square error. It can be shown that an appropriate unbiased estimate is given by:

$$\frac{1}{K-3} \sum_{n=1}^K (\tilde{Z}_n - Z_n^{trend})^2 \quad (7-11)$$

\hat{Z} denotes estimated value from trend surface. Therefore, fitting planar surfaces to the height points, which project into each image segment, and computing the average height, tilt angle and goodness of fit obtain DSM-based evidences (Figure 7-6).

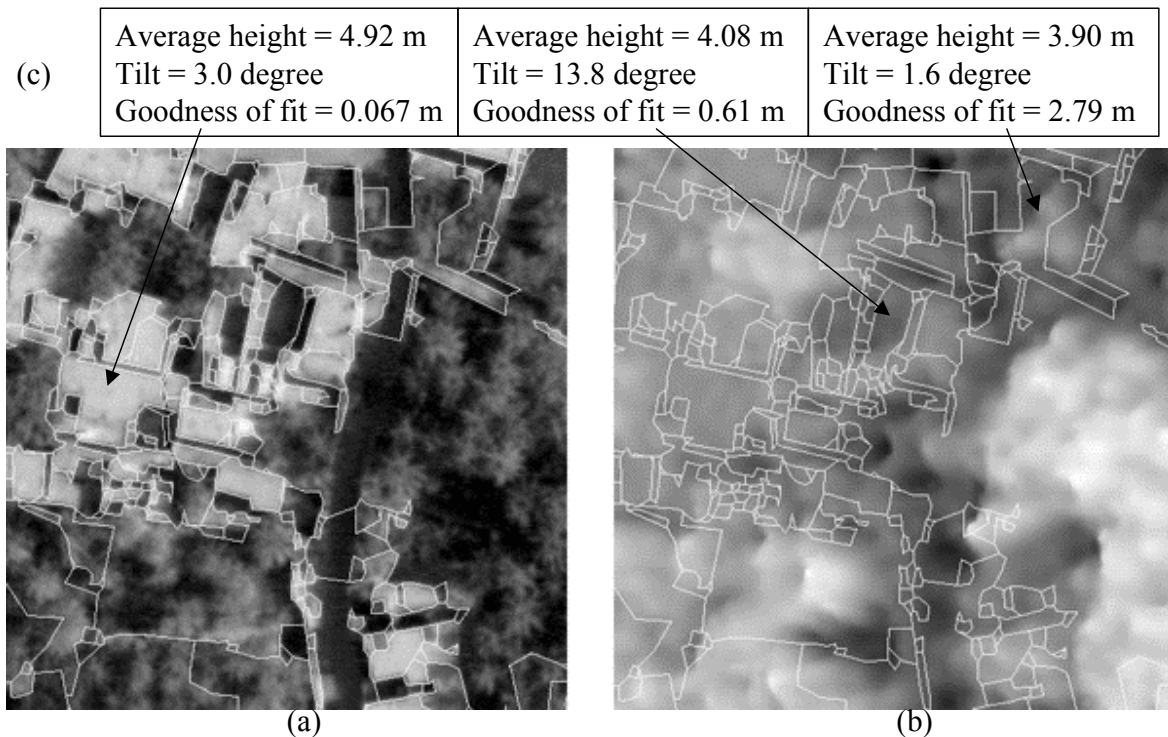


Figure 7-6: A sample window from Bam aerial image –left photo (a) Segmented image, (b) Corresponding DSM generated automatically (c) Attributes of trend surface for 3 sample segments

7.4.2. Features Extracted from Images

7.4.2.1. Pixel Intensity and Color

Image formation based on radiation from electromagnetic spectrum is the most familiar and the subject of what sensors consist of and how they perform is important and wide-ranging. The visual band of electromagnetic spectrum is the most prevailing method for imaging and the infrared band often is used in conjunction with visual imaging. In remote sensing usually it is utilized several bands in the visual and infrared regions of the spectrum. The characteristics and uses of each band are different. Pixels intensity and pattern have long been recognized as important attributes of high-resolution image data.

A further classification can use multi-spectral images to separate points on buildings from points on trees and vegetations. It is difficult to classify the vegetations from the buildings using only the height information. There are techniques pursued by using height texture to tackle this problem (Niederöst 2003). These solutions evaluate the local surface roughness. With multi-spectral images, the normalized difference vegetation index (NDVI) is well suited for vegetation classification (Rouse et al. 1973). This is a combination of the red and the infrared channel, for the elimination of vegetation regions:

$$NDVI = \frac{IR - R}{IR + R} \quad (7-12)$$

where IR and R denote pixel values of the infrared and red channels, respectively. NDVI is related to the proportion of photosynthetically absorbed radiation and vegetation is characterized by high NDVI value.

The detection of vegetation areas without infrared channel is difficult. One possibility to separate man-made objects from vegetation is to use the color information of the aerial images. There are numerous color models, which can be categorized as colorimetric, subtractive, video, and nonstandard (Pratt 2001). In the RGB model, each color appears in its primary spectrum components of red (R), green (G) and blue (B). The RGB color space is a model for color monitors and a broad class of color video camera. One method to derive useful information for vegetation detection is to use arithmetical combinations proposed by Sibiryakov 1996 (Degree of Artificiality):

$$GR = \frac{G - R}{G + R} \quad (7-13)$$

The HSI (hue, saturation, intensity) color model decouples the intensity component from the color carrying (hue and saturation) in a color image (Gonzalez and Woods 2002):

$$H = \begin{cases} \theta & B \leq G \\ 360 - \theta & B > G \end{cases} \quad \theta = \cos^{-1} \left(\frac{\frac{1}{2}[(R-G)+(R-B)]}{\sqrt{(R-G)^2+(R-B)(G-B)}} \right) \quad (7-14a)$$

$$S = 1 - \frac{3}{(R+G+B)} [\min(R, G, B)] \quad I = \frac{R+G+B}{3} \quad (7-14b)$$

Hue is a color attribute that describes a pure color whereas saturation gives a measure of the degree to which a pure color is diluted by white light. Saturation helps to discriminate between shadow and non-shadow regions and hue is used to support separation of vegetation.

CIE $L^*a^*b^*$ (CIELAB) cube root color coordinate system was designed by the International Commission on Illumination to approximate human vision. It describes all the colors visible to the human eye and was created to serve as a device independent model to be used as a reference. The definition of $L^*a^*b^*$ is based on an intermediate system, known as the CIE XYZ space (ITU-Rec. 709), which is derived from RGB as follows (Wyszecki and Stiles 1982):

$$\begin{bmatrix} X \\ Y \\ Z \end{bmatrix} = \begin{bmatrix} 0.4125 & 0.3576 & 0.1804 \\ 0.2127 & 0.7152 & 0.0722 \\ 0.0193 & 0.1191 & 0.9502 \end{bmatrix} \begin{bmatrix} R \\ G \\ B \end{bmatrix} \quad (7-15)$$

Based on this definition, $L^*a^*b^*$ is defined as follows:

$$L^* = \begin{cases} 116(\frac{Y}{Y_0})^{1/3} - 16 & \frac{Y}{Y_0} > 0.008856 \\ 903.3 \frac{Y}{Y_0} & 0 \leq \frac{Y}{Y_0} \leq 0.008856 \end{cases}, \quad a^* = 500 \left[f(\frac{X}{X_0}) - f(\frac{Y}{Y_0}) \right], \quad b^* = 200 \left[f(\frac{X}{X_0}) - f(\frac{Z}{Z_0}) \right] \quad (7-16)$$

where

$$f(w) = \begin{cases} w^{1/3} & w > 0.008856 \\ 7.787w + 01379 & 0 \leq w \leq 0.008856 \end{cases}$$

Here X_0 , Y_0 and Z_0 are the tristimulus values of the reference white point. L^* represents the lightness of the color ($L^* = 0$ yields black and $L^* = 100$ indicates diffuse white), a^* is correlated with redness-greenness (negative values indicate green while positive values indicate magenta) and b^* with yellowness-blueness (negative values indicate blue and positive values indicate yellow). Sibiryakov (1996) did some tests and proposed to use a^* and b^* of the CIELAB color space. Channel a^* has the advantage that any roof parts are represented with about the same gray value, regardless if they are under the sun or in the shade (Niederöst 2003). Applying a supervised classification system using GR and a^* can detect vegetations successfully (Figure 7-7).

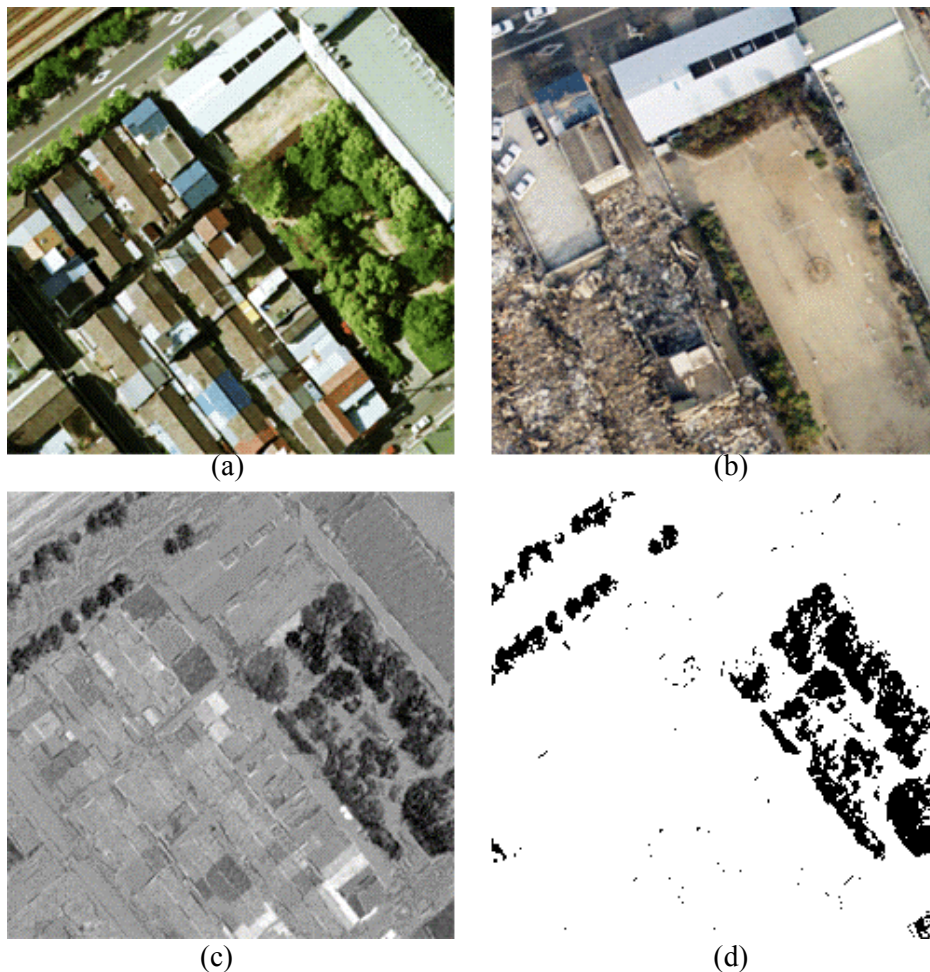


Figure 7-7: Sample window of Kobe, (a) before and (b) after earthquake. Before earthquake, the green yard was removed, which may be misclassified as damaged area. (c) Channel a^* , (d) vegetation detection

7.4.2.2. Segment Shape

Segments appearance could be another cue for our inferring system. The regions surrounded by long straight lines may indicate the undamaged buildings and are directly applicable to the inferring system. Moreover, those segments, which appeared as polygons with parallel sides, could be likely candidates for being rooftop segment. We propose an index to quantify similarity between extracted segments and such polygon. For this purpose, the histogram of edge pixels with respect to lines direction is generated. The line detector (Hough transform) has already generated the direction angles. A window with specified width (e.g. 10 degrees) moves on histogram and computes the total number of pixels located about specific direction. We define following index, so called *shape index*:

$$SI = \frac{\text{summation of two sequent maximum values of no overlapped windows}}{\text{total number of pixels belong to segment edges}} \quad (7-17)$$

This quotient gives a positive number less than 1 and the number close to 1 indicates a polygon with parallel sides in two major directions. Figure 7-8 gives three sample polygons and their computed indices. Moreover, we use the quotient of region pixels to perimeter that gives a measure of compactness.

Therefore, for any segmented image, region boundaries are stored as a 2D polygon, with attributes for color range in the regions, greenness, compactness, and shape index (extracted from images) and trend surface information (extracted from DSMs).

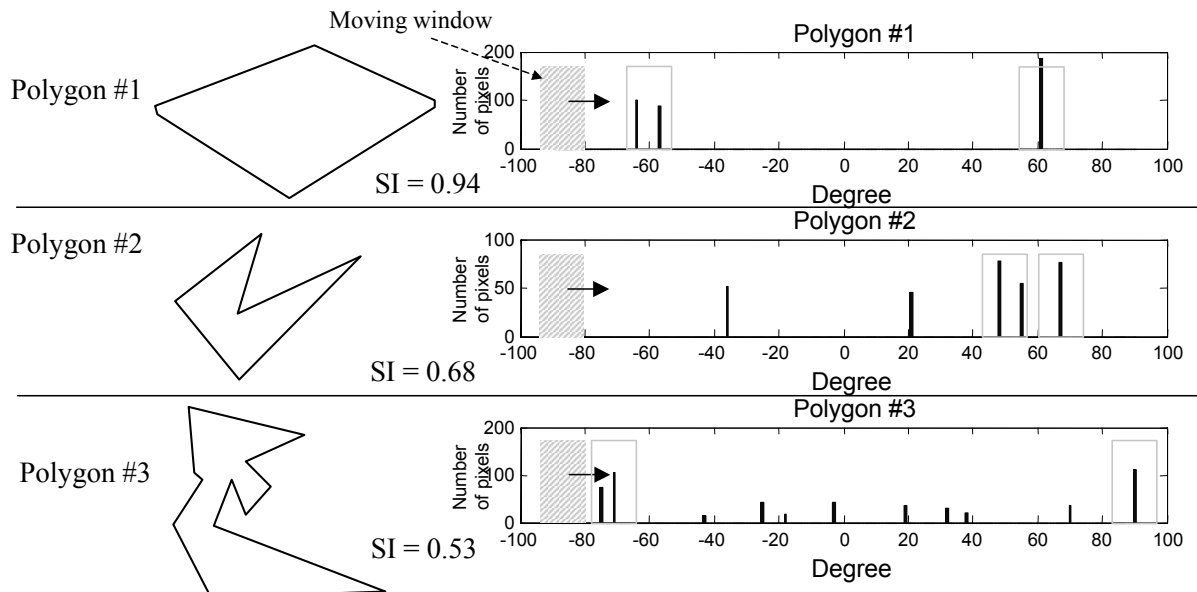


Figure 7-8: Three sample polygons and their indices

7.5. Reasoning System using Bayesian Network

All evidences extracted from DSMs and aerial images have to be integrated through a ‘decision maker system’ in order to detect buildings and then detect damaged ones. However, one important aspect that has to be considered is evidence uncertainty. Bayesian networks have been used by researchers in decision analysis and artificial intelligence to build probabilistic expert system. Bayesian networks are very effective for modeling situations where some information is already known and incoming data is uncertain or partially unavailable. These networks also offer consistent semantics for representing causes and effects (and likelihood) via an intuitive graphical representation. The use of Bayesian networks to represent prior knowledge about the scene proves to be a straightforward technique for designing knowledge-based vision systems (Kim 2001). We use these networks to determine what evidence to collect and what to do with the evidence once it has been obtained. In Bayesian decision theory, decisions are made based on the probabilities of hypotheses given evidence. Explicit knowledge about an area is stored in a Bayesian network that is used to fuse information gathered from the execution of evidence acquisition (Figure 7-1) and forms the basis for automatic damage detection. The goal of processing in this chapter, then, is the reduction of uncertainty about information of damages for specific urban area after earthquake.

7.5.1. Bayesian Network

Belief or Bayesian networks (BN) have proved to be an effective knowledge representation and inference engine in artificial intelligence and expert systems. As BNs are diagrammatically based, it is relatively easy to understand the outputs provided by a decision support system built with them. This facilitates the communication of information to users without technical abilities so they can participate more fully in the decision making process. Graphical models are graphs in which nodes (the features) represent the variables and the arcs represent a causal (or probabilistic) relationship among the connected variables. Probability distributions are easily readable in combination with graphical representations of dependencies in graphical models.

Contrary to undirected graphical models (also called Markov Random Fields), a Bayesian network is a directed acyclic graph which means it is formed by a collection of vertices and directed edges, each edge connecting one vertex to another, such that there is no way to start at the vertex and follow a sequence of edges that eventually loops back to the same vertex again. Bayesian Networks have a more complicated notion of independence, which takes into account the directionality of the arcs. The most important advantage of directed models is that one can regard an arc from A to B as indicating that A causes B. This can be used as a guide to construct the graph structure. In addition, directed models can encode deterministic relationships, and are easier to learn (fit to data).

In addition to the graph structure, it is necessary to specify the parameters of the model. For a directed model, we must specify the Conditional Probability Distribution (CPD) for each variable (feature) which represented by graph nodes. Variables can either be discrete or continuous. If the variables are discrete, CPD can be represented as a table (CPT), which lists the probability that the child node takes on each of its different values for each combination of values of its parents. Accordingly, Bayesian networks are composed of three elements:

- A set of nodes, representing random variables that in our application would be the extracted features.
- A set of arcs (links), representing causal relationships between these nodes.

- A set of probabilities for each node, specifying the belief that a node will be in a particular state given the states of those nodes that affect it directly (its parent).

Figure 7-9 depicts an example, in which all nodes are binary, i.e., have two possible values, which denoted by T (true) and F (false).

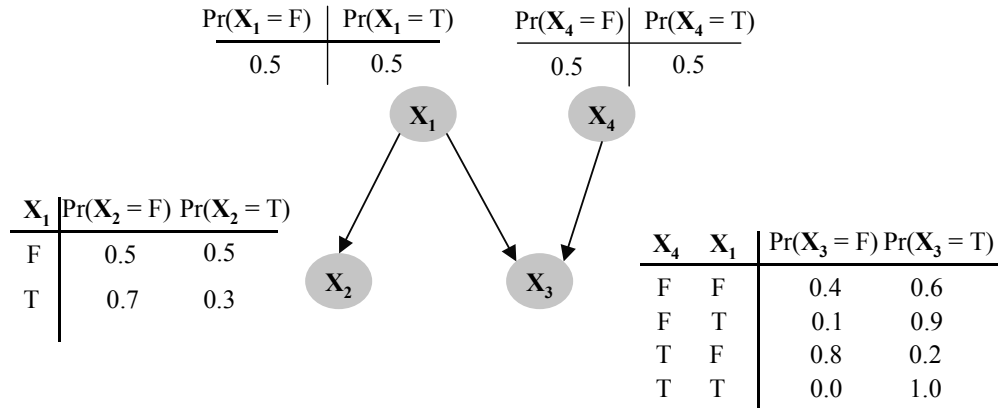


Figure 7-9: Bayesian network and relative conditional probability tables (CPTs)

In this example, a node (feature) is conditionally independent from its ancestors given its parents, where the ancestor/parent relationship is with respect to some fixed topological ordering of the nodes. Probabilistic parameters are encoded into a set of tables for each variable, in the form of local conditional distributions of a variable given its parents. The independences are encoded into the network. The joint distribution can be reconstructed by simply multiplying these tables. Probabilistic reasoning is done by applying Bayes' rule on the CPTs and the prior probabilities of the nodes and propagating it through the network. In general, the CPT associated with each node contains the probability of each state of the variable given every possible combination of states of its parents. The structure of the network encodes the assertion that each node is conditionally independent of its non-descendants given its parents. Thus the probability of an arbitrary event $\mathbf{X} = \{X_1, X_2, \dots, X_n\}$ can be computed as:

$$\Pr(\mathbf{X}) = \prod_{i=1}^n \Pr(X_i / \text{Parents}(X_i)) \quad (7-18)$$

Typically, the task of learning a Bayesian network can be divided into two subtasks: initially, the learning of the graph structure of the network, and then the determination of its parameters. However, structure learning is more difficult than parameters learning. Learning the structure of a Bayesian network (i.e., the graph) is a very important part of learning. When the relations between nodes are clear, the structure of a BN can be manually determined by adding edges (or causal links) between node pairs with direct causal relationships. In the simplest case, a Bayesian network is specified by an expert and is then used to perform inference. Otherwise, the network structure and the parameters of the local distributions must be learned from data. The structure may be learned by statistical methods. It requires a scoring function and a search strategy. A common scoring function

is posterior probability of the structure given the training data. An iterative search is performed to find a network that best matches the input data given a criterion (Van Allen and Greiner 2000).

A Naïve Bayesian network has the simple structure depicted in Figure 7-10. This network is composed of only one parent and several child nodes (attributes). The main assumption behind the naïve Bayes classifier is that every attribute is independent from the rest of the attributes given the state of the class variable (the root in the network). Domingos and Pazzani (1997) provided an interesting analysis that compared naïve Bayes with several classical learning algorithms with large ensemble of standard benchmark datasets. They reported that naïve Bayes classifier sometimes is superior to the other learning schemes, even on datasets with substantial feature dependencies.

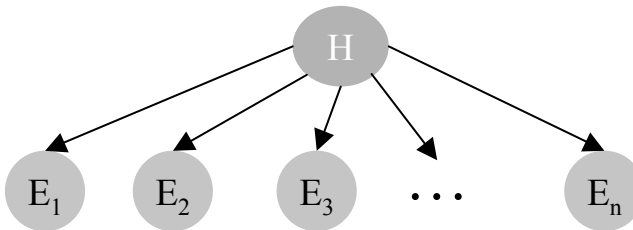


Figure 7-10: Naïve Bayesian network

The main advantages of naïve Bayesian network are that it is straightforward to understand as well as easy and fast to train. In this network, due to that all nodes (E) are conditionally independent then:

$$\Pr(\mathbf{E}/H) = \prod_{i=1}^n \Pr(E_i/H) \quad (7-19)$$

And therefore, by computing conditional probabilities, for binary hypothesis H , Bayes rule gives:

$$\Pr(H/\mathbf{E}) = \frac{\Pr(\mathbf{E}/H)P(H)}{\Pr(\mathbf{E})} = \frac{\Pr(\mathbf{E}/H)P(H)}{\Pr(\mathbf{E}/H)P(H) + \Pr(\mathbf{E}/\bar{H})P(\bar{H})} \quad (7-20)$$

In general, the probability distributions are continuous functions and need to be represented effectively. There are several considerations for an effective representation. It should be nonnegative and the total area of the distribution should sum up 1 since it is a probability distribution. Considering these conditions, two different approaches can be applied. The first is to use parametric curves such as normal distribution curves. Gaussian functions are widely used because they approximate various distributions fairly with known fitting algorithms. Another approach is to quantize the distributions into appropriate discrete levels using a variant of the methods (Fayyad and Irani 1993, Dougherty et al. 1995). Dougherty et al. (1995) conducted an empirical study comparing the performance of four well-known discretization methods and concluded that all of the methods can significantly outperform a version of naïve Bayes that assumes normal for all continuous variables whereas no significant difference between their performances was found. Their results showed that naïve Bayes classifier can achieve suitable results using a very simple method such as ten-bin. Ten-bin method simply divides the domain of each continuous variable into ten equal-width bins. Hsu et al. (2000) explained that discretized

variables have Dirichlet priors and since perfect aggregation holds for Dirichletes, we can show that generally, a wide variety of discretization methods can perform well with insignificant difference. Assuming the prior distributions to be Dirichlet generally does not result in a significant loss of accuracy, since precise priors aren't usually available, and Dirichlet functions can fairly flexibly fit a wide variety of simple functions.

Once a structure of network is given, the CPT values can be estimated by collecting the statistics from training data for parameters learning. However, learning when some of the nodes are hidden (hidden nodes are nodes whose values are not known) is much harder than when everything is observed. The goal of learning is to find the values of the parameters of each CPT, which maximizes the likelihood of training set: $T = \{\mathbf{X}_1, \mathbf{X}_2, \dots, \mathbf{X}_D\}$, which contain n cases: $\mathbf{X}_d = \{X_{d,1}, X_{d,2}, \dots, X_{d,n}\}$ assume to be independent. One approach is to find the network that maximizes the log-likelihood of the data:

$$L = \sum_{d=1}^D \log \Pr(\mathbf{X}_d) = \sum_{d=1}^D \sum_{i=1}^n \log \Pr(X_{d,i} / \text{Parents}(X_{d,i})) \quad (7-21)$$

When the structure of the network is known, this reduces to estimating $p_{i,j,k}$, the probability that variable i is in state k given that its parents are in state j , for all i, j, k . In the case of full-observability which means there are no examples with missing values in the training set and we assume parameter independence, the maximum likelihood estimates are simply the observed frequency estimates:

$$\hat{p}_{i,j,k} = \frac{n_{i,j,k}}{n_{i,j}} \quad (7-22)$$

where $n_{i,j,k}$ is the number of occurrences in the training set of the k th state of X_i with the j th state of its parents, and $n_{i,j}$ is the sum of $n_{i,j,k}$ over all k . Thus "learning" just amounts to counting in the case of multinomial distributions. Moreover, one approach is that all CPT probabilities start as uniform or entry of probabilities by an expert and then conditional probabilities could be modified for those nodes that training data supply a value and supply values for its parents.

When some of the nodes are hidden, we can use the Expectation Maximization (EM) algorithm to find a (locally) optimal maximum likelihood estimate of the parameters. EM learning repeatedly takes a Bayes net and uses it to find a better one by doing an expectation (E) step followed by a maximization (M) step. In the E step, it uses regular Bayes net inference with the existing Bayes net to compute the expected value of all the missing data, and then the M step finds the maximum likelihood Bayes net given the now extended data (i.e. original data plus expected value of missing data). This procedure is guaranteed to converge to a local maximum of the likelihood surface. Another classical approach to this problem is gradient ascent on the likelihood surface. Gradient descent learning searches the space of Bayes net parameters by using the negative log likelihood as an objective function it is trying to minimize. This approach can be expensive and lead to large dimension models. Both EM and gradient ascent learning work by an iterative process can get stuck in local minima, but in actual practice do quite well, especially the EM algorithm, is usually faster (since it uses the natural gradient) and simpler (since it has no step size parameter and takes care of parameter constraints automatically (e.g., the "rows" of the CPT having to sum to one)).

The applied criteria allow the separation of the two tasks of buildings detection and damage detection. In the following, we therefore describe our approaches using Bayesian networks for both tasks, focusing on the discrimination of rooftops by use of differential geometry and radiometry cues as a first step towards the extraction of damaged points.

7.5.2. Naïve Bayesian Network for Buildings Extraction

We initially start with a simple naïve Bayesian network to detect buildings using gray-scale images and digital surfaces. The main focus is on the detection, mainly on the use of height and differential geometric information to discriminate intact buildings amongst trees and vegetations. First of all, our approach for building detection exploits the fact that a normalized DSM provides information about buildings. As an evidence for finding roof planes, we utilize this information by computing the average height of detected segments for each image (φ_2). Fitting planar surfaces to the height points, which project into each image segment, and computing the goodness of fit can obtain another evidence (φ_3). This is based on the assumption that building parts are planar objects; thus buildings with curved surfaces are not taken into account in this method. Another criterion is the deviation from a horizontal plane (φ_4). Beside, we utilize intensity information and segment shape of each image segment (φ_1, φ_5). The following notations summarize the applied features (c.f. section 7.2.2):

$$\text{For all } S_{i,j}^t, \exists \tilde{P}_n : \mathbf{p}_m = T_i^t(\tilde{P}_n) \& \text{pixel}_m \in S_{i,j}^t \rightarrow \{P_n^{\text{trend}}\} = \text{fit-plane}\{\tilde{P}_n\} \quad (7-23)$$

$$\Gamma^4 : \Phi_{i,j}^t = \begin{cases} \varphi_0 = \text{Compactness factor of segment polygon} \\ \varphi_1 = \frac{1}{M_{i,j}^t} \sum_{m=1}^{M_{i,j}^t} \lambda_m \\ \varphi_2 = \frac{1}{M_{i,j}^t} \sum_{m=1}^{M_{i,j}^t} (\tilde{Z}_m - Z_m^{\text{terrain}}) \\ \varphi_3 = \frac{1}{M_{i,j}^t - 3} \sum (\tilde{Z}_n - Z_n^{\text{trend}})^2 \\ \varphi_4 = \theta [\text{degree}] \\ \varphi_5 = \text{Shape Index (SI) of segment polygon} \end{cases}$$

Since, there are two images before and three images after earthquake, for every given point P_n :

$$\begin{aligned} \forall P_n : \\ \Omega_n^t &= \text{subset}(\{\Phi_1, \Phi_2, \dots, \Phi_{I^t}\}_n) = \{\Phi_{i,j}^t \mid \text{for } i = 1, 2, \dots, I^t \text{ find } j : \mathbf{p}_m = T_i^t(\tilde{P}_n) \& \text{pixel}_m \in S_{i,j}^t\} \\ t &= \text{before, after} \quad I^{\text{before}} = 2, \quad I^{\text{after}} = 3 \end{aligned} \quad (7-24)$$

then

$$\begin{aligned} \Omega_n^{\text{before}} &= \text{subset}(\{\Phi_1, \Phi_2\}_n^{\text{before}}) \\ \Omega_n^{\text{after}} &= \text{subset}(\{\Phi_1, \Phi_2, \Phi_3\}_n^{\text{after}}) \end{aligned} \quad (7-25)$$

The points without any related evidence ($\Omega'_n = \emptyset$) have to be ignored. On the other side, when features of more than one image are available, we have to select the best features set, or in other words, need to select the most appropriate image segment. Figure 7-11 depicts an artificial scene, which is projected on three image planes and with approximate DSM.

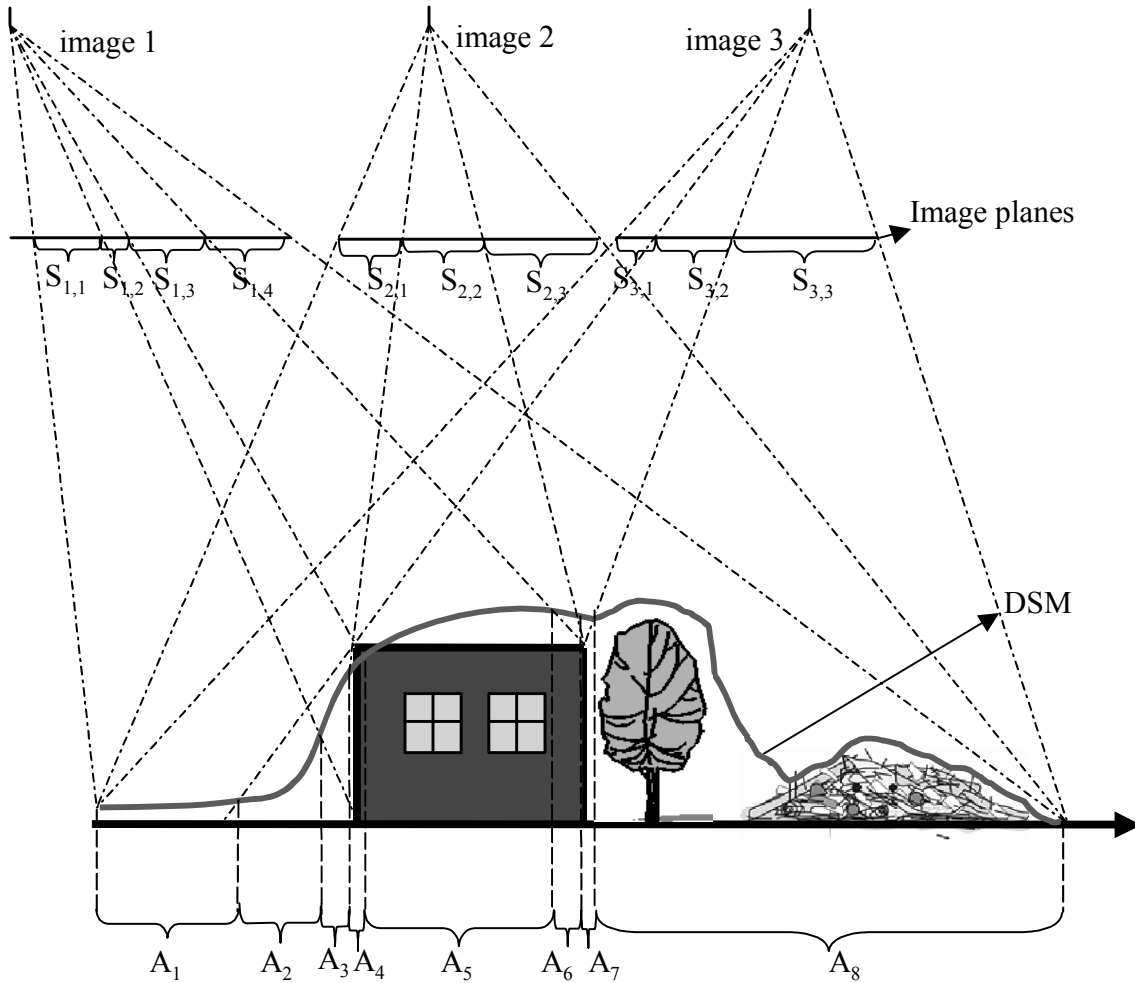


Figure 7-11: An artificial scene with three images of different view and approximate DSM

Ideally, using line-based segmentation, image plane is partitioned based on surfaces of hyperplane objects i.e. the building surfaces. In this example, eight distinct regions must be emphasized (A_1-A_8). The relationship between image segments and object regions can be explicated as follow:

$$\begin{aligned} A_1 &\in \{S_{1,1}, S_{2,1}, S_{3,1}\}, A_2 \in \{S_{1,1}, S_{2,1}, S_{3,2}\}, A_3 \in \{S_{1,2}, S_{2,1}, S_{3,2}\}, A_4 \in \{S_{1,2}, S_{2,2}, S_{3,2}\} \\ A_5 &\in \{S_{1,3}, S_{2,2}, S_{3,2}\}, A_6 \in \{S_{1,4}, S_{2,2}, S_{3,2}\}, A_7 \in \{S_{1,4}, S_{2,3}, S_{3,2}\}, A_8 \in \{S_{1,4}, S_{2,3}, S_{3,3}\} \end{aligned} \quad (7-26)$$

S_{ij} denotes j th segment of i th image. Given A_i , one needs to select the most appropriate segment amongst others and the best segment could be the one with the best view regarding surface topography and orientation. However, this process can be more complicated where a segment overgrowing would happen. In our design, first the segments with compactness factor (the quotient of region pixels to perimeter) less than one are excluded and then those segments with the best “trend plane” in terms of goodness-of-fit (φ_3) and tilt angle (φ_4) are selected for decision-making procedure. Accordingly in this example the following segments will be selected:

$$(A_1, S_{3,1}), (A_2, S_{1,1}), (A_3, S_{1,2}), (A_4, S_{1,2}), (A_5, S_{2,2}), (A_6, S_{2,2}), (A_7, S_{2,3}), (A_8, S_{3,3}) \quad (7-27)$$

Initially, the proposed network could be a naïve Bayesian network where all the evidence variables are children of the hypothesis node ($H_b, H_a: P_n \in \text{Building rooftop before/after earthquake}$) (Rezaeian and Grün 2010). In this implementation, the Bayesian Network is developed for discrete variables. Therefore, the continuous variables need to be quantized and divided into proper intervals. The quantization levels are set empirically. The results are:

- Hypotheses (H_b, H_a). Two states: False, True.
- Average intensity (φ_1). Four intervals: (0-64), (64-128), (128-192), (192-255).
- Average height of nDSM (φ_2). Six intervals: (less than 2m), (2-4), (4-6), (6-8), (8-10), (more than 10m).
- Goodness of plane fit (φ_3). Three intervals: (0-0.5m), (0.5-1m), (more than 1m).
- Deviation from horizontal plane (φ_4). Four intervals: (0-10°), (10°-30°), (30°-60°), (60°-90°).
- Segment shape index (φ_5): Three intervals: (less than 0.45), (0.45-0.75), (0.75-1).

For each root node (i.e. hypothesis node) we define initial uniform prior state probability densities. For each non-root node we then need to define conditional probability tables $P(\varphi_i/H)$, which quantify the edges of the network. Conditional probability tables contain two rows of $P(\varphi_i/H = \text{False})$ and $P(\varphi_i/H = \text{True})$. Each of these tables gives the conditional probability of a child node being in each of its states, given all possible parent state combinations. These probabilities can be entered by an expert or derived from the training data. We assume (nearly-) uniform probabilities for $P(\varphi_i/H = \text{False})$ and then adjust the second row for $P(\varphi_i/H = \text{True})$. Here, we use simplest algorithm for parameter learning of conditional probability table, called counting-learning. For example, the conditional probability of ‘average intensity’ being in ‘interval 1’, given H is true, is determined from data, by counting the number of points belong to building examples with an intensity within ‘interval 1’, and so on. For this purpose we have selected some points of building areas for generating probabilities table. From the building hypotheses, a learning dataset was created by displaying one hypothesis at a time to a human and asking for a decision on whether it is positive or not.

The proposed method has been implemented in (Rezaeian and Grün 2010). Figure 7-12 shows an area of Bam city of about 100m × 100m before earthquake. This sample area included buildings, walls, streets, palm gardens and single trees. We applied our method to every point of a regular grid at a spatial resolution of 2m. The features, extracted from left and right images, were compared and the best set in terms of goodness-of-fit and tilt angle are selected. Then, all probabilities were computed for these points. Based on the probability of pre-event data the classification with $\Pr(H_b =$

True) > 0.5 yields the building segments (Figure 7-12(b), green points). Seemingly, it works well in distinguishing building rooftops (or even courtyard walls) from vegetation.

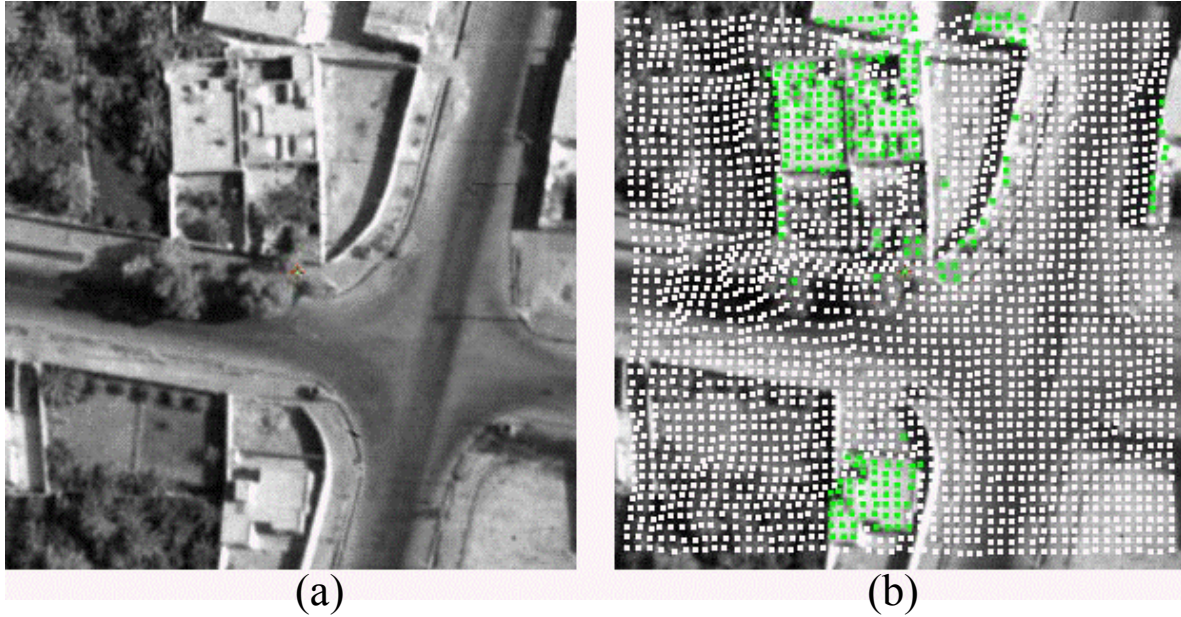


Figure 7-12: (a) Sample area of Bam city before earthquake, (b) Result of proposed method to discriminate man-made objects from vegetation

7.5.3. Augmented Bayesian Network for Buildings Extraction

It is noted that substantial blunders in DSM could unavoidably lead to erroneous results. Nevertheless, using multi-image data may give an estimation of features uncertainty. As a matter of fact, if there is conformity between corresponding features, which are extracted from different image planes, inferring system should be able to make more strong decision than where disparate attributes are detected. Actually, we attempt to represent the type of uncertainty that is particularly created from generally strong, but conflicting evidence i.e. ambiguity. For this purpose, we compare corresponding features extracted from different views and suggest a new variable so called “Features Conformity” (FC). One solution for low conformity could be neutrality strategy, which means the inferring system should organize a fifty-fifty chance between “H = *True*” and “H = *False*”. In the implemented system, this is obtained as follow:

$$\text{if } FC \rightarrow \text{low-value} \quad \text{then} \quad \Pr(\varphi_i / H = \text{True}, FC) \rightarrow \Pr(\varphi_i / H = \text{False}) \quad (7-28)$$

“Features Conformity” is quantized in three levels: High – Medium – Low. Figure 7-13 presents conditional probabilities of two features (φ_2 : height average, φ_4 : plane tilt) with three states of FC. The Bayesian network should be extend by adding FC node (Figure 7-13) and conditional probability tables (CPTs) will be modified with respect to features conformity states.

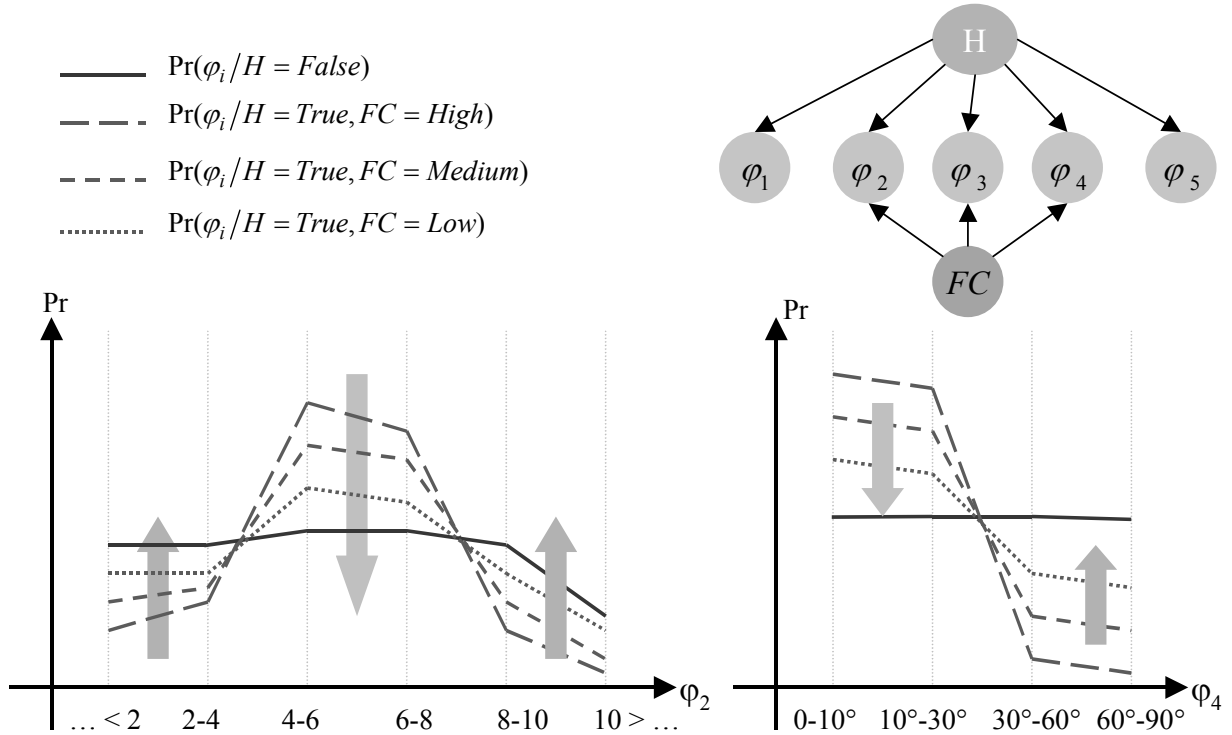


Figure 7-13: Augmented Bayesian network, the gravity of φ_i is attenuated when $FC \rightarrow low-value$

Experimental results revealed that the performance of the inferring system will improve by using the augmented Bayesian network and the proposed method gives significant and consistent performance efficiency. Obviously, the proposed method is unable to eliminate effects of blunders completely but cause decisions to be more confident for acceptance of hypotheses with probabilities close to one.

A typical sample is presented in Figure 7-14. Figures 7-14(a) and 7-14(b) show sample windows of left and right images in Bam city, respectively. In a particular point like P , due to 4.6m overestimation of DSM the point will be projected on disparate segments of left and right images (p_{left} , p_{right}) containing dissimilar attributes (because p_{left} , p_{right} belong to inhomogeneous segments). Due to this inconformity, the gravity of geometrical attributes is attenuated in the Bayesian network, which leads to increase influence of imagery attributes in inferring system. We applied our method to every point of a regular grid at a spatial resolution of 1m for this area. Figures 7-14(c) and (d) show the results of building detection ($\Pr(H_b = True) > 0.5$) using naïve BN and augmented BN, respectively. Green dots mark the area labeled as buildings. The region between adjacent buildings or those points close to walls are labeled correctly as “no-building” using augmented BN. In these regions, only “imagery features” play main role and low intensity value of φ_i cause to classify as no building.

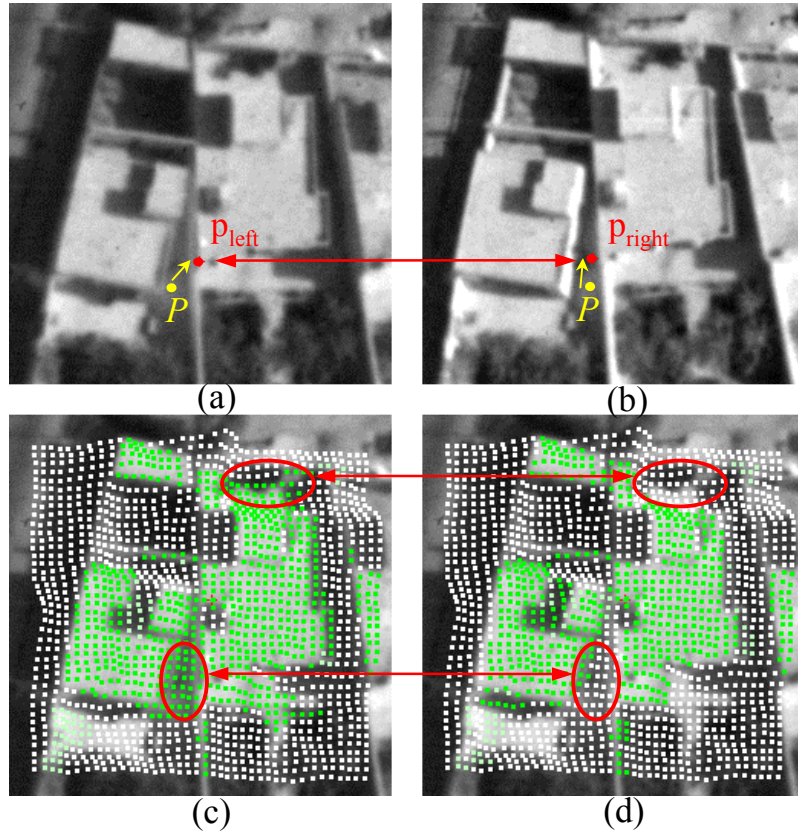


Figure 7-14: The point “P” is incorrectly projected on (a) left “ p_{left} ” and (b) right “ p_{right} ” images, due to the DSM error (c) Building detection using Naïve BN (d) Building detection using Augmented BN

Figure 7-15 shows the results of applying this method for three regions of Bam city. The proposed classifier has succeeded in discriminating buildings among palm trees using gray-scaled images. In addition, these data can be processed to extract information used for risk assessment and disaster management. Two of the important parameters for earthquake risk assessment are density and average height (i.e. number of storey) of buildings in each city block. In general, risk increases as population and building density increase. Taller buildings are more vulnerable than one- or two-story buildings when located on soft, unconsolidated sediments, but taller buildings tend to be the more stable when on a hard bedrock foundation. Table 7-1 gives an estimation of density and average heights of buildings for three specific regions in comparison with manual stereoscopic measurements. The building density is calculated with the quotient of building area to the region area, which is: $100\text{m} \times 100\text{m} = 10^4 \text{ m}^2$.

Table 7-1: Building density and average building height extracted manually and automatically

Figure 7-15	Stereoscopic measurement		Automatically estimation	
	Building density	Average building height [m]	Building density	Average building height [m]
Region #1	%32	4.5	%35	5.3
Region #2	%20	3.7	%18	5.1
Region #3	%12	5.5	%10	4.8



Figure 7-15: Left: three regions of Bam city before the earthquake, Right: results of proposed method to discriminate man-made objects from vegetation. For more information please refer to table 7-1

7.5.4. Bayesian Network for Damage Assessment

The main contribution of the previous part was to explore the use of Bayesian networks to combine various features obtained from DSM and imagery data to detect and extract man-made regions. Now, we can combine the results of before and after earthquake for damage detection of man-made objects (Figure 7-16).

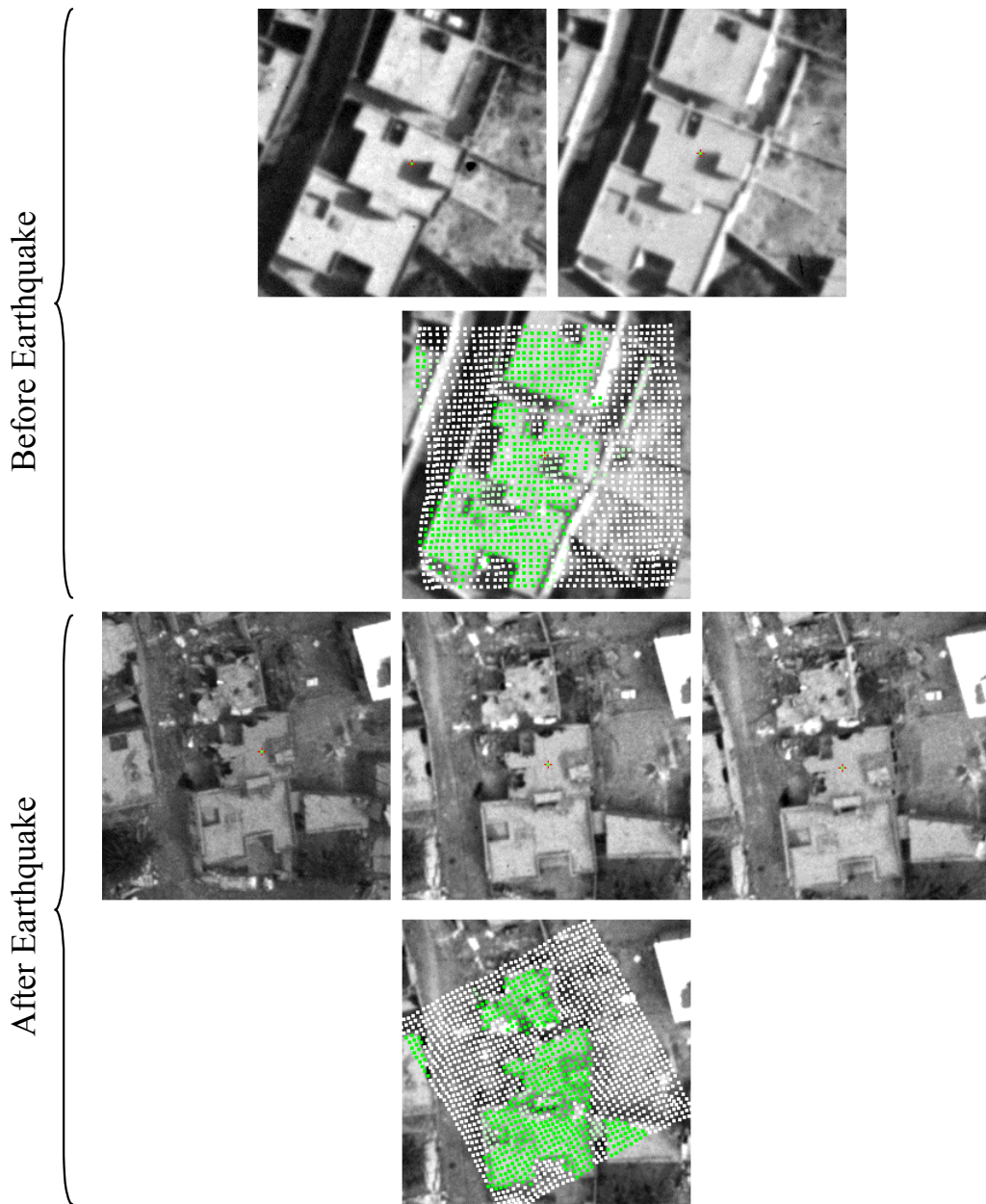


Figure 7-16: Comparing buildings before and after the earthquake of Bam – two images before and three images after the earthquake are available – green points represent undamaged parts of man-made objects extracted automatically using the augmented Bayesian networks

To detect damaged points we propose a symmetric form of Bayesian network includes two parts for building detection before and after earthquake (H_b and H_a). The final section of the network is organized based on perceptual concept of a damaged region. In this part, results of previous section are considered as input to estimate the final predicate ($H_d: P_n \text{ is damaged}$). Moreover, the reduction of average heights ($\varphi_2^{\text{before}} - \varphi_2^{\text{after}}$) is used as well (Figure 7-17).

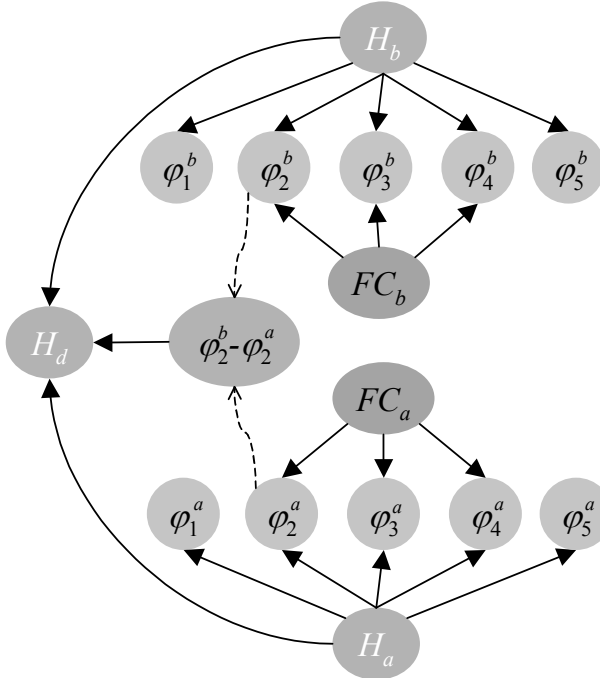


Figure 7-17: Bayesian network constructed for damage classification

We define random variables hb and ha , having normal distributions with means and standard deviations $(\mu_{\varphi_2}^{\text{before}}, \sigma_{\varphi_2}^{\text{before}})$ and $(\mu_{\varphi_2}^{\text{after}}, \sigma_{\varphi_2}^{\text{after}})$ respectively. In addition, we define the random variable $hr = hb - ha$, which has to be normal with mean and standard deviation:

$$\left(\mu_{hr} = \varphi_2^{\text{before}} - \varphi_2^{\text{after}}, \sigma_{hr} = \sqrt{(\sigma_{\varphi_2}^{\text{before}})^2 + (\sigma_{\varphi_2}^{\text{after}})^2} \right) \quad (7-29)$$

The standard deviations can be set regarding the DSM accuracies, which can be obtained by estimating checkpoints and/or taking sensor models and image scales into account. The probabilities $\Pr(H_b=True)$ and $\Pr(H_a=True)$ follow from:

$$\begin{aligned} \Pr(H_b = \text{True}) &\propto \\ &\sum_i \Pr(H_b = \text{True}/hb \in \text{interval } i) \Pr(hb \in \text{interval } i) \\ \Pr(H_a = \text{True}) &\propto \\ &\sum_i \Pr(H_a = \text{True}/ha \in \text{interval } i) \Pr(ha \in \text{interval } i) \end{aligned} \quad (7-30)$$

and the probability of $\Pr(H_d = S_i)$ follows from:

$$\Pr(H_d = S_i) \propto \sum_i \sum_{(S_1, S_2)} [\Pr(H_d = S_i / H_b = S'_1, H_a = S'_2, hr \in \text{interval } i) \times \Pr(H_b = S'_1, H_a = S'_2, hr \in \text{interval } i)] \quad (7-31)$$

Where the tuple (S'_1, S'_2) has the values $\{(True, True), (True, False), (False, True), (False, False)\}$ and

$$\begin{aligned} \Pr(H_b = S'_1, H_a = S'_2, hr \in \text{interval } i) &= \\ \Pr(H_b = S'_1, H_a = S'_2) \Pr(hr \in \text{interval } i / H_b = S'_1, H_a = S'_2) &= \\ \Pr(H_b = S'_1) \Pr(H_a = S'_2) \Pr(hr \in \text{interval } i / H_b = S'_1, H_a = S'_2) & \end{aligned} \quad (7-32)$$

We perform hypothesis test that hr is discretized into intervals: $hr < 1m$ and $hr \geq 1m$ (please refer to Chapter 5). The following conditional probability table is established (Table 7-2):

Table 7-2: Conditional probability table for H_d

H_b	H_a	$hr \geq 1m$	H_d
<i>True</i>	<i>True</i>	<i>True</i>	Dr: <u>Dropped</u> rooftop
<i>True</i>	<i>True</i>	<i>False</i>	U: <u>Undamaged building</u> rooftop
<i>True</i>	<i>False</i>	<i>True</i>	De: <u>Demolished</u> rooftop
<i>True</i>	<i>False</i>	<i>False</i>	C: <u>Changed</u> rooftop
<i>False</i>	<i>True</i>	×	U: <u>Undamaged building</u> rooftop
<i>False</i>	<i>False</i>	×	N: <u>No building</u>

In this table, two levels of damage: *Demolished* (De) and *Dropped* (Dr) rooftops are defined. Moreover, undamaged area is divided to: *Undamaged building* (U) and *No building* (N) regions. The attribute known as *Changed* (C) can translate to “probable damage”. This attribute would be assigned when “ $H_b = \text{True}$ ” and “ $H_a = \text{False}$ ” and null hypothesis for height variation is not rejected. Since, no rejection doesn’t mean to be accepted, we need to take more care with possibility of being damage with this attribute. Therefore:

$$\sum_{i=1}^5 \Pr(H_d = S_i) = 1 \quad \text{where} \quad S_i \in \{N, U, C, Dr, De\} \quad (7-33)$$

For final classification, the points will be marked by the attributes with maximum probability more than 0.5 (i.e. the attribute with absolute majority). If none of the attributes would attain absolute majority, that point has to be ignored or reinspect visually.

$$\forall P_n : \text{ if } \Pr(H_d = S_k) > 0.5 \text{ then } "P_n \text{ is attributed as } S_k" \quad (7-34)$$

7.6. Empirical Investigations

7.6.1. Experimental Results – Bam City (Gray-scale aerial images)

The proposed methods including segmentation, features extraction and classification by means of Bayesian Network have been implemented and produced as stand-alone software. Using the networks discussed in the previous section, the performance of the system was analyzed. In particular the ability of the proposed system for damage assessment was tested. Initially, different regions of Bam city were used in order to characterize the performance of the system across different degrees of damage using gray scale images. After network installation, the probabilities are calculated once with respect to entire compositions of states. All probabilities were computed for the points of a regular mesh at spatial resolution 1m. In the Bam dataset, most buildings were constructed of clay bricks in simple box shape with flat rooftops, and low-texture images resulted. Also, traditional adobe buildings respond very poorly to earthquake ground shaking, suffering serious structural damage or collapse. In Bam, the vast majority of buildings in the city collapsed and most of the remaining buildings were severely damaged. Thus, the interpretation of damages in our dataset is a bi-level choice mainly either fully collapsed or partly collapsed.

The results of ten sample windows of Bam city are shown in Figure 7-19. Each window covers an area about 40m×40m. The left two columns comprise digital aerial images before and after the earthquake (note that the images have different orientation). The right column shows the classified points that are superimposed on the image of after earthquake. Figures 7-19(a) to 7-19-(e) show fully and partially collapsed buildings. Red points, which are labeled as “Demolished rooftop” (De), represent collapsed parts of the buildings. Our investigations indicated that the suggested system is quite promising to detect full-collapse and partial-collapse buildings. We defined “Changed rooftop” (C) when “ $H_b = True$ ” and “ $H_a = False$ ” while height reduction is trivial. The “Changed rooftop” attribute usually represents a definite change in features of images before and after the earthquake without height reduction, which might be related to small-size debris over the rooftop (Figure 7-19(c), (h), (i)) or burned structures (Figure 7-20(d), (e) in the Kobe dataset).

Additionally, we defined another type of collapsed points, so called “Dropped rooftop” (Dr) that might be related to damage with broken planes or pancake collapse buildings. Figure 7-19(f) shows a sample building that the rooftop is broken into fragments after the earthquake. Applying the proposed method revealed fell-down planes, which is marked by pink colored points. The usefulness of the proposed method to detect small damages is exhibited by Figures 7-19(g) to 7-19(i). Figures 7-19(j) shows a location with palm trees that do not exist any more after the earthquake. The inferring system use the goodness of fit to detect vegetation areas. In this location, despite surface elevation (ca 4m), it is not classified as building and hereupon the classification is carried out correctly. The obtained results are promising, in the following our experiments will be repeated for colored aerial images of Kobe city.

7.6.2. Experimental Results – Kobe City (Colored aerial images)

The use of color for representing image data is very common image processing research, dictated primarily by the availability of such data as produced by the camera apparatus. We extend our method for available colored aerial images of Kobe city. The edges are obtained by computing gradients of each RGB component image and forming a composite gradient image by adding the corresponding values of the three component images at each coordinate. Next, the edge map will be used for the line detection procedure. In addition, green parts of images are estimated using RGB

and CIELAB color space by performing pixel-based classification (c.f. section 7.4.2.1). The percentage of green points within any given segment could represent the probability of being a greenery segment. This new feature is represented as a child node added to hypothesis nodes (H_b , H_a) in Bayesian network (Figure 7-18, φ_6^b, φ_6^a). As before, the conditional probability tables need to be adjusted properly. For this purpose, some sample buildings for training were selected and related probabilities were calculated using a counting-learning algorithm.

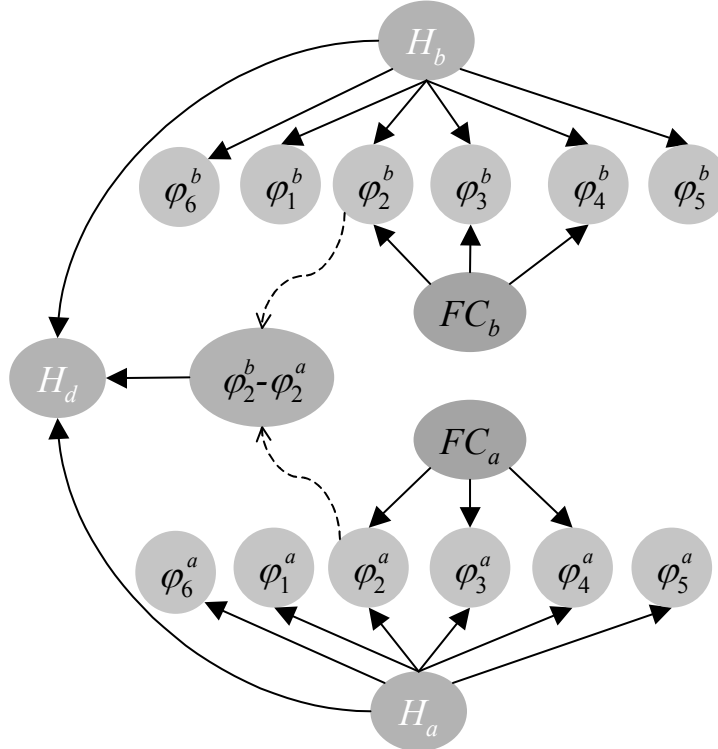
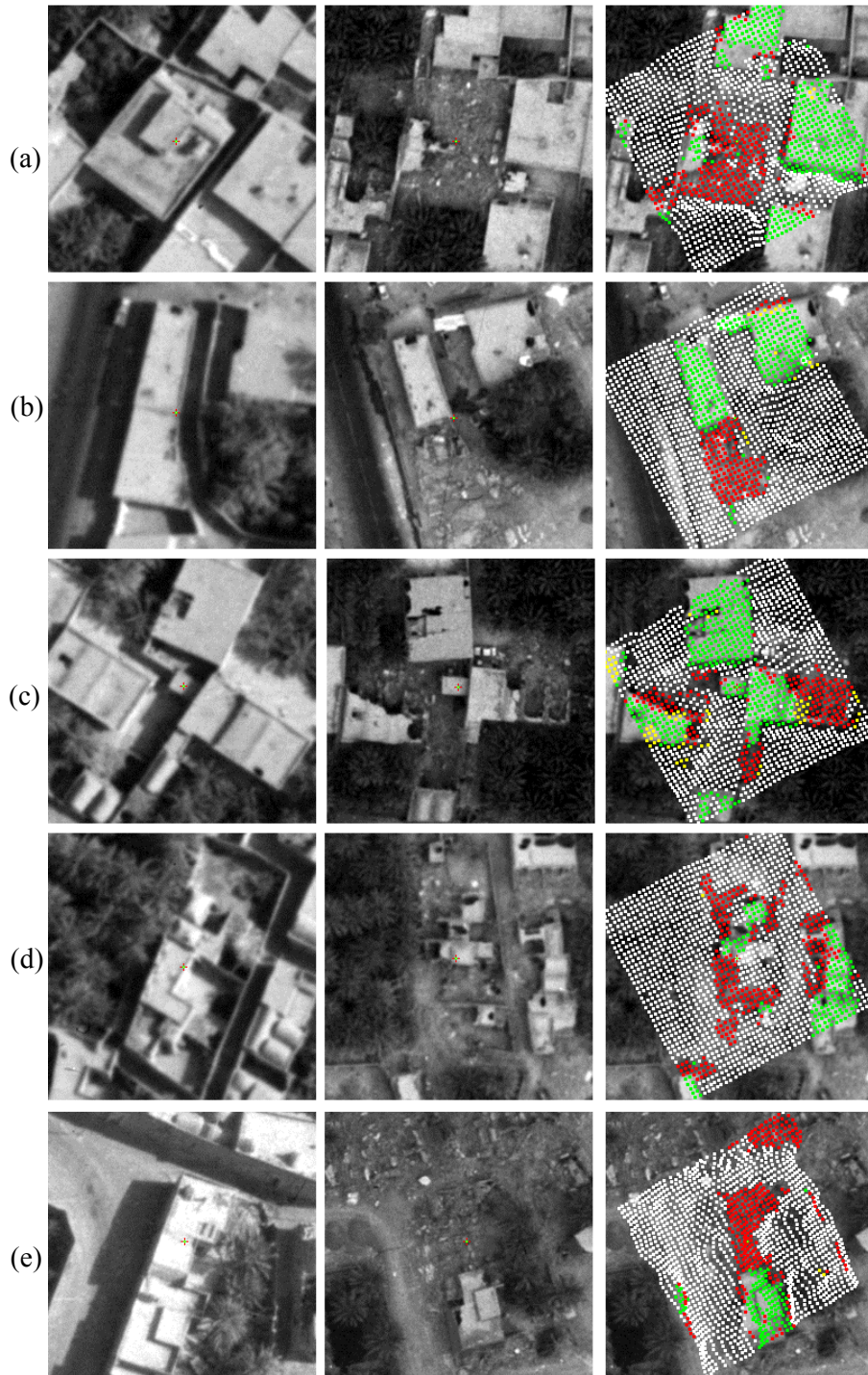


Figure 7-18: Bayesian network constructed for damage classification, two nodes for detecting the segments with green color (φ_6^b, φ_6^a) are added

Unlike the city of Bam, Kobe is composed of wide varieties of structures with the jam-packed high-rise and low-rise buildings. Some buildings exhibit complex shapes of rooftops with small details and some of them are partly occluded by the next building.

After the Kobe earthquake, older wood-frame houses with heavy clay tile roofs completely collapsed. Most of the older traditional houses had heavy tiled roofs and when the support frame gave way, the roof crushed the un-reinforced walls and floors in a "pancake" collapse. The collapse of buildings was followed by the ignition of fires within minutes of the earthquake and some buildings were ruined by fire. However, many of the structures had been designed to strict seismic codes, and most of these buildings withstood the earthquake.



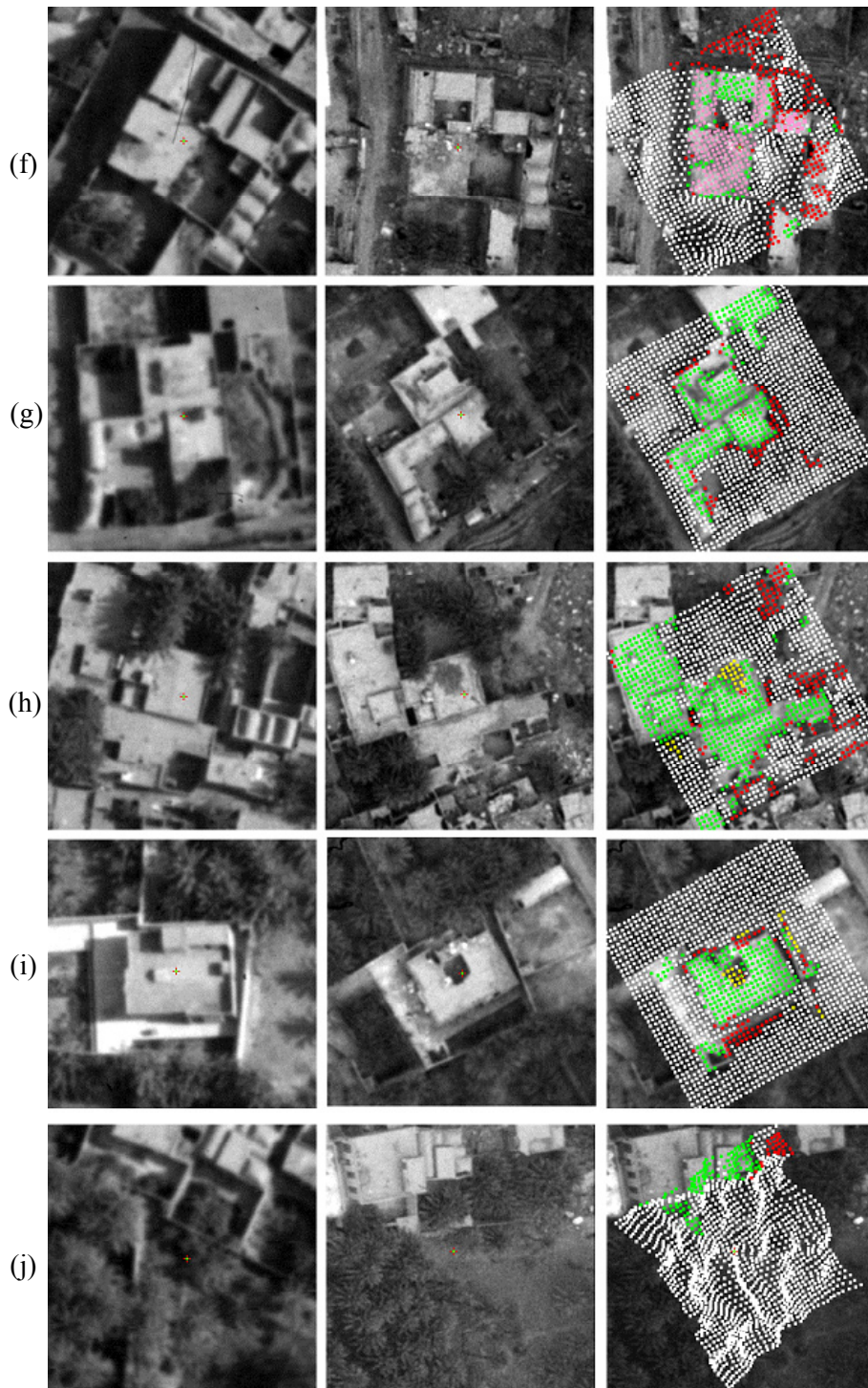
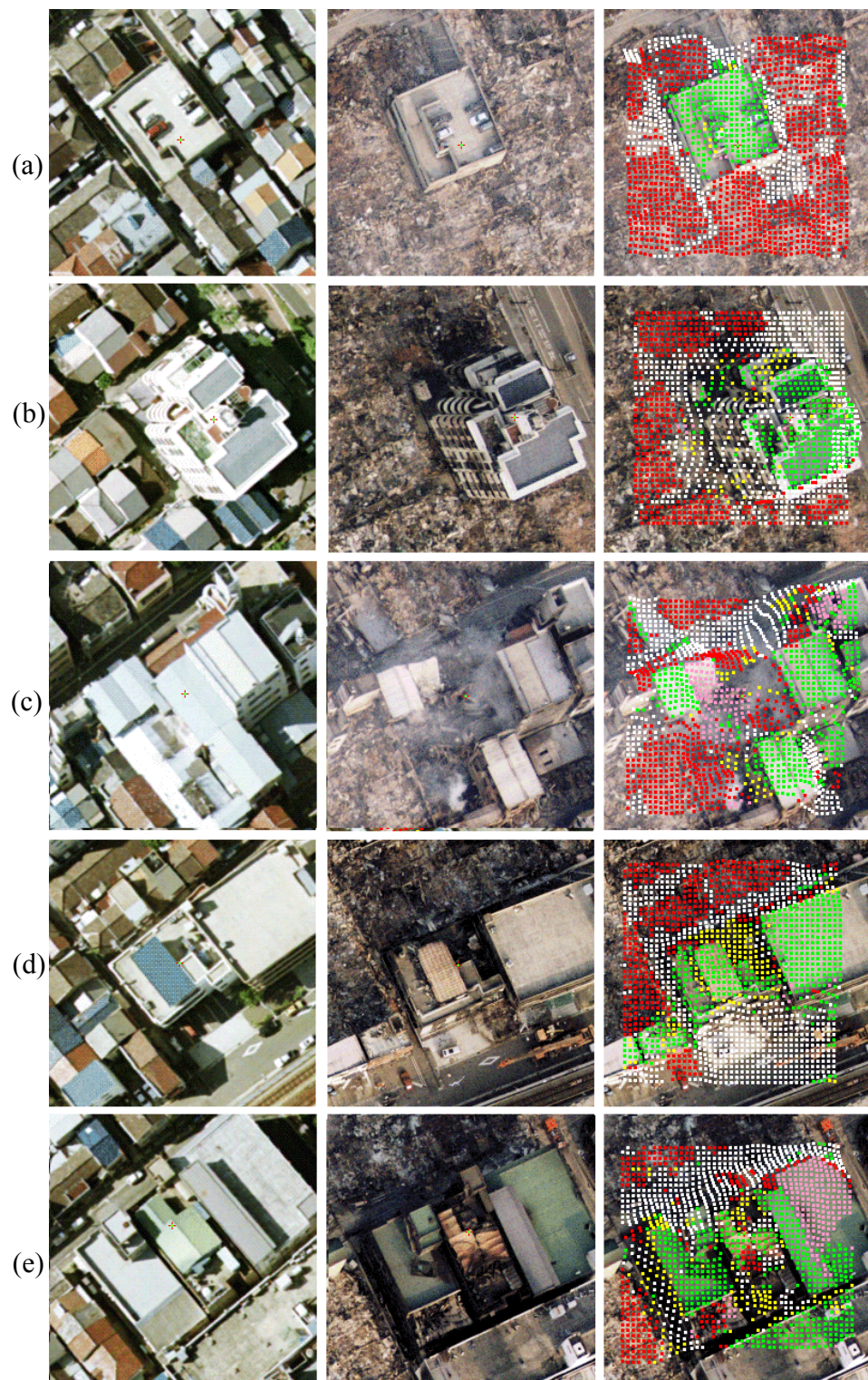


Figure 7-19: Results of BN classification on sample windows of Bam city - the left two columns: pair of aerial images before and after the earthquake, the right column: classified points, red: Demolished, pink: Dropped, yellow: Changed, green: Undamaged rooftop and white: No building



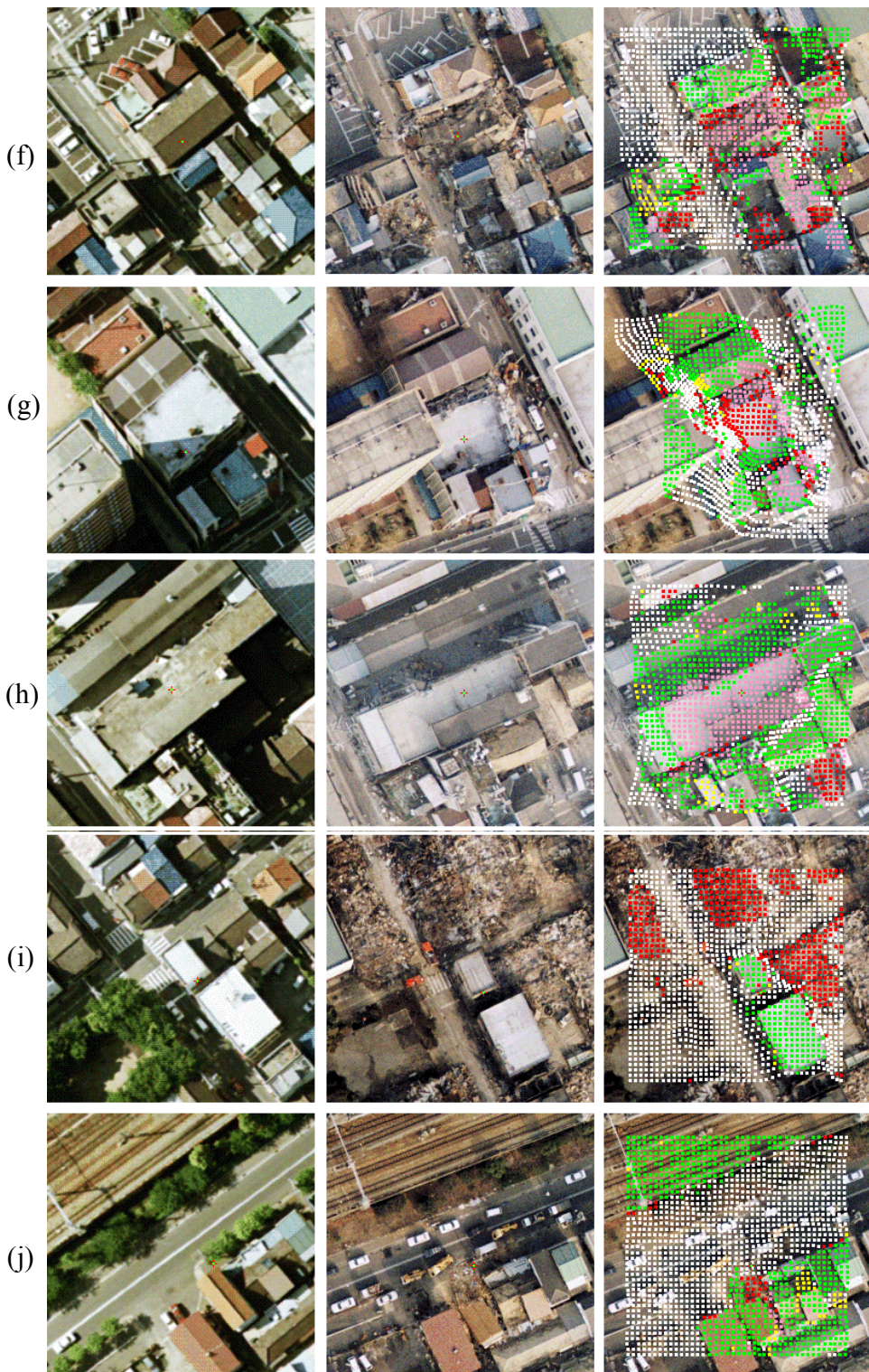


Figure 7-20: Results of BN classification on sample windows of Kobe city - the left two columns: pair of aerial images before and after the earthquake, the right column: classified points, red: Demolished, pink: Dropped, yellow: Changed, green: Undamaged rooftop and white: No building

Segmentation, feature extraction and classification by applying Bayesian Network are conducted and the probabilities are computed for the points of a regular mesh at a spatial resolution of 1m. Figure 7-20 demonstrates the final results for ten sample windows with a size about 40m×40m. Figure 7-20(a) shows some residential buildings that enclose a parking deck. Except the parking deck, all of buildings are demolished after the earthquake. In this sample, the area clearly is divided into “no damage” and “Demolished” regions while white points are representing “No building” locations such as alleys or courtyards. Figure 7-20(b) shows a multi-storey building that suffers no structural damage and all constructions are totally collapsed around the building, marked by red points as demolished area (De). Careful scrutiny of the high-rise building from different views revealed burns in the forth and fifth stories. Generally, after an earthquake, haze of dust and smoke obscure the view of the city, disturbing image interpretations. Figures 7-20(c), (d), (e) show some locations that were burned and demolished after the earthquake. A smoky fire has covered the collapsed buildings in Figure 7-20(c). The regions without attribute (vacant spaces) are not classified due to lack of complete confidence in assigning the foreseen attribute. Within smoky locations, we have vague features that prevent the inferring system from assigning any attribute to the points (please refer to Equation 7-34). Figure 7-20(d) shows a building ruined by fire but its frame is intact. In this case, the inferring system detects significant change in texture intensity without height reduction that leads to “Changed” labels (yellow points). Similarly, Figure 7-20(e) shows damaged buildings after the shake and consecutive fire. Figures 7-20(f), (g) show damaged buildings with broken planes, which are marked by pink points known as dropped planes (Dr). This attribute indicates that we encounter heavy big plates of a damaged rooftop. As well, pancake collapsed buildings may be exhibited by group of points classified as “Dr” (Figure 7-20(h)). The left window of Figure 7-20(i) shows a green area where trees had been pruned before the earthquake. In this location, colored imagery data cause a correct decision despite estimating height elevation about 7 meters. Figure 7-20(j) shows part of the railway-bridge detected by the classifier while the trees standing nearby. This sample shows the usefulness of the proposed method to detect other manmade objects.

We should note that substantial blunders in a digital surface model especially around steep slopes of buildings cause false alarms. In the Kobe dataset, the accuracy of the DSM - generated automatically - becomes worse in these areas with densely manmade objects. There are many points having more than 3.0 meters difference with manually measured points. These points are almost all located around the steep slopes of the buildings. This is caused by the fact that manually measured points and automatic extracted points refer to different object points due to the errors in image matching procedures and surface modeling problems (Zhang 2005). In addition, smoothing effects caused by utilizing the surface smoothness constraint can appear in cases where some edges cannot be successfully matched or the foot parts of buildings are totally occluded.

As mentioned earlier, the system is designed to detect planar manmade objects and may fail to detect a rooftop with curved surface. Figures 7-21(a) and 7-21(b) demonstrate two sample buildings with barrel-shaped and domical roofs from Kobe and Bam cities respectively. The Bayesian network trained for planar rooftops is unable to discern such structures.

The framework of the proposed system is designed to classify single points, however, the final decisions must be made based on the attribute of a group of points. Therefore, after removing single noisy points, we are able to report distribution, density and damage severity for a given area. Damages in surrounded regions are estimated based on attributes of the points inside. The estimate of debris volume from any given area could be one of the by-products of using such system.

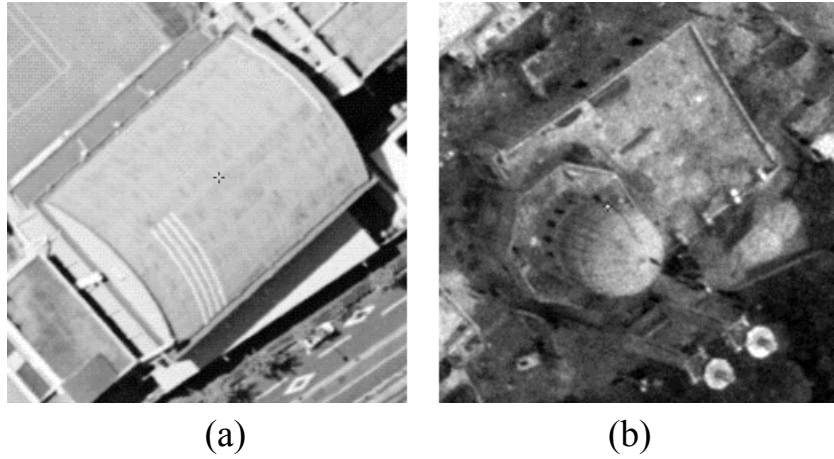


Figure 7-21: (a) Barrel-shaped rooftop in Kobe, (b) Domical rooftop (mosque dome) in Bam

7.7. Automatic Interpretation of Damaged Buildings

The goal of this section is to develop an artificial expert interpreter for classifying damaged buildings. For any desired and delineated region, the presented method is able to detect and classify damaged points. This region may be a polygon that identifies building rooftop. However, extracting details of damaged buildings would be possible if appropriate resolution in both imagery data and surface model is available. We should set prior probabilities concerning rooftop area of a man-made object. Before an earthquake, a prior probability should be set to one (i.e. $P(H_b = \text{True}) = 1$) and then only the second part of the BN will be active for detecting damages. After an earthquake, a prior probability for any specific building can be estimated if technical data about the building construction and/or severity level of earthquake are available. Otherwise, equal prior probabilities will be set. In this section we focus on the Kobe dataset with color images, more details for Bam can be found in (Rezaeian and Grün 2010).

Damaged parts of each building are highlighted by “Demolished” and “Dropped” attributes. Moreover, some points may be marked by “Changed” attribute when the BN classifier is doubtful about being damaged or undamaged (c.f. section 7.5.4). After pointwise assessment, with respect to the area of a building the ratio of damaged parts is estimated. Final classification is performed through “if-then” rules. Regarding the damaged parts of a rooftop, we define two levels of destruction for likely collapsed and certainly collapsed structures (DL1, DL2, e.g. 20% for likely collapsed and 50% for certainly collapsed). Those buildings that are certainly collapsed should be classified as “Partially” or “Totally” collapsed (EMS98: Grade 4,5 in Chapter 4). The certainly collapsed buildings are subject to more investigation to discover the details of demolition. Considering the proportion of “Demolished” and “Dropped” points, more details about collapsed buildings are extracted. In addition, we assume buildings with average height reduction less than one-meter per storey are recognized as “Partially collapsed” (still standing stories). The likely collapsed buildings have to be rechecked, this time including those points labeled by “Changed” attributes. The building is classified as “Partially collapsed” if $(De + Dr + C) > DL2$, otherwise it is classified as “*Substantial damage*” (EMS98: Grade 3). Also, we need to define a minimum level of “Undamaged” points for recognizing undamaged buildings (UL, e.g. 60%). Ultimately, the last if-then rule examines the structure for the final condition of an undamaged building or classifying it as

“Moderate damage” (EMS98: Grade 2). The following instructions summarize how to interpret and classify a damaged building automatically:

- Calculate ratios of “De”, “Dr”, “C”, “U” attributes and average heights of the building before and after earthquake (hb , ha).
- Calculate: $D = De+Dr$ and $d = hb-ha$ and estimate number of building stories: $s = hb \div 2.5$ (one-storey building height = 2.5m)
- Define two levels for partially and totally collapsed buildings: DL1 = 20%, DL2 = 50% and one level for undamaged buildings: UL = 60%

```
if (D > DL2) then {
    if ( d > s ) then
        Classified as: "Totally collapsed (G5)"
    else
        Classified as: "Partially collapsed (G4)"
    /* Looking for more details of collapsed building*/
    if (Dr > DL2) then
        Affix: "-inclined, overturned or pancake collapsed"
    elseif (Dr > DL1) then
        Affix: "-heap of debris with plates"
    else
        Affix: "-heap of debris"
}
elseif {
    if ( D > DL1) then {
        if (D + C > DL2) then
            Classified as "Partially collapsed (G4)"
        elseif
            Classified as "Substantial damage (G3)"
    }
    elseif (U > UL) then{
        Classified as: "Undamaged or no significant damage (G1)"
    }
    else
        Classified as: "Moderate damage (G2)"
}
```

Figures 7-22 to 7-26 show some sample buildings that first were segmented using the Bayesian reasoning network and then classified into damage categories using if-then rules (equal-appearing windows have different size). The attributes were recorded at equally spaced points (50 cm) within building polygons including: “Demolished”, “Dropped”, “Changed” and “Undamaged” represented by red, pink, yellow and green points respectively. Figures 7-22(a)-(d) and Figures 7-23(a)-(f) demonstrate some totally collapsed buildings from the Bam and Kobe datasets. In Bam, the majority of collapsed buildings were converted to a heap of debris either totally or partially. The developed system will be able to extract more details about remaining rubbles and debris type. Figure 7-23(c) shows a 7-storey building in Kobe that after the earthquake is completely collapsed. Automatic interpretation could give us a hint about huge debris with large plates. The secondary information about the type of debris facilitates rescue operations and recovery programs. Figures 7-23(d), (e) and (f) exhibit totally collapsed buildings where floor slabs form stacked layers. The case of Figure 7-23(g) a building is estimated to be 5-story and classified as partially collapsed into “one-story pancake collapse” category (Figure 3-4).

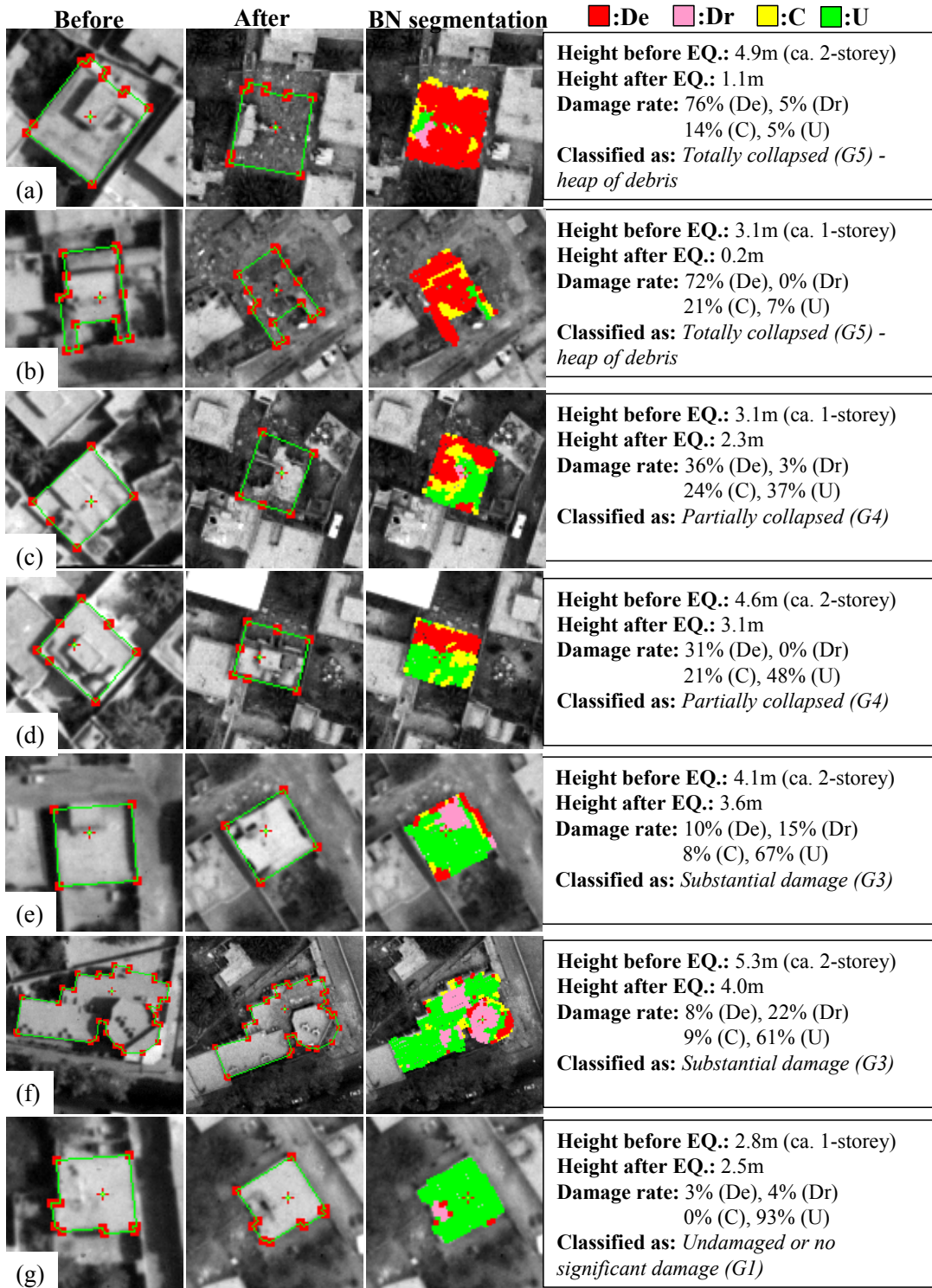


Figure 7-22: Results of automatic damage interpretation for sample buildings of Bam city - the left two columns: pair of aerial images before and after the earthquake, the right column: segmented buildings and their damage interpretation

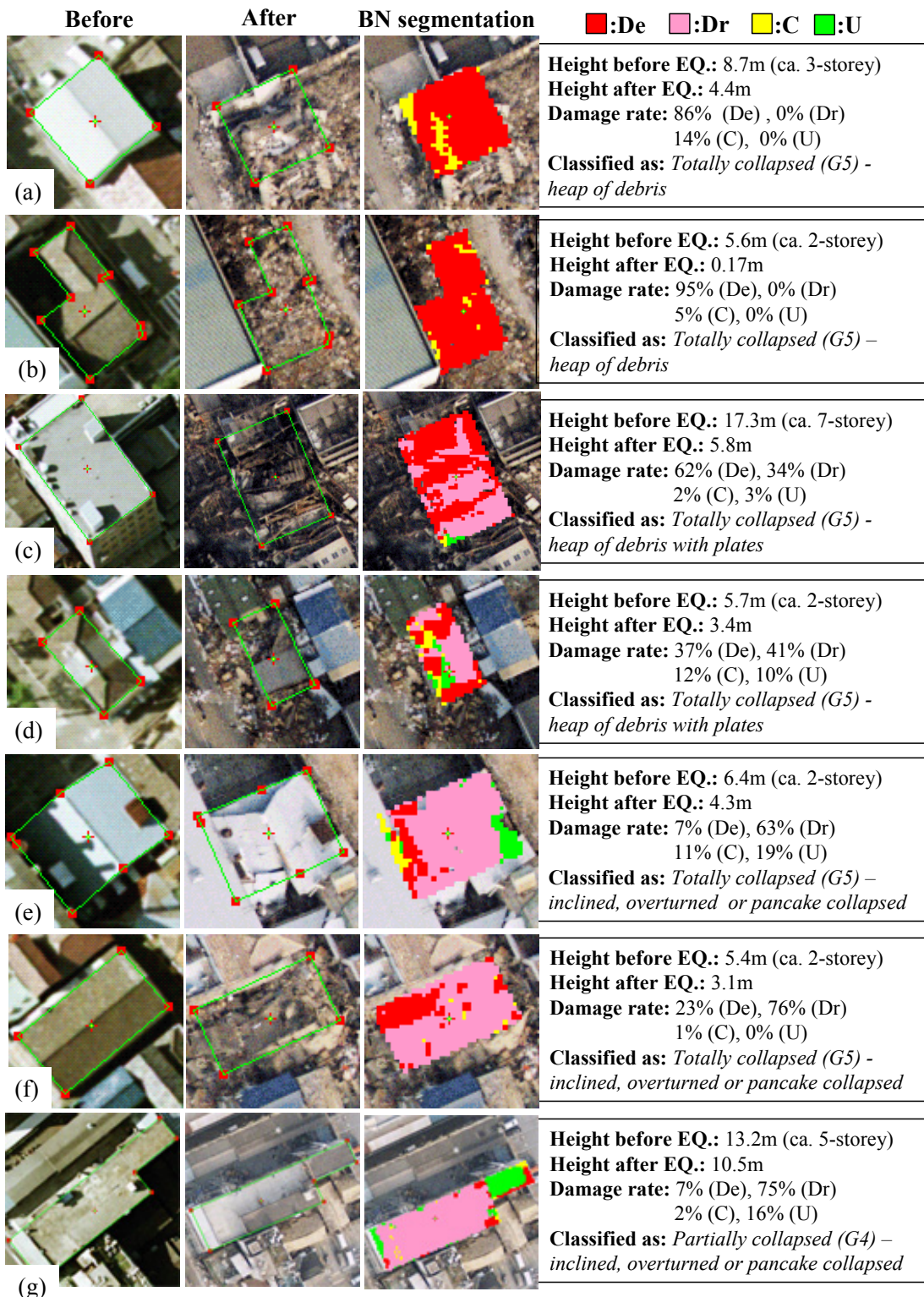


Figure 7-23: Results of automatic damage interpretation for sample buildings of Kobe city - the left two columns: pair of aerial images before and after the earthquake, the right column: segmented buildings and their damage interpretation – Collapsed buildings

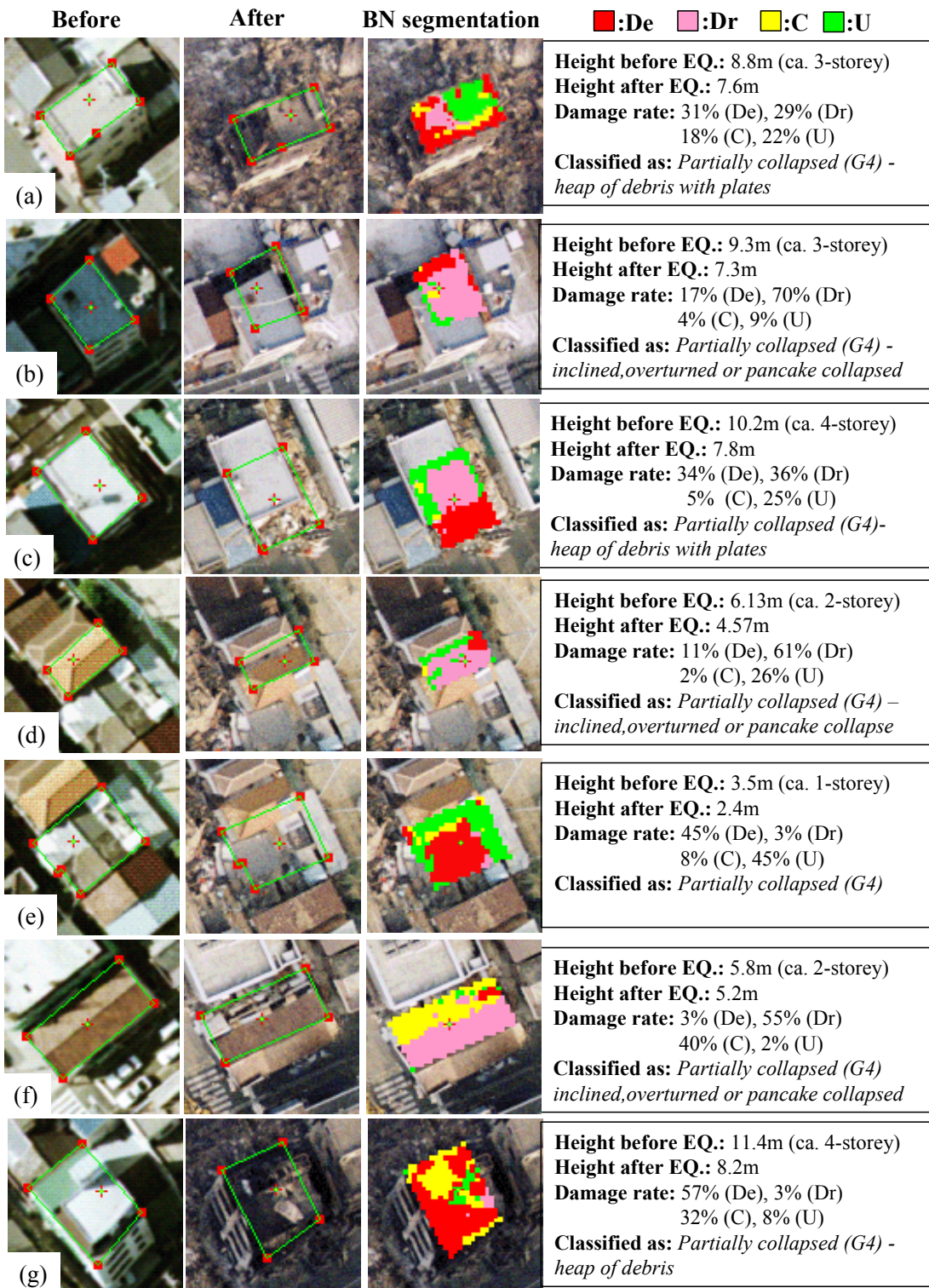


Figure 7-24: Results of automatic damage interpretation for sample buildings of Kobe city - the left two columns: pair of aerial images before and after the earthquake, the right column: segmented buildings and their damage interpretation – Partially collapsed buildings

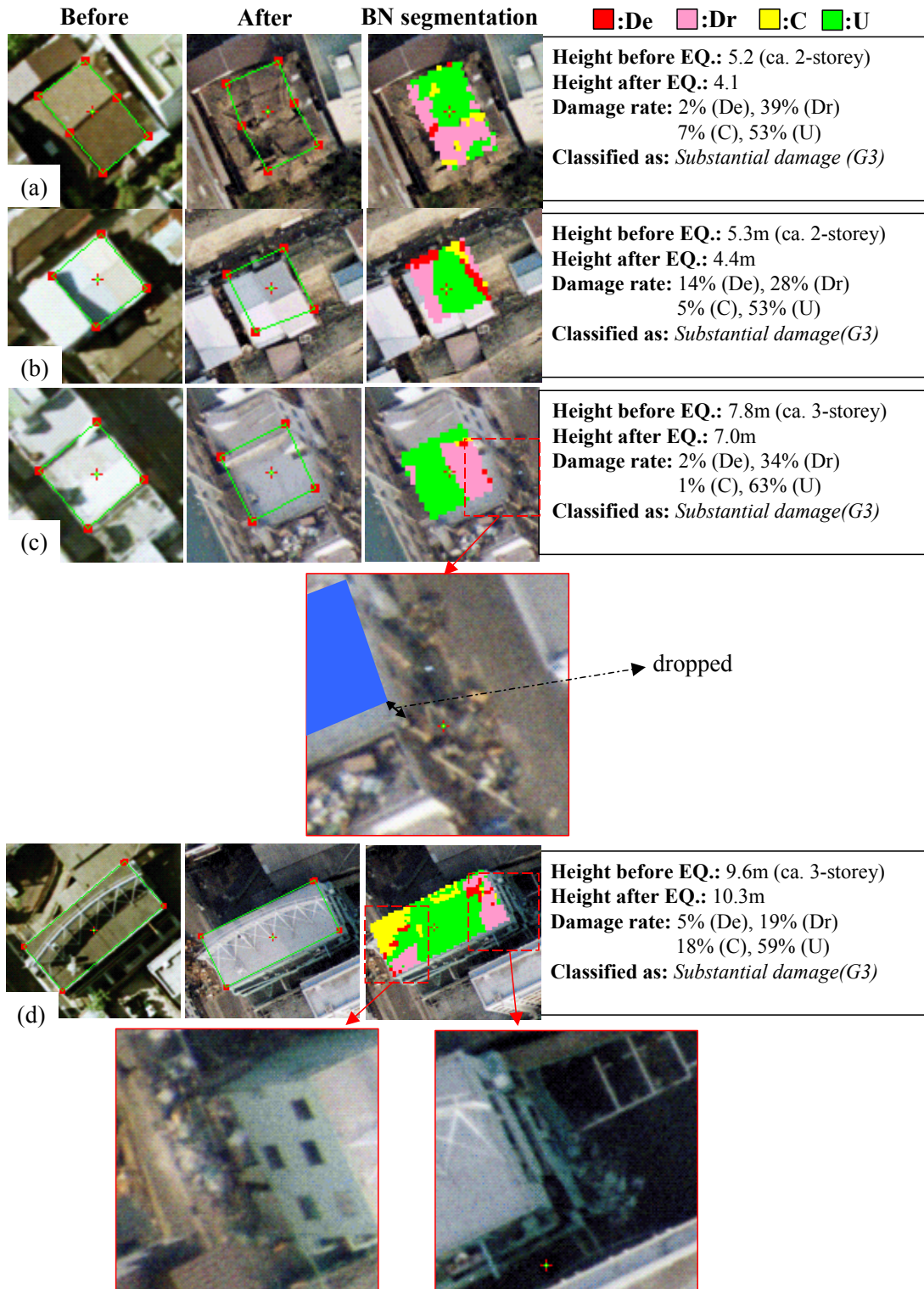


Figure 7-25: Results of automatic damage interpretation for sample buildings of Kobe city - the left two columns: pair of aerial images before and after the earthquake, the right column: segmented buildings and their damage interpretation – Substantially damaged (G3)

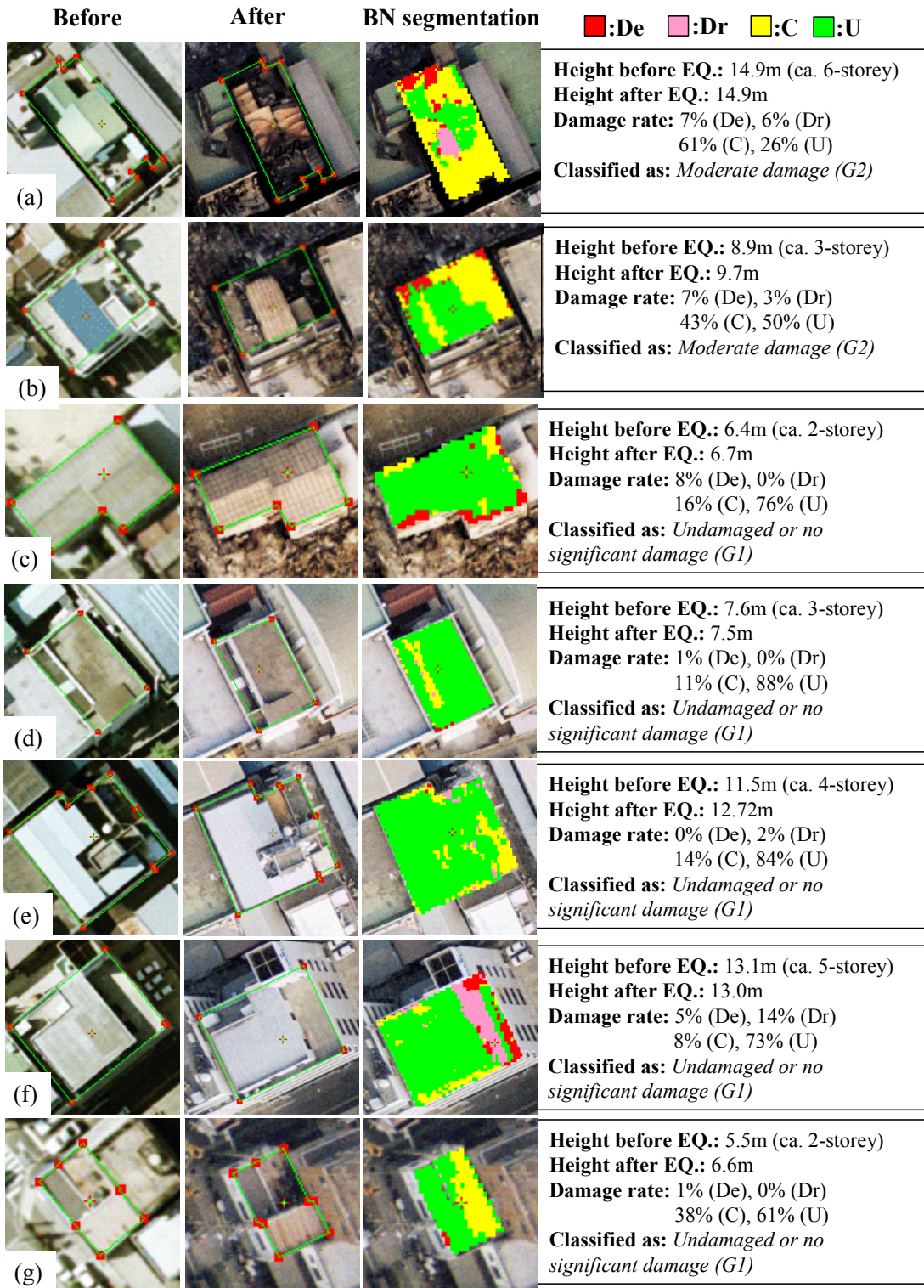


Figure 7-26: Results of automatic damage interpretation for sample buildings of Kobe city - the left two columns: pair of aerial images before and after the earthquake, the right column: segmented buildings and their damage interpretation – No structural damage (G1&G2)

Figure 7-24 demonstrates a collection of “Partially collapsed” buildings with different situations after Kobe earthquake. Figure 7-24(a) shows a single partly collapse surrounded by debris, which is correctly classified as Grade 4 of EMS98 levels. After an earthquake, buildings might be removed from their initial locations while still standing. Commonly, serious dislocations may cause to damage soft first storey and the resulting height reduction will be detectable (Figure 7-24(b), (c), (d)). Figure 7-24(d) shows a dislocated building that moved to the next neighboring building while it is completely collapsed (Figure 7-24(e)). When the dislocated house partly occupies adjacent footprint, it is quite likely to misclassify a totally collapsed as a partially collapsed building. Also, significant blunders of DSMs cause a similar mistake where low-rise collapsed buildings are located near to high-rise ones (Figure 7-24(f)). In addition, DSMs generated by image matching software may contain substantial errors in low-textured area of the image. For instance, the building in Figure 7-24(g) would be classified as non-structural damage (Grade 3) if the height of scorched building - appeared in dark and edgeless image- could be measured from precise DSMs, but in this area DSM points show an average error about of 3m (underestimation). Nevertheless, The experimental results to detect totally collapsed structures are quite promising and the proposed system is still successful for many structural damages containing either heap of debris or inclined layers. The erroneously categorized buildings were further investigated to find out what might have caused them to deviate from the reference data. It appears that the main reason for undamaged buildings to be wrongly categorized as “Partially collapsed” is problems in the DSM generation. Moreover, another reason is the absence of strong evidences in areas where buildings are hidden in the shadows or covered by trees.

Moderate structural damages are represented as Grade 3 of EMS98 (Table 3-1). This category describes buildings with large and extensive cracks in walls, detached roof tiles, failure of rooftop elements and gable walls and surrounded by debris and rubbles. However, the proposed system concentrates on building footprint regardless of its surrounding. In previous chapters, the features (e.g. average height reduction) are calculated on the whole assuming any building as one entity. In this chapter, objects are divided into segments with related attributes and therefore small damaged parts can be detected. Figure 7-25 presents some results of the proposed method to classify buildings with moderate structural damage (Grade 3). Figure 7-25(a) shows a building that is not collapsed but some segments of the rooftop have been damaged.

Figure 7-25(b) shows a pair of dislocated buildings. The proposed system succeeds to reveal small vacant spaces classified as damaged parts. Figures 7-25(c) and (d) exhibit two buildings where at first glance no damage is detected and comparing “average heights” of buildings before and after earthquake does not show any significant height reduction. Nonetheless, pointwise comparisons give strong evidence for detecting a damaged building. In Figure 7-25(d) the billboard on the rooftop makes a complex structure, which is not represented correctly by the DSM. For this building, the DSM errors cause to show a higher value for “average height” after the earthquake (before: 9.6m & after: 10.3m). Despite illusive data, the BN classifier succeeds to extract fell down parts of the rooftop assigning Grade 3 for damaged building.

We utilized the Bayesian network to combine pictorial and geometrical features. Consequently, this approach makes significant improvement to recognize heavy and moderate structural and presents a rather efficient method to discover non-structural damages. Figures 7-26(a) and (b) present two burned buildings with slight structural damages. In this case, the classifier is able to explore dark parts of the buildings attributing scorched sections into “Changed” points. With relation to damage rate and selected thresholds, these buildings are classified as Grade 2 of EMS98 categories (Moderate damage). Figures 7-26(c) to 7-26 (g) show five undamaged buildings that are classified correctly. We define a threshold value (UL), which indicates minimum rate of undamaged

points approving a building to be labeled as undamaged structure. In Figure 7-26(f) the rooftop's bi-level design located beside a tower-shape structure makes problems for surface modeling. This composition together with low-texture and dark shadow in pre-event images generates partly incorrect attributes (pink segment: "Dr"). However the ultimate decision is made correctly. The domain for finding intact buildings becomes restricted with increasing this threshold. There is a trade-off between the number of false negatives (undetected damages) and false positives (falsely detected damages). In this application, if the results are to be edited by a user, removing false positives may not be so critical, and if the results of the automated process are to be used directly, it may be important to weight the errors of false negatives more than those of false positives. Changing the thresholds for the output usually controls the relation between false positives and false negatives.

Table 7-3 presents numerical comparison of automatic damage interpretation with visually damage classification (Chapter 3). For tri-level classification ("Uncollapsed", "Partially collapsed" and "Totally collapsed") and in comparison with the results of previous chapters (e.g. Table 6-5) we achieve significant improvements. Out of 637 buildings in the Kobe dataset, 571 buildings are correctly classified resulting an overall accuracy 89.8%. The producer and user's accuracies of "Partially collapsed" buildings were computed as 56.4% and 53.5%, which show significant improvements as well. In addition, a validation for multi-level EMS classes is performed with respect to our referenced data extracted visually. Producer and user's accuracies for (G1&G2) and (G5) were calculated 90.3%, 86.8% and 94.4%, 97.3% respectively. Considering visual interpretation criteria, for G3 one needs to detect surrounding debris (Table 3-1). It is foreseen that the EMS-G3 being undetectable with only roof analysis approach. Nevertheless, the reasoning system considerably succeeds to extract details of collapsed buildings. It should be noted that due to inherent ambiguity in definition of collapse categories, the results of interpretation that are performed manually by different human interpreters could be dissimilar. In Table 7-3, we assume shaded cells exhibit correct classification. Accordingly, the proposed system achieves 85.6% of overall accuracy for damage classification with details about collapsed buildings.

Table 7-3: Results of automatic interpretation of damages compared with visual interpretation and accuracy assessments – Kobe dataset (637 buildings)

Bayesian Network Reasoning system	Visual interpretation		
	Uncollapsed	Partially collapsed	Totally collapsed
Uncollapsed	254	22	8
Partially collapsed	18	31	9
Totally collapsed	6	2	287
Accuracy Assessment			
Overall accuracy	89.8%		
Producer's accuracy	91.3%	56.4%	94.4%
User's accuracy	89.4%	53.5%	97.3%
Kappa	82.3%		

Table 7-3 (cont.)

Bayesian Network Reasoning system	Visual interpretation			
	Uncollapsed		Partially collapsed	Totally collapsed
	G1&G2	G3	G4	G5
G1&G2	223	16	13	5
G3	9	6	9	3
G4	11	7	31	9
G5	4	2	2	287
Accuracy Assessment				
Overall accuracy	85.9%			
Producer's accuracy	90.3%	19.4%	56.4%	94.4%
User's accuracy	86.8%	22.2%	53.5%	97.3%
Kappa	76.9%			

Table 7-3 (cont.)

Bayesian Network Reasoning system	Visual interpretation									
	Uncollapsed		Partially collapsed (G4)				Totally collapsed (G5)			
	G1&G2	G3	I	P	H	O	I	P	H	O
G1	198	10	0	3	2	7	0	0	2	0
G2	25	6	0	1	0	0	0	0	3	0
G3	9	6	3	0	1	5	0	1	2	0
G4	I, P, O	3	2	5	4	1	5	0	0	0
	H with plates	3	2	0	2	5	2	0	0	1
	H	3	1	0	1	3	0	0	1	0
G5	No detail	2	2	1	1	0	1	0	0	5
	I, P, O	0	0	0	1	0	0	4	0	3
	H with plates	1	0	0	0	0	0	0	2	9
H	3	2	0	0	1	0	0	0	268	0
	Accuracy Assessment									
Overall accuracy	85.6%									

7.8. Summary

This chapter showed an innovative approach for macro-seismic damage assessment in urban areas, using remote sensing techniques in high-resolution aerial imagery. In this contribution we focused on procedures, which start with gathering evidences from image segments and end up with inferring on every point in object space. Using line-based segmentation as an abstraction of building shape, it is possible to compare geometry of features, evidencing soft damages, reducing the effects

of DSM errors. We presented a methodology for using Bayesian networks to a multi-view and multi-modal damaged object description. An augmented Bayesian network, which handles the combination of varying numbers of evidence sets has been introduced. Experimental results show that the suggested approach is promising. The more critical aspects of this work refer to the degree to which the low-level image feature extractors are reliable enough to provide evidence for inferences about damaged buildings and to the issue of how well Bayesian inference, *per se*, is an adequate model for how experts combine such diverse information in the process of image understanding. The presented results support both aspects of the model with respect to recognition performance, although more extensive testing is clearly required. It is anticipated that this general theoretical approach has potential to yield automatic urban damage estimation.

CONCLUSIONS AND OUTLOOK

The presented dissertation has investigated methods for detecting and classifying damages caused by an earthquake in urban area. Our study mainly focused on multi-image, multi-temporal approaches (comparing images of before and after earthquake). Damage identification via space/airborne images is restricted to some structural type of visible damages and visibility of details relies on view direction as well as image resolution. The drawbacks of traditional photo interpretation methodology are linked firstly to the time and cost needed for manual processing of the data and secondly to the difficulty in maintaining coherent interpretation criteria in case there are large numbers of photo-interpreters working in parallel for interpretation of wide areas in a short time. The major contribution of this dissertation was to find solutions in order to automate interpretation tasks entirely or partially. Damage interpretation is divided into four main tasks: identifying objects, collecting relative attributes and evidences, detecting damaged objects and classification in meaningful categories. This research is divided into two main parts. In part one (Chapters 5 and 6) it is assumed that the objects of interest (i.e. buildings) are already identified using auxiliary pre-event data such as building polygons or 3D models. The polygon-based assessment depends on the availability of large scale and recently updated maps in the area. In the second part (Chapter 7) we made efforts to extract objects and damages at once. High-resolution and geo-referenced images are prerequisites for the presented methods.

8.1. Collapse Detection using DSMs Generated Automatically

Digital surface models (DSMs) play an important role for damage assessment. For automatic DSMs generation, we have used an advanced image matching software SAT-PP, which is an efficient in-house developed software of IGP-ETHZ.

The reduction of point's elevation will be a significant cue to detect collapsed objects. Simple pointwise comparison between pre- and post-event DSMs can't be a reliable evidence for damaged points. The critical parameter is an optimum threshold value, which cannot be defined generally due to stochastically behaviors of the model in different areas. The hypothesis test suggested in Chapter 5 shows that normalized value of "average height differences" (AHD) could provide the optimum overall accuracy for bi-level classification. However, the mean and variance should be estimated from some undamaged sample buildings. Buildings with one-meter average height reduction were translated as "Collapsed" buildings. Numerical results for collapse detection show to have 92% and 83% overall accuracies for the Kobe and Bam datasets, respectively. The experiments were extended by replacing the pre-event DSM with a 3D model of buildings extracted before the earthquake. Building models especially those, which contain enough details are priceless information for disaster management and damage assessments. The DSM blunders and error fluctuations especially in steep slopes of buildings are the main reasons for the misclassifications. The accuracy of the DSMs - generated automatically - becomes worse in these areas with densely manmade objects. Sample buildings selected for evaluating the mean and variance (Equation 5-7) need to be distributed almost uniformly in a test area including variety of the buildings. However,

airborne LIDAR systems can be used for a rapid and extensive acquisition of precise height and better results are attainable.

8.2. Imagery Data and Related Features for Collapse Detection

Various approaches have been used to investigate the textural and spatial structural characteristics of images for debris detection. In the course of this research several methods for extracting imagery features were examined. First and second order statistical descriptors including standard deviation, entropy and homogeneity were evaluated. They were computed for small windows around pixels and average values were assigned to each building polygon (ASD, AE, AH). The assessments show that this kind of descriptors, measuring image amplitude in terms of luminance or tristimulus values, are less sensitive to soft damage and suffer from miscellaneous textures in high-resolution images in urban area. We aimed to describe the look of building image as regular or irregular. Regularity indices were defined taking account of lines composition with regards to building footprint. Experimental results revealed fairly good performance of the proposed features for collapse detection. Three kinds of classification methods: k-NN, Bayesian and SVM were used and compared. The classification results were evaluated by a cross-validation method and by an independent visual interpretation test set. The Support Vector Machine (SVM) classifier is a relatively new method that proved to be quite effective for damage detection.

8.3. Collapse Classification using Image and Object Space Features

The integration of object (DSMs) and image space features was applied through classifiers for labeling three attributes of buildings (“Uncollapsed”, “Partially collapsed” and “Totally collapsed”). The results of the analysis showed that using multiple features can be useful to classify collapsed buildings automatically and with high success rate. Regularity indices combined with normalized average height difference through an OVO-SVM classifier yielded 79% of overall accuracy for collapse classification with the available dataset. However, “Partially collapsed” detection is not of sufficient accuracy, especially in the Kobe dataset. The first and main reason is the problems in the DSM generation which some uncollapsed buildings with error in their height values may be categorized as partially collapsed and vice versa. The second reason in the Kobe data is the varieties of “Partially collapsed” buildings, which mainly are classified as inclined, overturned and pancake buildings. Overturned buildings exhibit neither significant height reduction nor irregularity textures in the image.

8.4. Knowledge-Based Bayesian Framework for Damage Assessment

We developed a system that automatically interprets data produced by aerial sensors before and after an earthquake in order to arrive at a detailed damage map quickly after disaster. We assumed that no prior information about buildings position is available and the possibility of a near-real time damage assessment is examined and the results were compared. The proposed system applied image-understanding algorithms to recognize buildings prior to classifying the scene. Another aspect of the proposed system is to handle “uncertainty” using Bayesian networks. The network provides pointwise analysis based on prior information of multi-image segments.

8.4.1. Pointwise Analysis Using Object-Based Features

Traditionally, the approaches of classifications can be divided into two main categories: pixel-based and object-based analyses. In pixel-based analysis, each pixel is assigned a separate state based on the characteristics of the pixel or some contextual information from adjacent pixels. In object-based analysis, the original pixels are first segmented into objects and all subsequent analyses are performed on each object as a whole. Both of these approaches assign attributes to “image pixels” either one-by-one or segment-by-segment. In the proposed system attributes are assigned to “object points” based on features extracted from segments of multi-image data. In other words, the system starts with gathering evidences from multi-image segments and end up with inferring on every point in object space. This approach may be converted to a traditional object-based classifier employing single images because all pixels inside each segment of image are only classified based on the evidences extracted from that segment of image.

8.4.2. Image Segmentation and Shape Index

The goal of our segmentation algorithm was to partition the image into a number of regions that correspond to surfaces of man-made objects. Straight-line segments in urban areas provide important information. We designed and developed a multi-stage line detection method using Hierarchical Permissive Hough Transform (HPHT), a modified version of HT (Figure 6-7). This algorithm iteratively detects obvious and obscure lines. Assuming each segment is separated by a line, a specific line grouping technique that leads to complete closed polygons was presented. We looked for an index reflecting line regularities. In urban areas, parallel lines could represent line regularity. The shape index defined by Equation 7-17 gives a positive number for any given polygon. The index close to one indicates a polygon with parallel sides in two major directions. The shape index is used in Bayesian network for supporting polyhedral undamaged objects.

8.4.3. Bayesian Reasoning For Multi-view Multi-modal System

We started by establishing a naïve Bayesian network for building detection. The network is composed of five (or six for colored image) features as child nodes and one parent node (H_b , H_a : $P_n \in$ Building rooftop before/after earthquake). The evidence policy is to select out the best relative features and discard the rest. We first exclude the segments with compactness less than one and then those with the best “trend plane” in terms of goodness-of-fit and tilt angle are selected for the decision-making procedure. Adding a new node augments this structure. We called it “Features Conformity”. The idea is: corresponding features that are extracted from different segments while being closely similar should obtain more reliable evidence for the reasoning system. Hence, by adding FC node (Figure 7-13) the network became circumspect about inferring with disparate features. The investigations with the Bam and Kobe dataset show that augmented BN improve the performance of the reasoning system. To detect damaged points a symmetric form of the Bayesian network including two parts for detection before and after earthquake was suggested (Figure 7-17). By defining normal random variables, the conditional probability table for final hypothesis was established perceptually. The experimental results were presented in Figures 7-18 and 7-20.

One important aspect of Bayesian networks, compared to other decision-making systems (e.g. neural networks), is most certainly the possibility of taking into account prior information. A-priori knowledge, in the form of initial prior probabilities associated with each hypothesis, is used in the initial step. When no prior knowledge is available, equal probabilities are assigned to all possible states of the root nodes (i.e. $P(H = \text{True}) = 0.5$, $P(H=\text{False}) = 0.5$). When prior probabilities are chosen according to the expected class areas, classes with high prior probabilities are likely to be

overestimated. In the hypothetical case where we know the correct class areas beforehand and base prior probabilities on these, we would obtain an improved classification as compared to using equal priors. This prior knowledge is assumed to be supplied by an operator who is familiar with the site to be processed and is able to estimate the statistical distribution of the object. After an earthquake, the number of damaged buildings for each damage grade can be estimated by using fragility curves, peak ground velocity and buildings density in the studied area. These values reflect user knowledge about each test domain, which can be applied by a prior probability. The results show that only minor modifications of the network prior class expectations across regions before and after disaster can allow the system to achieve an effective performance level. For this purpose, we may readjust prior probabilities before and after earthquake considering information that may be derived from building characteristics such as construction class (e.g. wood-frame, steel-frame, reinforced concrete, etc.) age, height and so on.

8.4.4. EMS98 Damage and Collapse Classification by “if-then” Rules

Pointwise analysis enables us to develop an artificial damage interpreter. Within a building polygon, the presented method is able to detect and classify damaged points. However, we have to readjust the network and should set prior probabilities concerning the rooftop area of a man-made object. After pointwise assessment, with respect to the area of building, the ratio of damaged parts are estimated. The final classification is performed through “if-then” rules. These rules were suggested based on experiments achieved from visually damage interpretation. Empirical results show that the suggested approach is quite promising. In the Kobe dataset, it has attained 86% of overall accuracy by comparison with the reference data to extract EMS98 damage classes.

8.5. Future Investigations and Improvements

We have demonstrated a usable approach for automatic damage detection and classification from aerial images. This system has the ability to provide detailed information about damaged buildings. The most outstanding characteristics of this approach are an integration of features extracted from multi-images as well as DSMs and handling evidence uncertainties by an augmented Bayesian network. We focused on multi-temporal approaches comparing optical images before and after disaster. However, the experimental results of this study have been negatively influenced by a number of factors, which in the future can be avoided by the following measures:

- Use of digital images – compared with the film-based aerial photography, digital cameras have more dynamic range and optical sensitivity and the images are ready for computation after data acquisition. This improves the image information with better radiometric depth, which allows to look into the shadows and also opens the possibility of faster (on-line) processing.
- Use multi-image (more than stereo) approach - helps against occlusions and gives more reliability in image matching. Multiple overlap is easy to produce with digital images.
- Use larger focal length (“normal angle” images) or Linear Array camera images – helps against occlusions. Oblique images provide valuable information about the facades of the buildings. This makes it possible to see damages on the walls.
- Fly with larger image scale – this improves the interpretability of images (higher level of detail).
- Provide more comprehensive datasets of different earthquakes. The majority of the researches suffer from scarcity of actual data about damages. The developed system was applied on two study

areas of Bam and Kobe with more than 1500 buildings. The study area in Kobe includes various types of densely damaged buildings. We evaluated the results of classification with visual interpretations that is not quite reliable for EMS98 and then more extensive testing is clearly required.

Moreover, main topics that can contribute to the advancement of our system are:

- Develop the methods for applying different sensors. A practical damage assessment system needs to be operational with varieties of input supported or supplanted by other available data. In principle, the approach can be further extended to use other sources such as satellite and close-range images by just replacing sensor models. However, optical sensors work only in daylight and are restricted by weather conditions. Airborne Laser Scanning (ALS) is an active sensor, which can collect data at nighttime and can be operated in low sun angle condition. Moreover, Synthetic Aperture Radar (SAR) is one of the most promising technologies for monitoring damaged areas under independence of weather and sun illumination.
- Optimize the algorithms and reduce the processing time using parallel processing. The huge size of the images and DSMs data must be considered during the design of a practical system.
- The elapse time between successive dates of data acquisition might be a problem and more concentration should be directed toward post-event information.
- Although the experimental results have demonstrated that our approach has the capability to give good and encouraging results, there is a particular point about uncertainty handling. Mathematicians handle uncertainty with methods such as Dempster-Shafer theory, fuzzy logic, and probability theory as well. Fuzzy logic and probability refer to different kinds of uncertainty. Fuzzy logic is specifically designed to deal with imprecision of facts (fuzzy logic statements), while probability deals with chances of that happening (but still considering the result to be precise). A basic prerequisite for the interpretation is the development of the damage class description. It should contain possible damage types of entire buildings and their geometrical and therefore detectable features. This classification suffers from the fuzzy nature of damage types. Therefore, methods based on fuzzy logic could be used and the results are given in combination with a reasoning system.

BIBLIOGRAPHY

- Aach, T., Kaup, A. (1995). Bayesian algorithms for adaptive change detection in image sequences using Markov random fields. *Signal Processing: Image Communication*, 7(2), pp. 147-160.
- Adams, B.J., Huyck, C., Mansouri, B., Eguchi, R., Shinozuka, M. (2002). Post-disaster bridge damage assessment. Proceedings of the 15th Pecora Conference: Integrating Remote Sensing at the Global, Regional, and Local Scale, Denver, Colorado, 8p (on CD-ROM).
- Aha, D. (1997). Lazy Learning. Dordrecht: Kluwer Academic Publishers.
- Ahlqvist, O. (2008). Extending post-classification change detection using semantic similarity metrics to overcome class heterogeneity: A study of 1992 and 2001 U.S. National Land Cover Database changes. *Remote Sensing of Environment*, 112(3), pp. 1226-1241.
- Ajmar, A., Boccardo, P., Tonolo, F. G., Veloso C. (2010). Earthquake Damage Assessment Using Remote Sensing Imagery. The Haiti Case Study. *Geoinformation for Disaster and Risk Management, Examples and Best Practices*, O. Altan, R. Backhaus, P. Boccardo, S. Zlatanova (eds.), pp. 31-37.
- Alberga, V., Idrissa, M., Lacroix, V., Inglada, J. (2007). Comparison of similarity measures of multi-sensor images for change detection applications. In Proceeding: IEEE Geoscience and Remote Sensing Symposium, Barcelona, Spain, pp. 2358-2361.
- Alberga, V. (2009). Similarity Measures of Remotely Sensed Multi-Sensor Images for Change Detection Applications. *Journal of Remote Sensing*, ISSN 2072-4249, pp. 122-143.
- Altan, O., Toz, G., Kulur, S., Seker, D., Volz, S., Fritsch, D., Sester, M. (2001). Photogrammetry and geographic information systems for quick assessment, documentation and analysis of earthquakes. *ISPRS Journal of Photogrammetry & Remote Sensing* 55(2001), pp. 359-372.
- Altan, O., Kemper, G. (2008). System architecture for earthquake, tsunami preparedness and warning. *International Archive of Photogrammetry and Remote Sensing (IAPRS)*, 37 (B4), pp. 1061-1071.
- Ameri, B. (2000). Automatic Recognition and 3D Reconstruction of Buildings through Computer Vision and Digital Photogrammetry. Dissertation, Fakultät für Bauingenieur- und Vermessungswesen, Universität Stuttgart, DGK Series C, No. 526.
- Baltsavias, E., Mason, S., Stallmann, D. (1995). Use of DTMs/DSMs and Orthoimages to Support Building Extraction. In: *Automatic Extraction of Man-Made Objects from Aerial and Space Images*, A. Grün, O. Kübler & P. Agouris (eds.). Birkhäuser Verlag, Basel, pp. 199-210.
- Baltsavias, E., Gruen, A. and Van Gool, L., (eds). (2001). *Automatic Extraction of Man-made Objects from Aerial and Space Images (III)*. Rotterdam: Balkema.
- Baltsavias, E. (2004). Object Extraction and Revision by Image Analysis using Existing Geodata and Knowledge: Current Status and Steps Toward Operational Systems. In: *ISPRS Journal of Photogrammetry and Remote Sensing*, 58 (3-4), pp. 129-151.

- Bendea, H., Boccardo, P., Dequal, S., Giulio Tonolo, F., Marenchino, D., Piras, M. (2008). Low Cost UAV For Post-Disaster Assessment. International Archive of Photogrammetry and Remote Sensing (IAPRS), 37 (B8), pp. 1373-1379.
- Bitelli, G., Camassi., R., Gusella., L., Mognol, A. (2004). Image Change Detection on Urban Areas: The Earthquake Case. International Archive of Photogrammetry and Remote Sensing (IAPRS), 35 (B7), pp. 692-697.
- Bovolo, F., Bruzzone, L. (2007). A Theoretical Framework for Unsupervised Change Detection Based on Change Vector Analysis in the Polar Domain. IEEE Transactions on Geoscience and Remote Sensing, 45(1), pp 218-236.
- Brenner, C. (2005). Building Reconstruction from Images and Laser Scanning. In: International Journal of Applied Earth Observation and Geoinformation, Theme Issue on “data Quality in Earth Observation Techniques”, 6(3-4), Elsevier, March, pp. 187-198.
- Bresenham , J. E. (1965). Algorithm for Computer Control of a Digital Plotter. IBM Systems Journal, Vol. 4, No.1, January, pp. 25–30.
- Brinkhoff, T. (2008). Supporting Mobile Device Applications By Geospatial Web Services. International Archive of Photogrammetry and Remote Sensing (IAPRS), 37 (B4), pp. 865-870.
- Brunn, A. and Weidner, U. (1997). Extracting buildings from digital surface models. ISPRS Workshop on 3D Reconstruction and Modeling of Topographic Objects, Stuttgart, Germany, pp. 27-34.
- Bruzzone , L., Prieto, D. F. (2000). Automatic Analysis of the Difference Image for Unsupervised Change Detection. IEEE Transactions on Geoscience and Remote Sensing, 38(3), pp. 1171-1182.
- Bruzzone, L., Prieto, D. F. (2002).An adaptive semiparametric and context-based approach to unsupervised change detection in multitemporal remote-sensing images. IEEE Trans. Image Processing, 11(4), pp. 452–466.
- Buchheister, J., Rezaeian, M. (2008). Identification of liquefaction failures based on aerial images. The 14th World Conference on Earthquake Engineering, Beijing, China, 9p (on CD-ROM).
- Byrne, G., Crapper, P., Mayo, K. (1980). Monitoring Land-Cover Change by Principle Components Analysis of Multitemporal Landsat Data. Remote Sensing of Environment, 10, pp. 175-184.
- Canny, J. F. (1986). A Computational Approach to Edge Detection. IEEE Transactions on Pattern Analysis and Machine Intelligence, Vol. 8, No. 6, pp. 679-698.
- CBS/AP (2010), "Red Cross: 3M Haitians Affected by Quake". CBS News. 13, <http://www.cbsnews.com/stories/2010/01/13/world/main6090601.shtml>, Retrieved 2010-01-18.
- Chengfeng, L., Zhengjun, L., Jixian, Z. (2009). Geoinformation and Standard for Synthetical Emergency Management System. Proceedings of International Conference on Geo-spatial Solutions for Emergency Management, Beijing, China, pp. 192-195.

- Chesnel, A.-L., Binet, R., Wald, L. (2007). Quantitative Assessment Of Building Damage In Urban Area Using Very High Resolution Images. Urban Remote Sensing Joint Event, Paris, pp. 11-13 April, pp.1-5.
- Chung, H., Sarabandi, P. (2006). Remote sensing for building inventory updates in disaster management, Proceedings of the Smart Structures and Materials and NDE for Health Monitoring and Diagnostics Conference, San Diego, February 26–March 2, 8p (on CD-ROM).
- Coburn, A., Pomonis, A., Sakai, S., Spence, R. (1991). Assessing Human Casualties Caused by Building Collapse in Earthquakes. Summaries of the International Conference on the Impact of Natural Disasters, University of California, Los Angeles, USA.
- Cohen, J. (1960). A coefficient of agreement for nominal scales. *Educational and Psychological Measurement*, 20, pp. 37–46.
- Collins, R., Hanson, A., Riseman, E. and Schultz, H. (1995). Automatic extraction of buildings and terrain from aerial images. In: A. Gruen, O. Kuebler and P. Agouris (eds.). *Automatic Extraction of Man-Made Objects from Aerial and Space Images*. Basel, Boston, Berlin: Birkhauser Verlag, pp. 169-178.
- Cygan, M., Patterson. T. (2010). GIS for Emergency Management. . *Geoinformation for Disaster and Risk Management, Examples and Best Practices*, O. Altan, R. Backhaus, P. Boccardo, S. Zlatanova (eds.), Vienna, Austria, pp. 95-98.
- Danneels, G., Pirard, E., Havenith, H.B. (2007). Automatic landslide detection from remote sensing images using supervised classification methods. *Geoscience and Remote Sensing Symposium*. IEEE, pp. 3014-3017.
- De Groot, T., Peter, T., Annunziato, A., Vernaccini, L. (2010). Global Disaster Alert and Coordination System. *Geoinformation for Disaster and Risk Management, Examples and Best Practices*, O. Altan, R. Backhaus, P. Boccardo, S. Zlatanova (eds.), Vienna, Austria, pp.1-6.
- Deng, J. S., Wang, K., Deng, Y. H., Qi, G. J. (2008). PCA-based land-use change detection and analysis using multitemporal and multisensor satellite data. *International Journal of Remote Sensing*, 29(16), pp. 4823-4838.
- Diermayer, E., Hostert, P. (2007). Assessing post-socialist urban change with Landsat data; Case study Berlin, Germany. *Urban Remote Sensing Joint Event*, 2007, Paris, pp. 1-4.
- Domingos, P., Pazzani, M. (1997). On the optimality of the simple Bayesian classifier under zero-one loss. *Machine Learning* 29, pp. 103-130.
- Dorninger, P., Nothegger, C. (2007). 3D segmentation of unstructured point clouds for building modeling. *International Archives of the Photogrammetry, Remote Sensing and Spatial Information Sciences*, 35 (3/W49A), pp. 191–196.
- Dougherty, J., Kohavi, R., Sahami, M. (1995). Supervised and unsupervised discretization of continuous features. In:A. Prieditis & S. Russel (eds.), *Proceedings of the Twelfth International Conference on Machine Learning*, San Francisco, pp. 194-202.

- Durrett, Richard (1996). Probability: theory and examples (Second ed.)
- Durupt, M., Taillandier, F. (2006). Automatic building reconstruction from a digital elevation model and cadastral data: An operational approach. International Archives of the Photogrammetry, Remote Sensing and Spatial Information Sciences, 35 (3), pp. 142–147.
- Eisenbeiss, H. (2009). UAV Photogrammetry. PhD dissertation, Institute of Geodesy and Photogrammetry, IGP Mitteilungen Nr. 105.
- Estrada, M., Kohiyama, M. (2001). Detection of damages due to the 2001 El Salvador earthquake using Landsat images. Paper presented at: The 22nd Asian Conference on Remote sensing, Singapore, pp. 1372-1377.
- Fayyad, U. M., Irani, K. B. (1993). Multi-interval discretization of continuous valued attributes for classification learning. In: Proceeding of the Thirteenth International Joint Conference on Artificial Intelligence, pp. 1022-1027.
- Fiedrich, F., Gebauer, F. and Rickers, U. (2000) Optimized resource allocation for emergency response after earthquake disasters. Safety Science 35 (1-3), pp. 41-57.
- Fisher, P. F., Tate, N. J. (2006). Causes and consequences of error in digital elevation models. Progress in Physical Geography 30, pp. 467–489.
- Förstner, W., Plümer, L., eds. (1997). Semantic Modeling for the Acquisition of Topographic Information from Images and Maps. Basel, Boston, Berlin: Birkhäuser Verlag.
- Förstner, W. (1999). 3D-City Models: Automatic and Semiautomatic Acquisition Methods. In: Fritsch, D. and Spiller, R. (eds.): Photogrammetric Week '99, Wichmann, Karlsruhe.
- French, S. P., Muthukumar, S. (2006). Advanced Technologies For Earthquake Risk Inventories. Journal of Earthquake Engineering, 10 (2), pp. 207–236.
- Fuchs, C., Förstner, W. (1995). Polymorphic grouping for image segmentation. Fifth International Conference on Computer Vision, Massachusetts Institute of Technology, Cambridge, Massachusetts, pp. 175-182.
- Fung, T., Ledrew, E. (1988). The determination of optimal threshold levels for change detection using various accuracy indices. Photogrammetric Engineering and Remote Sensing, 54(10), pp. 1449–1454.
- Genton, M. (2001). Classes of Kernels for Machine Learning: A Statistics Perspective. Journal of Machine Learning Research 2: pp. 299-312.
- Gonzalez, R. C., Woods, R. E. (2002). Digital Image Processing - Second Edition. Prentice-Hall, Inc., New Jersey.
- Gruen, A., Kübler, O. and Agouris, P. (eds.). (1995). Automatic Extraction of Man-Made Objects from Aerial and Space Images. Basel, Boston, Berlin: Birkhäuser Verlag.

- Gruen, A., Baltsavias, E. and Henricsson, O. (eds.). (1997). Automatic Extraction of Man-Made Objects from Aerial and Space Images (II). Basel, Boston, Berlin: Birkhäuser Verlag.
- Gruen, A. (2000). Semi-automated Approaches to Site Recording and Modeling. In: International Archive of Photogrammetry and Remote Sensing (IAPRS), 33 (5/1), pp. 309-318.
- Gua, H., Lu, L., Ma, J., Pesaresi, M., Yuan F. (2009). An improved automatic detection method for earth-quake-collapsed buildings from ADS40 image. Chinese Science Bulletin, pp. 3303-3307.
- Gueguen, L., Pesaresi, M., Soille, P., Gerhardinger, A. (2009). Morphological Descriptors and Spatial Aggregations for Characterizing Damaged Buildings in Very High Resolution Images. Presented in 6th Conference on Image Information Mining: automation of geospatial intelligence from Earth Observation, Madrid (Spain), November 3-5, 5p (on CD-ROM).
- Guler, M.A., Turker, M. (2003). Detection of the Earthquake Damage Buildings from Post-Event Aerial Photographs Using Perceptual Grouping. In: International Archives of Photogrammetry Remote Sensing and Spatial Information Science, vol. 35 (3), pp. 451-454.
- Guo, G., Wang, H., Bell, D., Bi, Y., Greer, K. (2003). KNN Model-Based Approach in Classification. Lecture Notes in Computer Science, Volume 2888, pp. 986 – 996.
- Gusella, L., Adams, B. J., Bitelli, G., Huyck, C. K., Mognol, A. (2005). Object-Oriented Image Understanding and Post-Earthquake Damage Assessment for the 2003 Bam, Iran, Earthquake. Earthquake Spectra, 21 (S1), pp. S225–S238.
- Haralick, R. M., Shanmugam, K., Dinstein, I. (1973). Textural fatures for image Classification. IEEE Transaction on systems, Man and Cybernetics, 3(6), pp. 610-621.
- Heuel, S. (2004). Uncertain Projective Geometry-Statistical Reasoning for Polyhedral Object Reconstruction. Lecture notes in computer science, Springer-Verlag Berlin Heidelberg.
- Hosokawa, M., Jeong, B., Takizawa, O., Matsuoka, M. (2008). Disaster risk evaluation and damage detection using remote sensing data for global rescue operations. International Archive of Photogrammetry and Remote Sensing (IAPRS), 37 (B8), pp. 183-186.
- Hsu, C.-N., Huang, H.-J., Wong, T.-T. (2000). Why Discretization Works for Naïve Bayesian Classifiers. Presented in the 17th International Conference on Machine Learning (ICML-2000), Stanford University, June 29-July 2, pp. 309-406.
- Huertas, A., Nevatia, R. (1988). Detecting buildings in aerial images. Computer Vision, Graphics and Image Processing, 41(2), pp. 131-152.
- Huertas, A., Lin, C. and Nevatia, R. (1993). Detection of buildings from monocular views of aerial scenes using perceptual organization and shadows. Proceeding of the 1993 ARPA Image Understanding Workshop, pp. 253-260.
- Huyck, C. K., Adams, B. J., Cho, S. Chung, H., Eguchi, R. T. (2005). Towards Rapid Citywide Damage Mapping Using Neighborhood Edge Dissimilarities in Very High-Resolution Optical

- Satellite Imagery—Application to the 2003 Bam, Iran, Earthquake. *Earthquake Spectra*, Volume 21, No. S1, pp. S255–S266.
- Ip, A.W.L., Mostafa, M.M.R., Hutton, J., Barriere, J.P. (2008). An optimally integrated direct georeferencing and flight management system for increased productivity of airborne mapping and remote sensing. *International Archive of Photogrammetry and Remote Sensing (IAPRS)*, 37 (B1), pp. 579-584.
- Irvin, R., McKeown, D. (1989). Methods for exploiting the relationship between buildings and their shadows in aerial imagery. *IEEE Transactions on Pattern Analysis and Machine Intelligence*, 19(6), pp. 1564-1575.
- Jaw, J. J., Cheng, C.C. (2008). Building Roof Reconstruction by Fusing Laser Range Data and Aerial. *International Archive of Photogrammetry and Remote Sensing (IAPRS)*, 37 (B3b), pp. 707-712.
- Jaya, I., Abe, N. (2006). Methods for Detecting Landslide within Mountains Area Using Multitemporal SPOT HRV Imageries: A Case Study in Niigata, Japan. *Study Report of Faculty of Agriculture, Niigata University*, Vol. 58, No. 2, pp. 109-116.
- Jaynes, C. O. (2000). Automatic Model Acquisition and Aerial Image Understanding. Ph.D. dissertation, University of Massachusetts, Department of Computer Science, May.
- Jiping, L., Shenghua, W., Liang, W., Fuhamo Z. (2009). Development and Demonstration Application of Government Geographic Information Service Platform. *Proceedings of International Conference on Geo-spatial Solutions for Emergency Management*, Beijing, China, pp. 73-77.
- Jiugang, L., Xinming, T., Zhengjun, L., Minyan, D. (2009). Design and Implementation of WEBGIS For Government Emergency Management Based on SOA. *Proceedings of International Conference on Geo-spatial Solutions for Emergency Management*, Beijing, China, pp. 149-152.
- Kasetkasem, T., Varshney, P. K. (2002). An image change detection algorithm based on Markov random field models", *IEEE Transaction of Geoscience and Remote Sensing*, 40, pp. 1815-1823.
- Kim, T., Müller, J. (1995). Building Extraction and Verification from Spaceborne and Aerial Imagery Using Image Understanding Data Fusion Techniques. In: A. Gruen, O. Kübler and P. Agouris (eds.), *Automatic Extraction of Man-Made Objects from Aerial and Space Images*, Basel, Boston, Berlin: Virkhauser Verlag, pp. 221-230.
- Kim, Z. (2001). Multi-Vie 3-D Object Description with Uncertain Reasoning and Machine Learning. Ph.D. dissertation, Faculty of the Graduate Scholl University of Southern California.
- Kerle, N., Heuel, S., Pfeifer, N. (2008). Real-time data collection and information generation using airborne sensors. *Geospatial Information Technology for Emergency Response*, Taylor & Francis Group, London, pp. 43-74.

- Kobe City FIRE Bureau (2006-01-17). On the Site in Japanese of Kobe City Fire Bureau.
<http://www.city.kobe.jp/cityoffice/48/quake/higai.html>. Retrieved 2008-05-25.
- Kohiyama, M., Yamazaki, F. (2005). Damage detection for 2003 Bam, Iran earthquake using Terra-ASTER satellite imagery. *Earthquake Spectra*, 21(S1), pp. S267-S274.
- Kolbe, T.H., Gröger, G., Plümer, L. (2008). CityGML – 3D city models and their potential for emergency response. *Geospatial Information Technology for Emergency Response*, Taylor & Francis Group, London, pp. 257-238.
- Kotsiantis, S.B. (2007). Supervised machine learning: A review of classification techniques. *Informatica*, 31, pp. 249-268.
- Kouchi, K., Yamazaki, F., Kohiyama, M., Matsuaka, M., Muraoka, N. (2004). Damage detection from QuickBird high-resolution Satellite images for the 2003 Boumerdes, Algeria Earthquake. Proceeding of the Asian Conference on Earthquake Engineering. Manila, Philippines, pp. 215-226 (on CD-ROM).
- Kreimer, A., Munasinghe, M., and Preece, M. (1992). Reducing environmental vulnerability and managing disasters in urban areas. in *Environmental Management and Urban Vulnerability*. Kreimer, A. and Munasinghe, M., Eds., World Bank Discussions Papers, Washington.
- Kulszewski, K., Koch, K. R. (1997). Building recognition with bayesian networks. Workshop on Semantic Modeling for the Acquisition of Topographic Information from Images and Maps, SMATT'97, pp. 196-210.
- Li, M., Cheng, L., Gong, J., Liu, Y., Chen, Z., Li, F., Chen, G., Chen, D. Song, X. (2008). Post-earthquake assessment of building damage degree using LiDAR data and imagery. *Science in China press* , co-published with Springer-Verlag GmbH. Vol. 51, pp.133-143.
- Li, S., Fan, Y., Yang, S., Wang, L. (2010). Space Technology Application for Wenchuan Earthquake Relief. *Geoinformation for Disaster and Risk Management, Examples and Best Practices*, O. Altan, R. Backhaus, P. Boccardo, S. Zlatanova (eds.), pp. 39-44.
- Li, X., Yeh, A. (1998). Principle Component Analysis of Stacked Multi-Temporal Images for the Monitoring of Rapid Urban Expansion in the Pearl River Delta. *International Journal of Remote Sensing*, 19(8), pp. 1501-1518.
- Lillesand, T. M., Kiefer, R.W. (1994). *Remote Sensing and Image Interpretation*, 3rd edn (New York: John Wiley & Sons, Inc.).
- Lin, C. Lin, Huertas, A., Nevatia, R. (1994). Detection of Buildings using perceptual grouping and shadows. presented at IEEE Conferecne on Computer Vision and Pattern Recognition, pp. 62-69.
- Lin, C., Huertas, A. and Nevatia, R. (1995). Detection of buildings from monocular images. In A. Gruen, O. Kuebler and P. Agouris (eds.), *Automatic Extraction of Man-Made Objects from Aerial and Space Images*. Basel, Boston, Berlin: Birkhauser Verlag, pp. 125-134.

- Liu, W., Yamazaki, F. (2008). Damage Detection of the 2008 Sichuan, China Earthquake from ALOS Optical Images. Proceeding 28th Asian Conference on Remote Sensing, Paper No. 119, 6p (on CD-ROM).
- Lu, D., Mausel, P., Brondizio, E., and Moran, E. (2004). Change Detection Techniques. International Journal of Remote Sensing, 25(12), pp. 2365–2407.
- Mansouri, B., Shinozuka, M., Huyck, C., Houshmand, B. (2005). Earthquake-induced change detection in the 2003 Bam, earthquake by complex analysis using Envisat ASAR data. Earthquake Spectra, 21(81), pp.8275-8284.
- Markus, M., Fiedrich, F., Gebauer, F., Hirschberger, S. (2000). Strong Earthquakes, Rapid Damage Assessment and Rescue Planning. In: Contingency, Emergency, Crisis, and Disaster Management: Emergency Management in the Third Millennium, Proceedings of the Seventh Annual Conference of The International Emergency Management Society, K.M. Kowalski and M.A. Trevits (eds.), 16.-19. Orlando, Florida, pp. 369-378.
- Maas, H.-G. (1999). The potential of height texture measures for the segmentation of airborne laserscanner data. Fourth International Airborne Remote Sensing Conference, Ottawa, 21-24 June, (I), pp. 154-161.
- Maes, F., Collignon, A., Vandermeulen, D., Marchal, G., Suetens, P. (1997). Multimodality image registration by maximization of mutual information. IEEE Transactions on Medical Imaging, 16, pp. 187–198.
- Malila, W.A. (1980). Change Vector Analysis: an Approach for Detecting Forest Changes with Landsat. Proceedings of the 6th Annual Symposium on Machine Processing of Remotely Sensed Data, Purdue University, IN, pp. 326–335.
- Mas, J. F. (1999). Monitoring Land-Cover Changes: A Comparison of Change Detection Techniques. International Journal of Remote Sensing, 20(1), pp. 139–152.
- Matsuoka, M., Yamazaki, F. (2004). Use of Satellite SAR Intensity Imagery for Detecting Building Areas Damaged due to Earthquakes. Earthquake Spectra EERI, 20 (3), pp. 975-994.
- Mitomi, H., Yamazaki, F., Matsuoka, M. (2001). Development of automated extraction method for building damage area based on maximum likelihood classifier. In Proceedings of the 8th International Conference on Structural Safety and Reliability, 8p (on CD-ROM).
- Moffiet, T., Mengerson, K., Witte, C., King, R., Denham, R. (2005). Airborne laser scanning: Exploratory data analysis indicates variables for classification of individual trees or forest stands according to species. In ISPRS Journal of Photogrammetry & Remote Sensing, Vol. 59 (2005), pp. 289-309.
- Mohan, R., Nevatia, R. (1989). Segmentation and description based on perceptual organization. In Proc. IEEE Computer Society Conference on Computer Vision and Pattern Recognition, San Diego, CA, pp. 333-341.

- Murao, O., Miyamoto, A., Sasaki, T. (2007). Virtual Chi-Chi City on Digital Earth Model as Post-Earthquake Recovery Digital Archive. Presented in 5th International Workshop on Remote Sensing Applications to Natural Hazards, The George Washington University, Washington, D.C. September 10-11, 6p (on CD-ROM).
- Nevatia, R., Lin, C., Huertas, A. (1999). A system for building detection from aerial images. In A. Gruen, O. Kuebler and M. Baltsavias (eds.). Automatic Extraction of Man-Made Objects from Aerial and Space Images (II), Basel, Boston, Berlin: Birkhauser Verlag, pp. 77-86.
- Niederöst, M. (2003). Detection and Reconstruction of Buildings for Automated Map Updating. Ph. D. Dissertation, Report No. 78, Institute of Geodesy and Photogrammetry, ETH Zurich, Switzerland.
- Nolte, E. M., Adams, B. J., Wenzel, F. (2010). Population Estimation for Megacities: Solving Disaster Management Challenges Using Remote Sensing, Web-GIS and Advanced Technologies. Geoinformation for Disaster and Risk Management, Examples and Best Practices, O. Altan, R. Backhaus, P. Boccardo, S. Zlatanova (eds.), pp. 89-94.
- Ogawa, N., Yamazaki, F. (2000). Photo-Interpretation of Building Damage due to Earthquakes using Aerial Photographs. 12th World Conference on Earthquake Engineering, 8p (on CD-ROM).
- Oude Elberink, S., Maas, H.-G. (2000): The use of anisotropic height texture measures for the segmentation of airborne laser scanner data. IAPRS, Vol. XXXIII, Part B3/2, pp. 678-684.
- Pacifici, F., Del Frate, F., Solimini, C., Emery, W. J. (2007). An Innovative Neural-Net Method to Detect Temporal Changes in High-Resolution Optical Satellite Imagery. IEEE Transactions on Geoscience and Remote Sensing, 45(9), pp. 2940- 2952.
- Platt, J. C., Cristianini, N., Shawe-Taylor, J. (2000). Large Margin DAGs for multiclass classification. Advances in Neural Network Information Processing Systems, 12, pp. 547-553.
- Pluim, J., Maintz, J., Viergever, M. (2003). Mutual information based registration of medical images: a survey. IEEE Transactions on Medical Imaging, 22, pp. 986–1004.
- Pratt, W. K. (1991). Digital image processing. John Wiley & Sons Inc, New York.
- Purohit, S., Mantri, S. (2009). Formulation of Geo-spatial Solution for Disaster Management. Proceedings of International Conference on Geo-spatial Solutions for Emergency Management, Beijing, China, pp. 67-72.
- Qiao, Q., Zhang, T. (2009). 3D-GIS for Barrier Lake Disaster Reduction and Risk Management. Proceedings of International Conference on Geo-spatial Solutions for Emergency Management, Beijing, China, pp. 224-226.
- Radke, R. J., Andra S., Al-Kofahi, O., Roysam, B. (2005). Image change detection algorithms: A systematic survey. IEEE Transactions on Image Processing, 14(3), pp. 294–307.

- Rathje, E. M., Crawford, M., Wo, K. (2005). Damage Patterns from Satellite Images of the 2003 Bam, Iran, Earthquake. *Earthquake Spectra*, Volume 21, No. S1, pp. S295–S307.
- Rehor, M., Bähr H.-P. (2007). Detection and analysis of building damage caused by earthquakes using Laser scanning data. International Symposium on Strong Vrancea Earthquakes and Risk Mitigation, Bucharest, Romania, pp. 457-47.
- Rehro, M., Bähr, H., Tarsha-Kurdi, F., Landes, T., Grussenmeyer, P. (2008). Contribution of two plane detection algorithms to recognition of intact and damaged buildings in lidar data. *The Photogrammetric Record*. 23(124), pp. 441-456.
- Rehor, M., Vögtle, T. (2008). Improvement of building damage detection and classification based on laser scanning data by integrating spectral information. *International Archive of Photogrammetry and Remote Sensing (IAPRS)*, 37 (B7), pp. 1599-1605.
- Rejaie, A., Shinozuka, M. (2004). Reconnaissance of Golcuk 1999 Earthquake Damage using Satellite Images. *Journal of Aerospace Engineering*, 17(1), January, pp. 20-25.
- Rezaeian, M. and Gruen, A. (2007). Automatic classification of collapsed buildings using object and image space features. In: J. Li, S. Zlatanova and A. Fabbri (eds.), *Geomatics solutions for Disaster Management*. Springer, pp. 135-148.
- Rezaeian, M. and Gruen, A. (2008). Automatic classification of collapsed buildings using Digital surface models. Presented at Second Disaster Management Conference, Tehran, Iran, 8p (on CD-ROM).
- Rezaeian, M., Grün, A. (2010). Automatic 3D building extraction from aerial and space images for earthquake risk management. *Journal of Georisk (Taylor & Francis): Assessment and Management of Risk for Engineered Systems and Geohazards*, 4(3), 1-20.
- Richards, P. B. (1982). The Utility of Landsat-D and Other Satellite Imaging Systems in Disaster Management, Final Report. NASA Goddard Space Flight Center Disaster Management Workshop, NASA DPR S-70677 (Washington, D.C.: Naval Research Laboratory, March 29-30).
- Rogan J., Chen, D. (2004). Remote sensing technology for mapping and monitoring land-cover and land-use change. *Progress in Planning*, 61, pp. 301–325.
- Rogerson, P.A. (2002). Change detection thresholds for remotely sensed images. *Journal of Geographical Systems*, 4, pp. 85–97.
- Rosin, P. (2002). Thresholding for change detection. *Computer Vision and Image Understanding*, 86(2), pp. 79–95.
- Rouse, J. W., Haas, R. H., Schell, J. A., Deering, D. W. (1973). Monitoring vegetation systems in the great plains with ERTS. Third ERTS Symposium, NASA SP-351, 1, pp. 309-317.
- Russakoff, D. B., Tomasi, C., Rohlfing, T., Maurer C. R. (2004). Image similarity using mutual information of regions. In Proceedings of the 8th European Conference on Computer Vision (ECCV), LNCS 3023, pp. 596-607.

- Saito, K., Spence, R. (2004). Rapid Damage Mapping using Post-Earthquake Satellite Images. In: Proceedings of International Geoscience and Remote Sensing Symposium, IEEE, vol. 4, 20-24 September, pp. 2272-2275.
- Sarabandi, P., Adams, B., Kiremidjian, A.S., and Eguchi, R.T. (2005). Infrastructure inventory compilation using single high resolution satellite images, Proceedings of the 3rd International Workshop on Remote Sensing for Post-Disaster Response, Chiba University, Japan, September 12–13, 8p (on CD-ROM).
- Samadzadegan, F., Rastiveisi, H. (2008). Automatic detection and classification of damaged buildings, using high resolution satellite imagery and vector data. International archives of Photogrammetry Remote Sensing and Spatial Information Sciences, 37 (B8), pp. 415-420.
- Schiavon, G., Del Frate, F., Solimini, C. (2003). High resolution multi-spectral analysis of urban areas with QuickBird imagery and synergy with ERS data. Proceedings of the International Geoscience And Remote Sensing Symposium, Toulouse, France, pp. 1972-1974.
- Schweier, C., Markus, M. (2004). Assessment of the search and rescue demand for individual buildings. Proceedings of the 13th World Conference on Earthquake Engineering, Vancouver, Canada, Paper No. 3092, 11p (on CD_ROM).
- Sertel, E., Kaya, S., Curran, P.J. (2007). Use of Semivariograms to identify Earthquake Damage in an Urban Area. In:IEEE Transactions on Geoscience and Remote Sensing, 45(6), pp. 1590-1594.
- Sharma, R.K., Kumar, B.S., Desai, N.M., Gujrati, V.R. (2008). SAR for disaster management. Aerospace and Electronic systems Magazine, IEEE, 23(6), pp. 4-9.
- Shinozuka, M., Rejai, S. A. (2001). Damage assessment from remotely sensed images using PCA. In Proceeding SPIE: Smart Structures and Materials 2001: Smart Systems for Bridges, Structures, and Highways, Newport Beach, CA, USA, pp. 1-10.
- Sibiryakov, A. (1996). House Detection from Aerial Color Images. Internal Report, Institute of Geodesy and Photogrammetry. Swiss Federal Institute of Technology, Zurich (ETH).
- Singh, A. (1989). Digital change detection techniques using remotely-sensed data, International Journal of Remote Sensing, 10(6), pp. 989-1003.
- Singh, D., Chamundeeswari, V.V., Singh, K., Wiesbeck, W. (2008). Monitoring and change detection of natural disaster (like subsidence) using Synthetic Aperture Radar (SAR) data. In International Conference on Recent Advances in Microwave Theory and Applications, 21-24th Nov., Jaipur, pp. 419-42.
- Shirzaei, M., Mansouri, B., Shinozuka, M. (2006). Multiresolution Analysis of Satellite Optical Images for Damage Detection using Wavelet Transform. 4th International Workshop on Remote Sensing for Disaster Response, 25-26th, Cambridge, UK, 8p (on CD_ROM).
- Shaoqing Z., Lu X. (2008). The Comparative Study of Three Methods of Remote Sensing Image Change Detection. International archives of Photogrammetry Remote Sensing and Spatial Information Sciences, 37 (B7), pp. 1595-1598.

- Smith, K. (1996). Environmental Hazards: Assessing Risk and Reducing Disaster. 2nd ed. London and New York: Routledge.
- Sohl, T. L. (1999). Change analysis in the United Arab Emirates: an investigation of techniques. *Photogrammetric Engineering and Remote Sensing*, 65, pp. 475–484.
- Sohn, G., Dowman, I. (2007). Data fusion of high-resolution satellite imagery and LiDAR data for automatic building extraction, *ISPRS Journal of Photogrammetry & Remote Sensing*, 62, pp. 43–63.
- Song, Z., Pan, C., Yang, Q., Li, F., Li, W. (2008). Building roof detection from a single high-resolution satellite image in dense areas. *International Archives of Photogrammetry Remote Sensing and Spatial Information Sciences*, 37 (B3a), pp. 271-278.
- Steinle, E., Bähr H.-P. (1999). Laserscanning for change detection in urban environment. In: O. Altan & L. Gründig (eds.), *Proceedings of the Third Turkish-German Joint Geodetic Days - Towards A Digital Age(I)*, Istanbul, Turkey, pp. 147-156.
- Steinle, E. and Vögtle, T. (2000). Effects of different laser scanning modes on the results of building recognition and reconstruction. *International Archive of Photogrammetry and Remote Sensing (IAPRS)*, 33 (B3/2), pp. 858-865.
- Sumer, E., Turker, M. (2005). Building Damage Detection from Post-Earthquake Aerial Imagery Using Building Grey-Value and Gradient Orientation Analyses. *Proceedings of 2nd International Conference on Recent Advances in Space Technologies (RAST'05)*, Istanbul, Turkey, pp. 577-582
- Sumer, E., Turker, M. (2006). An integrated earthquake damage detection system. In Proceeding 1st International Conference on Object-based Image Analysis (OBIA 2006). July, Salzburg, Austria, 6p (on CD-ROM).
- Suzuki, D., Yamazaki, F. (2008). Extraction of Building Damages in the 2007 Niigata-Ken Chuetsu-Oki Earthquake Using Digital Aerial Images. Proc. 28th Asian Conference on Remote Sensing, Paper No. 156, 6p (on CD-ROM).
- Tan, J., Fan, X. (2009). Researches on Software Architecture in Emergency Response Network Spatial Information System. *Proceedings of International Conference on Geo-spatial Solutions for Emergency Management*, Beijing, China, pp. 250-254.
- Theodoridis, S., Koutroumbas, K. (2003). Pattern Recognition – Second edition. Elsevier, Academic Press, London, UK.
- Tovari, D., Vögtle, T. (2004). Object Classification in Laser-Scanning Data. In *Int. Arch. of Photogrammetry and Remote Sensing*, 36(8/W2), pp. 45-49.
- Trianni, G., Dell'Acqua, F., Gamba, P., Lisini, G. (2008). Fusion of GIS and SAR statistical features for earthquake damage mapping at the block scale. *International Archive of Photogrammetry and Remote Sensing (IAPRS)*, 37 (B4), pp. 1665-1670.

- Turker, M., San, B. T. (2003), "SPOT HRV Data Analysis for Detecting Earthquake-induced Changes in Izmit, Turkey. International Journal of Remote Sensing, 24(12): pp. 2439–2450.
- Turker, M. and San, B. T. (2004). Detection of collapsed buildings caused by the 1999 Izmit, Turkey earthquake through digital analysis of post-event aerial photographs. Int. Journal of Remote Sensing, 25 (21), pp. 4701–4714.
- Turker M, Cetinkaya B. (2005). Automatic detection of earthquake damaged buildings using DEMs created from pre- and post-earthquake stereo aerial photographs. International Journal of Remote Sensing, 26(4), pp. 823–832.
- Turker, M., Sumer, E. (2008). Building-based Damage Detection due to Earthquake using the Watershed Segmentation of Post-event Aerial Images. International Journal of Remote Sensing, 29(11), pp. 3073-3089.
- Tuytelaars , T., Proesmans, M., Van Gool , L. J. (1997). The Cascaded Hough Transform as Support for Grouping and Finding Vanishing Points and Lines. Proceedings of the International Workshop on Algebraic Frames for the Perception-Action Cycle, September 08-09, pp. 278-289.
- Van Allen, T., Greiner, R. (2000). Model Selection Criteria for Learning Belief Nets: an Empirical Comparison. Proc. 17th Int'l Conf. Machine Learning, pp. 1047-1054.
- Van Oort, P. A. J. (2005). Improving land cover change estimates by accounting for classification errors. International Journal of Remote Sensing, 26(14), pp. 3009 – 3024.
- Vapnik, V. (1995). The nature of statistical learning theory. New York: Springer
- Viola, P., Wells III, W. M. (1997). Alignment by maximization of mutual information. International Journal of Computer Vision, 24, pp. 137–154.
- Volpi, M., Tuia, D., Kanevski, M., Bovolo, F., Bruzzone, L. (2009). Supervised change detection in VHR images: A comparative analysis. IEEE International Workshop on Machine Learning for Signal Processing, Grenoble, France, pp. 1-6.
- Voorhees, H., Poggio, T. (1987). Detecting textons and texture boundaries in natural images. In Proc. 1st Int. Conf. on Computer Vision, London, England, June 8-11.
- Vu, T. T., Matsuoka, M., Yamazaki, F. (2004a). LIDAR for updating 3D information in building database. Proceeding of ASIA Conference on Earthquake Engineering (ACEE), Manila, Philippines 2, pp. 365-372.
- Vu, T. T., Matsuoka, M., Yamazaki, F. (2004b). Shadow Analysis in Assisting Damage Detection Due to Earthquakes from Quickbird Imagery. International archives of Photogrammetry Remote Sensing and Spatial Information Sciences, 35 (7), pp. 607-610.
- Vögtle, T., Steinle, E. (2004). Detection and recognition of changes in building geometry derived from multitemporal laserscanning data. International Archive of Photogrammetry and Remote Sensing (IAPRS), 35 (B2), pp. 428-433.

- Wang, Z., Schenk, T. (1992). 3D urban area surface analysis. International Archive of Photogrammetry and Remote Sensing (IAPRS), 29 (B3), pp. 720-726.
- Wechsler, S. P. (2006). Uncertainties associated with digital elevation models for hydrologic applications: A Review. *Hydrology and Earth System Sciences Discussions* 3, pp. 2343–2384.
- Weidner, U. (1997). Digital Surface Models for Building Extraction. In: A. Gruen, E. Baltsavias & O. Henricsson, (eds.), *Automatic Extraction of Man-Made Objects from Aerial and Space Images (II)*, Basel: Birkhäuser Verlag, pp. 193-202.
- Wyszecki, G.W., Stiles, S.W. (1982). *Color Science: Concepts and Methods, Quantitative Data and Formulas*. New York: Wiley.
- Yamazaki, F., Nishimura, A., Ueno, Y. (1996). Estimation of Human Casualties due to Urban Earthquakes. 11th World Conference on Earthquake Engineering, 8p (on CD-ROM).
- Yamazaki, F., Yano, Y., Matsuoka, M. (2005). Visual damage interpretation of buildings in Bam City using QuickBird images. *Earthquake Spectra*, 21 (S1), pp. S329-S336.
- Yano, Y., Yamazaki, F., Matsuoka, M., Vu, T.T. (2004). Building Damage Detection of the 2003 Bam, Iran Earthquake Using QuickBird Images. Proceeding 25th Asian Conference on Remote Sensing, CD-ROM, pp. 618-623.
- Yong, L., Huayi, W. (2008). Adaptive Building Edge Detection by Combining LIDAR Data and Aerial Images. *International archives of Photogrammetry Remote Sensing and Spatial Information Sciences*, 37 (B1), pp. 197-202.
- Yusuf, Y., Matsuoka, M. and Yamazaki, F. (2001). Damage assessment after 2001 Gujarat earthquake using Landsat-7 satellite images. *Journal of the Indian Society of Remote Sensing*, 29 (1), pp. 233-239.
- Zlatanova, S. (2008). SII for emergency response: The 3D challenges. International Archive of Photogrammetry and Remote Sensing (IAPRS), 37 (B4), pp. 1631-1637.
- Zhang, L. (2005). Automatic Digital Surface Model (DSM) Generation from Linear Array Images. Ph. D. Dissertation, Report No. 88, Institute of Geodesy and Photogrammetry, ETH Zurich, Switzerland.
- Zhang, S., Na, X., Kong, B., Wang, Z., Jiang, H., Yu, H., Zhao, Z., Li, X., Liu, C., Dale, P. (2009). Identifying wetland change in China's Sanjiang Plain using remote sensing. *WETLANDS*, 29(1), DOI: 10.1672/08-04.1, pp. 302-313.
- Zhou, G. (2009). Future Intelligent Earth Observing System (FIEOS) for Fast Response Disaster. Proceedings of International Conference on Geo-spatial Solutions for Emergency Management, Beijing, China, pp. 7-12.
- Zimmermann, P. (2005). Modellbasierte Gebäudeextraktion aus Farbluftbildern mit Höhendaten und Zusatzinformationen. Thesis (PhD). Swiss Federal Institute of Technology (ETH), Zurich, Switzerland, Nr. 16161.

ACKNOWLEDGEMENTS

It is an honor for me to thank those who made this thesis possible and first and foremost I would like to express my gratitude to my supervisor Prof. em. Dr. Armin Gruen for his support, scientific guidance and critical reviews during this research. I would be grateful that he gave me the chance for working in the multidisciplinary project with MERCI group. I also would like to thank Prof. Dr. Pollefeyts and Prof. Dr. Altan for being my co-examiners and for their valuable contribution.

I would like to acknowledge all my friends in Zurich for their support and deep friendship, in particular Dr. Henri Eisenbeiß for translating the abstract to German, Dr. Zhang Li for his fruitful help, Beat Rüedin for constant and useful help on the hardware and software problems and Dr. Jafar Amiri Parian and Soheil Sotoodeh for their help during my stay in Zurich.

The meetings and discussions with my former colleagues at MERCI group were also very important for the success of this work, in particular our joint study with Dr. Juliane Buchheister. The help and care of Liliane Steinbrückner, Susanne Sebestyen and Brigitte Cuperus have also been greatly appreciated. I wish to thank the National Cartography Center of Iran (NCC) for the provision of aerial imagery, ground control information and the digital map of Bam city.

Last but by no means least, my sincerest thanks go to my whole family for their support and motivation during this very trying period. This thesis is dedicated to my wife and daughter - Maryam and Yasaman - who have always stood by me and borne all my absence from many family occasions with a smile. I could have never completed this thesis without their greatest support.

CURRICULUM VITAE

Personal Data

Name & Surname: Mehdi Rezaeian

Date & place of birth: September, 22, 1970, Tehran – Iran

Education:

Since February 2005

Ph.D. student at Institute of Geodesy and Photogrammetry Swiss Federal Institute of Technology, Zürich, Switzerland

Feb. 1995 - Dec. 1997

M.Sc. Electrical Engineering (Bioelectric) University of Tehran (Honor)

Thesis: Parallelization of ML Algorithms for PET Image Reconstruction

Sept. 1989 - Sept. 1994

B.Sc. Electrical Engineering (Electronics) K.N.T. University of Technology (Honor)

Thesis: Designing and Producing a Developed 80188 System

Academic positions:

1999-2004

Lecturer, Department of Geomatics, University of Tehran-Iran

2001-2002

Assistant to Chairman in Educational Affairs, Department of Surveying and Geomatics, University of Tehran-Iran

2002-2004

Manager of Faculty in Educational Affairs, Faculty of Engineering, University of Tehran-Iran

2004-2007

Research Assistance, research project: Management of Earthquake Risks using Condition Indicators (MERCI), ETH Zürich- Switzerland.

Publications

Journal paper:

Rezaeian, M., Grün, A. (2010). Automatic 3D building extraction from aerial and space images for earthquake risk management. Journal of Georisk (Taylor & Francis): Assessment and Management of Risk for Engineered Systems and Geohazards, Vol. 4, No. 3, 1-20.

Book chapter:

Rezaeian, M. and Gruen, A. (2007) Automatic classification of collapsed buildings using object and image space features. In: J. Li, S. Zlatanova and A. Fabbri (eds.), Geomatics solutions for Disaster Management. Springer .

Conference papers:

Buchheister, J., Rezaeian M. (2008). Identification of liquefaction failures based on aerial images. The 14th World Conference on Earthquake Engineering, Beijing, China.

Rezaeian, M. and Gruen, A. (2008). Automatic classification of collapsed buildings using Digital surface models. Presented at Second Disaster Management Conference, Tehran, Iran, 8p (on CD-ROM).

Rezaeian M. (2007) Automatic detection of collapsed buildings due to earthquake using aerial images. Presented at International Conference on Seismology and Earthquake Engineering, Tehran, Iran, 8p (on CD-ROM).

Hashemi L., Azizi A., Rezaeian M. (2004) The Reflectance Modeling In Shape From Shading. International Society for photogrammetry and Remote Sensing, Istanbul Turkey.

Rezaeian M. (2004) Designing and Developing a Parallel DEM software based on Cluster Processing. Published in the Proceedings of the Iranian Geomatics Conference, Tehran, Iran (in Farsi).

Rezaeian M. and Soltanian-Zadeh H. (2002) Parallel PET image reconstruction based on SAGE algorithms. Published in the Proceedings of the Iranian Computer Vision Conference, Tehran, Iran (in Farsi).

Samadzadegan F., Rezaeian M., Gharashi M. P., Hahn M. (2000) Automatic Robust Digital Terrain Modeling Based on Fuzzy Logic. Published in the Proceedings of the Iranian Geomatics Conference, Tehran, Iran.

Azizi A., Samadzadegan F., Rezaeian M., Gharashi M. P. (2000) A Design of New Generation of Digital Photogrammetric Workstations. Published in the Proceedings of the Iranian Geomatics Conference, Tehran, Iran (in Farsi).

Samadzadegan F., Rezaeian M., Hahn M. (2000) A Robust automatic digital terrain modeling method based on fuzzy logic, Published in the Proceedings of ISPRS Congress, Amsterdam, Netherlands.

Rezaeian M. and Soltanian-Zadeh H. (1997) "Time-Frequency Analysis of Noise." Presented at the Fifth Iranian Conference on Electrical Engineering, Tehran, Iran (in Farsi).

Rezaeian M. and Soltanian-Zadeh H. (1996) A New Multi-Grid Method for PET Image Reconstruction Using EM Algorithm, Published in the Proceedings of the 8th Conference on Biomedical Eng, Tehran, Iran (in Farsi).